Dipl.-Ing. Markus Bainschab, BSc

Automotive Exhaust Particle Sensing Down to Ten Nanometer

PhD Thesis

to achieve the university degree of

Doktor der Technischen Wissenschaften

Doctoral Programme: Electrical Engineering

submitted to

Graz University of Technology

Supervisor

Univ.-Prof. Dipl.-Ing. Mag.rer.nat. Dr.rer.nat. Alexander Bergmann

Institute of Electrical Measurement and Sensor Systems
Head: Univ.-Prof. Dipl.-Ing. Mag.rer.nat. Dr.rer.nat. Alexander Bergmann

Graz, June 2020

Affidavit

I declare that I have authored this thesis independently, that I have not used other than the declared sources/resources, and that I have explicitly indicated all material which has been quoted either literally or by content from the sources used. The text document uploaded to TUGRAZonline is identical to the present doctoral thesis.

Date

Signature

Acknowledgements

I want to pronounce my honest gratitude to my supervisor, Alexander Bergmann, for inspiring, supporting, and teaching me during the last years. In addition to the technical expertise he shared with me, I could learn a lot from his way of leading and interacting with people. Supervising me, he found the perfect balance between guidance and leaving space for creative solutions and often estimated my capabilities better than I could.

I want to thank all people who were involved in DownToTen. Being part of an international project where many people from different countries and institutions collaborate constructively, was an excellent experience for me. I want to thank Zissis Samaras and his team for the superb organization and leadership and Lukas Landl, Stefan Hausberger (both IVT TUG), Jon Andersson (Ricardo Ltd.) and Athanasios Mamakos (AVL GmbH) for their efforts and fruitful discussions during our collaborations. I am especially grateful for the joint activities with Sampsa Martikainen, Panu Karjalainen, and Jorma Keskinen from Tampere University. During my numerous enjoyable stays in Tampere, they seamlessly integrated me into their research group and generously shared their expertise in aerosol science.

I want to thank Adam Boise for enabling me to temporarily join his research group at Cambridge University and for his inspiration during this time. I want to express my sincere gratitude to Simone Hochgreb and her family for having me in their home during my stay in Cambridge. Meeting and working with Simone was genuinely inspiring for me. I gratefully acknowledge the efforts of Hassan Imran and George Giannopoulos during our joint work in the laboratory.

I am grateful for the delightful and enriching environment created by the people of the Institute of Electrical Measurement and Sensor Systems. I had the pleasure to experience support from and fruitful discussions with my

friends and Ph.D. colleagues, Alexander, Anton, Benjamin, Georg, Mario, Markus, Martin, Paul, Philipp, Reinhard, Stefan, Tanja, Theresa, and Ulrich. I want to thank Sitaram and Thomas for supporting me in technical issues and Julia and Esther for their efforts in administration. I acknowledge the staff from the machine shops of the Institute of Electronics, the Institute of Electrical Measurement and Sensor Systems, and the Institute of Internal Combustion Engines and Thermodynamics, for their expertise and support. I am thankful for an enriching group of friends and the time we spent together. I want to express my special gratitude to Paul Maierhofer, who has been a great companion at the university and outside.

Most of all, I want to thank my family for their unrestricted support, and Sara for her love and endurance.

Abstract

Particulate matter suspended in the air causes adverse health effects and contributes to global climate warming. Regulations around the world, therefore, limit the emissions of particles by motor vehicles. With progressing engine and exhaust after-treatment technologies, these regulations need to be updated and extended to ensure further reductions of emissions. On the one hand, this work aims to contribute to the adaptation of European particle number emission regulations to account for new engine technologies that may emit notable levels of particles below the current legislative size limit of 23 nm. On the other hand, extending existing regulations towards particle number concentration measurement during periodic technical inspections to identify vehicles with after-treatment malfunctions is investigated in this thesis.

Large portions of this thesis were conducted in the project DownToTen; a European Union-funded project focused on the particle size fraction below the current regulatory size threshold of 23 nm. The main emphasis of this thesis was the transportation of the exhaust from the tailpipe to the particle number sensing element, along with adequate dilution and conditioning. The solutions for this challenging task elaborated within this thesis are twofold. First, the DownToTen sampling system was designed and constructed by using existing technologies that were modified and redesigned to address the challenges that arise in the sub-23 nm size regime. Stationary measurements of exhaust from a large number of different vehicles and engine technologies accompanied the system's development in multiple generations. Finally, the system was applied as a portable emission measurement system to assess real driving particle emissions below the current legislative size limit. The development and characterization of the aerosol gas exchange system constitute a second contribution to the progress of instrumentation for particle number measurement in the size regime below

23 nm. The instrument developed can act as an alternative approach for engine exhaust conditioning. With its function principle based on diffusion, it can furthermore be a useful tool in other fields of aerosol science.

The final part of the thesis is dedicated to low-cost particle number concentration measurements during periodic technical inspections. The effectiveness of under-discussion instrument specifications to guarantee the unambiguous distinction of high and low emitters among the vehicles of a fleet was evaluated in a dedicated experimental study supported by simulations. Additionally, this study comprises the first quantitative assessment of the potential reduction of overall fleet emissions associated with particle number concentration measurements during periodic technical inspections.

Contents

List of Figures

Nomenclature

Abbreviations

AGES	Aerosol Gas Exchange System
APi-TOF	Atmospheric Pressure Interface Time-of-Flight
BC	Black Carbon
CAST	Combustion Aerosol Standard
CE	Counting Efficiency
CPC	Condensation Particle Counter
CVS	Constant Volume Sampling
DC	Diffusion Charger
DCS	Diffusion Charging Sensor
DEG	Diethylene Glycol
DMA	Differential Mobility Analyzer
DMS	Differential Mobility Spectrometer
DPF	Diesel Particle Filter
ED	Ejector Diluter
EEPS	Engine Exhaust Particle Sizer

EPA	Environmental Protection Agency
ET	Evaporation Tube
FMPS	Fast Mobility Particle Sizer
GDI	Gasoline Direct Injection
GSA	Gaseous Sulfuric Acid
HEPA	High-Efficiency Particulate Air
ICE	Internal Combustion Engine
ICP-MS	Inductively Coupled Plasma Mass Spectrometer
ISC	In-Service Conformity
MISG	Miniature Inverted Soot Generator
nCNC	nano Condensation Nucleus Counter
NEDC	New European Driving Cycle
NO_x	Nitrogen Oxides
PFI	Port Fuel Injection
PM	Particle Mass
PN	Particle Number
PSL	Polystyrene Latex
PSM	Particle Size Magnifier
PTD	Porous Tube Diluter
PTI	Periodic Technical Inspection

PVT	Polyvinyltoluene
RDD	Rotating Disk Diluter
RDE	Real Drive Emissions
SMPS	Scanning Mobility Particle Sizer
SPG	Shirasu Porous Glass
TAT	Type Approval Testing
TD	Thermodenuder
TPN	Total Particle Number
VPR	Volatile Particle Remover
WLTC	Worldwide Harmonized Light Vehicles Test Cycle

Symbols

η	Kinematic Viscosity
μ	Dimensionless Deposition Parameter
μ_d	Location Parameter in Log-Normal Distribution
μ_e	Electrical Mobility
ρ_p	Particle Density
σ_d	Width Parameter in Log-Normal Distribution
$c_\mathrm{p,CVS}$	Pollutant Concentration in the CVS tunnel
$c_\mathrm{p,TP}$	Pollutant Concentration at the Tailpipe
C_c	Cunningham Slip Correction Factor

D	Diffusion Coefficient
d_p	Particle Diameter
f	Rotation Frequency
H	Molecular Accommodation Coefficient
k	Boltzmann Constant
k_g	Gas Thermal Conductivity
k_p	Particle Thermal Conductivity
L	Tube Length
P	Relative Particle Penetration
q	Particle Charge
Q_{ex}	Exhaust Flow Rate
Q_{tot}	Total Flow Rate
Q_v	Volumetric Flow Rate
Q_{dil}	Dilution Air Flow Rate
R	Particle Size Resolution in Channels per Decade
RE	Removal Efficiency
T	Absolute Temperature
V_{cav}	Rotating Disk Cavity Volume
v_{th}	Thermophoretic Velocity
X_p	Pollutant Emission Rate

GMD	Geometric Mean Diameter
GSD	Geometric Standard Deviation

1. Introduction

1.1. Motivation

Many studies prove that particulates suspended in the air cause adverse health effects [1–5]. In addition to that, black carbon (BC) particles are among the most significant contributors to global warming[6–9]. Especially in densely populated areas, a significant fraction of the particle air pollution is anthropogenic, with road transport being a major source[10–12]. Particles emitted by vehicles may be generated by tire wear, road wear, brake wear, or the combustion process of the internal combustion engine (ICE) . While the particles generated by abrasion mechanisms are not subject to regulations at the moment, many countries all over the world have legislatively limited the emission of combustion generated particles. These emission regulations have reduced vehicle particle emissions substantially in the last decades. As a result, the related adverse health effects have been mitigated, and the quality of life of millions of people has been improved notably. Despite these improvements, particulate matter still causes thousands of premature deaths worldwide each year[13]. In changing times with the rapid evolution of transportation technologies, it is challenging to maintain this trend of decreasing emissions further and improving air quality with corresponding regulations. It is the task of researchers to provide the required scientific progress to enable the regulations to keep up with technological developments. This task is especially demanding for particulate exhaust emissions. The system of exhaust particles and the air they are suspended in is considered an aerosol. A large number of different physical and chemical effects relevant to aerosol science are responsible for a broad range of related topics that remain insufficiently understood. With applications in manufacturing processes[14], environmental science [6], the transmission of pathogens[15] and other fields, the relevance of gaining a better understanding of these

effects and developing the required measurement instrumentation goes far beyond limiting the emissions of internal combustion engines.

1.2. Problem Statement

Type Approval Testing

In September 2015, the United States Environmental Protection Agency (EPA) revealed that NO_x emission control systems of certain Volkswagen vehicles were only active during emission testing in laboratories. As a result, the said vehicles fulfilled the US emission standards but emitted multiples of the regulatory limit in real-world operation[16–18]. This issue, commonly known as the "Volkswagen emission scandal", raised concerns on the emissions of vehicles on the road. These concerns, which were shared by the public and lawmakers, should be addressed with real drive emissions (RDE) regulations to assess the emissions under realistic operation conditions. This major change in regulatory emission testing and recent findings that diesel and gasoline direct injection (GDI) emit solid particles smaller than the active smaller particle size limit[19, 20] triggered a reconsideration of this lower size limit in particle number emission regulations in Europe. The lower size limit was established at 23 nm by the Particle Measurement Programme (PMP)[21–24] and implemented in the European emission standards in 2011 (EURO5b). This introduction of particle number based emission regulations was mainly motivated by a higher sensitivity than gravimetric methods. This higher sensitivity allowed capturing the low particle emissions of vehicles equipped with diesel particle filters (DPF) more repeatably [25]. Initially, the particle number emission regulation only targeted diesel-powered vehicles with a limit value of 6×10^{11} #/km. With the implementation of Euro 6b in September 2014, the particle number emissions of GDI vehicles have been regulated with the same limit value but with an exception within a monitoring phase of three years where the limit value was 6×10^{12} #/km. Port fuel injection gasoline vehicles generally exhibit significantly lower particle emissions than GDI vehicles and are therefore excluded from particle emission regulations in Europe[26].

In 2016, three parallel projects funded by the EU Horizon 2020 program were launched to investigate sub-23 nm automotive particle number measurements and the feasibility for regulatory purposes. The names of the projects are SUREAL-23[27], PEMs4Nano[28] and DownToTen[29]. The sampling and exhaust conditioning procedure was identified as a key component for the feasibility of reproducible sub-23 nm automotive exhaust particle number measurement. The exhaust has to be transported to the measurement instrument in a way, that the sub-23 nm fraction of the particles is not overly suppressed by diffusional losses while guaranteeing that volatile particles are efficiently removed. Furthermore, at the inlet of the measurement device, temperature, and particle number concentration of the aerosol have to match the operation limits of the measurement instrument. There are commercially available systems for automotive particle number measurement above 23 nm, but the extension of the particle size range down to 10 nm or below is a non-trivial task. Therefore, sampling and conditioning methods received significant attention not only in this thesis and DownToTen but also in the two sister projects.

Periodic Technical Inspections

The above mentioned regulative actions and methods focus on type approval testing (TAT), for the accurate assessment of the emissions of a limited number of vehicles of a specific type before the introduction to the market. These tests are performed using high-end measurement in dynamometer facilities and PEMS equipment to assess real drive emissions. While guaranteeing the compliance with emission standards at the beginning of vehicles' life cycles, type approval testing does not assess the in-use compliance with emission standards.

However, there are additional regulative measures also to assess the emissions of real-world vehicles beyond type approval. During in-service conformity (ISC) tests, a limited number of vehicles in circulation are selected according to prescribed procedures and tested for their emissions in a dynamometer facility[30]. In-service conformity RDE testing was introduced for heavy-duty vehicles in 2014[31]. The non-governmental organization

Transport & Environment in 2016 suggested to extend RDE in-service conformity testing towards light-duty vehicles, to ensure compliance with legal emission limits during the lifetime of vehicles(160 000 km)[18].

In addition to in-service conformity testing, many countries prescribe simple emission tests in the course of periodic technical inspections (PTI) . The particle emissions are commonly assessed with opacity tests[30, 32, 33]. However, it has been proven repeatedly that these tests are insufficient. Boveroux et al., for example, could only identify 1 % of the vehicles as high emitters employing opacity testing, while reliable detecting all of them by measurements of the emitted particle number concentration in low idle operation. Other studies found a good agreement of particle number concentrations in low idle with the total number of particles emitted over type approval compliant driving cycles like the New European Driving Cycle (NEDC) or the Worldwide Harmonized Light Vehicles Test Cycle (WLTC)[34, 35].

Malfunctions of exhaust after-treatment systems may occur at certain times in vehicles' lives, causing emissions that exceed the regulative limits by orders of magnitudes. This scenario is especially relevant for vehicles with DPFs. In a study by Boveroux et al., the particle emissions of more than 300 EURO5 and EURO6 diesel cars were measured[36]. It was found that only 15 % of the vehicles cause 97 % of the overall particle emissions. Thus, identifying these high emitters and reestablishing the functionality of their malfunctioned after-treatment systems that cause high emissions, would have a substantial impact on the overall fleet emissions.

There is a broad agreement in the scientific community that a valid and reliable identification of particulate filter malfunctions can be achieved utilizing particle number concentration measurements. This common sense induced the prescription of particle number measurements during PTIs for on-road or off-road vehicles in several European countries (Belgium, the Netherlands, Germany, Switzerland). The underlying national regulations include instrument specifications like particle size-dependent limits for the counting efficiency. The instrument specifications are a vital factor for the success of the PN PTI measurements. The specified technical properties have to guarantee that malfunctioned particle filters are reliably detected.

Simultaneously, the instruments' complexity should remain limited to facilitate their usage by non-expert personnel in workshops. It is crucial to have a profound knowledge of the particle size distributions of the emissions in idling operation for the definition of limits for the particle size-dependent counting efficiency. However, the corresponding available data set in the literature is limited. This lack of stressable data, up to now, inhibited a comprehensive analysis of the specifications that are under discussion. Another open question is the magnitude of the potential reduction of the fleet particle emissions that can be achieved by the introduction of particle number measurements in PTI. While there is no doubt in the scientific community that PTI PN measurements can reduce the emissions, there is no published quantitative assessment of the potential impact.

1.3. Scope

The first aim of this thesis is to design, construct, and apply a sampling system, enabling the mobile measurement of automotive particle number measurement down to at least 10 nm. The system is developed within the project DownToTen, by selecting and modifying existing technologies based on literature review and the results of a dedicated laboratory measurement campaign. The system is applied in mobile measurements to assess currently unregulated sub-23 nm particle emissions during real driving.

Additionally, a novel method for engine exhaust aerosol conditioning called the Aerosol Gas Exchange System (AGES) is modeled, materialized, and tested in laboratory experiments. With a complementary working principle to existing exhaust conditioning technologies, the AGES can be especially useful for the measurement of sub-23 nm particles and applications in other fields of aerosol science.

The third part of the thesis contributes to reducing automotive particle emissions beyond type approval testing. A study on the particle size distributions of vehicles in idling operation is conducted to comprehensively assess under-discussion instrument specifications for particle number concentration measurements in periodic technical inspections. In addition to the specification analysis, a first assessment of the potential impact these

measurements can have on the overall particle emissions of a vehicle fleet is performed.

1.4. Organization of the Thesis

After this introduction, chapter 2 provides a brief description of basic concepts and definitions in aerosol science. In chapter 3, the concepts, and instruments of aerosol measurement technologies that are relevant in this thesis are introduced. The results of the thesis that are presented in the form of the journal publications listed below are discussed in chapter 4, which is followed by concluding remarks in chapter 5. After the conclusion, reprints of the following papers are attached:

Paper 1 Markus Bainschab, Lukas Landl, Jon Andersson, Athanasios Mamakos, Stefan Hausberger, and Alexander Bergmann. "Measuring Sub-23 Nanometer Real Driving Particle Number Emissions Using the Portable DownToTen Sampling System." In: *Journal of Visualized Experiments* (2020). DOI: doi:10.3791/61287. URL: https://www.jove.com/video/61287

Paper 2 Markus Bainschab, Sampsa Martikainen, Jorma Keskinen, Alexander Bergmann, and Panu Karjalainen. "Aerosol gas exchange system (AGES) for nanoparticle sampling at elevated temperatures: Modeling and experimental characterization." In: *Scientific Reports* (2019). DOI: 10.1038/s41598-019-53113-5. URL: https://www.nature.com/articles/s41598-019-53113-5

Paper 3 Markus Bainschab, Mario Anton Schriefl, and Alexander Bergmann. "Particle Number Measurements within Periodic Technical Inspections: A First Quantitative Assessment of the Influence of Size Distributions and the Fleet Emission Reduction." Graz, 2020

Paper 1 and **Paper 2** are peer-reviewed and published. At the time this thesis is submitted, **Paper 3** is under peer-review at the journal *Atmospheric Environment: X*. The version of **Paper 3** attached, is based on the submitted paper and additionally comprises corrections and clarifications as suggested by Prof. Jason Olfert (Department of Mechanical Engineering, University of Alberta).

The appendix provides supplementary technical and organizational information. Additionally, self-contained elaborations of two aerosol dilution concepts are described in Appendix D and Appendix E. Finally, in Appendix F, a patent application, describing an invention that was conceived in this thesis is attached.

1.5. Author Contributions to the Papers

Paper 1 The author of this thesis designed, constructed, and tested the DownToTen sampling system. He wrote the entire manuscript except for the introduction (Jon Andersson) and the instructions for installing the exhaust flow meter and the time alignment procedure (Lukas Landl). The author handled the submission of the manuscript, correspondence with the editor, and the rebuttal of the reviewer's comments.

Paper 2 The author of this thesis conceived the idea to use the counter flow denuder as an alternative approach for engine exhaust conditioning. The author designed and constructed the Aerosol Gas Exchange System and performed the oxygen removal test. The author set up the mathematical model and the CFD simulations and participated in the laboratory measurement campaign. Furthermore, the author performed the entire data evaluation except for the GSA data from API-TOF (Sampsa Martikainen). The author of this thesis prepared all figures except for Figure 7 (Sampsa Martikainen). The author wrote the "Instrument Description," and the "Results" sections and parts of the "Introduction," "Methods," and "Discussion" sections. The author handled the submission of the manuscript, correspondence with the editor, and the rebuttal of the reviewer's comments.

Paper 3 The author of this thesis participated in the conceptualization and execution of the measurement campaign. The author performed the entire measurement data evaluation. He conceived and performed the quantitative emission reduction assessment. The author prepared all figures in the manuscript and wrote the manuscript except for some paragraphs in the "Introduction" and the "Assessment of Instrument Specifications" sections (Mario Schriefl). The author of this thesis handled the submission of the manuscript.

2. Aerosol Background

This chapter introduces the basic definitions and concepts of aerosol science and exhaust particle measurement required for the comprehension of this thesis. The explanations in this chapter are limited to the essentials and by no means claim to be exhaustive. The following books are recommended for more comprehensive elaborations:

- William C Hinds. *Aerosol technology: properties, behavior, and measurement of airborne particles*. John Wiley & Sons, 1999. ISBN: 0-471-19410-7
- Peter Eastwood. *Particulate Emissions from Vehicles*. John Wiley & Sons, 2008. ISBN: 978-0-470-72455-2
- Ian Colbeck and Lazaridis Mihalis. *Aerosol Science*. John Wiley and Sons, 2014. ISBN: 978-1-119-97792-6
- Pramod Kulkarni, Paul A Baron, and Klaus Willeke. *Aerosol measurement: principles, techniques, and applications*. Third Edit. John Wiley & Sons, 2011. ISBN: 978-0-470-38741-2
- Sheldon K Friedlander. *Smoke, Dust, and Haze: Fundamentals of Aerosol Dynamics*. Second Edi. Oxford, New York: Oxford University Press, 2000. ISBN: 0-19-512999-7

2.1. Particle Size

Aerosols are systems consisting of a gaseous carrier medium and liquid or solid particles suspended in the carrier gas. The particles sizes usually range between 2 nm to more than 100 µm[40]. The definition of the particle size itself is usually done utilizing equivalent diameters, which indicate that the particle, this equivalent diameter is assigned, has the same physical property as a sphere with this diameter. One example of an equivalent diameter is

the aerodynamic equivalent diameter. The aerodynamic equivalent diameter is the diameter of a sphere with a density of $1000\,\mathrm{kg\,m^{-3}}$ that exhibits the same terminal velocity as the particle under consideration[43]. Different equivalent diameters may be used to describe aerosol particles depending on the particle size and other properties of interest. Examples are:

- aerodynamic equivalent diameter
- electrical mobility equivalent diameter
- volume equivalent diameter
- mass equivalent diameter
- projected area equivalent diameter
- envelope equivalent diameter
- Sauter mean diameter

The electric mobility equivalent diameter is the most commonly used one in the field of automotive exhaust particle measurement. It is the diameter of a sphere with the same electrical mobility μ_e as the considered particle. The mobility μ_e can be described as a function of the particles charge q, the absolute temperature T, the Boltzmann constant k, and the diffusion coefficient D:

$$\mu_\mathrm{e} = \frac{qD}{kT} \tag{2.1}$$

The diffusion coefficient of a spherical particle in a gas can be computed as follows:

$$D = \frac{kTC_\mathrm{c}}{3\pi\eta d_\mathrm{p}} \tag{2.2}$$

Where η is the kinematic viscosity of the particle's carrier gas and C_c is the Cunningham slip correction factor, that accounts for the particle kinetics in the transition and free molecular regimes where the particle radii $d_\mathrm{p}/2$ are comparable to or smaller than the mean free path λ of carrier gas molecules. For air and standard conditions, the Cunningham slip correction factor is calculated as follows[45, 46]:

$$C_\mathrm{c} = 1 + \frac{2\lambda}{d_\mathrm{p}} \cdot \left(1.257 + 0.400 \cdot \exp\left(\frac{-0.55 d_\mathrm{p}}{\lambda}\right)\right) \tag{2.3}$$

2.2. Particle Size Distributions

The particles an aerosol comprises may differ from each other in many properties like chemical composition, shape, or density. It is highly unlikely that two given aerosol particles are identical in any physical property. The particle size is no exception to this. The sizes of aerosol particles are subject to size distributions. These size distributions are most commonly of log-normal nature and may comprise one or multiple modes. The statement that log-normal distributions accurately describe particle size distributions stems from empirical observations. It has not emerged from a derivation based on fundamental physical correlations. A general mathematical expression for a unimodal log-normal size distribution as function of the parameters a, μ_d, σ_d and the particle diameter d_p is given in Equation 2.4.

$$p(d_\mathrm{p}) = \frac{a}{d_\mathrm{p}} \frac{1}{\sigma_\mathrm{d}\sqrt{2\pi}} \exp\left(-\frac{(\ln(d_\mathrm{p}) - \mu_\mathrm{d})^2}{2\sigma_\mathrm{d}^2}\right) \tag{2.4}$$

The parameter a is proportional to the total number of particles. The parameter μ_d and σ_d define the location and width of the mode, respectively. They are related to the geometric mean diameter (GMD) and the geometric standard deviation (GSD) as follows:

$$\mathrm{GMD} = \exp(\mu_\mathrm{d}) \text{ and } \mathrm{GSD} = \exp(\sigma_\mathrm{d}) \tag{2.5}$$

In engine exhaust particle measurement, the size distributions commonly comprise three distinct modes. Figure 2.1 shows a generic illustration of these three modes weighted by the particle size to the power of different exponents. Particle number (d_p^0) and particle mass (d_p^3) are the most commonly used metrics in exhaust particle measurement. The size distribution weighted with the particle length (d_p^1) and surface area (d_p^2) are also included. These two metrics are less common but can also be of interest. For example, when applying charge based measurement devices for the characterization of the aerosol. As further elaborated in section 3.1, the responses of charge based particle measurement devices typically scale with the particle diameter to the power of 1 to 2 [43, 47–49].

As indicated in Figure 2.1, the three modes are usually labeled as nucleation mode, accumulation mode, and coarse mode. The nucleation mode $(d_p \lesssim 30\,\text{nm})$ predominantly consists of volatile organic and sulfur compounds but can also have a non-volatile core[50–52]. The volatile nucleation mode particles form upon dilution and cooling. As shown in Figure 2.1, this mode usually dominates the particle number weighted size distribution.

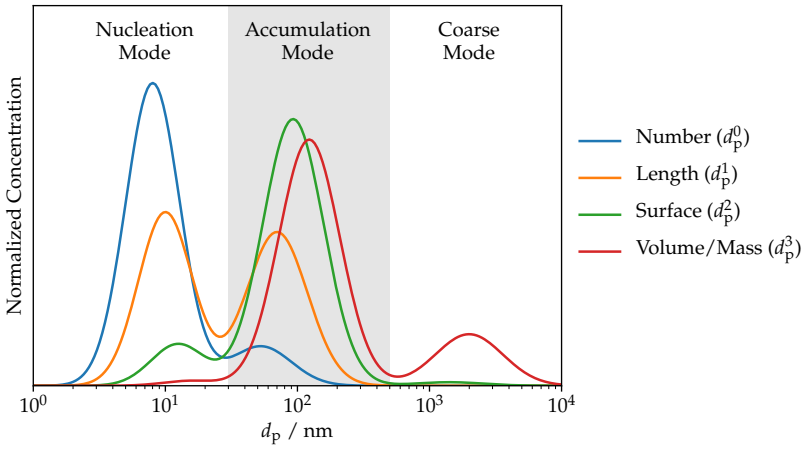

Figure 2.1.: Typical engine exhaust particle size distribution consisting of three log-normal modes. The different colors indicate different weights. The differently weighted distributions are normalized to have the same area under the curves.

The emitted particle mass is dominated by the accumulation mode ($30\,\text{nm} \lesssim d_p \lesssim 500\,\text{nm}$). The particles in this mode predominantly consist of soot and volatile material adsorbed thereon. The soot particles form in locally fuel-rich regions during the combustion process. Considering vehicles without particle filters equipped, typical mean diameters of diesel and gasoline exhaust accumulation mode particles are 60 nm to 120 nm and 40 nm to 80 nm respectively[25, 53]. Diesel particle filters typically reduce the particle number emissions by more than two orders of magnitude[25]. However, the effect of DPFs on the geometric mean particle is limited. When analyzing particle emissions of gasoline-powered vehicles, it is important to distinguish between direct injection and port fuel injection (PFI). The particle emissions of GDI vehicles generally tend to be significantly higher than those of PFI vehicles. The reason is that there is less time for fuel droplets to evaporate

and mix with the oxidation air if directly injecting fuel into the cylinder. Incomplete combustion in fuel-rich regions results in the generation of soot particles[54–56]. In particle size distributions of GDI vehicle exhaust a lobe at approximately 20 nm can occur[19]. Increased emissions of small particles have been observed in combination with the use of 85 % ethanol fuel[57].

The coarse mode $\left(d_\mathrm{p} \gtrsim 500\,\mathrm{nm}\right)$ consists of soot particles that deposited on surfaces in the exhaust duct system and later aerosolized again by vibrations, heat or flow forces, in the form of larger agglomerates[58]. As indicated in Figure 2.1, the coarse mode's contribution to the total particle number is negligible.

This thesis extensively covers particle size distributions of vehicles operating in idle speed in **Paper 3**. The instruments used to measure the particle size distributions are described in section 3.2. Due to the low volatility of accumulation mode particles, they are the main focus of automotive particle number measurements in emission regulations and this thesis.

2.3. Temporal Exhaust Aerosol Evolution

The nature of engine exhaust particles released into the atmosphere changes over time. The temporal evolution they undergo is schematically and simplified, shown in Figure 2.2. The temporal change of engine exhaust particles involves a large number of different chemical reactions, evaporation, condensation, and other effects that are not fully understood. Quantitative descriptions of the effects involved and corresponding definitions and models can be found in the literature[59–61]. The picture of this evolution drawn here is very simplified and should provide a rough description of commonly used terms.

Due to the high temperature ($> 400\,^\circ\mathrm{C}$) in the tailpipe, volatile compounds of the exhaust are in the gas phase. This state of the exhaust is often referred to as "hot exhaust" or "primary aerosol." Apart from soot, other non-volatile material like metals, ashes, or pyrolyzed hydrocarbons can be in the particle phase. The non-soot particles in this stage are usually of sizes smaller than

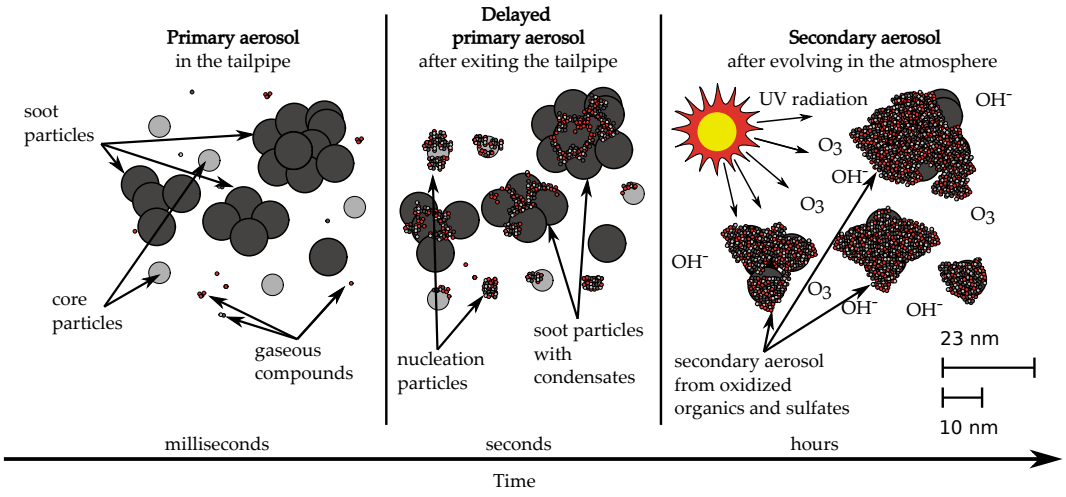

Figure 2.2.: Illustration of the temporal evolution of engine exhaust particles and gaseous compounds.

10 nm. They are referred to as "core particles" because they act as non-volatile cores of volatile particles that form upon cold dilution[50–52].

Upon release into the atmosphere, the exhaust is diluted by $\approx 1000:1$ and cools down to ambient temperature within seconds[62]. Volatile organic material goes into particle-phase by condensing on existing particles or forming volatile nucleation mode particles (sulfur driven process). The middle section of Figure 2.2 schematically shows this phase. The particles in this stage of their temporal evolution are referred to as "delayed primary aerosol" or "fresh aerosol particles." Due to further agglomeration and condensation of volatile material on the fractal soot particles, they become more spherical, and their effective density is increased [63]. Under the influence of ultraviolet radiation, atmospheric oxidants (e.g., O_3, OH^-, NO_3^-) and temperature variations, the exhaust transitions into "secondary aerosol"

within a time frame of hours to days[61]. Volatile material is deposited on the particles by physisorption and chemisorption. The ultraviolet radiation ionizes organic material, triggering different chemical reactions. Due to the chemical composition of secondary aerosol particles, their influence on human health and the climate is considerably different from the impact of primary aerosol[60]. However, their emissions are not yet directly limited by regulation.

Predominantly for the sake of reproducibility, the European particle number based emission standards are limited to the emission of solid particles. The restriction to solid particles is effectively equivalent to the particle number in the ”hot exhaust.” By additionally limiting the emissions of gaseous compounds like SO_2, or NO_x, that can act as precursors for the formation of secondary aerosol; its formation is indirectly targeted by regulations[61].

The DownToTen sampling system described in **Paper 1**, is primarily used for the measurement of solid engine exhaust particles. However, the system can also be used to assess ”fresh exhaust” and ”secondary aerosol”. The total particle number (TPN) of ”fresh exhaust”, can be measured by operating the system at room temperature.

2.4. Deposition Mechanisms

The deposition of aerosol particles, may be desired or to be avoided depending on the application. Offline particle analysis methods for example can rely on the deposition of particles on filters. In automotive particle number measurement, in contrast, the deposition of particles on the surfaces of sampling the sampling and measurement system is referred to as ”particle losses” and is usually not desirable. Different physical effects may drive the deposition of aerosol particles on surfaces. The six most relevant aerosol particle deposition mechanisms are the following[40, 41]:

Interception Particles following the streamlines of gas in motion get close enough to an object to be captured.

Sedimentation Particles are driven towards surfaces by gravity.

Inertial Impaction Particles with high inertia cannot follow bending streamlines of the carrier gas, causing them to colloid with the object the carrier gas low around.

Electrostatic Attraction Charged particles are driven towards surfaces in electric fields.

Thermophoresis Particles are deposited on cold surfaces by thermophoretic forces driven by a temperature gradient.

Diffusion Brownian motion of particles causes them to collide with surfaces randomly.

Thermophoresis and diffusion are two particle-deposition mechanisms that are the most relevant in automotive exhaust particle number measurement and this thesis. The following paragraphs cover these two mechanisms in further detail.

2.4.1. Thermophoresis

Thermophoresis describes particle transport by a temperature gradient. The gas molecules hitting the particle on the hotter side carry more momentum than the gas molecules on the cooler side. As a result, there is a net momentum transfer onto the particle, pushing it in the direction of decreasing temperature. This effect can be seen in everyday life, for example, at the wall behind a radiator. The radiator's hot surface tends to stay clean, while the cold wall behind it is often polluted with particulate matter. In engine exhaust particle measurement, the temperature of the exhaust at the tailpipe of a vehicle is usually not within the specifications of measurement instruments. It has to be cooled in the course of the sampling procedure. The cooling is usually done by using a coil or mixing the hot aerosol with particle-free dilution air. In both techniques, substantial temperature gradients in the sampling line are unavoidable, causing thermophoretic losses of particles. For a particle that is smaller than the mean free path λ of the carrier gas the thermophoretic velocity v_{th} is[43]:

$$v_{\mathrm{th}} = \frac{0.55\eta}{\rho_{\mathrm{p}}} \nabla T \quad \text{for } d_{\mathrm{p}} < \lambda \tag{2.6}$$

Where ρ_p is the density of the particle,η is the kinematic viscosity of the carrier gas and ∇T is the temperature gradient. As Equation 2.6 shows, there is no dependence of the thermophoretic velocity v_{th} on the particle diameter d_p. For particles larger than the mean free path, there is a small particle size dependence, which is accounted for in Equation 2.7 by the inclusion of the Cunningham slip correction factor C_c and the molecular accommodation coefficient H [43].

$$v_{th} = \frac{-3\eta C_c H}{2\rho_p T}\nabla T \quad \text{for } d_p > \lambda \tag{2.7}$$

The molecular accommodation coefficient depends on the particle diameter, the mean free path, and the thermal conductivities of the particle and the carrier gas k_p and k_g[43].

$$H \approxeq \left(\frac{1}{1+6\lambda/d_p}\right)\left(\frac{k_g/k_p + 4.4\lambda/d_p}{1+2k_g/k_p+8.8\lambda/d_p}\right) \tag{2.8}$$

The fact that thermophoretic velocity only has a small dependence on the particle diameter facilitates correcting for the corresponding particle losses. For the correction of thermophoretic particle losses in sampling systems for automotive exhaust particle number measurement, the small particle size dependence for large particles is usually neglected, and a constant factor is applied. This is illustrated in the results section of **Paper 1**. The ISO standard 29904 describes how thermophoretic particle deposition is accounted for in aerosol measurement systems [64].

2.4.2. Diffusion

In contrast to thermophoresis, described above, diffusional particle deposition is highly particle size-dependent. The diffusion of aerosol particles appears due to stochastic collisions of carrier gas molecules with the particles. Momentum is randomly transferred to the particles by this process, resulting in the particles' random motion. The smaller the particles are, the more pronounced this effect is. This trend is reflected in the particle size dependence of the diffusion coefficient D, that was already introduced in Equation 2.2 in section 2.1. It is approximately proportional to the inverse of

the particle diameter d_p for particles much larger than the mean free path λ of the carrier gas. In the transition regime ($d_p \approx \lambda$) and the free molecular flow regime ($d_p \ll \lambda$), the Cunningham slip correction factor C_c accounts for the additional dependence on the particle size. Diffusional particle losses in particle number measurement systems are usually considered to be relevant below a particle size of $d_p = 100\,\text{nm}$. The particle size-dependent magnitude of diffusional particle losses in tubes under laminar flow conditions can be estimated employing analytical expressions that were first found by Gormley and Kennedy in 1948[65]. A dimensionless deposition parameter μ is introduced for the calculation of the relative particle penetration P. It is defined as the diffusion coefficient D times the length of the tube L divided by the volumetric flow rate Q_v. [43]

$$\mu = \frac{DL}{Q_v} \tag{2.9}$$

Only considering diffusional particle deposition, the relative particle penetration of on aerosol flowing through a cylindrical tube can be computed as in Equation 2.10 and Equation 2.11.

$$P = 0.819e^{-11.49\mu} + 0.098e^{-70.07\mu} + 0.033e^{-179.0\mu} + 0.015e^{-338.1\mu} \;\; ; \;\; \mu > 0.006 \tag{2.10}$$

$$P = 1.0 - 5.50\mu^{\frac{2}{3}} + 3.77\mu + 0.81\mu^{\frac{4}{3}} \;\; ; \;\; \mu < 0.006 \tag{2.11}$$

The related diffusional particle losses $(1 - P)$ as a function of μ are shown in Figure 2.3. Points that correspond to different particle sizes, a tube length of $L = 1\,\text{m}$, and a flow rate of $Q_v = 1\,\text{lpm}$ under standard conditions are marked to relate the shown curve to real-world systems.

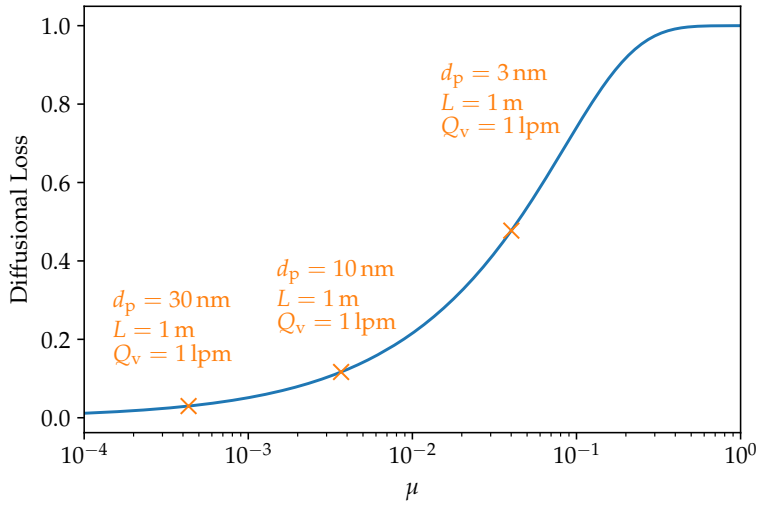

Figure 2.3.: Diffusional particle loss $(1 - P)$ in a cylindrical tube under laminar flow conditions as a function of the dimensionless deposition parameter μ. Points corresponding to a tube length of $L = 1\,\mathrm{m}$, a flow rate of $Q_v = 1\,\mathrm{lpm}$ and different particle diameters are marked.

In addition to Equation 2.10 and Equation 2.11, that hold for cylindrical tubes, also analytical expressions for diffusion-limited particle penetration in other geometries like rectangular tubes or parallel circular plates can be found in the literature[40, 43].

Paper 1 shows the diffusional particle losses of the DownToTen sampling system. The diffusional particle losses in the aerosol gas exchange system losses down to a particle size of 1.2 nm are experimentally investigated in **Paper 2**. Furthermore, the diffusional exchange of the carrier gas in the aerosol gas exchange system is modeled analytically and numerically in **Paper 2**. As elaborated in detail in the paper, the underlying differential equations are the same as for diffusional particle deposition, but the boundary conditions are different. As a result, the mathematical description of the exchange of carrier gas is not the same but of a similar form as the one for diffusional particle deposition.

3. Instrumentation

This chapter describes the aerosol particle measurement, sampling, and generation technologies used within this thesis. Additionally, some relevant alternatives to the technologies used are introduced. In section 3.1, the two PN measurement approaches, that are the most common in automotive particle measurement is described. Basic concepts and selected techniques for the measurement of particle size distributions are described in section 3.2. The measurement devices described in these first two sections of this chapter cannot be applied directly to the measurement of automotive exhaust particles. In aerosol science, it is often the case that one or more physical parameters of the aerosol to be characterized experimentally are not compatible with the specifications of the available measurement devices. For example, the pressure level of the aerosol exceeds the maximal inlet pressure of the device. If this is the case, the aerosol has to be treated in a certain way to meet the specifications of the measurement devices. This treatment, together with the conveyance of the aerosol to the measurement device, is referred to as "sampling." Also, in automotive emission particle measurements, sampling is required to be able to apply state-of-the-art measurement devices to characterize the exhaust. The parameters of the exhaust aerosol that are not compatible with measurement device limitations are most commonly the temperature and the particle number concentration. Furthermore, the specification of a certain sampling often acts as a definition of the regulated quantity. The processes applied in sampling procedures are divided into dilution and conditioning. These two processes and selected technical implementations are described in section 3.3 and section 3.4 respectively. In section 3.5, methods for the generation of aerosols to test measurement and sampling instrumentation in the laboratory are discussed.

3.1. Aerosol Particle Number Sensing

There are many different techniques to assess various properties of airborne particles. The properties that can be measured include mass, carried charge, chemical composition, electrical mobility, aerodynamic size, and others. The aerosol properties used for the definition of limit values in emission regulations are particle number, particle mass, and opacity. This thesis's primary focus is the measurement of particle number concentrations in automotive exhaust. The traditional approaches to evaluating the particle number concentrations are the condensation particle counter (CPC) and the diffusion charger (DC). The following paragraphs briefly describe both techniques.

3.1.1. Condensation Particle Counter

The condensation particle counter (CPC) is the most commonly used particle number measurement device in the field of automotive emissions measurement. The CPC offers reliable single particle detection down to particle diameters in the single-digit nm range. The upper PN concentration detection limit of CPCs operating in single count mode usually is in the range of $1 \times 10^4 \,\#/\mathrm{cm}^3$ to $1 \times 10^5 \,\#/\mathrm{cm}^3$. Beyond this upper limit, coincidence correction algorithms have to be applied to maintain the linearity of the instrument response with particle number concentration. There are numerous different embodiments of condensation particle counters, varying in the technical realization of different components. However, all of them rely on the optical detection of magnified particles[66].

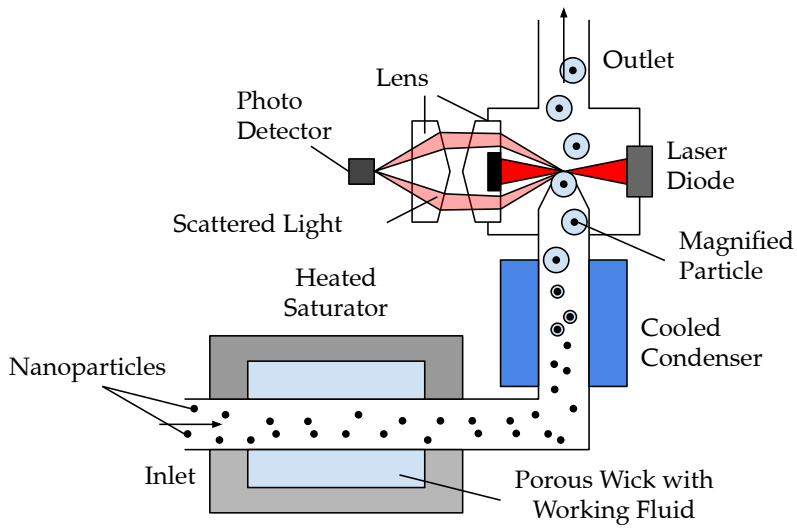

Figure 3.1.: Schematic drawing of a CPC and its working principle. The aerosol particles' depictions are not true to scale.

Figure 3.1 schematically shows the main components and illustrates the working principle of one embodiment of a CPC. An aerosol is drawn into the device by an underpressure, created by an internal or external pump. Directly downstream the inlet of the CPC, the aerosol is conveyed through the saturator section. In this heated section, the aerosol to be characterized is in contact with a liquid working fluid (e.g., n-butanol, water, isopropanol, n-decane). A porous wick absorbs the working fluid. Evaporation of the working fluid leads to saturation of the aerosol with the gaseous working fluid. Downstream the saturator, the aerosol is conveyed through a cooled condenser section. The lower temperature in this section induces a supersaturation of the aerosol with the working fluid. The particles suspended in the aerosol act as nucleation nuclei, and the working fluid condenses onto them. The condensation of working fluid on the particles magnifies them from their initial size (a few nm to several hundreds of nm) to a size that enables their optical detection (typically a few µm). Adiabatic expansion and mixing hot and cold streams, constitute alternative methods to achieve supersaturation and condensation. A laser diode is typically used as the light source for optical detection of the magnified particles. A beam dump and a lens system ensure that only light scattered

by the magnified particles falls onto the photodetector. The electronic signal from the photodetector is processed to detect and count the peaks that are generated by the light scattered from the particles. The particle number concentration can be calculated from the number of counted peaks and the known flow rate at the optical detection section.

Figure 3.2 shows a typical CPC counting efficiency curve. The lower particle size-dependent counting efficiency cutoff of a CPC is characterized by the d_{50}. The d_{50} refers to the diameter of a particle detected with an efficiency of 50 %. It is mainly dependent on the working fluid and the temperatures of the saturator and the condenser. Typical values of the d_{50} of commercially available CPCs are between 2.5 nm and 30 nm. For particle sizes exceeding the d_{50} by more than a factor of 2, the response of a CPC has a very low dependence on the particle size over a broad range, which makes it suitable for particle number concentration measurements[67].

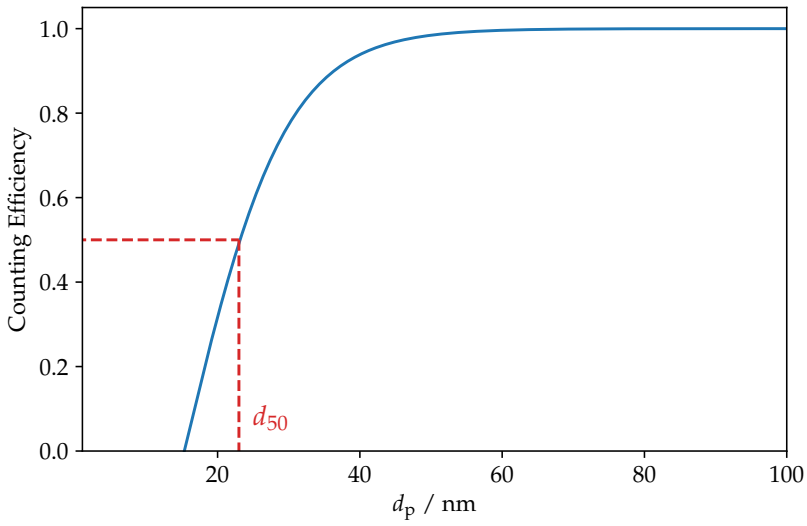

Figure 3.2.: Typical counting efficiency (CE) curve of a CPC. The particle diameter where the counting efficiency amounts to 50 % is referred to as d_{50}.

The nano Condensation Nucleus Counter (nCNC) described in subsection 3.2.4, is a different embodiment of a CPC enabling particle size distribution measurements by employing two condensation stage with different

working fluids in series and alternating the saturation ratio in the first condensation stage.

Different CPCs have been used for particle concentration measurements in **Paper 1**, **Paper 2** and **Paper 3**. An alternative approach to the realization of a CPC, which enabled operation at elevated temperatures, was conceived in this thesis. The concept of this alternative approach is subject to a patent application that is attached in Appendix F.

3.1.2. Diffusion Charger

Diffusion chargers (DC) or diffusion charging sensors (DCS) are charge-based devices for the measurement of aerosol particle concentrations. Diffusion chargers rely on unipolar charging of aerosol particles and measurement of the charge carried by the particles. Figure 3.3 shows a schematic of a diffusion charger. The main components of a diffusion charger are the charger, an ion trap, and the measurement stage. The charging of the particles is most commonly realized by employing a positive corona creating ions that subsequently attach to the aerosol particles by diffusion. Direct photoelectric charging using UV light enables material selective detection of particles[48, 68]. Alternative charging methods (soft X-ray, radioactive) exist but exhibit major drawbacks (price, safety regulations). Furthermore, the application of these bipolar charge sources would result in poor sensitivity if a Faraday-cup was used as the detection unit. These disadvantages compared to unipolar corona charging limit the applications of alternative charging methods in commercial instruments[43]. Downstream the charging stage, an ion trap removes ions that are not attached to particles. In the measurement stage, the charge that is carried by the particles is measured using an electrometer. Different realizations of this stage exist. One possibility is that the particles are captured in a filter inside a Faraday cup, as indicated in Figure 3.3. An electrometer measures the current compensating the charge carried by the captured particles. In different embodiments, where the charging stage or the ion trap are operated in pulsed modes, the charged particles pass through a Faraday cup. The electrometer measures an alternating current induced by clouds of charged particles entering and exiting the Faraday cup[47, 49]. The electrometer characteristics primarily determine

the limit of detection of a diffusion charger, which typically corresponds to a particle number concentration on the order of 1000 #/cm^3.

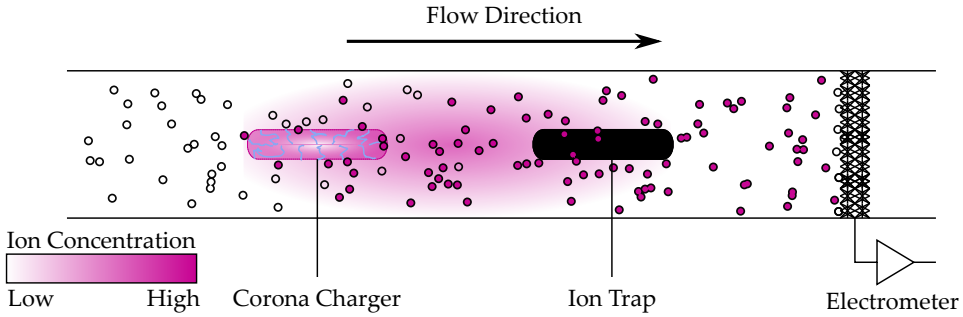

Figure 3.3.: Schematic drawing of a diffusion charger and its working principle. Void and filled circles indicate electrically neutral and charged particles, respectively. The purple cloud indicates a region of elevated ion concentration.

Due to charging characteristics and particle losses, the response of DCs is dependent on the diameter of the measured aerosol particles. Depending on the technical realization of the measurement device, the dependence on the particle diameter can be approximately linear to quadratic ($d_\mathrm{p}^1 - d_\mathrm{p}^2$)[43]. The deduction of a particle number concentration from a diffusion charger's response requires calibration and assumptions on the particle size distributions.

The relatively narrow range of mean particle sizes and distribution widths to be expected in the soot mode of automotive exhaust (section 2.2) enables accurate measurement of particle number emissions employing diffusion chargers. Diffusion chargers are widely applied as particle sensors in portable emission measurement systems (PEMS) for real driving emissions (RDE). Furthermore, they are used for particle number concentration measurements of the exhaust of vehicles in idling operation, to test the integrity of exhaust after-treatment systems. **Paper 3** describes this application, the possible impact of such measurements performed during periodic technical inspections, and the implications of different particle size distributions.

3.2. Aerosol Particle Size Distribution Measurement

There are certain upper and lower size boundaries for particles that are subject to emission regulations. A detailed assessment of the size distribution of the emitted particles is usually not required in emission testing. However, for research and development purposes, the size distribution of the emitted particles can be of interest. There are different methods to measure the particle size distribution of an aerosol. The particles are usually classified by electrical mobility or aerodynamic particle size and subsequently electrically or optically detected. The following paragraphs introduce some basic concepts of aerosol particle size distribution measurement and selected techniques utilized in this thesis.

3.2.1. Basic Concepts

As mentioned in section 2.2, aerosol particles sizes are commonly log-normal distributed. Therefore, some basic concepts and conventions are illustrated on the example of a log-normal distribution as introduced in section 2.2:

$$p(d_\mathrm{p}) = \frac{a}{d_\mathrm{p}} \frac{1}{\sigma_\mathrm{d}\sqrt{2\pi}} \exp\left(-\frac{(\ln(d_\mathrm{p}) - \mu_\mathrm{d})^2}{2\sigma_\mathrm{d}^2}\right) \tag{3.1}$$

The mathematical description of log-normal size distributions as in Equation 3.1 is valid for linearly spaced particle size intervals $d_\mathrm{p} + \mathrm{d}d_\mathrm{p}$. However, in aerosol science it is common to describe size distributions for logarithmically spaced particle size intervals $d_\mathrm{p} + \mathrm{d}\ln(d_\mathrm{p})$. This representation is often more convenient because the size distributions can expand more than one order of magnitude in particle size. In this case, a unimodal log-normal size distribution can be described as:

$$p(\ln(d_\mathrm{p})) = \frac{a}{\sigma_\mathrm{d}\sqrt{2\pi}} \exp\left(-\frac{(\ln(d_\mathrm{p}) - \mu_\mathrm{d})^2}{2\sigma_\mathrm{d}^2}\right) \tag{3.2}$$

The difference between Equation 3.1 and Equation 3.2 is the factor of $\frac{1}{d_\mathrm{p}}$ that is compensated by the logarithmic spacing of particle size intervals and the correlated bin widths. The difference between the two underlying concepts of constant and logarithmic particle size bin widths and the impact on visualized measurement data is demonstrated below in Figure 3.5. However, before this figure is discussed, the discretization of the particle size is introduced.

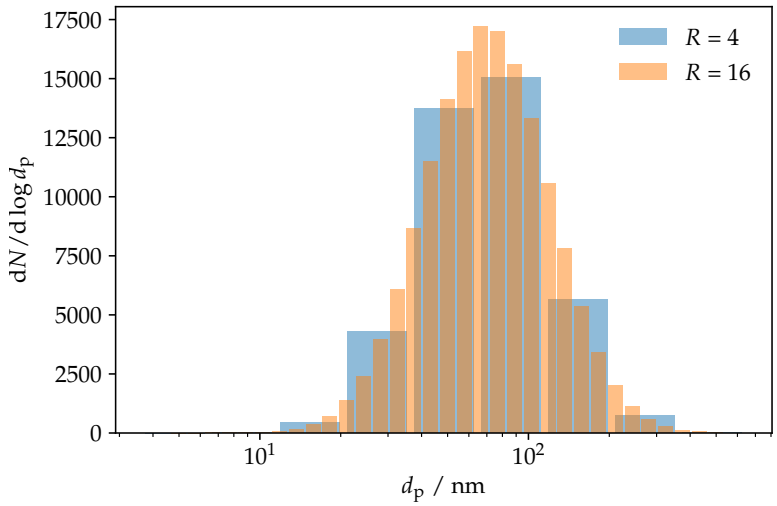

Figure 3.4.: Exemplary depiction of a log-normal size distribution with a GMD of 70 nm, a GSD of 1.7 and a total particle number concentration of 1×10^4 #/cm^3 as captured by simulated generic particle size distribution measurement instruments with resolutions of 4 and 16 channels per decade respectively. The widths of the shown bars are proportional to the respective bin widths. The number of particles in each bin is normalized with the number of channels per decade.

The particle diameter d_p is treated as a continuous variable in the equations stated above. In real-world measurement instruments, the particles are categorized into discrete size bins. The locations of the bin centers and the bin widths are typically spaced logarithmically. The resolution R of size distribution measurement instruments is usually defined as a number of channels per decade (see section 3.2). The number of particles $\mathrm{d}N$ in a size bin is normalized with the resolution to facilitate comparing data from

instruments with different resolutions.

$$\mathrm{d}N/\mathrm{d}\log(d_\mathrm{p}) = \frac{\mathrm{d}N}{\mathrm{d}\log(d_\mathrm{p})} = \frac{\mathrm{d}N}{\log(d_\mathrm{p,u}) - \log(d_\mathrm{p,l})} \tag{3.3}$$

Where the difference of the logarithm of the upper boundary of a size bin $\log(d_\mathrm{p,u})$ minus the logarithm of the lower boundary of the size bin $\log(d_\mathrm{p,l})$ is precisely 1 over the resolution R in number of channels per decade:

$$\left(\frac{d_\mathrm{p,u}}{d_\mathrm{p,l}}\right)^R = 10 \tag{3.4}$$

$$R\left(\log(d_\mathrm{p,u}) - \log(d_\mathrm{p,l})\right) = \log(10) \tag{3.5}$$

$$\log(d_\mathrm{p,u}) - \log(d_\mathrm{p,l}) = \frac{1}{R} \tag{3.6}$$

Figure 3.4 demonstrates the concept of this normalization with the instrument resolution for two simulated generic instruments with resolutions of 4 and 16 channels per decade, respectively. The plot shows a log-normal distribution with a GMD of 70 nm, and a GSD of 1.7. The total number concentration amounts to 1×10^4 #/cm^3. The normalization of the number of particles in the bins with the number of channels per decade enables similar bin heights at corresponding particle diameters. The similar bin heights facilitate a convenient comparison of the data reported by the two instruments with different particle size resolutions. Because the bins of both virtual instruments in Figure 3.4 are spaced logarithmically, as it is common for instruments of this kind, the envelope functions of the histograms are described by Equation 3.2 in good approximation.

Figure 3.5 shows the comparison of simulated data from instruments with constant and logarithmic spacings. The plot demonstrates how a logarithmic or constant spacing changes the representation of size distribution data. The underlying particle size distribution is identical to the one shown in Figure 3.4. It is a unimodal log-normal size distribution with a GMD of 70 nm, a GSD of 1.7 and a total number concentration of 1×10^4 #/cm^3. The simulated instruments both have 33 channels in the range of 5 nm to

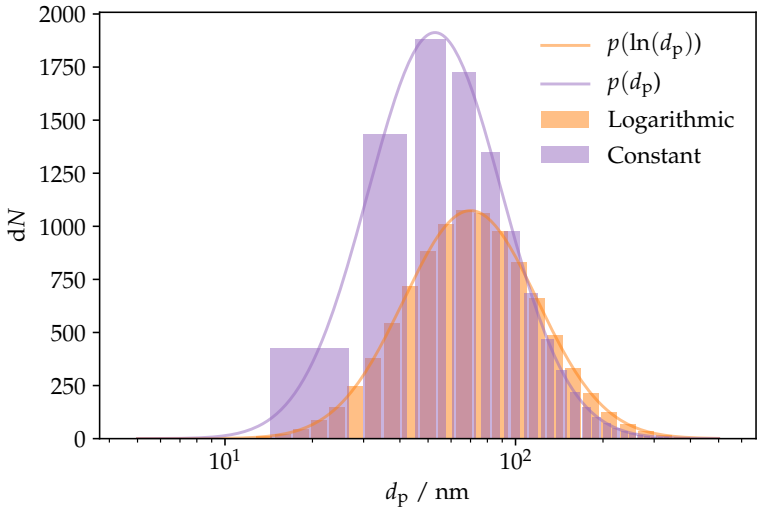

Figure 3.5.: Exemplary depiction of a log-normal size distribution with a GMD of 70 nm, a GSD of 1.7, and a total particle number concentration of 1×10^4 #/cm^3 as captured by simulated generic particle size distribution measurement instruments with logarithmic and constant bin widths.

500 nm. The simulated data from the instrument with constant bin widths are represented in purple, and the simulated data for the instrument with logarithmic spacing is shown in orange. In contrast to Figure 3.4, the number of particles in the bins is not normalized in Figure 3.5. Note that the logarithmic x-scale influences the appearance of the bin widths. As a result, the bins with constant widths appear to be broadened for smaller particle sizes. The purple size distribution appears to be shifted towards smaller particle sizes compared to the orange one. The envelopes of the histograms are approximated by Equation 3.1 and Equation 3.2. For infinitesimally small bin widths, the histogram heights would transition to the continuous log-normal distributions indicated by the orange and purple lines. Reconsidering these two equations illustrates the appeared shift of the mode of the data from the instrument with constant spacing as the number of particles in the bins is suppressed by the factor $\frac{1}{d_p}$ for increasing particle diameters.

3.2.2. Scanning Mobility Particle Sizer

The Scanning Mobility Particle Sizer (SMPS) [69] is one of the most commonly used particle size distribution measurement devices in aerosol science. It consists of a differential mobility analyzer (DMA) for the classification of particles by electrical mobility and a CPC as a detection unit. With the SMPS, particle size distributions can be measured over a relatively broad range of particle diameters. Depending on the configurations of the DMA and the CPC and the operation parameter settings, particle sizes from a few nm to a few 100 nm are scanned by varying the classified particle mobility using the DMA. The size resolution of the SMPS is typically 64 channels per decade. The temporal resolution, which is determined by the scan time is on the order of 1 min. This relatively low temporal resolution restricts the SMPS application for automotive emission measurements to stationary operation points. Transient events on the order of seconds cannot be resolved with the SMPS.

In this thesis, the SMPS was used for several laboratory-based experiments and the size distribution measurements of the emissions of vehicles in low and high idling operation described in **Paper 3**.

3.2.3. Engine Exhaust Particle Sizer

The Engine Exhaust Particle Sizer (EEPS) is a charge based size distribution measurement device for the real-time assessment of particle size distributions of engine exhaust. At the inlet of the EEPS, the particles are charged with a unipolar charger. An electric field subsequently classifies the particles by their electrical mobility. The charges carried by the classified particles in the size-range between 5.6 nm and 560 nm are measured with 22 electrometers. The temporal resolution can be as high as 10 Hz. This high temporal resolution makes the EEPS suitable for the analysis of transient events like the regeneration of particulate filters. The manufacturer of the EEPS is TSI. Instruments based on the same operation principle are the Fast Mobility Particle Sizer (FMPS) , which is also manufactured by TSI, and the Differential Mobility Spectrometer (DMS) 500 by Cambustion. The technical details

in that these three instruments differ from each other are described in the literature [43, 70].

The EEPS was used for real monitoring of particle size distributions in the laboratory experiments described in **Paper 2**. With the EEPS, it was possible to detect nucleation events caused by gaseous sulfuric acid (GSA). The real-time monitoring of the particle size distribution enabled precise dosing of GSA so that the GSA could be detected with the atmospheric pressure interface time-of-flight (APi-TOF) mass spectrometer. In **Paper 3**, the EEPS was used to detect possible transient events during the emission measurements of the vehicles in low and high idle operation.

3.2.4. nano Condensation Nucleus Counter

The nano Condensation Nucleus Counter (nCNC) system by Airmodus is a measurement device to assess aerosol particle size distributions in the size range between 1 nm and 4 nm[71, 72]. The system consists of a particle size magnifier (PSM) and a CPC (subsection 3.1.1). The particles to be analyzed are magnified to droplets in the size range of 90 nm to 100 nm by condensation of diethylene glycol (DEG) in the PSM. Subsequently, they are detected with a CPC. Size distribution measurements are enabled by the variation of the saturation of DEG in the PSM. By this variation, the smallest particle size that is activated by the PSM is changed. By the application of a data inversion algorithm, a size distribution in the range between 1 nm and 4 nm is deduced from the saturation dependent particle number concentration measured by the CPC.

The nCNC system was used to determine particle penetration of the aerosol gas exchange system for particle sizes down to 1.2 nm as described in **Paper 2**.

3.3. Aerosol Dilution

Dilution generally refers to a process to reduce the concentration of a given substance. In the case of particle number concentration, this can be

achieved by mixing the original aerosol with an aerosol of a lower particle number concentration or removing a fraction of the particles by filtration or other loss mechanisms. Particle number concentration dilution often comes with changes in temperature and concentration changes of volatile components of the aerosol's carrier gas. The effects and side effects of dilution on a given aerosol may be spatially limited so that additional mixing is required downstream of the dilution to ensure a spatially homogeneous particle distribution. The homogeneity of the spatial particle distribution of the aerosol is crucial if the aerosol flow is divided downstream of the dilution. It ensures that the aerosol in both branches comprises the same particle concentration. This equality in concentration is essential to correctly account for the dilution during the post-processing of the measurement data. Dilution can be realized in multiple stages and by applying different techniques to achieve the desired reduction of the particle concentration or reduction of the partial pressure of volatile compounds.

3.3.1. Ejector Diluter

The ejector diluter (ED) is a Venturi pump, that is modified for the application as an aerosol diluter [24, 30, 73, 74]. A flow of particle-free dilution gas passes by a nozzle to create an underpressure (Venturi-effect). The underpressure draws the aerosol into the ejector diluter. Directly downstream the nozzle, there is a mixing volume, where the aerosol and the dilution gas are turbulently mixed. A downside of the ejector diluter is the relatively large dependence of the dilution ratio on the inlet pressure. This large dependence limits the applicability of the ejector to sources that do not exhibit large fluctuations or drifts in the pressure level. Ejector diluters provide a relatively high flow rate of diluted aerosol ($\approx 40\,\mathrm{l\,min^{-1}}$), which makes them useful for comprehensive aerosol characterizations, where many measurement instruments need to be supplied with sample aerosol. The ejector diluter can be applied at temperatures up to 450 °C without the need for special customizations.

In this thesis, ejector diluters have been used in the experiments described in **Paper 2**. Early prototypes of the DownToTen sampling system described

in **Paper 1** comprised an ejector diluter as secondary or tertiary dilution stages.

3.3.2. Porous Tube Diluter

In a porous tube diluter (PTD) , the aerosol is diluted with particle-free dilution gas, which enters the sampling line radially through a porous material. Figure 3.6a shows a drawing of a porous tube diluter. The relatively simple shape of porous tube diluters allows for a straightforward application of heating or cooling devices for temperature regulation of the aerosol. In contrast to the ejector diluter, porous tube diluters do not independently generate underpressure to draw sample aerosol. Consequently, the sample flow through the diluter has to be induced by external means. The radial ingress of dilution counteracts particle losses because the flow has a negative radial component near the walls, pushing particles towards the center-line. This pushing towards the center-line is advantageous if low particle losses are desired. However, the radial ingress of dilution air also leads to a non-uniform particle concentration over the cross-section of the sampling line directly downstream of the porous tube diluter. There is an increased particle concentration at the center-line compared to regions near the walls. Mixing has to be applied to establish a homogeneous particle distribution. Mixing can be achieved, by a sudden change in diameter to induce turbulence or the application of static mixing elements directly downstream the porous diluter.

In this thesis, a porous tube diluter, including mixing elements, was developed. Figure 3.6b shows a drawing of this porous tube diluter. Diluters of this kind are used in the DownToTen sampling system described in **Paper 1** for the realization of the primary and the secondary dilution stage. The configuration with integrated mixing elements allows for a more compact design of the overall sampling system. The reduced length of the sampling lines contributes to a further reduction of diffusional particle losses. The relevance of proper mixing in aerosol sampling and the concept of directly including mixing elements in the porous tube diluter was published in an oral presentation at the International Aerosol Conference in St. Louis,

Missouri, 2018[75]. Jonathan Symonds (Cambustion Ltd.) held the oral presentation. The author of this thesis contributed in the form of simulation results and PTD design proposals (Appendix A).

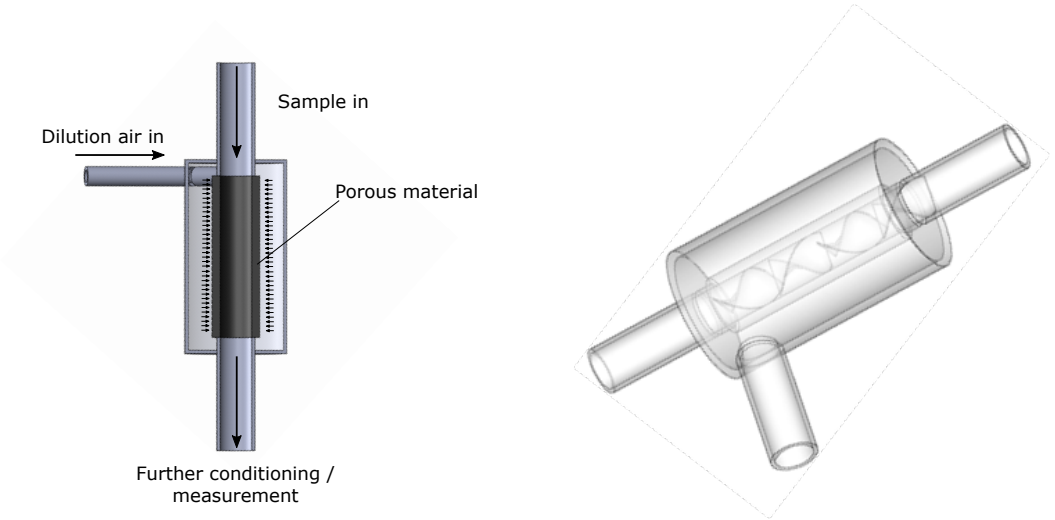

(a) Drawing of a porous tube diluter. Cut through center plane.

(b) Drawing of a porous tube diluter with integrated mixing elements.

Figure 3.6.: Drawings of porous tube diluters.

3.3.3. Rotating Disk Diluter

A rotating disk diluter (RDD) transfers defined volumes of an aerosol sample into a defined dilution airflow. The cavities of a rotating disk are filled with the sample aerosol in the sample channel. By rotation, the cavities are transferred into the dilution gas channel, where the sample aerosol is diluted. The dilution ratio DR can be calculated from the dilution air flow rate Q_{dil} the rotation frequency f and the volume of a cavity V_{cav} and the n number of cavities in the disk:

$$DR = \frac{Q_{\text{dil}}}{n f V_{\text{cav}}} + 1 \tag{3.7}$$

The cavities can be dome-shaped, as shown by Hueglin et al. [76] or cylindrical to penetrate the rotating disk completely[30]. The RDD is commonly

used in automotive exhaust particle measurements as a primary diluter. It decouples the measurement system downstream of the RDD from the pressure fluctuations at the tailpipe of a vehicle. Another application of the RDD aerosol dilution with argon to enable an elemental analysis of aerosol particles using an inductively coupled plasma mass spectrometer (ICP-MS)[77, 78].

Due to relatively high particle losses in the sub-23 nm particle size regime, the application of different dilution technologies were preferred over the RDD within the project DownToTen and this thesis. However, a particle loss characterization of an AVL RDD was performed and is described in Appendix E.

3.3.4. Bifurcated Flow Diluter

A bifurcated flow diluter is a passive device that splits the aerosol flow into two branches and removes the particles in one of the two branches before they are merged again[30, 79–81]. The removal of particles is typically realized with a high-efficiency particulate air (HEPA) filter. The dilution ratio of a bifurcated flow diluter can be adjustable by regulating the pressure drop over one of the two branches with a needle valve. The bifurcated flow diluter does not change the concentrations of the aerosol's gaseous components. This has to be kept in mind when applying it for automotive exhaust particle measurements where it is often desirable to lower the partial pressure of volatile compounds to avoid particle formation by nucleation and condensational growth of sub-cut-sized particles.

In this thesis, a bifurcated flow diluter was designed, constructed, and applied as a tertiary dilution stage in the DownToTen sampling system. It was used to attenuate the particle number concentration further downstream of the first two dilution stages. The fact that it is a passive element made it suitable for the mobile measurement application where low energy and dilution air consumption is beneficial. Appendix D provides a detailed description of the designed device in the form of a reprint of a corresponding conference proceedings paper.

3.3.5. Constant Volume Sampling

Constant volume sampling (CVS) is a method in emission measurement, where the full flow of the exhaust is fed into a tunnel and diluted in a way that the total flow rate Q_{tot} is constant. The dilution ratio is typically on the order of 10. This method is often advantageous because the determination of the emission rate of a pollutant (particulate or gaseous) per unit time X_p does not require the measurement of the exhaust flow rate Q_{ex}. The emission rate of a pollutant per unit time is the exhaust flow rate multiplied with the concentration of the emitted pollutant at the tailpipe ($c_{p,TP}$). The emission rate per unit time is not to be mixed up with the emission factor, that relates the emissions of a pollutant to an activity like the emission of a different pollutant (e.g., CO_2, NO, NO_x,...)[82] or the distance driven[83]. Equation 3.8 demonstrates that the concentration of the pollutant $c_{p,CVS}$ in the CVS tunnel multiplied with the total flow rate Q_{tot} also yields the emission rate per unit time of the pollutant X_p.

$$X_p = Q_{ex} c_{p,TP} = Q_{ex} \frac{c_{p,CVS} Q_{tot}}{Q_{ex}} = c_{p,CVS} Q_{tot} \tag{3.8}$$

Disadvantages of the CVS are a large size, high costs, and the fact that dilution with the CVS can induce the generation of nucleation mode particles[84].

The DownToTen sampling system developed in this thesis and described in **Paper 1** has been applied for CVS particle number measurements at the Insititute of Internal Combustion Engines and Thermodynamics (Graz, Austria), Ricardo Ltd. (Shoreham-by-Sea, UK), AVL List GmbH (Graz, Austria), Laboratory of Applied Thermodynamics (Thessaloniki, Greece) and Centro Ricerche Fiat (Orbassano, Italy).

3.4. Aerosol Conditioning

It is necessary to condition the aerosol to isolate a fraction of particles that exhibit a certain degree of volatility. In automotive exhaust particle measure-

ment, the solid particles are usually the particles of interest. In this context, the term "solid" refers to the property to withstand a temperature of 300 °C for ≈ 0.2 s [22, 23]. Volatile or semi-volatile particles are removed from the aerosol before the particle number concentration is determined with a CPC or diffusion charger. Conditioning the exhaust aerosol furthermore inhibits the growth of particles with sizes below the specified cut point and prevents the formation of particles by nucleation of volatile compounds in the gas phase. There are three state-of-the-art methods for engine exhaust conditioning. In this thesis, another method was developed and characterized that can be seen as an alternative approach for engine exhaust aerosol conditioning. The three established methods and the method developed in this thesis are briefly introduced in the following paragraphs.

3.4.1. Evaporation Tube

The evaporation tube (ET) is a simple approach for aerosol conditioning. The aerosol is provided a given residence time in a heated tube (typically 300 °C to 400 °C), to evaporate volatile particles. This method does not actively remove the volatile material from the sampling line. The evaporation tube is usually accompanied by dilution to lower the partial pressure of the volatile compounds. The additional dilution reduces the risk of renucleation of the volatile material upon cooling down. Dilution, in combination with the ET, is often referred to as volatile particle remover (VPR). A sampling system compliant with the particle number measurement procedure defined in the UNECE Regulation No. 83 comprises a VPR for aerosol conditioning[85]. The volatile particle remover that defined in this regulation consists of a primary diluter, an evaporation tube, and a secondary diluter. The VPR has to achieve 99 % vaporization of 30 nm tetracontane ($CH_3(CH_2)_{38}CH_3$) particles with a concentration $> 1 \times 10^4$ #/cm^3 at the inlet.

Earlier prototypes of the DownToTen system described in **Paper 1** had the option of using an evaporation tube instead of the catalytic stripper (described below) to further lower diffusional particle losses.

3.4.2. Thermodenuder

The thermodenuder (TD) relies on heating the aerosol to evaporate volatile material and subsequent adsorption of the evaporated material using a cooled activated carbon section[86–90]. The storage of removed material can raise the practical issue of limited storage capacity and mandates periodic maintenance of the device. The thermophoretic particle losses in thermodenuders are typically 25 % to 30 %. However, special designs can help to reduce these losses significantly[91]. Thermodenuders are considered useful research tools but are not as prevalent as other methods of engine exhaust conditioning methods.

3.4.3. Catalytic Stripper

A catalytic stripper is a device with a catalytically active surface for the oxidation of organic material [88, 90, 92, 93]. Some embodiments also comprise a section for sulfur trapping to prevent the poisoning of the catalytic surface and further reduce the potential of nucleation. The transport of the organic material to the catalytic surface is driven by diffusion. Therefore, the aerosol is heated to evaporate volatile material upstream the catalytically active. This significantly increases the removal efficiency because the diffusivity of gas-phase material is by orders of magnitude higher than the diffusivity of the particles. Due to the relatively large surface area required for efficiently oxidizing organic material, catalytic strippers are significant sources of diffusional particle losses. The choice of the size of a catalytic is a trade-off between acceptable particle losses and desired volatile removal.

The DownToTen system described in **Paper 1** uses a catalytic stripper for the removal of volatile particles. The model used is commercially available and supplied by AVL. DownToTen's sister project SUREAL-23 developed a catalytic stripper for the application of sub-23 nm particle measurement[94]. The CS was developed there and was also provided to DownToTen. The CS was integrated into the DownToTen system for a performance assessment. Appendix C describes the modification of the sampling system and the particle penetration assessment performed in this thesis.

3.4.4. Aerosol Gas Exchange System

The aerosol gas exchange system (AGES) [38] has been developed in the course of this thesis as an alternative approach for engine exhaust conditioning. The system's core component is a device called "counter flow denuder" [95]. The working principle of this instrument illustrated in Figure 3.7 is based on the diffusional exchange of aerosol carrier gas by a chosen purge gas through a porous glass membrane (SPG, Shirasu Porous Glass). Compared to nanoparticles, the much higher diffusion coefficient of gas molecules allows for high gas exchange efficiencies and limited particle losses.

Paper 2 comprises a detailed description of the AGES, a mathematical model for the gas removal efficiency, and the experimental characterization of the device.

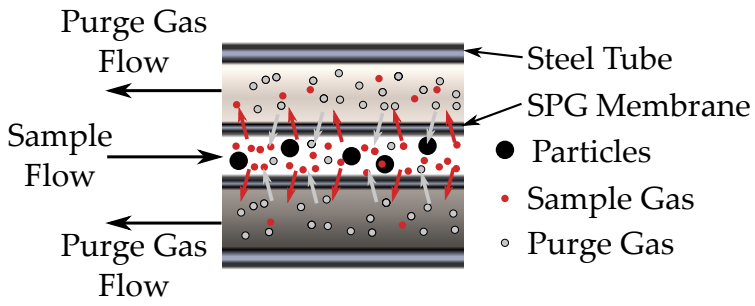

Figure 3.7.: Illustration of the working principle of the counter flow denuder. The flow directions of the aerosol sample and the purge gas are anti-parallel. Red and grey circles respectively represent sample and purge gas molecules. The red and gray arrows indicate a net diffusive flux of the particular species, driven by a concentration gradient. Black circles represent aerosol particles.

3.5. Aerosol Generation

To test and calibrate aerosol sampling and measurement equipment, it is often necessary to generate test aerosol in a stable, reproducible way. Different artificial aerosol sources may be used depending on the requirements on

particle concentration, particle size, chemical composition, charge, or other properties. The following paragraphs introduce different classes of aerosol generators used in this thesis.

3.5.1. Burners

Burners enable the generation of soot particles by a controlled supply of fuel (e.g., propane, ethylene, acetylene) and oxidation air to a diffusion flame or premixed flame. In locally fuel-rich regions, incomplete combustion of the fuel results in the production of soot particles. Depending on the burner's complexity, additional control mechanisms may further tweak different properties of the generated aerosol. The combustion aerosol standard (CAST)[96, 97] for example, allows for controlled quenching of the flame by supplying nitrogen. The miniature inverted soot generator (MISG) [98, 99] enables the production of aerosols with very high concentrations of soot by employing a downward flowing open-tipped flame. Another commonly used burner is the McKenna burner [100–102], that supplies a premixed flat flame for controlled soot generation.

Olfert and Rogak[103] reviewed a variety of different non-premixed-flame combustion sources. They showed a correlation between primary particle size and aggregate size for fresh soot with coatings removed for a broad range of soot sources.

A catalytic stripper can be used downstream of the burner to remove coatings of unburnt hydrocarbons. The coatings change the effective density of soot particles and can cause undesirable effects like nucleation in the sampling system.

Because of soot particles being generated in a combustion process, burners are especially relevant for testing and calibrating equipment that is intended to be applied for engine exhaust particle measurements. The matching chemical composition, primary particle size, and fractal nature of particles generated by burners make burners a good laboratory surrogate for internal combustion engines.

Different kinds of burners have been used in laboratory experiments in this thesis. For calibration measurements of the DownToTen system, a CAST was used as described in **Paper 1** and Appendix C. In the laboratory in Tampere, a flat flame burner was used in early experiments with the aerosol gas exchange system.

3.5.2. Spark generator

Apart from burners described above also spark generators can be used to produce carbonaceous aerosols. A spark discharge between two graphite electrodes in inert gas produces primary aerosol particles (3 nm to 10 nm in diameter) by sublimation of graphite and subsequent resublimation[104, 105]. The primary particles form agglomerates of sizes up to a few hundred nanometers depending on the flow rate, discharge voltage, discharge frequency, and dilution flow rate. The formed agglomerates consist of loosely connected primary particles. The smaller primary particle size and the low effective density of spark-generated graphite particles constitute notable differences to soot particles generated by combustion. Studies show that spark-generated graphite agglomerates are, therefore, significantly more difficult to detect employing incandescence methods[106]. Also, metal or metal oxide aerosols can be produced utilizing the spark generation process,

A graphite spark generator (Palas DNP 3000) was used for the calibration measurements described in **Paper 3**.

3.5.3. Nebulizers

A variety of different aerosol particles can be produced by nebulization. A liquid is dispersed either by ultrasonic means or by high-velocity air that draws liquid from a reservoir (Bernoulli effect) and then breaks the liquid into small droplets [43]. The generated aerosol can directly be used for testing purposes. Nebulizers (also called atomizers) can also be used to produces solid aerosol particles. One possibility is to put monodisperse polystyrene latex (PSL) or polyvinyltoluene (PVT) into the liquid that is to be nebulized. A diffusion dryer removes the liquid after the nebulization

of the liquid containing the spheres. This process results in aerosolized monodisperse particles. Another way of producing solid aerosol particles with atomizers is to put a soluble solid substance (e.g., NaCl in water) into the nebulized liquid. Again, the liquid is removed after the droplets are formed by nebulization. This process produces a polydisperse aerosol of the soluble solid substance.

3.5.4. Evaporation/Condensation

Evaporation of material and subsequent nucleation or condensation constitutes another standard aerosol generation method. A broad range of different materials ranging from metals, salts to organic compounds can be aerosolized with this method. Depending on the material, different furnace or heating elements may be used to achieve the temperatures that are required to evaporate the desired amount of material. The evaporated material is convectively transported off by a flow of adequate carrier gas (usually chemically inert, e.g., Ar, N_2). Downstream the evaporation, conductive cooling or dilution with cooler gas induces nucleation or condensation onto existing particles of the evaporated material.

The silver particles that were used for the particle penetration measurements of the aerosol gas exchange system described in **Paper 2** were generated by evaporating silver in a tube furnace and subsequent conductive cooling. The removal efficiency requirements for PMP compliant particle measurement systems of $< 99\,\%$ of 30 nm tetracontane particles at a concentration of $\geq 1 \times 10^5\,\#/\mathrm{cm}^3$ [85] is commonly tested with tetracontane aerosol generated as described above.

3.5.5. Electrospray

With the electrospray method, liquid droplets are generated by conveying fluid through a capillary tube. A high electric field is applied at the capillary tip[107]. The liquid breaks up into droplets in a certain mode[43], depending on the field strength and properties of the liquid and the surrounding gas. For certain combinations of parameter values, the fluid forms a conical

jet that breaks up into a stream of charged particles. With commercialized embodiments like the TSI model 3480, it is possible to create monodisperse particles (GSD = 1.1) in the size-range between a few nanometers and approximately 100 nm. Substances dissolved in a solvent or suspended nanoparticles are nebulized as described above before the solvent is removed, and the particles are electrically neutralized.

Athanasios Mamakos (AVL) tested the volatile particle removal efficiency of the DownToTen system with electrospray polydisperse emery oil particles ($>$ 50 nm, 3.5 mg m^{-3} to 5.5 mg m^{-3})(**Paper 1**). This test is defined in the RDE regulations[108] and is more rigorous than the tetracontane test prescribed in the PMP protocol. The chemical composition of emery oil is supposed to be representative of synthetic lube oil. Emery oil consists of 82 % to 85 % C_30H_60 and 13 % to 16 % $C_{40}H_{80}$ polyalphaolefins by volume[109].

4. Results and Discussion

The results of this thesis are presented in the form of the three journal publications attached. This section seeks to provide a summary of the results and critical messages presented rather than a full replication. The supplementary information and results presented in the appendix are discussed in the respective appendix chapters and are not elaborated further.

4.1. DownToTen Sampling System

Paper 1 describes the DownToTen sampling system, particle penetration calibration measurements, and the system's application for the mobile measurement of particle number emissions in the currently regulated size regime larger than 23 nm and below. This paper is published in the *Journal of Visualized Experiments*. As this journal focuses on providing practical guides on applying scientific methods, large portions of the manuscript are written in the form of step-by-step instructions. Furthermore, the manuscript comes with a video showcasing the application of the DownToTen system. The results presented in this paper include laboratory particle penetration measurements and the data from mobile particle number emission measurements using the DownToTen system with a 10 nm and a 23 nm cutoff CPC, in comparison to a commercially available AVL PN-PEMS using a diffusion charger as the sensor element.

The particle penetration measurement results (Figure 11) show that the particle size independent thermophoretic particle amount to $\approx 15\,\%$. The particle size-dependent diffusional losses yield a d_{50} cut point of 11 nm. This cutoff characteristic makes the system suitable for sub-23 nm particle measurement.

The PN emission data shown in Figure 12 of the paper was acquired in a test drive with a light-duty compression ignition vehicle (BMW 218d). Lukas Landl from the Institute of Internal Combustion Engines and Thermodynamics performed the measurement and the driving. The data shown in the paper demonstrates a generally good agreement of the DownToTen system with the AVL PN-PEMS reference system. The data reported by the two CPCs operated with the DownToTen system show that the emission rates $> 23\,\text{nm}$ are comparable to the $> 10\,\text{nm}$ emission rates for the majority of the time shown in this plot. An exception to this was identified in an event shortly after the start. In this cold start event, more than 50 % of the total number of particles emitted is in the size-range of 10 nm to 23 nm. The identification of this event showcases the relevance of sub-23 nm particle number emission measurement.

4.2. Aerosol Gas Exchange System

The Aerosol Gas Exchange System (AGES), described and characterized in **Paper 2**, was developed in this thesis. This development is based on the counter flow denuder presented in a publication by Hagino in *Aerosol Science & Technology* in 2017 [95]. The counter flow denuder described in this publication was replicated and integrated into a system. Said system enables precise control of the purge gas flow rate, the purge gas temperature, and the pressure difference between the sample channel and the purge gas channel. The integration of the counter flow denuder into the aerosol gas exchange system makes it applicable under a broad range of conditions.

One major part of **Paper 2** is the derivation of an analytical model to describe the removal efficiency RE as a function of the dimensionless parameter $\mu(= \frac{DL}{Q_\text{v}})$, which is the diffusion coefficient D of the gas to be removed, times the actual length L of the counter flow denuder, divided by the volumetric flow rate Q_v. The derived analytical model is of the following form:

$$RE = 1 - \sum_{n=1}^{\infty} \frac{\exp(-b_n \mu)}{c_n} \tag{4.1}$$

Where the parameters b_n and c_n, depend on the material-specific diffusion resistance of the porous glass membrane R_m plus an additional contribution R_{flow} attributed to the laminar flow profile in the sample channel. The model was calibrated with data from an oxygen removal experiment. It was found that only including the first term of the series described in Equation 4.1 yields a description that deviates less than 0.01 from the infinite sum:

$$RE = 1 - 0.990 \exp(-3.982\mu) \tag{4.2}$$

Numerical CFD simulations verified the validity of the analytical model before a dedicated measurement campaign was conducted. In the measurement campaign, the removal efficiency of different engine exhaust related species was determined at different flow rates and temperatures. Additionally, the particle losses down to 1.2 nm were evaluated. The results generally show a good agreement with the derived model. However, there are significant deviations for hydrocarbons at elevated temperatures. The removal efficiency for the corresponding measurement points was significantly lower than the model predicted. The measurement results furthermore indicate that gaseous sulfuric acid is removed by adsorption to the porous membrane, rather than diffusive transport through the membranes like the other substances investigated. This finding is in line with previously published literature, where it was found that gaseous sulfuric acid is very prone to sticking to surfaces. The particle losses down to 6 nm were found to be below 10 % for the tested operating conditions. The data for the particle losses in the size-range of 1 nm to 3 nm was acquired with the nano Condensation Nucleus Counter (nCNC) described in subsection 3.2.4. Despite considerable measurement uncertainties, it can be stated that the particle losses of the AGES are below 50 % down to 1.2 nm for the tested operating conditions. The AGES is a potentially handy tool for engine exhaust particle measurement and other fields of aerosol science. The complementary operation principle to established aerosol conditioning technologies and the relatively low particle losses open a manifold of possible applications. Especially the possibility to efficiently remove water vapor from the aerosol is a feature that is often desirable in particle measurement. The model developed allows for an application targeted design of the device and a corresponding choice of operation parameters to find an adequate trade-off between particle losses and gas exchange efficiency.

4.3. PN Measurements in Periodic Technical Inspections

In **Paper 3**, the impact of particle size distributions on possible measurement deviation in particle number measurements during periodic technical inspections (PTI) is assessed. The potential impact of these measurements on the fleet emissions is estimated based on previously published data and the prescribed PTI schedules in different countries.

A dedicated measurement campaign was conducted to assess the particle number concentrations and particle size distributions of the exhaust of 21 light-duty vehicles operating in low idle and high idle speed. The particle number concentrations measured with a PMP compliant AVL APC system and three prototype diffusion chargers were in good agreement with previously published data in other studies. The particle number concentrations of diesel vehicles without diesel particle filter (DPF) exceeded 1×10^6 #/cm^3 and could reliably be discriminated from vehicles with a functional DPF ($< 5 \times 10^4$ #/cm^3) from the results reported by any of the PN measurement devices applied in this study. This discrimination by exhaust particle number concentration was not possible for GDI vehicles, where the exhaust PN concentrations of vehicles with particle filter and without particle filter are within the same order of magnitude. The particle size distribution data collected in the measurement campaign was used to evaluate different automotive PN measurement instrument specifications. In particular, the particle size-dependent counting efficiency limits of said specifications were evaluated, if they guarantee an unambiguous distinction between highly emitting vehicles with malfunctioned after-treatment systems and low emitters compliant with emission regulations. The size distributions measured were weighted with limit-functions defining the upper and lower boundaries of counting efficiency compliance for the investigated specifications. The integration and normalization of the weighted size distributions, yield the maximal underestimations and overestimations of PN concentrations reported by instruments compliant with the respective specifications. This evaluation was extended and generalized for unimodal log-normal size distributions. It was found that the size distributions emitted during low idle operation are favorable compared to the size distributions emitted

during high idle operation for PN concentration measurements in PTI. The larger sizes of the particles emitted in low idle operation lead to a less pronounced maximal underestimation of the particle number concentration and a reduction of the risk for scenarios where vehicles pass the prescribed test despite exhibiting exhaust particle number concentrations exceeding 1×10^6 #/cm^3.

In the PTI PN measurement impact assessment, a total number of 45 different scenarios of vehicle age distributions, PTI schedules, and DPF aging behaviors were evaluated. It was found that PN PTI measurement can reduce the fleet emissions of diesel vehicles that are equipped with particle filters by more than 80 % in the most optimistic scenarios. The most pessimistic scenarios predict a reduction of 60 %. While the scientific community previously agreed that the impact of PN PTI measurements on the overall emissions could be substantial, this assessment, for the first time, provides an estimate for the magnitude of the achievable emission reduction.

5. Conclusion and Outlook

This thesis aimed to address new challenges in automotive particle emission measurement. As a part of the Horizon 2020 project DownToTen, sampling, and characterization methods of automotive exhaust aerosol with a particular focus on particle sizes below 23 nm were being researched. In particular, the transportation of the exhaust from the tailpipe to the particle number sensing element, together with adequate dilution and conditioning was the main focus of this thesis. The solutions for this challenging task elaborated within this thesis are twofold. First, the DownToTen sampling system was designed and constructed by using existing technologies that were modified and redesigned to address the challenges that arise in the sub-23 nm size regime. The development and characterization of the aerosol gas exchange system constitute a second contribution to the progress of instrumentation for particle number measurement in this size regime.

The DownToTen sampling system was built from carefully selected existing technologies. The reduction of diffusional particle losses, which are especially pronounced in the sub-23 nm regime, was emphasized. These extraordinary efforts are necessary to maintain a comparable degree of accuracy in particle measurements when extending the lower particle size cut off from 23 nm (current limit in regulations) to 10 nm (near -future limit). A high degree of versatility is another unique feature of the system. The versatility enables studies on unregulated secondary aerosol, besides the regulated solid particle number. The measurement system was successfully applied in stationary and mobile measurements identifying vehicles and events of significant currently unregulated emissions of solid sub-23 nm nanoparticles. The system's versatility enabled further applications beyond solid particle number measurement down to 10 nm. At the Institute of Internal Combustion Engines and Thermodynamics (Graz University of

Technology), it has recently been used for the mobile measurement of total particle emissions of heavy-duty vehicles and the characterization of a particle source for cloud seeding. It is about to be used in measurements of different kinds in the upcoming years.

In addition to the development of a measurement system from existing technologies, also novel instrumentation originated from the activities in DownToTen. An Aerosol Gas Exchange System (AGES) was developed as an alternative approach for engine exhaust conditioning. The instrument was designed, constructed, and tested in laboratory measurements. The AGES relies on the exchange of (semi-)volatile species with a different gas (e.g., air, argon, nitrogen...). Volatile compounds in an aerosol are exchanged by diffusional transport through a nano-porous glass membrane. The structure-function relationship of this porous material has been studied using experiments, the development of a mathematical model, and numerical multiphysics simulations. The exchange efficiencies of several engine exhaust related species and sub-23 nm particle losses have been studied extensively in comprehensive laboratory experiments. The diffusional exchange of gases distinguishes the AGES from existing technologies. Undesired (semi-)volatile material can be removed from engine exhaust while exhibiting low particle losses and avoiding chemical reactions. An application-specific design of the AGES can furthermore make dilution utterly redundant in a variety of applications. Avoiding dilution can improve the quality of aerosol measurements in automotive exhaust measurements and other fields of aerosol measurements like atmospheric studies and nanoparticle chemical analysis to derive a better understanding of health effects related to particulate matter. The AGES' working principle that only relies on diffusion and does not involve chemical reactions, together with the relatively low particle losses, has raised considerable interest in the scientific and related industrial community. Its application in field measurements and commercialization will require further development and testing. It is planned to conduct this further development in a joint project of the Aerosol Physics Department, Tampere University, and the Institute of Electrical Measurement and Sensor Systems (Graz University of Technology), which are the institutions that were involved in the development so far.

Complementarily to the activities in DownToTen, where highly accurate measurements in type approval testing were the main focus, the topic of

PN measurements in the course of periodic technical inspections (PTI) was addressed in this thesis. Soon, these measurements will be implemented in emission regulations to ensure vehicles' in-use compliance with emission limits. High emitters with malfunctioned exhaust after-treatment systems can be identified based on the results of these garage-based measurements. The reestablishment of the functionality of these broken after-treatment systems will have a significant impact on the overall fleet emissions. A dedicated measurement campaign has been carried out in the course of this thesis to evaluate instrument specifications for PTI particle number measurement devices that are currently under discussion. In this measurement campaign, particle emissions of more than 20 light-duty vehicles in idling operation have been analyzed. The emitted aerosol has been analyzed employing number concentration and size distribution using high-end type approval equipment, laboratory aerosol measurement instruments, and prototype PTI particle emission measurement devices. With the data acquired during the measurement campaign, it was possible to demonstrate the division of vehicles into regulation-compliant low emitters and high emitters with malfunctioned exhaust after-treatment systems. Furthermore, simulations show how regulatory specifications for PTI particle measurement instruments may affect the accuracy of measurement results. Hence, the validity of categorization into low and high emitters is based on these measurement results. Finally, an assessment of the potential impact of PN PTI measurements on the fleet emissions was performed. The simulation of 45 scenarios of PTI schedules, vehicle age distributions and particle filter aging behaviors shows that particle number concentration measurements during periodic technical inspections have the potential to reduce the fleet emissions by more than 80 %. The assessment of the magnitude of the potential impact, together with the evaluation of the instrument specifications under discussion, will hopefully support the introduction of PN measurements in periodic technical inspections in more and more countries. In the future, the potential impact of PN concentration measurements of idling vehicles could be further enhanced by remote sensing technologies. While remote sensing techniques are established for gaseous pollutants, they are still under development for particulates. The Institute of Electrical Measurement and Sensor Systems currently contributes to these developments in the course of the EU Horizon 2020 project CARES[110]. The techniques developed there seek to identify candidates for highly emitting vehicles directly on the road

to prescribe a technical inspection subsequently. This way, the time high emitters are on the road could be further reduced significantly to contribute to a cleaner environment.

Bibliography

[1] Günter Oberdörster, Eva Oberdörster, and Jan Oberdörster. *Nanotoxicology: An emerging discipline evolving from studies of ultrafine particles*. July 2005. DOI: 10.1289/ehp.7339 (cit. on p. 1).

[2] G Oberdörster et al. "Translocation of Inhaled Ultrafine Particles to the Brain." In: *Inhalation Toxicology* 16.6-7 (Jan. 2004), pp. 437–445. ISSN: 0895-8378. DOI: 10.1080/08958370490439597. URL: https://doi.org/10.1080/08958370490439597 (cit. on p. 1).

[3] Annette Peters et al. "Exposure to traffic and the onset of myocardial infarction." In: *New England Journal of Medicine* 351.17 (Oct. 2004), pp. 1721–1730. ISSN: 00284793. DOI: 10.1056/NEJMoa040203. URL: http://www.nejm.org/doi/abs/10.1056/NEJMoa040203 (cit. on p. 1).

[4] H. R. Anderson. "Air pollution and mortality: A history." In: *Atmospheric Environment* 43.1 (Jan. 2009), pp. 142–152. ISSN: 13522310. DOI: 10.1016/j.atmosenv.2008.09.026 (cit. on p. 1).

[5] Shanshan Li, Yuming Guo, and Gail Williams. "Acute impact of hourly ambient air pollution on preterm birth." In: *Environmental Health Perspectives* 124.10 (Oct. 2016), pp. 1623–1629. ISSN: 15529924. DOI: 10.1289/EHP200 (cit. on p. 1).

[6] V. Ramanathan and G. Carmichael. *Global and regional climate changes due to black carbon*. Apr. 2008. DOI: 10.1038/ngeo156 (cit. on p. 1).

[7] Christopher D. Cappa et al. "Radiative absorption enhancements due to the mixing state of atmospheric black carbon." In: *Science* 337.6098 (Aug. 2012), pp. 1078–1081. ISSN: 10959203. DOI: 10.1126/science.1223447 (cit. on p. 1).

[8] T. C. Bond et al. "Bounding the role of black carbon in the climate system: A scientific assessment." In: *Journal of Geophysical Research Atmospheres* 118.11 (June 2013), pp. 5380–5552. ISSN: 21698996. DOI: 10.1002/jgrd.50171 (cit. on p. 1).

[9] Hilkka Timonen et al. *Adaptation of Black Carbon Footprint Concept Would Accelerate Mitigation of Global Warming*. Nov. 2019. DOI: 10.1021/acs.est.9b05586 (cit. on p. 1).

[10] Federico Karagulian et al. *Contributions to cities' ambient particulate matter (PM): A systematic review of local source contributions at global level*. Nov. 2015. DOI: 10.1016/j.atmosenv.2015.08.087 (cit. on p. 1).

[11] Prashant Kumar et al. *Ultrafine particles in cities*. May 2014. DOI: 10.1016/j.envint.2014.01.013 (cit. on p. 1).

[12] Alfredo Sanchez Vicente. *The contribution of transport to air quality TERM 2012: transport indicators tracking progress towards environmental targets in Europe*. Tech. rep. European Environment Agency, 2012. URL: https://www.eea.europa.eu/publications/transport-and-air-quality-term-2012/download (cit. on p. 1).

[13] Nick Watts et al. *The 2019 report of The Lancet Countdown on health and climate change: ensuring that the health of a child born today is not defined by a changing climate*. Nov. 2019. DOI: 10.1016/S0140-6736(19)32596-6 (cit. on p. 1).

[14] Sotiris E. Pratsinis. *Flame aerosol synthesis of ceramic powders*. Jan. 1998. DOI: 10.1016/S0360-1285(97)00028-2 (cit. on p. 1).

[15] Yannis Drossinos and Nikolaos I. Stilianakis. "What aerosol physics tells us about airborne pathogen transmission." In: *Aerosol Science and Technology* (Apr. 2020), pp. 1–5. ISSN: 0278-6826. DOI: 10.1080/02786826.2020.1751055. URL: https://www.tandfonline.com/doi/full/10.1080/02786826.2020.1751055 (cit. on p. 1).

[16] USEPA. *Volkswagen Light Duty Diesel Vehicle Violations for Model Years 2009-2016*. 2016. URL: https://www.epa.gov/vw (cit. on p. 2).

[17] Leonidas Ntziachristos et al. "Implications of diesel emissions control failures to emission factors and road transport NO x evolution." In: *Atmospheric Environment* 141 (Sept. 2016), pp. 542–551. ISSN: 18732844. DOI: 10.1016/j.atmosenv.2016.07.036 (cit. on p. 2).

[18] Greg Archer. *Dieselgate: Who? What? How?* Tech. rep. Transport & Environment, Sept. 2016. URL: https://www.transportenvironment.org/sites/te/files/publications/2016_09_Dieselgate_report_who_what_how_FINAL_0.pdf (cit. on pp. 2, 4).

[19] Barouch Giechaskiel, Urbano Manfredi, and Giorgio Martini. "Engine Exhaust Solid Sub-23 nm Particles: I. Literature Survey." In: *SAE International Journal of Fuels and Lubricants* 7.3 (Oct. 2014), pp. 950–964. ISSN: 19463960. DOI: 10.4271/2014-01-2834 (cit. on pp. 2, 13).

[20] B. Giechaskiel et al. "Investigation of vehicle exhaust sub-23 nm particle emissions." In: *Aerosol Science and Technology* 51.5 (May 2017), pp. 626–641. ISSN: 15217388. DOI: 10.1080/02786826.2017.1286291. URL: https://www.tandfonline.com/action/journalInformation?journalCode=uast20%20http://dx.doi.org/10.1080/02786826.2017.1286291 (cit. on p. 2).

[21] Mike Dunne. "GRPE Particulate Measurement Programme (PMP)." In: *7th ETH-Conference on Combustion Generated Nanoparticles*. Geneva, 2003 (cit. on p. 2).

[22] Jon Andersson et al. *Particle Measurement Programme (PMP) Light-duty Inter-laboratory Correlation Exercise (ILCE_LD) Final Report*. Tech. rep. 2007 (cit. on pp. 2, 38).

[23] Barouch Giechaskiel et al. "Particle measurement programme (PMP) light-duty inter-laboratory exercise: Comparison of different particle number measurement systems." In: *Measurement Science and Technology* 19.9 (Sept. 2008), p. 95401. ISSN: 13616501. DOI: 10.1088/0957-0233/19/9/095401 (cit. on pp. 2, 38).

[24] Barouch Giechaskiel, Panagiota Dilara, and Jon Andersson. "Particle measurement programme (PMP) light-duty inter-laboratory exercise: repeatability and reproducibility of the particle number method." In: *Aerosol Science and Technology* 42.7 (2008), pp. 528–543 (cit. on pp. 2, 33).

[25] Barouch Giechaskiel et al. "Measurement of automotive nonvolatile particle number emissions within the European legislative framework: A review." In: *Aerosol Science and Technology* 46.7 (2012), pp. 719–749 (cit. on pp. 2, 12).

[26] Barouch Giechaskiel et al. "European Regulatory Framework and Particulate Matter Emissions of Gasoline Light-Duty Vehicles: A Review." In: *Catalysts* 9.7 (July 2019), p. 586. ISSN: 2073-4344. DOI: 10.3390/catal9070586. URL: https://www.mdpi.com/2073-4344/9/7/586 (cit. on p. 2).

[27] *SUREAL-23*. URL: http://sureal-23.cperi.certh.gr/ (cit. on p. 3).

[28] *PEMs4Nano*. URL: https://pems4nano.eu/ (cit. on p. 3).

[29] *DownToTen*. URL: http://www.downtoten.com/ (cit. on p. 3).

[30] Barouch Giechaskiel et al. "Review of motor vehicle particulate emissions sampling and measurement: From smoke and filter mass to particle number." In: *Journal of Aerosol Science* 67 (2014), pp. 48–86. DOI: https://doi.org/10.1016/j.jaerosci.2013.09.003 (cit. on pp. 3, 4, 33, 35, 36).

[31] Nils Hooftman et al. *A review of the European passenger car regulations – Real driving emissions vs local air quality*. Apr. 2018. DOI: 10.1016/j.rser.2018.01.012 (cit. on p. 3).

[32] Christie-Joy Brodrick et al. *UC Berkeley Earlier Faculty Research Title Multiple Smoke Opacity Measurements as Indicators of Particulate Emissions for Heavy-Duty Diesel Vehicle Inspection and Maintenance Programs Permalink https://escholarship.org/uc/item/1g26w44p Publication Date*. Tech. rep. Sept. 2000. URL: https://escholarship.org/uc/item/1g26w44p (cit. on p. 4).

[33] Michael St Denis and Jim Lindner. "Review of Light-Duty Diesel and Heavy-Duty Diesel Gasoline Inspection Programs." In: *Journal of the Air and Waste Management Association* 55.12 (2005), pp. 1876–1884. ISSN: 21622906. DOI: 10.1080/10473289.2005.10464773 (cit. on p. 4).

[34] G. Kadijk et al. *Investigation into a Periodic Technical Inspection (PTI) test method to check for presence and proper functioning of Diesel Particulate Filters in light-duty diesel vehicles - part 2*. Tech. rep. TNO, 2017, pp. 1–85 (cit. on p. 4).

[35] Barouch Giechaskiel et al. "Particle number measurements in the European legislation and future JRC activities." In: *Combustion Engines* 174.3 (2018), pp. 3–16. DOI: 10.19206/CE-2018-301 (cit. on p. 4).

[36] François Boveroux et al. "Feasibility study of a new test procedure to identify high emitters of particulate matter during periodic technical inspection." In: *SAE Technical Papers* 2019-April.April (2019), pp. 2–9. ISSN: 01487191. DOI: 10.4271/2019-01-1190 (cit. on p. 4).

[37] Markus Bainschab et al. "Measuring Sub-23 Nanometer Real Driving Particle Number Emissions Using the Portable DownToTen Sampling System." In: *Journal of Visualized Experiments* (2020). DOI: doi:10.3791/61287. URL: https://www.jove.com/video/61287 (cit. on p. 6).

[38] Markus Bainschab et al. "Aerosol gas exchange system (AGES) for nanoparticle sampling at elevated temperatures: Modeling and experimental characterization." In: *Scientific Reports* (2019). DOI: 10.1038/s41598-019-53113-5. URL: https://www.nature.com/articles/s41598-019-53113-5 (cit. on pp. 6, 40).

[39] Markus Bainschab, Mario Anton Schriefl, and Alexander Bergmann. "Particle Number Measurements within Periodic Technical Inspections: A First Quantitative Assessment of the Influence of Size Distributions and the Fleet Emission Reduction." Graz, 2020 (cit. on p. 6).

[40] William C Hinds. *Aerosol technology: properties, behavior, and measurement of airborne particles*. John Wiley & Sons, 1999. ISBN: 0-471-19410-7 (cit. on pp. 9, 15, 19).

[41] Peter Eastwood. *Particulate Emissions from Vehicles*. John Wiley & Sons, 2008. ISBN: 978-0-470-72455-2 (cit. on pp. 9, 15).

[42] Ian Colbeck and Lazaridis Mihalis. *Aerosol Science*. John Wiley and Sons, 2014. ISBN: 978-1-119-97792-6 (cit. on p. 9).

[43] Pramod Kulkarni, Paul A Baron, and Klaus Willeke. *Aerosol measurement: principles, techniques, and applications*. Third Edit. John Wiley & Sons, 2011. ISBN: 978-0-470-38741-2 (cit. on pp. 9–11, 16–19, 25, 26, 32, 42, 43).

[44] Sheldon K Friedlander. *Smoke, Dust, and Haze: Fundamentals of Aerosol Dynamics*. Second Edi. Oxford, New York: Oxford University Press, 2000. ISBN: 0-19-512999-7 (cit. on p. 9).

[45] Emma Cunningham. "On the velocity of steady fall of spherical particles through fluid medium." In: *Proceedings of the Royal Society of London. Series A, Containing Papers of a Mathematical and Physical Character* 83.563 (Mar. 1910), pp. 357–365. DOI: 10.1098/rspa.1910.0024 (cit. on p. 10).

[46] CN Davies. "Definitive equations for the fluid resistance of spheres." In: *Proceedings of the Physical Society* 57.4 (1945), p. 259. DOI: 10.1088/0959-5309/57/4/301 (cit. on p. 10).

[47] M. A. Schriefl, A. Bergmann, and M. Fierz. "Design principles for sensing particle number concentration and mean particle size with unipolar diffusion charging." In: *IEEE Sensors Journal* 19.4 (Feb. 2019), pp. 1392–1399. ISSN: 1530437X. DOI: 10.1109/JSEN.2018.2880278 (cit. on pp. 11, 25).

[48] Robert Takeo Nishida. "Measuring Aerosol Nanoparticles by Ultraviolet Photoionisation." PhD thesis. University of Cambridge, 2018 (cit. on pp. 11, 25).

[49] Mario A. Schriefl. "Particle Number Sensing Based on Electrical Charging Techniques." PhD thesis. Graz University of Technology, 2019, p. 144 (cit. on pp. 11, 25).

[50] Topi Rönkkö et al. "Nucleation mode particles with a nonvolatile core in the exhaust of a heavy duty diesel vehicle." In: *Environmental Science and Technology* 41.18 (Sept. 2007), pp. 6384–6389. ISSN: 0013936X. DOI: 10.1021/es0705339 (cit. on pp. 12, 14).

[51] Tero Lähde et al. "Heavy duty diesel engine exhaust aerosol particle and ion measurements." In: *Environmental Science and Technology* 43.1 (Jan. 2009), pp. 163–168. ISSN: 0013936X. DOI: 10.1021/es801690h (cit. on pp. 12, 14).

[52] Andrea De Filippo and M. Matti Maricq. "Diesel nucleation mode particles: Semivolatile or solid?" In: *Environmental Science and Technology* 42.21 (Nov. 2008), pp. 7957–7962. ISSN: 0013936X. DOI: 10.1021/es8010332 (cit. on pp. 12, 14).

[53] Stephen J. Harris and M. Matti Maricq. "Signature size distributions for diesel and gasoline engine exhaust particulate matter." In: *Journal of Aerosol Science* 32.6 (2001), pp. 749–764. ISSN: 00218502. DOI: 10.1016/S0021-8502(00)00111-7 (cit. on p. 12).

[54] Georgios Karavalakis et al. "Evaluating the regulated emissions, air toxics, ultrafine particles, and black carbon from SI-PFI and SI-DI vehicles operating on different ethanol and iso-butanol blends." In: *Fuel* 128 (July 2014), pp. 410–421. ISSN: 00162361. DOI: 10.1016/j.fuel.2014.03.016 (cit. on p. 13).

[55] Piotr Bielaczyc, Joseph Woodburn, and Andrzej Szczotka. "Particulate Emissions from European Vehicles Featuring Direct Injection Spark Ignition Engines Tested Under Laboratory Conditions." In: *SAE International Journal of Fuels and Lubricants* 7.2 (2014), pp. 580–590. ISSN: 19463960. DOI: 10.4271/2014-01-1608 (cit. on p. 13).

[56] Brian Mackenzie Graves, Charles Robert Koch, and Jason Scott Olfert. "Morphology and volatility of particulate matter emitted from a gasoline direct injection engine fuelled on gasoline and ethanol blends." In: *Journal of Aerosol Science* 105 (Mar. 2017), pp. 166–178. ISSN: 18791964. DOI: 10.1016/j.jaerosci.2016.10.013 (cit. on p. 13).

[57] James P. Szybist et al. "Ethanol blends and engine operating strategy effects on light-duty spark-ignition engine particle emissions." In: *Energy and Fuels* 25.11 (Nov. 2011), pp. 4977–4985. ISSN: 08870624. DOI: 10.1021/ef201127y (cit. on p. 13).

[58] David B. Kittelson. *Engines and nanoparticles: A review*. June 1998. DOI: 10.1016/S0021-8502(97)10037-4 (cit. on p. 13).

[59] Jesse H. Kroll and John H. Seinfeld. *Chemistry of secondary organic aerosol: Formation and evolution of low-volatility organics in the atmosphere*. May 2008. DOI: 10.1016/j.atmosenv.2008.01.003 (cit. on p. 13).

[60] Neil M. Donahue, Allen L. Robinson, and Spyros N. Pandis. "Atmospheric organic particulate matter: From smoke to secondary organic aerosol." In: *Atmospheric Environment* 43.1 (Jan. 2009), pp. 94–106. ISSN: 13522310. DOI: 10.1016/j.atmosenv.2008.09.055 (cit. on pp. 13, 15).

[61] Allen L. Robinson et al. *Updating the conceptual model for fine particle mass emissions from combustion systems*. 2010. DOI: 10.3155/1047-3289.60.10.1204 (cit. on pp. 13, 15).

[62] K. Max Zhang and Anthony S. Wexler. "Evolution of particle number distribution near roadways - Part I: Analysis of aerosol dynamics and its implications for engine emission measurement." In: *Atmospheric Environment* 38.38 (Dec. 2004), pp. 6643–6653. ISSN: 13522310. DOI: 10.1016/j.atmosenv.2004.06.043 (cit. on p. 14).

[63] J. S. Olfert, J. P.R. Symonds, and N. Collings. "The effective density and fractal dimension of particles emitted from a light-duty diesel vehicle with a diesel oxidation catalyst." In: *Journal of Aerosol Science* 38.1 (Jan. 2007), pp. 69–82. ISSN: 00218502. DOI: 10.1016/j.jaerosci.2006.10.002 (cit. on p. 14).

[64] International Organization for Standardization. *ISO 29904:2013 - Fire chemistry — Generation and measurement of aerosols*. Geneva, Switzerland. URL: https://www.iso.org/standard/45735.html (cit. on p. 17).

[65] P G Gormley and M Kennedy. "Diffusion from a stream flowing through a cylindrical tube." In: *Proceedings of the Royal Irish Academy. Section A: Mathematical and Physical Sciences*. Vol. 52. JSTOR. 1948, pp. 163–169 (cit. on p. 18).

[66] P. H. McMurry. "The history of condensation nucleus counters." In: *Aerosol Science and Technology* 33.4 (2000), pp. 297–322. ISSN: 02786826. DOI: 10.1080/02786820050121512 (cit. on p. 22).

[67] M. Hermann et al. "Particle counting efficiencies of new TSI condensation particle counters." In: *Journal of Aerosol Science* 38.6 (June 2007), pp. 674–682. ISSN: 00218502. DOI: 10.1016/j.jaerosci.2007.05.001 (cit. on p. 24).

[68] Heinz Burtscher. "Measurement and characteristics of combustion aerosols with special consideration of photoelectric charging and charging by flame ions." In: *Journal of Aerosol Science* 23.6 (1992), pp. 549–595 (cit. on p. 25).

[69] Shih Chen Wang and Richard C. Flagan. "Scanning electrical mobility spectrometer." In: *Aerosol Science and Technology* 13.2 (Jan. 1990), pp. 230–240. ISSN: 15217388. DOI: 10.1080/02786829008959441 (cit. on p. 31).

[70] Naomi Zimmerman et al. "Comparison of three nanoparticle sizing instruments: The influence of particle morphology." In: *Atmospheric Environment* 86 (Apr. 2014), pp. 140–147. ISSN: 13522310. DOI: 10.1016/j.atmosenv.2013.12.023 (cit. on p. 32).

[71] J. Kangasluoma et al. "Sizing of neutral sub 3nm tungsten oxide clusters using Airmodus Particle Size Magnifier." In: *Journal of Aerosol Science* 87 (Sept. 2015), pp. 53–62. ISSN: 18791964. DOI: 10.1016/j.jaerosci.2015.05.007 (cit. on p. 32).

[72] J Kangasluoma and J Kontkanen. "On the sources of uncertainty in the sub-3 nm particle concentration measurement." In: *Journal of Aerosol Science* 112 (2017), pp. 34–51 (cit. on p. 32).

[73] Maik Bergmann et al. "Using ejector diluters to sample vehicle exhaust at elevated pressures and temperatures." In: *SAE International Journal of Engines* 1.2008-01-2434 (2008), pp. 1167–1178. ISSN: 19463936. DOI: 10.4271/2008-01-2434 (cit. on p. 33).

[74] Jussi Lyyränen et al. "Comparison of Different Dilution Methods for Measuring Diesel Particle Emissions." In: *Aerosol Science and Technology* 38.1 (Jan. 2004), pp. 12–23. ISSN: 15217388. DOI: 10.1080/02786820490247579 (cit. on p. 33).

[75] Jonathan Symonds et al. "Uniformity of Particle Concentration after Mixing Aerosol Flows." In: *International Aerosol Conference 2018*. St. Louis, MO: AAAR, Sept. 2018. URL: https://www.researchgate.net/publication/327624013_Uniformity_of_Particle_Concentration_after_Mixing_Aerosol_Flows (cit. on p. 35).

[76] Ch Hueglin, L. Scherrer, and H. Burtscher. "An accurate, continuously adjustable dilution system (1:10 to 1:104) for submicron aerosols." In: *Journal of Aerosol Science* 28.6 (1997), pp. 1049–1055. ISSN: 00218502. DOI: 10.1016/S0021-8502(96)00485-5 (cit. on p. 35).

[77] Mohamed Tarik et al. "A Practical Guide on Coupling a Scanning Mobility Sizer and Inductively Coupled Plasma Mass Spectrometer (SMPS-ICPMS)." In: *Journal of visualized experiments: JoVE* 125 (2017) (cit. on p. 36).

[78] Adrian Hess, Mohamed Tarik, and Christian Ludwig. "A hyphenated SMPS–ICPMS coupling setup: size-resolved element specific analysis of airborne nanoparticles." In: *Journal of Aerosol Science* 88 (2015), pp. 109–118 (cit. on p. 36).

[79] Markus Bainschab and Alexander Bergmann. "An Intrinsically Pressure Insensitive Low Cost Particle Number Diluter Featuring Flow Monitoring." In: *Proceedings* 2.13 (Dec. 2018), p. 981. ISSN: 2504-3900. DOI: 10.3390/proceedings2130981. URL: http://www.mdpi.com/2504-3900/2/13/981 (cit. on p. 36).

[80] Abdelhakim Djebara, Victor Songmene, and Ali Bahloul. "Performance of a Capillary Dilution System for High-Concentration Sampling of Ultrafine Aerosols." In: *Aerosol Science and Engineering* (2018), pp. 1–6 (cit. on p. 36).

[81] Aaron Collins. "Ultrafine Particle Loss in Aerosol Diluters." PhD thesis. University of Minnesota, 2010, p. 210 (cit. on p. 36).

[82] Sara Janhäll et al. "Size resolved traffic emission factors of submicrometer particles." In: *Atmospheric Environment* 38.26 (Aug. 2004), pp. 4331–4340. ISSN: 13522310. DOI: 10.1016/j.atmosenv.2004.04.018 (cit. on p. 37).

[83] Stefan Hausberger et al. "Emission factors for heavy-duty vehicles and validation by tunnel measurements." In: *Atmospheric Environment*. Vol. 37. 37. Elsevier Ltd, Dec. 2003, pp. 5237–5245. DOI: 10.1016/j.atmosenv.2003.05.002 (cit. on p. 37).

[84] H. Burtscher. "Physical characterization of particulate emissions from diesel engines: A review." In: *Journal of Aerosol Science* 36.7 (July 2005), pp. 896–932. ISSN: 00218502. DOI: 10.1016/j.jaerosci.2004.12.001 (cit. on p. 37).

[85] United Nations Economic Commission for Europe. "Regulation No 83 of the Economic Commission for Europe of the United Nations (UN/ECE) – Uniform provisions concerning the approval of vehicles with regard to the emission of pollutants according to engine fuel requirements." In: *Publications Office of the European Union* (Dec. 2006). URL: https://op.europa.eu/en/publication-detail/-/publication/2f8f0ce5-66fb-4a38-ae68-558ae1b04a5f/language-en (cit. on pp. 38, 43).

[86] H. Burtscher et al. "Separation of volatile and non-volatile aerosol fractions by thermodesorption: instrumental development and applications." In: *Journal of Aerosol Science* 32.4 (2001), pp. 427–442. ISSN: 00218502. DOI: 10.1016/S0021-8502(00)00089-6 (cit. on p. 39).

[87] B. Wehner, S. Philippin, and A. Wiedensohler. "Design and calibration of a thermodenuder with an improved heating unit to measure the size-dependent volatile fraction of aerosol particles." In: *Journal of Aerosol Science* 33.7 (2002), pp. 1087–1093. ISSN: 00218502. DOI: 10.1016/S0021-8502(02)00056-3 (cit. on p. 39).

[88] Jacob Swanson and David Kittelson. "Evaluation of thermal denuder and catalytic stripper methods for solid particle measurements." In: *Journal of Aerosol Science* 41.12 (2010), pp. 1113–1122 (cit. on p. 39).

[89] Provat K. Saha, Andrey Khlystov, and Andrew P. Grieshop. "Determining Aerosol Volatility Parameters Using a "dual Thermodenuder" System: Application to Laboratory-Generated Organic Aerosols." In: *Aerosol Science and Technology* 49.8 (Aug. 2015), pp. 620–632. ISSN: 15217388. DOI: 10.1080/02786826.2015.1056769. URL: http://www.tandfonline.com/doi/full/10.1080/02786826.2015.1056769 (cit. on p. 39).

[90] Stavros Amanatidis et al. "Comparative performance of a thermal denuder and a catalytic stripper in sampling laboratory and marine exhaust aerosols." In: *Aerosol Science and Technology* 52.4 (Jan. 2018), pp. 1–13. ISSN: 15217388. DOI: 10.1080/02786826.2017.1422236 (cit. on p. 39).

[91] Martin Fierz, Martine G.C. Vernooij, and Heinz Burtscher. "An improved low-flow thermodenuder." In: *Journal of Aerosol Science* 38.11

(Nov. 2007), pp. 1163–1168. ISSN: 00218502. DOI: 10.1016/j.jaerosci.2007.08.006 (cit. on p. 39).

[92] Imad. Abdul-Khalek and David Kittelson. "Real Time Measurement of Volatile and Solid Exhaust Particles Using a Catalytic Stripper." In: *SAE Technical Paper* 950236 (1995). URL: http://papers.sae.org/950236/ (cit. on p. 39).

[93] Jacob Swanson et al. "A Miniature Catalytic Stripper for Particles Less Than 23 Nanometers." In: *SAE International Journal of Fuels and Lubricants* 6.2 (Apr. 2013), pp. 1570–2013. ISSN: 1946-3960. DOI: 10.4271/2013-01-1570. URL: http://papers.sae.org/2013-01-1570/ (cit. on p. 39).

[94] A. D. Melas et al. "Development and evaluation of a catalytic stripper for the measurement of solid ultrafine particle emissions from internal combustion engines." In: *Aerosol Science and Technology* (Jan. 2020), pp. 1–14. ISSN: 15217388. DOI: 10.1080/02786826.2020.1718061. URL: https://www.tandfonline.com/doi/full/10.1080/02786826.2020.1718061 (cit. on pp. 39, 170).

[95] Hiroyuki Hagino. "Laboratory evaluation of nanoparticle penetration efficiency in a cylindrical counter flow denuder for non-specific removal of trace gases." In: *Aerosol Science and Technology* 51.4 (2017), pp. 443–450 (cit. on pp. 40, 46).

[96] Richard H Moore et al. "Mapping the operation of the miniature combustion aerosol standard (Mini-CAST) soot generator." In: *Aerosol Science and Technology* 48.5 (2014), pp. 467–479. ISSN: 15217388. DOI: 10.1080/02786826.2014.890694. URL: https://www.tandfonline.com/action/journalInformation?journalCode=uast20 (cit. on p. 41).

[97] Lianpeng Jing. "Standard Combustion Aerosol Generator (SCAG) for Calibration Purposes." In: *Atmospheric Environment* 27.8 (1999), pp. 1271–1275 (cit. on p. 41).

[98] Mohsen Kazemimanesh et al. "A novel miniature inverted-flame burner for the generation of soot nanoparticles." In: *Aerosol Science and Technology* 53.2 (Feb. 2019), pp. 184–195. ISSN: 15217388. DOI: 10.1080/02786826.2018.1556774 (cit. on p. 41).

[99] Alireza Moallemi et al. *Characterization of black carbon particles generated by a propane-fueled miniature inverted soot generator*. Sept. 2019. DOI: 10.1016/j.jaerosci.2019.05.004 (cit. on p. 41).

[100] Dwight W. Senser, John S. Morse, and Vic A. Cundy. "Construction and novel application of a flat flame burner facility to study hazardous waste combustion." In: *Review of Scientific Instruments* 56.6 (June 1985), pp. 1279–1284. ISSN: 00346748. DOI: 10.1063/1.1137992. URL: http://aip.scitation.org/doi/10.1063/1.1137992 (cit. on p. 41).

[101] F. Migliorini et al. "How "flat" is the rich premixed flame produced by your McKenna burner?" In: *Combustion and Flame* 153.3 (May 2008), pp. 384–393. ISSN: 00102180. DOI: 10.1016/j.combustflame.2008.01.007 (cit. on p. 41).

[102] Rouzbeh Ghazi et al. "Mass, mobility, volatility, and morphology of soot particles generated by a mckenna and inverted burner." In: *Aerosol Science and Technology* 47.4 (Apr. 2013), pp. 395–405. ISSN: 02786826. DOI: 10.1080/02786826.2012.755259. URL: http://www.tandfonline.com/doi/abs/10.1080/02786826.2012.755259 (cit. on p. 41).

[103] Jason Olfert and Steven Rogak. *Universal relations between soot effective density and primary particle size for common combustion sources*. May 2019. DOI: 10.1080/02786826.2019.1577949. URL: https://www.tandfonline.com/doi/full/10.1080/02786826.2019.1577949 (cit. on p. 41).

[104] C. Helsper et al. "Investigations of a new aerosol generator for the production of carbon aggregate particles." In: *Atmospheric Environment Part A, General Topics* 27.8 (June 1993), pp. 1271–1275. ISSN: 09601686. DOI: 10.1016/0960-1686(93)90254-V (cit. on p. 42).

[105] *DNP digital 3000 - Product Lines - Palas*. URL: https://www.palas.de/en/product/dnpdigital3000 (cit. on p. 42).

[106] M. Gysel et al. "Technical Note: The single particle soot photometer fails to reliably detect PALAS soot nanoparticles." In: *Atmospheric Measurement Techniques* 5.12 (Dec. 2012), pp. 3099–3107. ISSN: 1867-8548. DOI: 10.5194/amt-5-3099-2012. URL: https://www.atmos-meas-tech.net/5/3099/2012/ (cit. on p. 42).

[107] Da Ren Chen, David Y.H. Pui, and Stanley L. Kaufman. "Electrospraying of conducting liquids for monodisperse aerosol generation in the 4 nm to 1.8 μm diameter range." In: *Journal of Aerosol Science* 26.6 (Sept. 1995), pp. 963–977. ISSN: 00218502. DOI: 10.1016/0021-8502(95)00027-A (cit. on p. 43).

[108] EC. "Commission Regulation (EU) 2017/1154." In: *Official Journal of the European Union* (2017). URL: https://eur-lex.europa.eu/eli/reg/2017/1154/oj (cit. on p. 44).

[109] B. Giechaskiel et al. "Calibration of condensation particle counters for legislated vehicle number emission measurements." In: *Aerosol Science and Technology* 43.12 (Nov. 2009), pp. 1164–1173. ISSN: 02786826. DOI: 10.1080/02786820903242029. URL: http://www.tandfonline.com/doi/abs/10.1080/02786820903242029 (cit. on p. 44).

[110] CARES. *CARES — City Air Remote Emission Sensing*. 2019. URL: https://cares-project.eu/ (cit. on p. 53).

[111] Willard C. Losinger. "A Review of the GUM Workbench." In: *American Statistician* 58.2 (2004), pp. 165–167. ISSN: 15372731. DOI: 10.1198/0003130043312 (cit. on pp. 151, 153).

Papers

Paper 1

Measuring Sub-23 Nanometer Real Driving Particle Number Emissions Using the Portable DownToTen Sampling System

Video Article

Measuring Sub-23 Nanometer Real Driving Particle Number Emissions Using the Portable DownToTen Sampling System

Markus Bainschab[1], Lukas Landl[2], Jon Andersson[3], Athanasios Mamakos[4], Stefan Hausberger[2], Alexander Bergmann[1]

[1]Institute of Electrical Measurement and Sensor Systems, Graz University of Technology

[2]Institute of Internal Combustion Engines and Thermodynamic, Graz University of Technology

[3]Ricardo UK Ltd.

[4]AVL List GmbH

Correspondence to: Markus Bainschab at m.bainschab@tugraz.at

URL: https://www.jove.com/video/61287
DOI: doi:10.3791/61287

Keywords: Engineering, Issue 159, automotive, emissions, particle number, sub-23 nm, portable emission measurement, real driving emissions, sampling, dilution

Date Published: 5/22/2020

Citation: Bainschab, M., Landl, L., Andersson, J., Mamakos, A., Hausberger, S., Bergmann, A. Measuring Sub-23 Nanometer Real Driving Particle Number Emissions Using the Portable DownToTen Sampling System. *J. Vis. Exp.* (159), e61287, doi:10.3791/61287 (2020).

Abstract

The current particle size threshold of the European Particle Number (PN) emission standards is 23 nm. This threshold could change because future combustion engine vehicle technology may emit large amounts of sub-23 nm particles. The Horizon 2020 funded project DownToTen (DTT) developed a sampling and measurement method to characterize particle emissions in this currently unregulated size range. A PN measurement system was developed based on an extensive review of the literature and laboratory experiments testing a variety of PN measurement and sampling approaches. The measurement system developed is characterized by high particle penetration and versatility, which enables the assessment of primary particles, delayed primary particles, and secondary aerosols, starting from a few nanometers in diameter. This paper provides instruction on how to install and operate this Portable Emission Measurement System (PEMS) for Real Drive Emissions (RDE) measurements and assess particle number emissions below the current legislative limit of 23 nm.

Introduction

The Particle Measurement Programme (PMP) was founded by the UK Government for the “development of type approval test protocols for assessing vehicles fitted with advanced particulate reduction technology that would complement or replace current legislative measurement procedures”[1]. The PMP is the world’s first particle number-based emissions regulation, targeted specifically at carbonaceous particles ≥23 nm. Recent measurements indicate that it may be necessary to include smaller particles.

Negative health impacts of diesel soot are well understood[2], and therefore, the ‘precautionary principle’ was invoked on the basis that the elimination of carbon particles from diesel exhaust, via the mandatory use of diesel particulate filters (DPFs), was imperative on health grounds. However, because in European legislation a limit value must force adoption of emissions control technologies, this could not be achieved without an appropriate measurement method. With strong political backing across Europe, the UK Government led the conception of the PMP to improve particulate measurements. The PMP, under the auspices of the United Nations Economic Commission for Europe (UN-ECE)[3], included the expertise of others from around the globe. Two particle research projects were completed in 2001. One of them (Particulate Research[4]) was carried out by the UK Government Department of the Environment, Transport and the Regions (DETR), in partnership with the Society of Motor Manufacturers and Traders (SMMT) and the Oil Companies European Organisation for Environment, Health and Safety (CONCAWE). The other one (PARTICULATES[5]) was funded by the European Union's 5th Framework and was carried out by 14 different European partners. The results of both projects indicated that particle number-based procedures were promising, but that challenges for repeatable and reproducible measurements remained.

In 2007 the final report of the PMP Light-duty Inter-laboratory Correlation Exercise was published[6], including some improvements on the filter-based mass measurement method, primarily demonstrating the feasibility of a number count-based method for regulatory purposes based upon a defined particle size range and particle volatility. Both methods were implemented based upon sampling from the existing constant volume sampler (CVS) dilution tunnel approach originally developed for particulate matter mass and bagged dilute gaseous emissions measurements.

Within the number count-based method, a lower particle size limit of ~20 nm was selected. The primary objective of the project was to ensure particles of this size and above were controlled by legislation. It is now known that the primary particle size in engine exhaust can be <20 nm[7,8,9]. For practical reasons, a particle counter with a 50% counting efficiency (d_{50}) at 23 nm was selected, and this size became the accepted lower size threshold. It was recognized that due to the high sensitivity to properties such as dilution, air temperature, humidity, and ratio[10], volatile particle size distribution and integrated number measurements could be repeatable in one CVS-equipped facility with one vehicle, but much less so from facility to facility. Thus, for rigorous regulations, it was necessary to focus purely on nonvolatile particles, with the measurement approach effectively defining the regulatory particle boundary conditions on size and volatility. European diesel fuel has back-end volatility such that only a few percent boils at temperatures above 350 °C, and early work within the PMP indicated that short residence times at this temperature were suitable for the complete evaporation of tetracontane, a linear hydrocarbon containing 40 carbon atoms with volatility towards the end boiling

point of engine lubricant[11]. Consequently, a temperature of 350 °C has become the de facto reference point for regulatory >23 nm particle volatility.

The PMP measurement system specification comprises components for sampling, sample conditioning, and measurement, summarized in **Table 1**.

Stage	Identity	Purpose
0	Sample source	Origin of sample
1	Particle Transport	Conduct sample from origin to measurement system
2	Volatile Particle Remover	Eliminate volatiles and define non-volatile particles to be measured
3	Particle Number Counter	Enumerate non-volatile particles and define the lower size limit

Table 1: Elements of the PMP Measurement System.

The European PMP PN approach is being implemented and now applies to light-duty diesel (September 2011, EURO 5b) and GDI vehicles (September 2014, EURO 6), and to diesel and gas heavy-duty engines (February 2013, EURO VI).

Recent measurements showed that some light-duty vehicles and, in particular, spark ignition technologies, can emit substantial levels of particles <23 nm[12,13,14]. This led the European Commission to fund research projects to develop new or extended methods that can be rapidly implemented as a replacement, or addition to, the current >23 nm regulation.

One such project, DownToTen (DTT), aims to preserve the general approach of PMP and extend the measurement range down to a d_{50} ≤10 nm. To this end, the configuration of the DTT measurement system was designed to include the same basic elements described in **Table 1**, but with the conditioning and measurement steps optimized to enable efficient transport and detection of the <23 nm particles. The DTT system was initially developed for laboratory use but was modified to operate as a portable emissions measurement system (PEMS). For the DTT PN-PEMS system, the components were optimized to reduce weight and power consumption and increase physical robustness without substantially diverging from the original design. For mobile application, the system must be resistant to harsher and erratic temperatures, pressures, and vibration environments likely encountered in light- and heavy-duty PEMS testing. The impact of pressure variations at the inlet of the system was modelled and studied experimentally[15]. The resistance to vibrations was assessed using a dedicated test bed[16]. Vibrations and accelerations that occur during typical RDE drives did not impair the measurement results of the condensation particle counters used. The DTT system is also designed for use at low temperatures, where the volatile removal function is inactive, to feed an aging chamber and study secondary organic aerosol formation[17].

The thermal conditioning elements of the DTT measurement system that define the regulatory volatility boundary of particles closely parallel the elements of the PMP system in that both systems contain the sequence:

1. First particle number dilution stage
2. HC/volatile elimination stage
3. Second particle number dilution stage

The primary differences between the DTT and PMP systems are that the DTT system components are selected to:

1. Maximize transmission of ~10 nm PN from the sample source to the particle counter using low loss dilution and particle transmission approaches
2. Comprehensively remove volatiles using oxidative particle elimination rather than merely reducing partial pressures of condensable HC species through evaporation and dilution
3. Count particles of ~10–50 nm with greater efficiency than current PMP systems

The objective of this paper is to present the use of the DTT PN-PEMS system for measuring nonvolatile particles ≥10 nm from an in-use road vehicle. This includes an introduction to the measurement system and its main components, performing laboratory-based calibration measurements, installing the device for a mobile application, conducting a real driving emission measurement, and processing the collected measurement data.

Instrumentation

The DTT PN-PEMS was designed to provide high particle penetration down to a few nanometers, robust particle number dilution, removal of volatile particles, and prevention of artificial particle formation. The components of the system were selected based on results from laboratory experiments comparing a variety of technologies for dilution and aerosol conditioning. This section provides an overview of the system, its working principle, and the components used. **Figure 1** shows a schematic of the system. **Figure 2** shows a photo of the system. The DTT system is 60 cm high and has a footprint of 50 cm x 50 cm. The weight of the system is approximately 20 kg. Including the required peripheral elements (i.e., battery and gas bottle) the total weight is approximately 80 kg. The major elements of the system are the two dilution stages (i.e., first hot, second cold), a catalytic stripper, and at least one condensation particle counter (CPC).

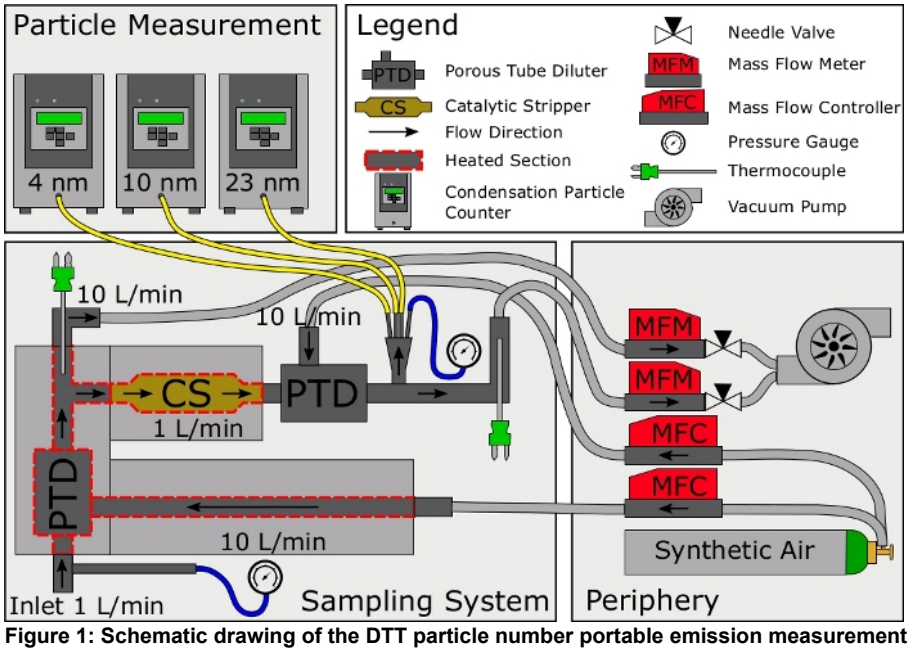

Figure 1: Schematic drawing of the DTT particle number portable emission measurement system. Please click here to view a larger version of this figure.

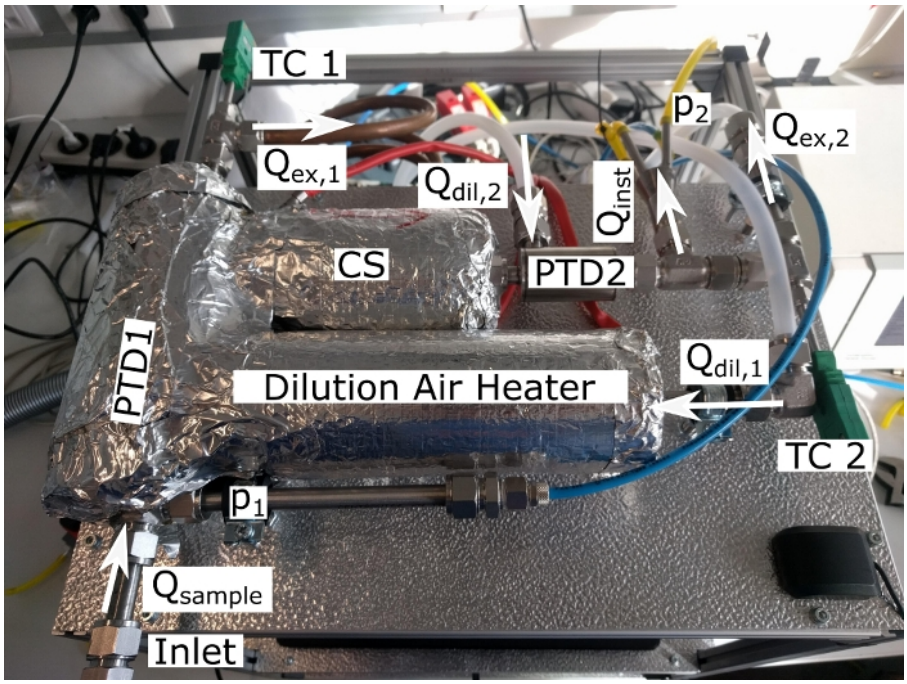

Figure 2: Top view picture of the DTT sampling system. Please click here to view a larger version of this figure.

Two dilution stages reduce the particle number concentrations to levels measurable by condensation particle counters (<10^4 #/cm^3). Custom-made porous tube diluters are used for both dilution stages. This technology was selected because of its low particle loss[18,19]. The radial ingress of dilution air convectively keeps particles away from the walls, which reduces particle losses. Furthermore, these diluters can be very small and can withstand temperatures of 400 °C. The porous material used is a sintered hastalloy X tube (GKN Filters Metals GmbH, Radevormwald, Germany). Static mixing elements inside the porous tube provide a well-mixed aerosol directly downstream of the diluter. This allows taking a representative sample of the diluted aerosol for further conditioning or measurement by splitting the aerosol flow directly downstream of the diluter, and allows for a compact sampling system. The primary dilution stage is typically heated to 350 °C, while the second stage is operated at ambient temperature. The dilution factor of the system is approximately 80. The exact value is dependent on the inlet flow and the mass flow management: The flow rates in the sampling system are managed by a system of two mass flow controllers and two mass flow meters. The mass flow controllers control the dilution air flow rates. The mass flow meters monitor the flow rates extracted downstream of dilution stages 1 and 2. The differences between the flows extracted and the flows supplied can be changed. In other words, the net flow added or subtracted in one dilution stage can be defined. The sample flow rate, Q_{sample}, is defined as the sum of all other flow rates: 1) Flow rate drawn by the

measurement instruments (Q_{inst}); 2) the dilution air flow rates ($Q_{dil,i}$); and 3) the excess flow rates $Q_{ex,i}$. For the calculation of the sample flow, the contributions of the flows extracted from the system are positive and the contributions of the flows fed into the system are negative.

$$Q_{sample} = Q_{ex,1} + Q_{ex,2} + Q_{inst} - Q_{dil,1} - Q_{dil,2}$$

The total dilution ratio *DR* is calculated by:

$$DR = DR_1 \times DR_2 = \left(\frac{Q_{dil,1}}{Q_{sample}} + 1\right) \times \left(\frac{Q_{dil,2}}{Q_{sample} + Q_{dil,1} - Q_{ex,1}} + 1\right)$$

A catalytic stripper (CS) is situated between dilution stage 1 and 2 and is operated at 350 °C at a flow rate of 1 liter per minute (L/min). The catalytic stripper provides oxidation of organic compounds and sulphur storage. The removal of these substances ensures the isolation of the solid particle fraction. The undesired formation of volatile and semivolatile particles and growth of subcut size particles is prevented. The catalytic stripper used is commercially available (AVL GmbH). The volatile particle removal efficiency of the CS was verified with polydisperse emery oil particles >50 nm and >1 mg/m^3 (3.5–5.5 mg/m^3) showing an efficiency of >99% (actual value 99.9%) as defined by RDE regulations[20]. This is a more rigorous test than the tetracontane test prescribed in the current PMP protocol.

One or more condensation particle counters are used to measure the particle number concentration downstream of the second dilution stage. A CPC with a d_{50} of 23 nm enables the measurement of the currently regulated emission of solid particles larger than 23 nm. Additionally, measuring the particle number concentration with one or more CPCs with a lower d_{50} cut point (e.g., 10 nm, 4 nm) enables the assessment of the currently unregulated solid particle fraction <23 nm down to the d_{50} cut size of the applied CPC.

The dilution air supply line, the primary porous tube diluter, and the catalytic stripper have independent heating elements containing k-type thermocouples (TC). Independently heating different sections controls the temperature distribution in the system.

In addition to the thermocouples in the heating elements, two thermocouples are placed downstream of dilution stage 1 and 2. These two thermocouples directly measure the aerosol temperature.

Two absolute pressure sensors (NXP MPX5100AP) are used to monitor the pressure at the inlet and the outlet of the sampling system.

For mobile measurements, a Clayton Power LPS 1500 battery pack is used. A 10 L synthetic air bottle supplies the system with dilution air during mobile applications. The sizes of the battery and the gas bottle are chosen so that the system can operate independently for 100 min.

The system is controlled via a NI myRIO running a LabVIEW virtual instrument. The virtual instrument allows for control of the flow rates and heater temperatures. Apart from the controlled parameters, the aerosol temperatures, pressures, and acceleration (via the sensor integrated in myRIO) can be monitored and logged. A myRIO accessory GPS module enables logging of the position data. **Figure 3** and **Figure 4** show the user interface of the virtual instrument used for controlling the DTT system.

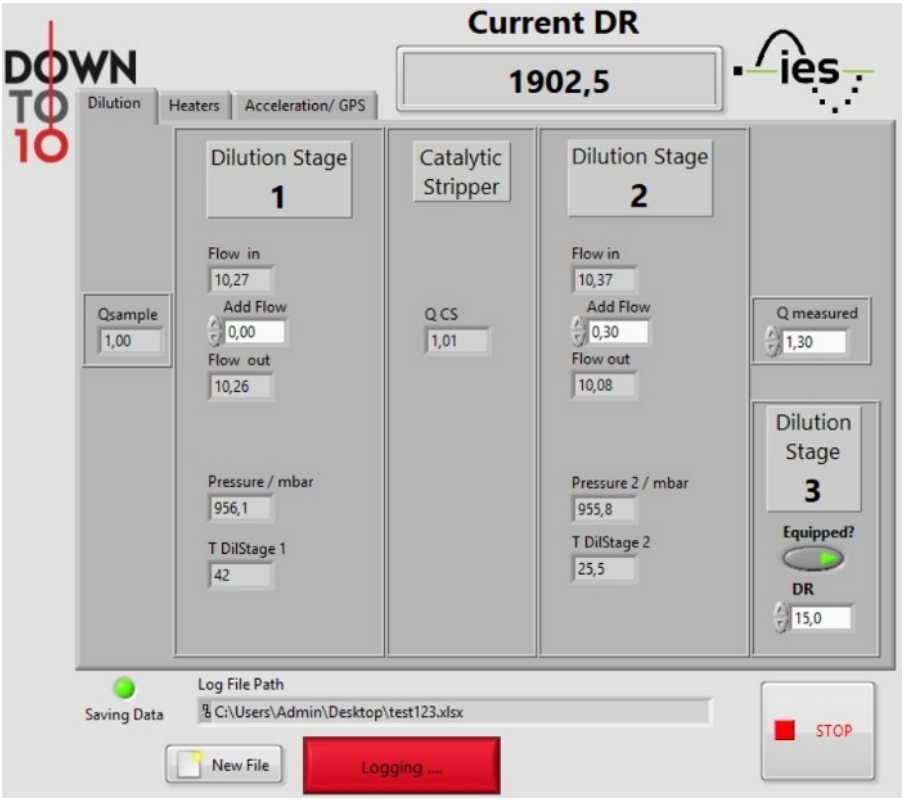

Figure 3: DTT virtual instrument dilution stage parameter overview. Please click here to view a larger version of this figure.

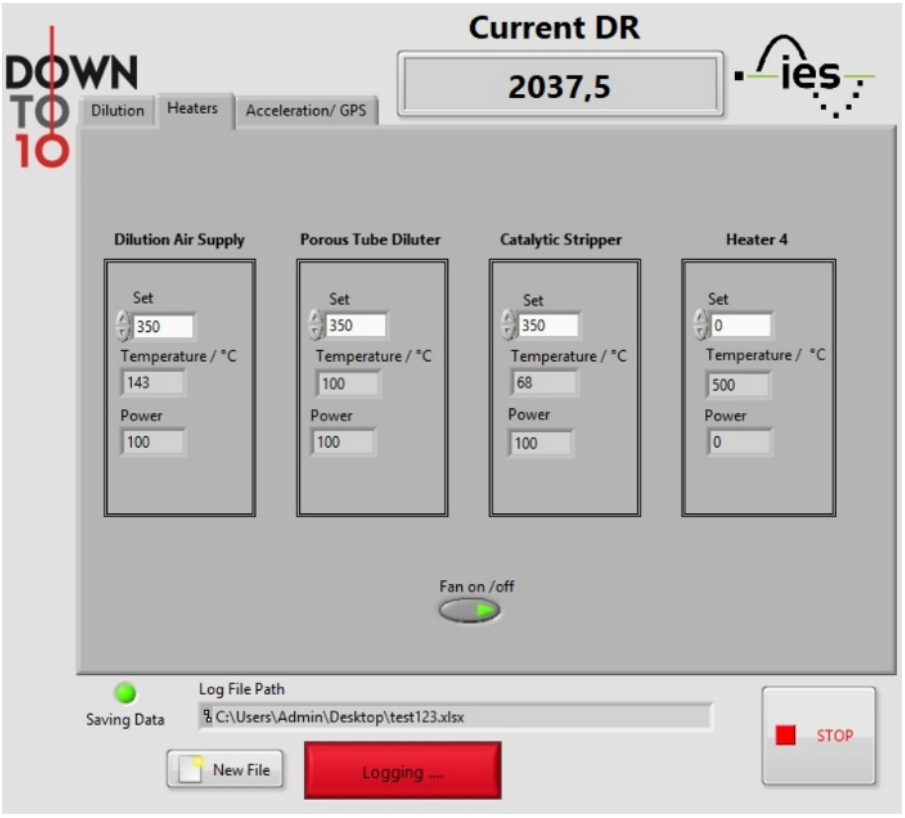

Figure 4: DTT virtual instrument heater control panel. Please click here to view a larger version of this figure.

Any kind of sampling procedure causes particle losses. To be able to account for these losses, laboratory measurements are performed to determine the particle size dependent particle penetration through the DTT sampling system. In these measurements, the particle concentration of monodisperse aerosol is measured upstream and downstream of the sampling system using two condensation particle counters. **Figure 5** shows the experimental setup for the calibration measurements. In this setup, a Jing miniCAST is used as a particle source[21,22]. Mass flow controllers (MFC) are used to control the gas flows into the burner. A dilution bridge enables the adjustment of the particle number concentration. The dilution bridge is a high-efficiency particulate air (HEPA) filter parallel to a needle valve. Adjusting the position of the needle valve alters the dilution ratio by changing the ratio between the fraction of the aerosol passing through the HEPA filter and the fraction of the aerosol passing through the needle valve. The filtered and the unfiltered aerosols are recombined with a T-piece to form a diluted aerosol. A catalytic stripper is used to remove possibly abundant volatile compounds generated as byproducts of the combustion process. A TSI 3082 electrostatic classifier together with a TSI 3085 differential mobility analyzer (nano DMA) are used for the size selection of particles. Two TSI CPCs 3775 (d_{50} = 4 nm) are used to measure the particle number concentration upstream and downstream of the DTT sampling system. The counters' cut point of d_{50} = 4 nm allows for the penetration determination at particle sizes as low as 10 nm and below.

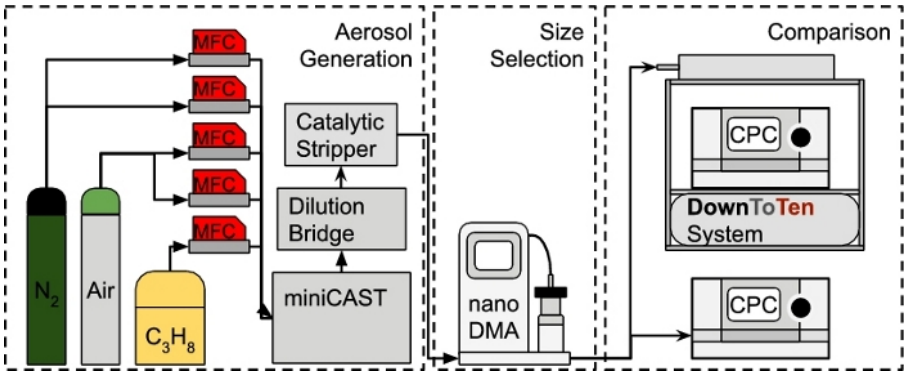

Figure 5: Schematic drawing of the experimental setup used for the calibration of the DTT sampling system. Please click here to view a larger version of this figure.

Protocol

1. Calibration procedure

1. Set up and prepare instruments.
    1. Place the instruments described, shown in **Figure 5**, in an organized and compact way in a laboratory with an extraction system.
    2. Connect the instruments as indicated by the arrows in **Figure 5** using conductive tubing. Keep the tubing as short as possible to minimize diffusional particle losses.
    3. Connect the instruments requiring power (i.e., DTT system, DTT system pump, two CPCs, DMA, catalytic stripper, and MFCs) to sockets.
    4. Connect the CPCs, the DTT system, and the MFC to a laptop.
    5. Make sure the laptop has the required software installed to communicate with the connected devices.
    6. Install missing software if required.

2. Warm up experimental components at least 30 minutes before starting the calibration measurements to ensure a thermally stable measurement setup.
    1. Start the operation of the burner by setting the gas flow controlled by the external MFC to the start setting specified in the user's manual.
    2. Ignite the flame.
    3. Feed the generated soot into the extraction system.
    4. Produce soot particles with a mean diameter of 50 ± 5 nm by setting the MFC-controlled flows accordingly. A table of settings and expected particle size distribution can be found in the burner manual or in the literature[23]. For the miniCAST settings in **Table 2** can be used:
    5. Start heating the catalytic stripper by setting the corresponding temperature controller to 350 °C.
    6. Switch on the CPCs and set to low flow mode (i.e., inlet flow of 0.3 L/min).
    7. Set up the communication of the CPCs with the laptop using the CPCs manufacturer's software or serial communication.
    8. Start up the DTT system warm up procedure as described in section 3.1.
    9. Install the impactor with a 0.071 cm nozzle at the inlet of the classifier according to the user's manual.
    10. Switch on the classifier. The display on the classifier should show an impactor flow of 1.30 ± 0.05 L/min. If the flow shown is different, double check the tubing connecting the classifier with the CPC and the DTT system.
    11. Set the sheath flow rate of the classifier to 13 L/min using the user interface.
    12. If a soft X-ray source (TSI 3088) is used, switch on the classifier's neutralizer.

Gas	Flow rate
Propane	20 mL/min
Quench gas (N_2)	2 L/min
Dilution air	5 L/min
Oxidation air	0.5 L/min
Mixing gas (N_2)	0 L/min

Table 2: Suggested miniCAST flow rates for calibration measurements.

3. After at least 30 min of warm up time perform the calibration measurements.
    1. Stop feeding the generated soot into the extraction system and connect the outlet of the burner to the dilution bridge.
    2. Set the particle size selected by the classifier to 10 nm using the user interface.
    3. Using the dilution bridge needle valve, adjust the particle number concentration upstream of the DTT system to be $10^4 \pm 10^3$ #/cm^3. This particle concentration yields a relatively high signal, enabling short measurement times while the CPCs operate in single-count mode, which ensures high accuracy. If the desired concentration of $10^4 \pm 10^3$ #/cm^3 cannot be reached because of exceedingly low particle concentrations emitted by the soot generator, maximize the throughput through the dilution bridge by fully opening the valve.
    4. Start logging the data of the DTT system (if not started already) by clicking the "**Start Data Logging**" button in the DTT Labview software.
    5. Start logging the data of the two CPCs using the proprietary software or serial communication.
    6. Wait 30 s for the experimental setup to stabilize.
    7. Note down a timestamp and the set particle size to mark the start of the measurement.
    8. Run the measurement for 2 min.
    9. Note down a timestamp to mark the end of the measurement.
    10. Repeat steps 1.3.3–1.3.9 for particle sizes of 15 nm, 30 nm, 50 nm, and 100 nm. Additional measurements can be taken if better size resolution is desired.
    11. Perform another set of measurements at the same particle sizes as before by repeating steps 1.3.2–1.3.10.
    12. Stop logging the measurement data of the two CPCs and the DTT system.
    13. Shut down all the instruments.

4. Evaluate the collected calibration data with a spreadsheet program.
    1. Export the particle concentration data measured by the CPCs into a .csv or .txt file.

2. Import the CPC and the DTT system data into a data evaluation tool.
3. Assign the data to the corresponding measurements by allocating data from each instrument (i.e., 2 CPCs, DTT system) with a timestamp between the start and the end timestamp of a measurement to the corresponding measurement. It is recommended to automate this task with a data evaluation tool.
4. Time average the two particle concentration datasets (CPCs) and the dilution ratio (DTT system) for all measurement points.
5. Calculate the relative particle penetration for all measurement points according to the following formula:

$$P_n = \frac{\bar{C}_{d,n}}{\bar{C}_{u,n}} \bar{DR}_n$$

Where P_n is the relative particle penetration at a certain measurement point *n*. $\bar{C}_{d,n}$ is the particle concentration measured by the CPC downstream of the DTT system averaged over the timespan of the measurement point *n*. $\bar{C}_{u,n}$ is the corresponding particle concentration measured by the CPC upstream of the DTT system averaged over the timespan of the measurement point *n*. $\bar{DR}_n$ is the dilution ratio from the DTT system, averaged over the timespan of the measurement point *n*.

6. Calculate the mean particle penetration P_{mean} by averaging over the average particle penetrations at 30 nm, 50 nm, and 100 nm particle size.

$$P_{mean} = \frac{P_{30nm} + P_{50nm} + P_{100nm}}{3}$$

This value is used for the calculation of the Particle Concentration Reduction Factor (PCRF) dividing the dilution ratio *DR* with the mean penetration efficiency P_{mean}.

$$PCRF = \frac{DR}{P_{mean}}$$

The *PCRF* is calculated from the penetration at 30 nm, 50 nm, and 100 nm to be comparable with PMP compliant, commercially available instruments. The measurements at sizes other than 30 nm, 50 nm, and 100 nm are used to determine the d_{50} cutoff size of the system to better characterize the system outside the regulatory frame.

2. Installation and preparation for real driving emissions measurements

1. Select a vehicle to assess for particle number emissions for particles <23 nm.
2. Select a route to measure the particle number emissions of the selected vehicle. There are guides on how to select appropriate routes in the literature[24].
3. Exhaust flow meter (EFM) installation
    1. Choose an EFM with a measurement range matching the expected exhaust flow range of the vehicle to be measured[24].
    2. Place the EFM control box in the trunk of the vehicle.
    3. Install the EFM outside of the car, according to the manufacturer's specification sheet. **Figure 6** shows an example of an installed EFM, mounted externally on shaped pipes leading into the trunk.
    4. Make sure the distance upstream and downstream of the EFM comply with EU regulations (i.e., 4x the pipe diameter or 150 mm straight pipe, whichever is larger, should be upstream and downstream of the flow sensor).
    5. When measuring vehicles with multiple exhaust manifolds, the individual exhaust pipes should be joined in front of the EFM and the cross-sectional area of this pipe increased accordingly to keep the increase in exhaust backpressure as low as possible. If this is not possible, the exhaust mass flow can be measured with several EFMs.
    6. Make sure the connectors from the EFM pipe to the exhaust pipe of the vehicle can withstand the exhaust gas temperatures (i.e., no plastic should be used).
    7. The pipe diameter, the connector diameter, and the diameter of any extensions required for sampling should not be smaller than the diameter of the exhaust pipe to keep the exhaust back pressure as low as possible.
    8. Start the piping at the exhaust of the vehicle.
    9. Connect the exhaust to the first pipe with connecting pipes and pipe clamps. Tighten the pipe clamps only at the end in order to be able to align the pipes during fitting.
    10. Connect one pipe at a time with connecting pipes and pipe clamps until there is a connection from the exhaust to the EFM. This should be as short as possible.
    11. Place the EFM control box and the EFM mounting bracket in the trunk to ensure that nothing slips during the measurement trip.
    12. Check that all the piping is tight and nothing comes loose during the measurement trip.
    13. Switch on the EFM.
    14. After a warm up time of up to 15 min depending on ambient temperature (see EFM user guide), the exhaust mass flow meter is ready to measure[25,26,27,28].

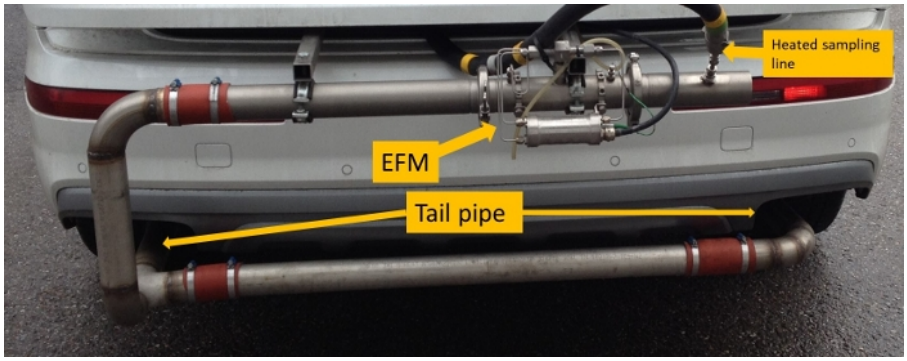

Figure 6: Picture of an installed EFM. Please click here to view a larger version of this figure.

4. Preparing and installing the DTT measurement system in the trunk of the vehicle
   NOTE: The measurements described here are conducted with two condensation particle counters as counting devices for the DTT system. One of the CPCs (TSI 3790A) has a lower d_{50} cutoff size of 23 nm, which equals the current legislative limit. The other CPC (commercially available 10 nm AVL CPC) has a lower d_{50} cutoff of 10 nm. Measuring particle emissions with these two instruments in parallel enables the assessment of the currently regulated emissions (>23 nm) and the <23 nm fraction.
   1. Take a laptop and install the DTT software and the software for logging the CPC measurement data.
   2. Place the synthetic air bottle in the trunk or on the floor in front of the rear seats and fix it using straps.
   3. Place the battery in the trunk of the vehicle and fix it. Plug in the AC input cable and connect it to a local power source.
   4. Place and fix the vacuum pumps for the sampling system and the condensation particle counters in the trunk of the vehicle and connect them to the battery.
   5. Place the DTT system in the trunk of the vehicle and fix its position using straps. **Figure 7** and **Figure 8** show the DTT system in the trunk of a car. Connect the system to the mobile battery pack.
   6. Connect the two inlet MFCs of the DTT system to a stationary pressurized air supply. Connect the two outlet MFMs of the DTT system to the vacuum pump.
   7. Use appropriate tubing to drive the exhaust of the pump outside the vehicle.
   8. Connect the DTT system to the measurement laptop using a USB cable.
   9. Connect the inlet of the system to the sampling point downstream of the EFM. Connect the system power inlet to the battery. Connect the condensation particle counters' power inlets to the battery pack.
   10. Connect the CPCs to the respective external vacuum pump.
   11. Mount the butanol bottles of the CPCs firmly on the frame of the dilution system as far away as possible from the vehicle occupants.
   12. Make sure that the cap is screwed on tight and does not open during the measurement drive when accelerating.
   13. Use appropriate tubing to drive the exhaust of the CPCs and/or the external pump outside the vehicle. Connect the CPCs to the measurement laptop using USB cables.
       NOTE: **Figure 9** shows the prepared vehicle. The DTT system is installed in the trunk of the vehicle. A commercially available PN-PEMS system is also installed to use as a reference for the regulated emission of solid particles >23 nm.

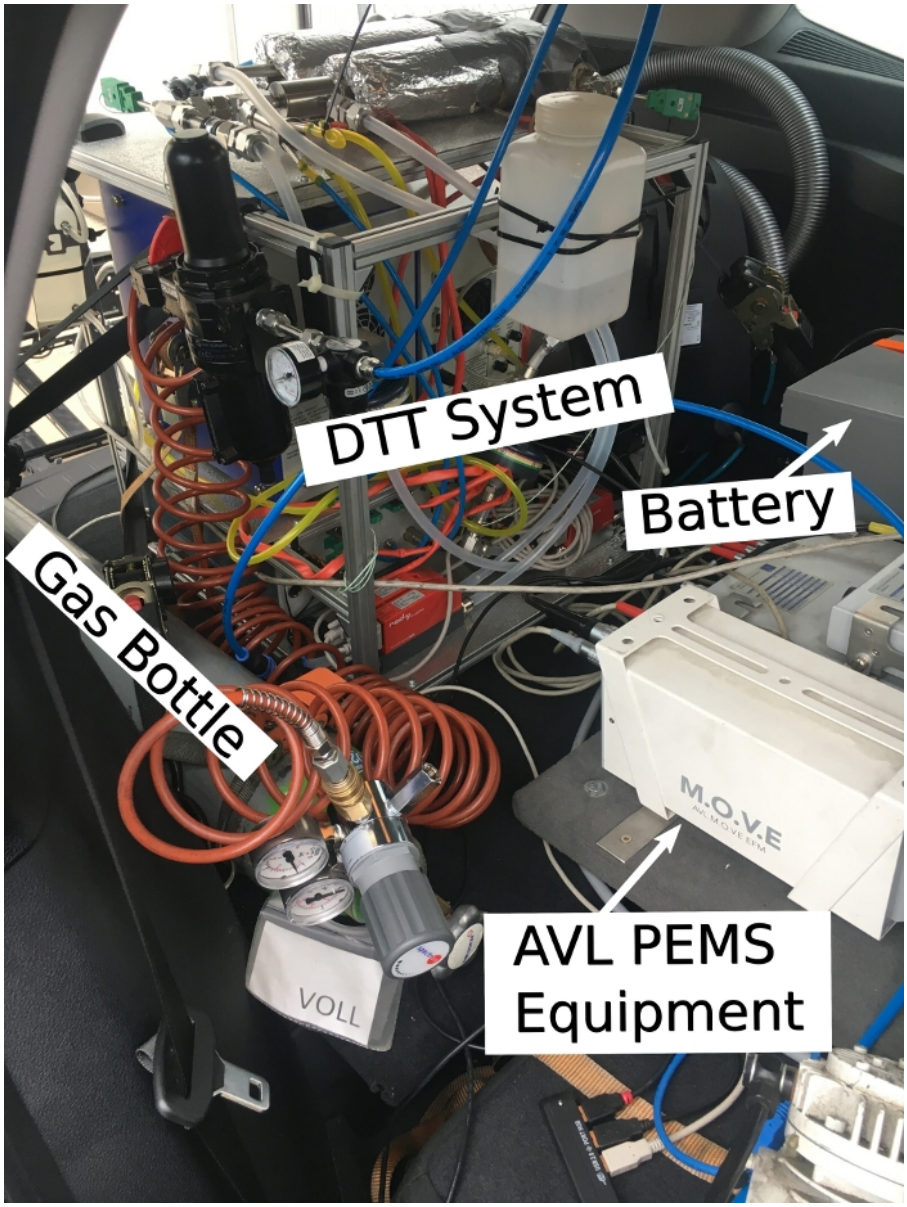

Figure 7: DTT PEMS from inside the vehicle. Please click here to view a larger version of this figure.

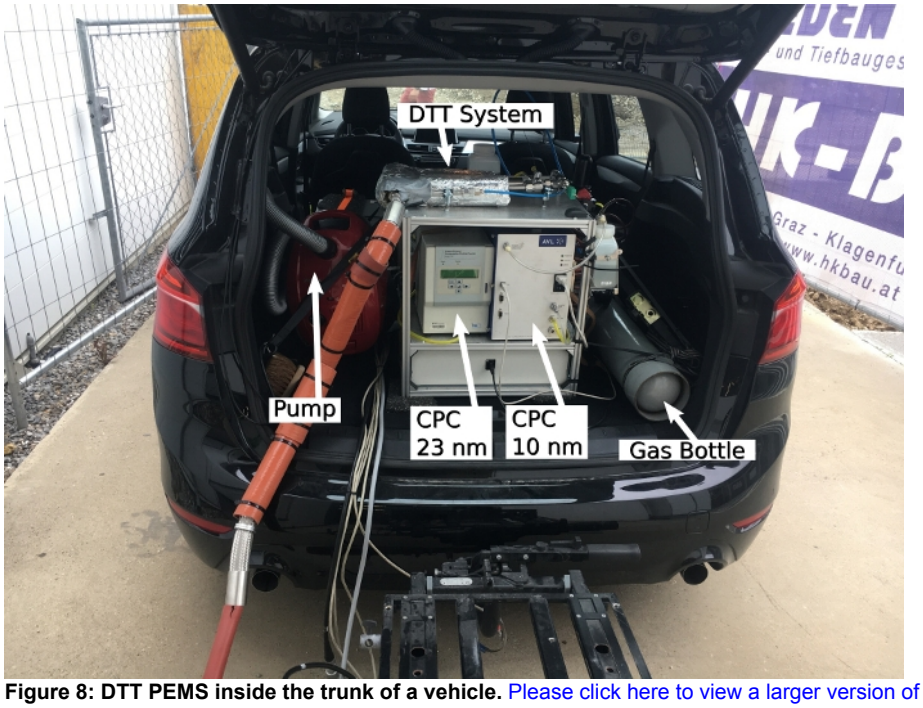

Figure 8: DTT PEMS inside the trunk of a vehicle. Please click here to view a larger version of this figure.

Figure 9: Vehicle with commercially available PN-PEMS (AVL MOVE) and DTT PEMS installed. Please click here to view a larger version of this figure.

3. Measurement operation

1. Heating and starting up the measurement system
    1. Switch on the two CPCs and their external vacuum supply.
    2. Open the CPCs software on the measurement laptop and establish communication with the CPCs. The communication can either run via the instrument's proprietary software or via serial communication as described in the CPC manual.
    3. Close the needle valves downstream of the MFMs.
    4. Switch on the DTT sampling system pump.
    5. Switch on the sampling system by pushing the red switch down.
    6. Open the LabVIEW DTT application on the computer. The communication with the system starts automatically.
    7. The graphical user interface (GUI) of the DTT LabVIEW application now displays the flows in and out at dilution stages 1 and 2, which should be 0.00 L/min. If not, double check that the needle valves are closed properly.
    8. Enter the mass flow drawn by the connected measurement instruments in sL/min. If the flow drawn by the instruments is unknown, measure it using a handheld mass flow meter (e.g., Vögtlin red-y compact series). Reconnect the tubing after measuring the flows drawn by the CPCs.
    9. Slowly open the needle valves until both "Flows out" reach 10.0 ± 0.5 sL/min. Both "Flows in" will increase to the same values as the corresponding "Flows out".
    10. Adjust the "Add Flow" (i.e., difference between dilution air flow and excess flow) of both dilution stages to get Q_{CS} = 1.0 ± 0.1 L/min through the catalytic stripper and a sample inlet flow of Q_{sample} = 1.0 ± 0.1 L/min.

11. Click on the "**Heater**" tab to set the heater temperatures.
12. Set the heater temperatures of the dilution air supply, the first porous tube diluter, and the catalytic stripper to 350 °C. The system will now start to heat up. Below the "**Set**" interfaces the current temperature and heating power percentages are displayed.
13. Wait until the gas temperature downstream dilution stage 1("T DilStage 1" in the GUI) reaches 290 °C before starting the measurement drive. This will take approximately 20 min.

2. Data logging
    1. Start to log the data on the measurement devices connected to the DTT sampling system.
    2. Start to log the data of the sampling system by pressing the "**Start Data Logging**" button and choose a path and a file name in the pop-up window. The log file path will be displayed and the green light will indicate that data are saved. The system data are logged at a frequency of 2 Hz.
    3. Log the particle concentration data of the CPC using appropriate software. This can either be the manufacturer's or a serial communication software (e.g., PuTTY).
    4. Start logging the exhaust flow with the EFM.

3. Driving
    1. Before driving the selected route, disconnect the battery's charging cable and switch from stationary pressurized air supply to the gas bottle.
    2. Drive the selected route.

4. After driving
    1. Press "**Logging ...**" to stop recording data. Shut down the instruments.

5. Recharge the battery to prepare for the next drive.

4. Data analysis

1. Import the data from the sampling system, the EFM (for exhaust flow), and the measurement devices into the same data analysis program.
2. Perform the time alignment considering the time the exhaust needs to be transported from the tailpipe to the measurement devices. The transport time t_{dil} through the dilution system is 2.5 s. The transport time t_{sample} through the sampling line can be calculated as follows:

$$t_{sample} = \frac{A_{sample} * l_{sample}}{\dot{Q}_{sample}}$$

Where t_{sample} is the transport time through the sampling line in seconds, t_{dil} is the transport time through the dilution system (2.5 s), A_{sample} is the cross section area of the sampling line in m^2, l_{sample} is the length of the sampling line from sample point to the dilution system inlet in meters, and $\dot{Q}_{sample}$ is the DTT dilution system sample flow in m^3/s. Add t_{sample} to t_{dil} to get the total delay time t_{total}:

$$t_{total} = t_{sample} + t_{dil}$$

NOTE: As an example, t_{total} for a pipe length of 0.5 m with an internal pipe diameter of 4 mm and sample flow of 1 L/min equals 2.88 s.
Figure 10 shows an example of the time alignment of the measured particle number (blue dotted line) to the time shifted particle number (blue line).

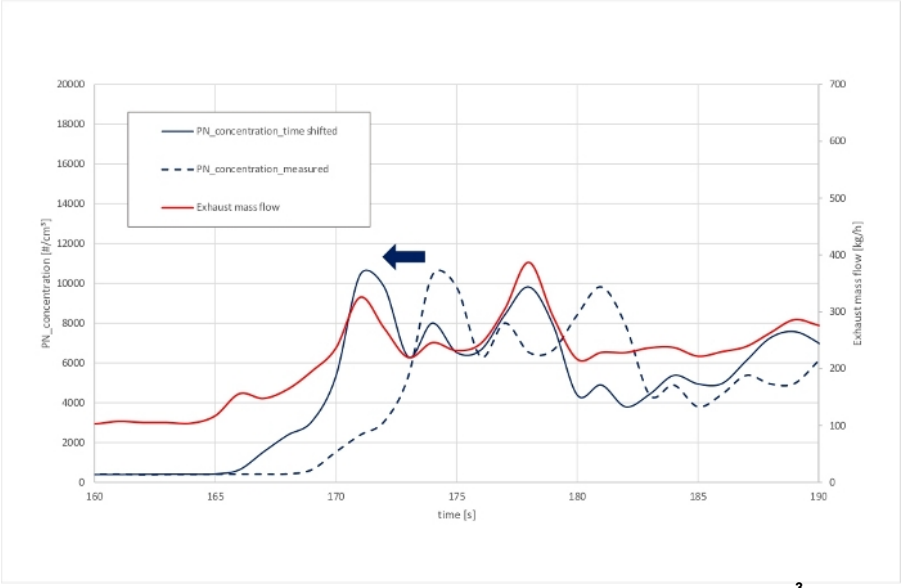

Figure 10: Example of time alignment of measured particle number PN in #/cm^3 compared to the measured exhaust mass flow in kg/h.
Please click here to view a larger version of this figure.

3. To be able to calculate the particle number in *PN* #/s, the exhaust gas volume flow $\dot{V}_{exhaust\_norm}$ in cm^3/s must be calculated first according to the following formula:

$$\dot{V}_{exhaust_{norm}} = \frac{\dot{m}_{exhaust} * R * T_{norm}}{p_{norm}}$$

where $\dot{V}_{exhaust\_norm}$ is the exhaust standard volume flow in m^3/s, $\dot{m}_{exhaust}$ is the measured exhaust mass flow in kg/s, R is the ideal gas constant for air (287.1 J/kg*K), T_{norm} is the temperature at standard conditions (273.15 K), and p_{norm} is the pressure at standard conditions (101,330 Pa). With this exhaust volume flow at standard conditions the particle number can be calculated by multiplying the $\dot{V}_{exhaust\_norm}$ with the dilution ratio DR of the sampling system, the concentration c_{PN} measured by the CPCs, and the factor 10^6 (for the conversion from m^3 to cm^3).

$$\dot{PN} = \dot{V}_{exhaust_{norm}} * c_{PN} * DR * 10^6$$

4. To correct for particle losses, multiply the particle exhaust flow times the particle number concentration rate with the system particle concentration reduction factor (*PCRF*) instead of the dilution ratio *DR*. The determination of *PCRF* is described in the calibration instruction section 1:

$$\dot{PN}_{corr} = \dot{V}_{exhaust_{norm}} * c_{PN} * PCRF$$

Representative Results

Calibration Data (Particle Penetration)**:**

Figure 11 shows an exemplary plot of the relative particle penetration of the DTT system as a function of the particle mobility diameter. The corresponding data have been measured and evaluated as described in instruction section 1. The plot shows that the deviations between two measurement points at the same mobility diameter were less than 5%. Deviations larger than 10% indicate instabilities in the experimental setup. In this case, the calibration had to be repeated with increased warm up stabilization times. Both the warm up time (typically 30 min) and the stabilization time (typically 30 s) increased by a factor of 1.5.

The particles passing through the DTT system were lost due to diffusion and thermophoresis. Thermophoretic losses were caused by a temperature gradient drawing particles towards the walls of the sampling system. This is a particle size independent effect[29]; in contrast, diffusion is highly particle size dependent. A concentration gradient caused a net particle flux towards the walls where particles were lost. The diffusivity rising with lower particle size made this the dominant loss mechanism for particles ≤10 nm. The lines in **Figure 11** indicating thermophoretic, diffusional, and total losses demonstrate the respective particle size dependencies. For the diffusional losses, this function was used to illustrate the approximate particle size dependency:

$$P = \exp\left(\frac{-a}{D(d_p)}\right)$$

The penetration P depends on a fit parameter a and the diffusion coefficient D:

$$D = \frac{kTC_c}{3\pi\eta d_p}$$

The diffusion coefficient depends on the Boltzmann constant k, the absolute temperature T, the viscosity η, the particle diameter d_p, and the Cunningham slip correction factor C_c, which is a function of the mean free path and the particle diameter[29].

The data illustrated in **Figure 11** resulted in the following mean particle penetration efficiency P_{mean}:

$$P_{mean} = \frac{P_{30nm} + P_{50nm} + P_{100nm}}{3} = \frac{0.795 + 0.825 + 0.825}{3} = \underline{0.815}$$

The particle size where the penetration efficiency amounts to 50% is referred to as d_{50}. The d_{50} describes the penetration cutoff characteristic of a system. For the DTT system the d_{50} was 11 nm. The d_{50} is shown in **Figure 11**.

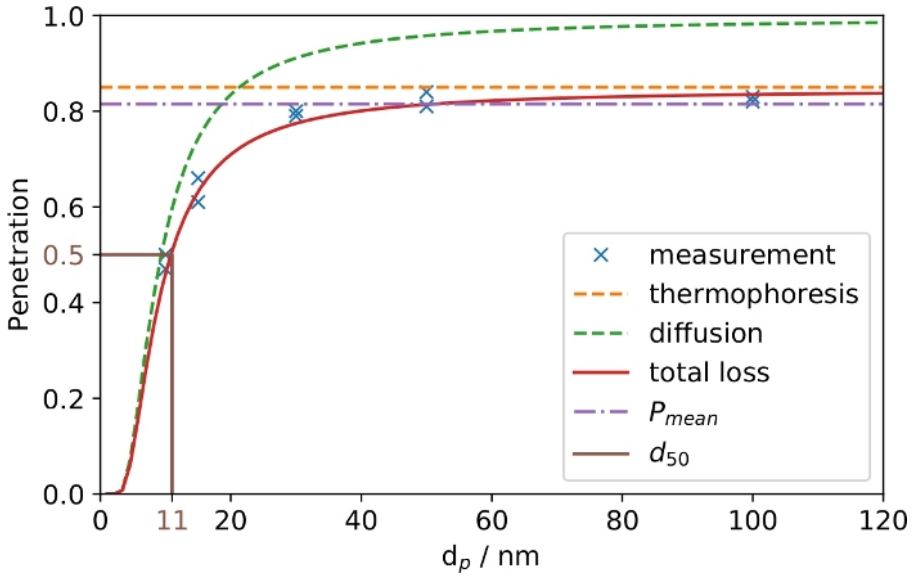

Figure 11: Particle penetration as a function of particle mobility diameter.
Points marked in blue are measurement results. The dashed lines in orange and green indicate the losses associated with thermophoresis and diffusion, respectively. The red line represents the total losses as the sum of diffusional and thermophoretic losses. The dotdashed purple line shows the average particle penetration Pmean as calculated in the calibration measurement instruction section 1. Please click here to view a larger version of this figure.

Solid Particle Number**:**

Figure 12 shows the particle number emission rate over time for the first ten minutes of an RDE measurement drive. The data from the DTT PEMS using a 10 nm and a 23 nm CPC are shown together with data from a commercially available 23 nm cut point system. The particle emission rates were calculated from the respective particle concentrations multiplied by the exhaust flow rate as described above in the data analysis instruction section 4. The reference instrument (AVL MOVE) relied on a diffusion charger for the particle number concentration measurement. Despite the different sensor principles, the data measured with the DTT PEMS were overall in very good agreement with the data measured by the commercially available PEMS. Sharp downwards pointing spikes in all three signals occurred because the particle measurement devices can report zero particle concentrations temporarily and zeros cannot be displayed in logarithmic plots. The particle emissions measured with the 10 nm CPC were very close to the emissions measured with the 23 nm CPC for the majority of the time period shown in **Figure 12**. However, right at the beginning between 10 s and 25 s there was an occurrence of significant <23 nm particle emission. The DTT 10 nm signal was significantly higher than the 23 nm signal of the DTT system and the AVL MOVE. In this case, >50% of the total number of particles emitted were between 10 nm and 23 nm. Cold start dynamic processes in non-thermal equilibrium can cause particle size distributions to differ from emissions from a hot vehicle[30]. The discussion of these complex processes is beyond the scope of this work. Further information on this topic can be found in the literature[31,32,33].

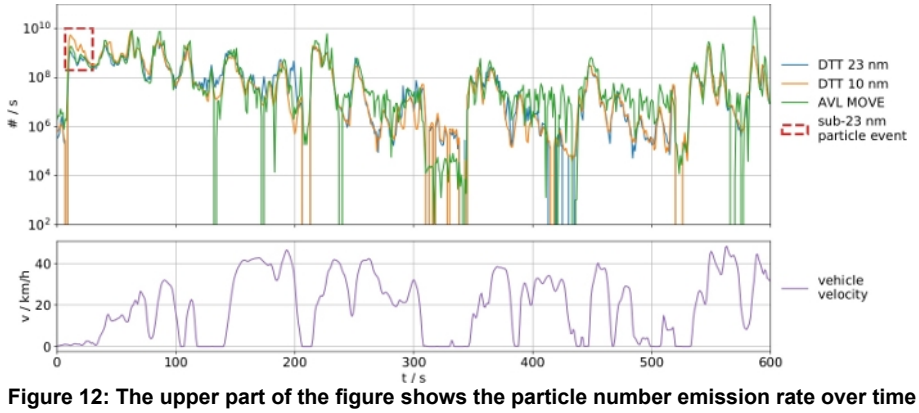

Figure 12: The upper part of the figure shows the particle number emission rate over time for the first 10 mins of an RDE measurement drive.
Data measured with the DTT PEMS using 10 nm and 23 nm CPC and a commercially available 23 nm cut point system (AVL MOVE) are used as a reference. The lower part of the figure shows the velocity of the vehicle. Please click here to view a larger version of this figure.

Discussion

This work presents the DTT sampling system and its application as a portable emission measurement system. The system was designed and constructed within the EU Horizon 2020 project DTT to enable particle number emission measurements below the current legislative particle size limit of 23 nm. The system's versatility enables the assessment of the regulated solid particle number emissions as well as total particle

emissions and studies on secondary aerosols. To interpret measurement results accurately, a calibration procedure is necessary with the DTT system. This is to evaluate the relative particle penetration for different particle sizes, to be able to calculate a correction factor that accounts for the particle losses. It is critical to provide sufficient warm up time for the sampling system itself and the rest of the experimental setup to reach thermal equilibrium and achieve accurate calibration measurement results.

The application of the DTT system for the measurement of solid particle number emissions with a lower particle size cutoff of 23 nm (current regulation) and 10 nm (experimental) is described. To be able to assess particle number emissions of a vehicle it is necessary to determine the particle number concentration and the exhaust mass flow rate. The DTT system covers the particle number concentration measurement. The exhaust mass flow is measured using an exhaust flow meter (EFM). It is critical to install the EFM according to the manufacturer's instructions. Erroneous measurements of the exhaust flow rate directly affect the deduced emission rates. When processing the measured data, it is important to perform an accurate time alignment of the particle concentration data and the exhaust flow data. This is necessary because the emission rate is the exhaust flow rate multiplied by the particle number concentration. If the two signals are not aligned correctly, the emissions over the whole drive can significantly deviate from the real emissions.

The DTT system is not a commercial device but a versatile research tool. It is used to investigate unregulated vehicle emissions as opposed to performing certification measurements validating compliance with current regulations. The high versatility comes at the cost of increased energy and dilution air consumption. When using the system for mobile measurements, the weight added to the vehicle due to the battery (30 kg) and gas bottle (20 kg) to cover the energy and air consumption of the system must be kept in mind. The total weight added to the car when measuring the PN emissions with the DTT system is approximately 80 kg, which is comparable to another person being transported in the vehicle. The added weight can lead to slightly increased emissions, especially if the drive includes a great deal of acceleration and/or hills.

The DTT system can be used to investigate the unregulated <23 nm particle number exhaust emissions. Both solid and total particle number emissions can be measured. Furthermore, it can be a useful tool to study the complex field of secondary aerosol formation. Another possible application of the system is the measurement of automotive brake wear particles. A significant fraction of the particles emitted during braking events can be smaller than 30 nm[34]. With a d_{50} of approximately 11 nm, the DTT system is suitable for studying these emissions. Although it is known that non-exhaust emissions contribute almost equally to traffic-related PM_{10} emissions[35], non-exhaust particle emissions are still unregulated. This is due to the complex and seldom reproducible process of particle generation, making it very difficult to set regulatory actions. Furthermore, the chemical composition and the related toxicity of organic brake wear particles is still widely unknown[35].

The DTT system is a useful tool to improve our understanding of both exhaust and non-exhaust traffic-related particle emissions.

Disclosures

The authors have nothing to disclose.

Acknowledgments

This work is conducted in the framework of the H2020 project DownToTen. This project has received funding from the European Union's Horizon 2020 research and innovation programme under grant agreement Nr. 724085.

References

1. Dunne, M. GRPE Particulate Measurement Programme (PMP). *7th ETH-Conference on Combustion Generated Nanoparticles.* (2003).
2. Sydbom, A. et al. Health effects of diesel exhaust emissions. *European Respiratory Journal.* **17** (4), 733–746 (2001).
3. *Vehicle Regulations - Transport - UNECE.* <https://www.unece.org/trans/main/welcwp29.html>. (2020).
4. Andersson, J., Wedekind, B. *DETR / SMMT / CONCAWE Particulate Research Programme 1998-2001 SUMMARY REPORT.* (2001).
5. Samaras, Z. et al. *Publication data form 1. Framework Programme European Commission-DG TrEn, 5 th Framework Programme Competitive and Sustainable Growth Sustainable Mobility and Intermodality 2. Contract No.* at <http://vergina.eng.auth.gr/mech/Lat/particulates/private/index.htm>. (2005).
6. Andersson, J., Giechaskiel, B., Muñoz-Bueno, R., Sandbach, E., Dilara, P. *Particle Measurement Programme (PMP) Light-duty Inter-laboratory Correlation Exercise (ILCE_LD) Final Report Institute for Environment and Sustainability 2007 EUR 22775 EN.* at <http://publications.jrc.ec.europa.eu/repository/bitstream/111111111/429/2/7386 - PMP_LD_final.pdf>. (2007).
7. Rönkkö, T. et al. Effects of gaseous sulphuric acid on diesel exhaust nanoparticle formation and characteristics. *Environmental Science and Technology.* **47** (20), 11882–11889 (2013).
8. Liati, A., Dimopoulos Eggenschwiler, P. Characterization of particulate matter deposited in diesel particulate filters: Visual and analytical approach in macro-, micro- and nano-scales. *Combustion and Flame.* **157** (9), 1658–1670 (2010).
9. Liati, A., Schreiber, D., Arroyo Rojas Dasilva, Y., Dimopoulos Eggenschwiler, P. Ultrafine particle emissions from modern Gasoline and Diesel vehicles: An electron microscopic perspective. *Environmental Pollution.* **239**, 661–669 (2018).
10. Kittelson, D. B. Recent Measurements of Nanoparticle Emissions from Engines. *Current Research on Diesel Exhaust Particles Japan Association of Aerosol Science and Technology.* 5 (2001).
11. Bruno, T. J., Ott, L. S., Smith, B. L. Composition-Explicit Distillation Curves of Waste Lubricant Oils and Resourced Crude Oil: A Diagnostic for Re-Refining and Evaluation. *American Journal of Environmental Sciences.* **6** (6), 523–534 (2010).
12. Giechaskiel, B., Vanhanen, J., Väkevä, M., Martini, G. Investigation of vehicle exhaust sub-23 nm particle emissions. *Aerosol Science and Technology.* **51** (5), 626–641 (2017).
13. Andersson, J. Call: H2020-GV-2016-2017: DownToTen. *48th PMP Update.* at <https://wiki.unece.org/download/attachments/73924923/PMP-48-10 DTT_Update_Nov_2018.pdf> (2018).
14. Andersson, J. *PMP 50th Session - Transport - Vehicle Regulations - UNECE Wiki.* at <https://wiki.unece.org/display/trans/PMP+50th+Session>. (2019).

15. Martikainen, S. et al. Dependence of Dilution Performance of a Prototype Setup for Sampling Non- volatile Engine Exhaust Particles down to ten Nanometer in Diameter on Pressure Variations in Sample Line. *22nd ETH Conference on Combustion Generated Particles.* 1, at <http://www.nanoparticles.ch/2018_ETH-NPC-22/2018_ETH-NPC-22_book_of_abstracts_posters.pdf> (2018).
16. Landl, L., Vuckovic, T., Hausberger, S. PEMS accuracies under harsh environmental conditions. *23rd Transport and Air Pollution Conference, Thessaloniki 2019.* at <https://www.tapconference.org/assets/files/previous-conferences/proceedings/2019_Proceedings.zip> (2019).
17. Karjalainen, P. et al. Time-resolved characterization of primary particle emissions and secondary particle formation from a modern gasoline passenger car. *Atmospheric Chemistry and Physics.* **16** (13), 8559–8570 (2016).
18. Mikkanen, P., Moisio, M., Keskinen, J., Ristimäki, J., Marjamäki, M. Sampling method for particle measurements of vehicle exhaust. *SAE Mobilus.* 2001-01-0219 (2001).
19. Giechaskiel, B. et al. Review of motor vehicle particulate emissions sampling and measurement: From smoke and filter mass to particle number. *Journal of Aerosol Science.* **67**, 48–86 (2014).
20. EC Commission Regulation (EU) 2017/1154. *Official Journal of the European Union.* at <https://eur-lex.europa.eu/eli/reg/2017/1154/oj> (2017).
21. Mamakos, A., Khalek, I., Giannelli, R., Spears, M. Characterization of combustion aerosol produced by a mini-CAST and treated in a catalytic stripper. *Aerosol Science and Technology.* **47** (8), 927–936 (2013).
22. Jing, L. Standard Combustion Aerosol Generator (SCAG) for Calibration Purposes. *Atmospheric Environment.* **27** (8), 1271–1275 (1999).
23. Moore, R. H. et al. Mapping the operation of the miniature combustion aerosol standard (Mini-CAST) soot generator. *Aerosol Science and Technology.* **48** (5), 467–479 (2014).
24. Giechaskiel, B. et al. Implementation of portable emissions measurement systems (PEMS) for the real-driving emissions (RDE) regulation in Europe. *Journal of Visualized Experiments.* (118), 54753 (2016).
25. EC Commission Regulation (EU) 2017/1151. *Official Journal of the European Union.* (692), 1–643, at <https://eur-lex.europa.eu/eli/reg/2017/1151/oj> (2017).
26. EC REGULATION (EC) No 715/2007 OF THE EUROPEAN PARLIAMENT AND OF THE COUNCIL. *Official journal of the European Union.* at <https://eur-lex.europa.eu/Legal-content/EN/ALL/?uri=CELEX:32007R0715> (2007).
27. EC DIRECTIVE 2007/46/EC OF THE EUROPEAN PARLIAMENT AND OF THE COUNCIL. *Official journal of the European Union.* at <https://eur-lex.europa.eu/Legal-content/EN/ALL/?uri=CELEX:32007L0046> (2007).
28. EC Commission Regulation 2790/99. *Official Journal of the European Communities.* at <https://eur-lex.europa.eu/Legal-content/EN/TXT/?uri=CELEX%3A31999R2790> (1999).
29. Hinds, W.C. *Aerosol technology: properties, behavior, and measurement of airborne particles.* John Wiley & Sons. (2012).
30. Badshah, H., Kittelson, D., Northrop, W. Particle Emissions from Light-Duty Vehicles during Cold-Cold Start. *SAE International Journal of Engines.* **9** (3), 1775–1785 (2016).
31. Andersson, J. et al. First results of vehicle technology effects on sub-23nm exhaust particle number emissions using the DownTo10 sampling and measurement system. *22nd ETH-Conference on Combustion Generated Nanoparticles,.* at <https://www.nanoparticles.ch/archive/2018_Andersson_PR.pdf> (2018).
32. Giechaskiel, B., Manfredi, U., Martini, G. Engine exhaust solid sub-23 nm particles: I. Literature survey. *SAE International Journal of Fuels and Lubricants.* **7** (2014-01–2834), 950–964 (2014).
33. Weiss, M., et al. Including cold-start emissions in the Real-Driving Emissions (RDE) test procedure. *Publications Office of the European Union.* https://op.europa.eu/en/publication-detail/-/publication/66874f0c-fd85-11e6-8a35-01aa75ed71a1/language-en/format-PDF/source-120155396, (2017).
34. Mathissen, M., Scheer, V., Vogt, R., Benter, T. Investigation on the potential generation of ultrafine particles from the tire-road interface. *Atmospheric Environment.* **45** (34), 6172–6179 (2011).
35. Grigoratos, T., Martini, G. Brake wear particle emissions: a review. *Environmental Science and Pollution Research.* **22** (4), 2491–2504 (2015).

Paper 2

Aerosol gas exchange system (AGES) for nanoparticle sampling at elevated temperatures: Modeling and experimental characterization

SCIENTIFIC REPORTS
nature research

OPEN

Aerosol gas exchange system (AGES) for nanoparticle sampling at elevated temperatures: Modeling and experimental characterization

Markus Bainschab[1*], Sampsa Martikainen[2], Jorma Keskinen[2], Alexander Bergmann[1] & Panu Karjalainen[2]

An aerosol gas exchange system (AGES) for nanoparticle sampling at elevated temperatures was developed, modeled, and further characterized with laboratory tests with respect to gas exchange efficiency and particle losses. The model describing the gas exchange was first verified with oxygen and later studied with several inert gases having molecular masses between 18 and 135 u. The exchange rate of the lightest compounds exceeds 90% efficiency at the flow rates used. In order to reach similarly high removal efficiencies for larger molecules, the residence time in the AGES has to be increased. The removal of sticky gases was studied with gaseous sulfuric acid. Results agreed with the model where the boundary condition is zero concentration on the wall. The AGES exhibits very limited particle losses (<5%) for mono-disperse 6 nm particles. Furthermore, diffusional losses for particles down to 1.2 nm were measured utilizing polydisperse aerosol. The experimental findings are in good agreement with the model derived. As both, gas exchange rate and particle losses, rely on the physical effect of diffusion, an optimization for enhanced gas exchange efficiency will come at the cost of increased diffusional particle losses. The presented model can be used as a tool to redesign and optimize the AGES for a desired application. With an application targeted design, particle dilution can be avoided, which can lead to improved results in many fields of aerosol measurement.

The quality of measurement results in aerosol studies is often not limited by the applied measurement instrument but by uncertainties introduced in the course of the sampling procedure. Sampling is especially difficult in the presence of the smallest nanoparticles and when the aerosol contains a large quantity of semi-volatile particulate matter that can be found in either gaseous or condensed states depending on sampling conditions, e.g. residence time and temperature in the sampling system. These extremely challenging aerosol measurement fields include for example engine emission studies[1–4] and atmospheric studies[5–7]. The sampling phase must (1) reduce particle concentrations to levels suitable for the measurement instruments, and (2) prevent condensation of gases on the surfaces of the sampling system itself or inside the measurement instruments. Often particles of a certain degree of volatility are of special interest. In engine emission studies, the fraction of particles that do not evaporate below 350 °C are most commonly the focus[8]. This focus sets additional requirements to the sampling procedure because the particle fraction of interest has to be isolated. However, existing methods for the isolation of non-volatile particles exhibit major drawbacks. This work presents an alternative method that can overcome many drawbacks of the existing solutions and is applicable to different fields of aerosol measurement.

Until recently, the type approval of vehicles required the determination of particulate mass emissions over a test cycle. The particle emissions were measured from the filter mass increase when diluted vehicle exhaust was collected on a paper filter. The introduction of diesel particulate filters (DPF) reduced emitted particle mass concentrations to levels where they can no longer be reliably measured gravimetrically. This made the transition to alternative particle measurement methods and metrics inevitable. Based on the studies of the Particle Measurement Programme (PMP) group (a programme managed by the UN-ECE), a methodology was introduced in the European legislation to count non-volatile particles – those that are not vaporized at 350 °C– of diameter >23 nm from diluted exhaust over a specific test cycle. Recently, the PMP methodology was extended

[1]Graz University of Technology, Insititute of Electronic Sensor Systems, Graz, 8010, Austria. [2]Tampere University, Aerosol Physics Laboratory, Tampere, 33720, Finland. *email: m.bainschab@tugraz.at

to assess real driving emissions (RDE) of particle number (PN) by Portable Emission Measurement Systems (PEMS), mounted on vehicles in real-world conditions. In this case, measurements must be conducted for practical reasons from the raw exhaust. While requirements exist for legislative measurements regarding sampling and transport of the aerosol sample, such requirements do not necessarily allow appropriate quantification of particle number emissions from raw exhaust measurements[8]. This is particularly prevalent for particle sizes smaller than 23 nm and especially below 10 nm. To reach the so called non-volatile particle fraction, heated sampling systems like thermodenuders (TDs)[9,10] or catalytic strippers (CSs)[11,12] have frequently been applied after sample dilution. TDs collect gases on the surface of activated charcoal, hence they require regular service. In the CS, gaseous organic compounds are oxidized and sulphuric acid is stored and thus these also require service and regeneration. Both TD and CS systems efficiently remove semi-volatile material, but due to their large surface areas, they often induce high losses of sub-10 nm particles. The current PMP protocol relies only on heated sampling and dilution to measure particles larger than 23 nm[8], and in the near future down to 10 nm. Maintaining comparable levels of accuracy in future regulatory particle number measurements would most likely require sampling systems that actively remove volatile compounds while exhibiting limited diffusional particle losses. This means that alternative exhaust conditioning approaches, apart from the existing CS, TD and the PMP method, are needed.

As an example, a concept of a counter flow denuder (CoFD) was recently published, where the working principle consists of an exchange of the carrier gas of an aerosol sample through diffusion across a cylindrical porous glass tube to a purge gas flow[13]. In the CoFD, the removal efficiency of gases increased with a lower sample flow rate and a higher purge-to-sample gas flow rate ratio. The pore size of the micro-porous glass did not affect the gas removal efficiency and particle penetration efficiency. High particle penetration (94% penetration for 20 nm particles) was observed experimentally. The values agreed with the theoretical estimation of diffusion losses.

In this work, a complete sampling system was constructed using the principles of CoFD. In addition, adjacent heaters, flow control, and a data collection system were implemented. The applicability of this aerosol gas exchange system (AGES) tolerating about 200 °C was tested with a synthetic laboratory aerosol. In the tests, both gas exchange efficiencies and particle losses were studied. Gas exchange efficiencies were studied using several gases of varying molecular masses. The particle losses were characterized down to 1.2 nm with Ag nanoparticles. A model describing the performance was derived, calibrated and experimentally validated.

The AGES system is a novel approach to the world of engine exhaust aerosol measurement, allowing robust quantification of particle properties down to the nanometre regime for research as well as legislative purposes. Apart from the application in exhaust particle measurements, the AGES can also allow for improved results in other fields of aerosol measurement. One example is the assessment of chemical properties of aerosol nanoparticles, where a separation of particles and carrier gas or comprehensive knowledge about the composition of the carrier gas is a requisite. Recently a method was presented that relies on dilution with argon to enable the application of an inductively coupled plasma mass spectrometer (ICP-MS) for the size-resolved elemental analysis of nanoparticles[14,15]. Carrier gas exchange instead of dilution would yield higher particle concentrations at the measurement instrument and hence a reduced limit of detection.

The operation parameters of the AGES can be tuned to meet the requirements of specific applications. This enables the AGES to act as a standalone sampler for aerosol instruments because all the gaseous impurities from the original exhaust can be removed in a single system. This opens new opportunities to sampling from exhaust flows containing very low levels of particulate matter at very low particle sizes like those from gas engines, jet engines or downstream of a particulate filter (PF).

Instrument Description

The AGES can be applied for removing gaseous compounds of an aerosol at temperatures up to 200 °C. The system's center piece is a counter flow denuder (CoFD)[13]. This device has previously been shown to enable a non-specific removal of gases from an aerosol while exhibiting fractional particle losses below 6% for polystyrene latex (PSL) particles larger than 20 nm. Gas molecules in the sample flow are exchanged by diffusive transport through a Shirasu Porous Glass (SPG, SPG Techno Co. Ltd., Japan)[16] membrane with the shape of a hollow cylinder. The membrane has an outer diameter of 5 mm, a wall thickness of 0.4 mm, a mean pore size of 100 nm and an active length of 200 mm. The anti-parallel flow directions of the the purge gas flow and the sample flow provide a high concentration gradient for the whole length of the denuder. Therefore, gas removal efficiencies close to 100% can be reached. To make the counter flow denuder applicable for challenging environments it is necessary to control the pressure difference between the sample flow line and the purge gas line and to control the temperature of the purge gas flow. A pressure difference between the sampling line and the purge gas line induces a flow through the porous glass membrane. Therefore the pressure difference has to be kept as low as possible to ensure that diffusion dominates the convective mass transport through the porous glass membrane. A pressure control unit was implemented in the AGES to control the pressure difference between purge gas line and sample line. A sensor (Honeywell TSCSNBN005PDUCV) measures the pressure difference between purge gas line and the sample line. A LabVIEW virtual instrument running on a NI myRIO takes the pressure difference as an input parameter for a PID controller that controls the valve of a mass flow controller to minimize the pressure difference. Figure 1 shows a drawing of the aerosol gas exchange system.

Mathematical model. In this section an analytical model is derived to find an approximate form of the removal efficiency as a function of operation parameters and species. The results of a laboratory experiment are used to find the membrane material and flow profile specific parameter R_m^* to adjust the derived general model for the specific denuder.

A mathematical expression for the removal efficiency of the counter flow denuder can be found in the literature[13,17]. However, the equation shown there is not generally applicable for the description of the presented type of denuder. Mathematically speaking, the reason why this equation cannot be applied for the description of the

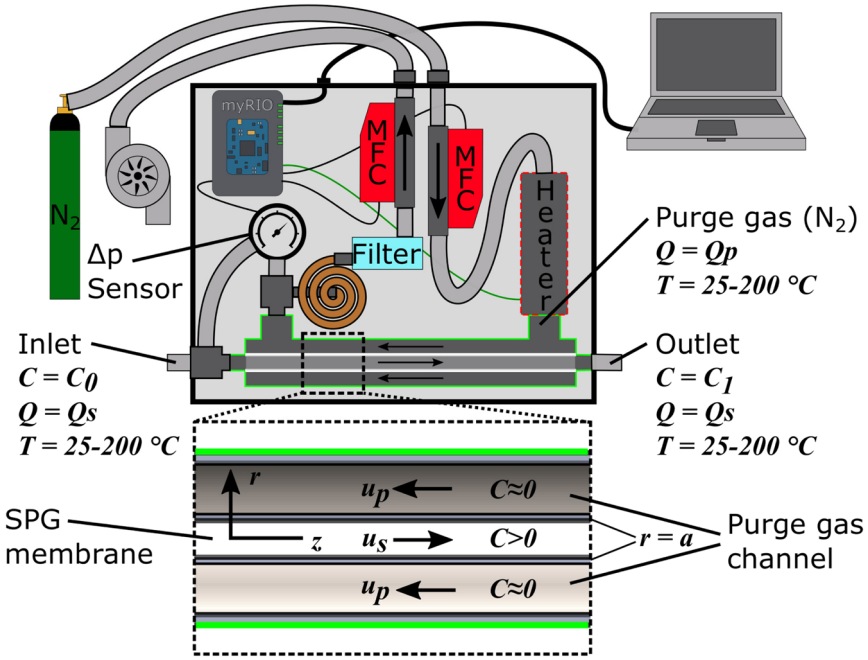

Figure 1. Drawing of the aerosol gas exchange system. The purge gas flow (N2) is controlled with a Vögtlin red-y mass flow controller. The pressure difference between the sample gas channel and the purge gas channel was measured with a Honeywell TSCSNBN005PDUCV. The controllable valve of another Vögtlin red-y MFC is programmed to keep the pressure difference as low as possible (typically <0.5 mbar). The part highlighted with a green frame represents the counter flow denuder. u_p and u_s are the flow velocity in the purge gas channel and the sample channel respectively. C_0 and C_1 are the concentrations of the substance to be removed at the inlet and the outlet of the system.

CoFD is that the boundary conditions do not match the conditions the solutions provided by several groups are based on[18–20]. The provided equations are based on the Dirichlet boundary condition that the concentration C of the substance to be removed is zero at the wall of the denuder ($r = a$).

$$C(r = a) = 0 \tag{1}$$

This condition only holds for gaseous species that are adsorbed at the porous glass membrane, and for particles that stick to the wall upon getting in contact with it. The transport of gaseous substances that are not absorbed by the glass membrane is described correctly with a Robin boundary condition. The diffusive mass flux J through the porous membrane of these substances is proportional to the difference between the concentrations C_s and C_p. C_s is the concentration at the inner wall of the membrane, which limits the sample channel. C_p is the concentration at the outer wall of the membrane, which is the boundary of the purge gas channel.

$$J(r = a) = D\frac{\partial C}{\partial r}\bigg|_{r=a} = \alpha(C_s - C_p) \tag{2}$$

D is the diffusion coefficient of the substance to be removed. The proportionality factor α depends on the diffusion resistance R_m and the convection coefficient h_m, which describes the effectiveness of the convective transport in the purge gas channel. The diffusion resistance R_m is the thickness of the porous membrane d_m divided by the diffusion coefficient of the substance to be removed in the porous membrane D_m. The convective transport in the the purge gas channel dominates the diffusive transport through the membrane ($Q_p = 8$ sl min^{-1}, Péclet number $Pe > 5000$) and the the bulk diffusion coefficient D is linearly proportional to the diffusion coefficient in the porous membrane because for the mean pore size of 100 nm constriction effects can be neglected[21,22]. Consequently, α can be assumed to be directly proportional to D in good approximation for the system described.

$$\alpha = \frac{1}{R_m + \frac{1}{h_m}} = \frac{1}{\frac{d_m}{D_m} + \frac{1}{h_m}} \propto D \tag{3}$$

The mass transport of substances that are not absorbed by the porous glass membrane are mathematically described by the convection-diffusion equation in cylinder coordinates (Eq. (4)) and the boundary condition in Eq. (2). Convection in r-direction is neglected because the sample flow velocities r-component is zero. Diffusion in z-direction is neglected because convection dominates the transport in z-direction ($Pe > 1000$) for typical values of the sample flow Q_s in the AGES.

$$\frac{1}{r}\frac{\partial}{\partial r}\left(r\frac{\partial C}{\partial r}\right) + \frac{u_z}{D}\frac{\partial C}{\partial z} = 0 \tag{4}$$

where u_z is the flow velocity in z-direction.

The mathematical problem as described above cannot be solved analytically. In order to provide an approximate mathematical expression for the removal efficiency RE, the analytical solution of a very similar but slightly simpler problem is adapted. Crank[23] provides a time dependent solution for a one-dimensional diffusion problem of the form:

$$\frac{1}{r}\frac{\partial}{\partial r}\left(r\frac{\partial C}{\partial r}\right) = 0 \tag{5}$$

and the boundary condition in Eq. (2). This equation describes the counter flow denuder for 0 sample flow rate. The removal efficiency RE of this system after time t can be written as[23]:

$$RE = 1 - \frac{C_1}{C_0} = 1 - \sum_{n=1}^{\infty} \frac{4L^2\exp(-\beta_n^2 Dt/a^2)}{\beta_n^2(\beta_n^2 + L^2)} \tag{6}$$

where β_n are the solutions of:

$$\beta J_1(\beta) - LJ_0(\beta) = 0 \text{ with } L = \frac{a\alpha}{D} \tag{7}$$

and J_i are the Bessel functions of the first kind of order i.

In order to adapt this solution to the counter flow denuder we first assume plug flow and later account for this simplification by modifying the parameter R_m that describes the diffusion resistance of the porous glass tube. Plug flow means that the flow velocity is equal at all points of the sample channel. As convection is the dominant transport mechanism in z-direction, diffusion in this direction can be neglected. Consequently, the residence time t in the counter flow denuder can be expressed in terms of the volumetric sample flow rate $Q_{s,vol}$, the length of the SPG membrane l and the inner radius of the SPG membrane a:

$$t = \frac{l}{v} = \frac{la^2\pi}{Q_{s,vol}} \tag{8}$$

According to Eq. (8), Eq. (6) can be reformulated as a function of the dimensionless parameter μ.

$$RE = 1 - \sum_{n=1}^{\infty} \frac{\exp(-b_n\mu)}{c_n} \text{ with } b_n = \beta_n^2\pi;\ c_n = \frac{4L^2}{\beta_n^2(\beta_n^2 + L^2)} \text{ and } \mu = \frac{Dl}{Q_{s,vol}} \tag{9}$$

To account for the simplified flow profile in the analytical model accompanied by an increased removal efficiency, the R_m is replaced by the modified parameter R_m^*. This parameter is an effective diffusion resistance, which is the material parameter R_m plus an additional resistance R_{flow} to account for the laminar flow profile.

$$R_m \rightarrow R_m^* = R_m + R_{flow} \tag{10}$$

The transition from R_m to R_m^* is motivated by the similarity of the velocity and concentration profiles in the sample channel. Both profiles have their maximum at the center line of the sample flow channel and decay towards the wall. Because of this overlap the mean residence time of molecules in the denuder is reduced compared to a device with plug flow conditions. Consequently, the probability of molecules reaching the SPG wall within the length of the denuder is decreased. This decrease in probability can be described as a diffusion resistance which is added to the material specific diffusion resistance R_m. It has been shown and applied successfully that kinetic resistances can be added to describe kinetic processes[24,25]. R_m^* is determined experimentally and R_m and R_{flow} are derived from CFD simulations.

Model calibration. In order to proof the validity of the mathematical expression derived, an experiment was performed. The results of this experiment are used to find the parameter R_m^* that describes the diffusion resistance of the SPG membrane and accounts for the laminar flow profile in the sample flow channel. The removal efficiencies RE of O_2 ($D = 0.2\ cm^2\ s^{-1}$) were measured for different sample mass flow rates (standard conditions: $T = 20\,°C$, $p = 1013\,hPa$) at room temperature. The acquired data is used to fit the parameter R_m^*. The dependency of the removal efficiency of R_m^* is described in Eqs (2, 3, 7, 9, and 10). Figure 2 shows a drawing of the experimental setup. Air was used as sample gas and nitrogen was used as a purge gas.

The nitrogen purge gas flow was set to 8 sl min^{-1}. The oxygen concentration in the pressurized air and the outlet of the AGES were measured with an electrochemical AlphaSense O2 A2 sensor. This measurement was repeated for flows between 0.2 sl min^{-1} and 10 sl min^{-1}. Figure 3 shows the O_2 removal efficiency as a function of the sample flow rate Q_s on the left and the removal efficiency as a function of μ on the right.

The sample flow measurement points are converted to values of μ before fitting the function in Eq. 6 with the parameter R_m^*. The right plot in Fig. 3 shows the result of this fit. It can be seen that the derived model fitted with only one parameter agrees with the measured data very well over a large range of removal efficiencies (from under 10% to over 90%. This result shows that the simplification of the problem and the inclusion of the effect

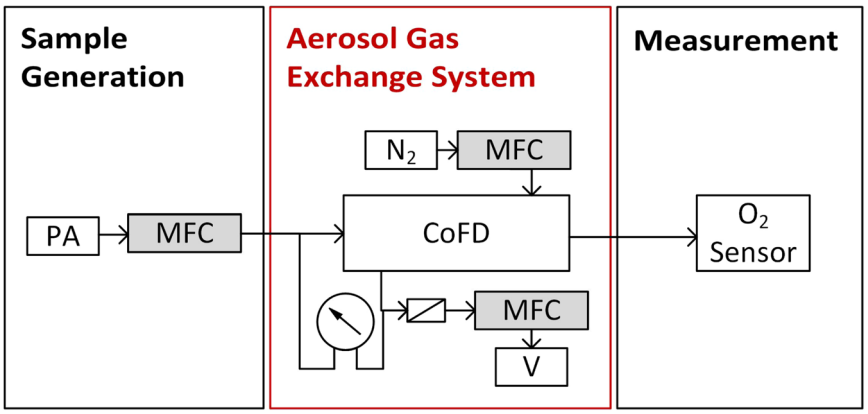

Figure 2. Schematic drawing of the experimental setup for the O_2 removal measurements to find the diffusion resistance R_m of the SPG membrane. The sample flow (air) is controlled with a Vögtlin red-y mass flow controller. The O_2 concentration at the outlet of the AGES is measured with an AlphaSense O2 A2 sensor.

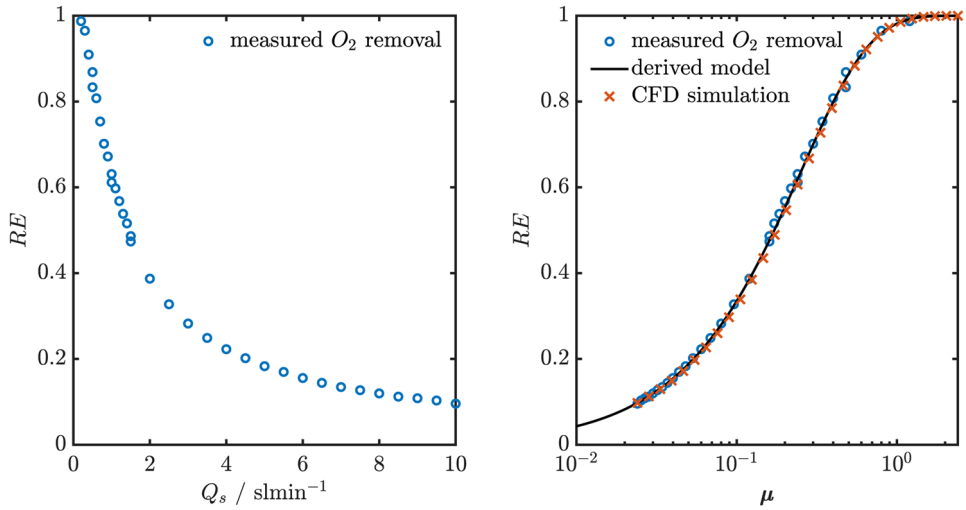

Figure 3. Left: Removal efficiency *RE* of O_2 as a function of the sample flow rate Q_s. Right: Measured O_2 removal efficiency, derived model and CFD simulation results as functions of the dimensionless parameter $\mu = \frac{Dl}{Q_{s,vol}}$. The derived model uses $R_m^* = 137.9\,\mathrm{sm}^{-1}$ as effective diffusion resistance. The CFD simulations were performed taking $R_m = 95.2\,\mathrm{sm}^{-1}$ as diffusion resistance of the porous glass tube.

of the laminar flow profile in the effective diffusion resistance R_m^* is an appropriate way to find a mathematical expression for the removal efficiency as a function of μ, which can be used to calculate the removal efficiency of different gases under different operation parameters. Only considering the first term of the infinite sum in Eq. 9 yields an approximation for the removal efficiency that deviates less than 0.01 from the infinite sum for all values of μ for the presented geometry and materials:

$$RE = 1 - 0.990 * \exp(-3.982\,\mu) \tag{11}$$

Computational fluid dynamics simulation. A 2D axismmetric model of the 20 cm long counter flow denuder was set up in COMSOL to simulate the oxygen removal laboratory experiment and to determine the diffusion resistance R_m of the porous membrane. The simulated geometry consisted of three rectangular domains each having a length of 20 cm. The innermost domain ($r < 2.1$ mm) represents the sample flow channel. The middle domain ($2.1 < r < 2.5$ mm) represents the porous glass membrane. In this domain the diffusion coefficient of the transported species is reduced to account for diffusion resistance R_m of the material. The modified diffusion resistance R_m^* determined experimentally is used as an initial value for R_m. The outermost channel ($2.5 < r < 5$ mm) represents the purge gas channel. The Reynolds number in the sample channel at a flow rate of $Q_s = 1$ sl min^{-1} is $Re = 282$, so the flow can assumed to be laminar at typical operation conditions of the counter flow denuder. Consequently, sample flow and the purge gas flow are simulated with the laminar flow interface. A no slip condition ($\mathbf{u} = 0$) is applied at the interfaces of the three domains and the outer boundary of the purge gas domain. The

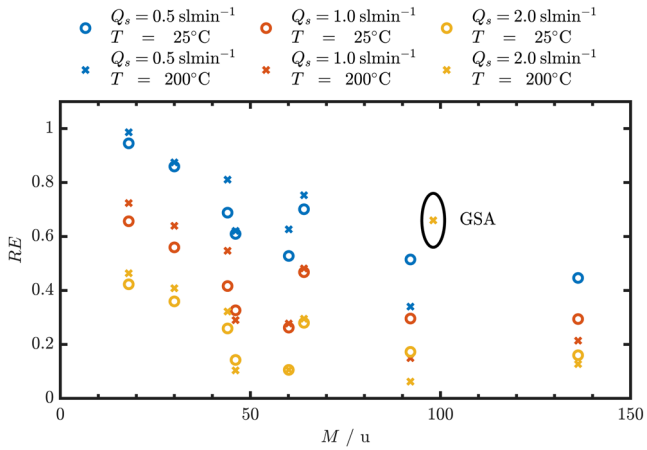

Figure 4. Gas removal efficiencies for the components listed in Table 1 as a function of the molecular mass at different temperatures and sample flow rates.

Substance	Chemical Formula	M/u	D/cm^2 s^{-1} @25 °C	D/cm^2 s^{-1} @200 °C	Typical Upstream AGES Concentration	Measurement Instrument
Water	H_2O	18.0	0.30	0.66	20000 ppm	LI-COR
Nitric oxide	NO	30.0	0.20	0.40	3000 ppm	SIDOR
Oxygen	O_2	32.0	0.20	0.40	21%	AlphaSense O2 A2
Carbon dioxide	CO_2	44.0	0.15	0.31	100000 ppm	LI-COR
Sulfur dioxide	SO_2	64.1	0.13	0.25	100 ppm	SIDOR
Ethanol	C_2H_5OH	46.1	0.12	0.23	3000 ppm	FID
Isopropanol	$CH_3CHOHCH_3$	60.1	0.10	0.20	3000 ppm	FID
Toluene	C_7H_8	92.1	0.09	0.17	4000 ppm	FID
Sulfuric acid	H_2SO_4	98.1	0.08[34]	0.18	7×10^8 molecules/cm^3	API-TOF
α pinene	$C_{10}H_{16}$	136.2	0.07[†]	0.13	4000 ppm	FID

Table 1. Table of substances tested listing the respective molecular weights M, the diffusion coefficients D at 25 °C and 200 °C as well as the measurement instrument used and typical concentrations upstream the AGES of the respective substance. [†]Indicates that the diffusion coefficient was calculated from Lenard-Jones potential parameters[35,36]. Values without superscripts are looked up and evaluated for 25 °C using the Chapman-Enskog theory[36,37].

purge gas flow rate is set to 8 sl min^{-1}. The sample flow rate Q_s is varied between 0.001 sl min^{-1} and 10 sl min^{-1} with 15 steps per decade. The transport of the oxygen is simulated using the transport of dilute species interface, which includes diffusion and convection as transport mechanisms. The oxygen concentration c_0 at the inlet of the sample channel is set to a normalized value of 1 mol m^{-3}. A stationary study is performed for all values of Q_s. The removal efficiency at each point of Q_s is evaluated. The described simulation is repeated for different values of R_m to find the value that leads to the most accurate reproduction of the experimentally found behavior. The value that fulfills this condition is found to be $R_m = 95.2$ sm^{-1}. The results of the simulations with this value of R_m are shown in Fig. 3. The difference of the experimentally determined effective diffusion resistance $R_m{}^* = 137.9$ sm^{-1} and the membrane diffusion resistance $R_m = 95.2$ sm^{-1} is assigned to the diffusion resistance induced by the laminar flow profile $R_{flow} = 42.7$ sm^{-1}.

Results

The data gathered in the experiments described in the methods section was evaluated to determine the AGES' performance in terms of exchange efficiency for different gaseous species and particle losses. The gas exchange efficiency is represented as a function of the molecular mass of the species' molecular mass and the dimensionless parameter μ. The particle losses are evaluated in two particle size regimes covered by the two different experimental approaches. Losses below 3 nm are determined from the data measured with the PSM whereas the losses between 6 nm and 23 nm are covered with the DMA-CPC approach.

Gas exchange. Figure 4 shows the removal efficiency of the tested substances listed in Table 1 as a function of the molecular weight. The removal efficiency was measured at three different sample flow rates at room temperature and at 200 °C with the exceptions of gaseous sulfuric acid (GSA, M = 98.1 u) where only measurements at elevated temperatures were performed.

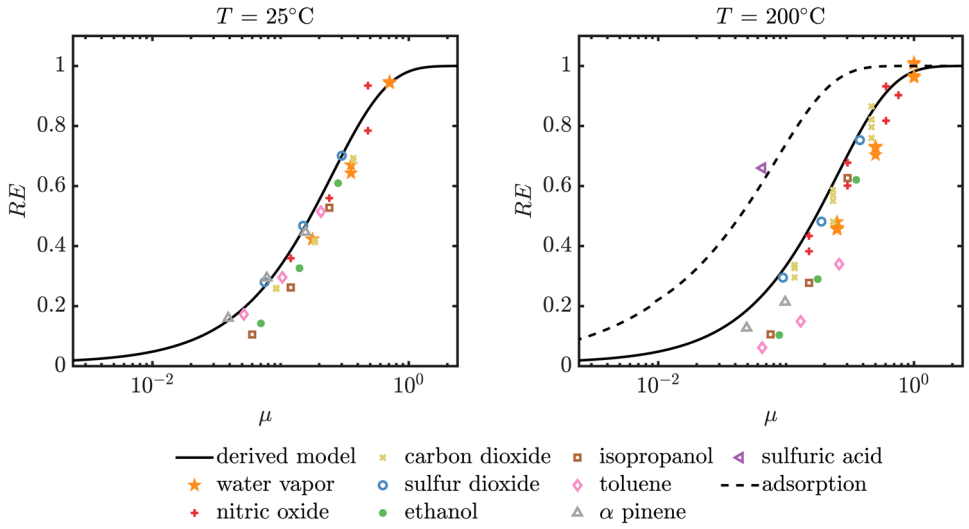

Figure 5. Removal efficiencies calculated from the measured upstream and downstream concentrations as a function of μ for different gaseous compounds at different flow rates. Left: Room temperature (25 °C experiment, Right: Experiment at elevated temperature (200 °C).

The highest removal efficiency observed was 99% measured for H_2O at 200 °C and a sample flow of 0.5 sl min^{-1}. The lowest efficiency value was 6% measured for toluene ($M = 92.1$ u) at 200 °C and a sample flow rate of 2.0 sl min^{-1}. As expected, there is a trend that the removal efficiency rises with lower molecular masses. This is due to the fact that the molecular mass is indirectly proportional to the diffusion coefficient of the respective gaseous substance. The data points at $M = 98.1$ u, which represent sulfuric acid are an exception to this general trend. The reason is the high probability of sulfuric acid molecules to adsorb to surfaces.

Also the SO_2 data points at $M = 64.1$ u protrude from neighboring data point measured under the same conditions. This behavior can be assigned to the relatively high diffusion coefficient of $D = 0.13\,cm^2\,s^{-1}$ given the molecular weight of $M = 64.1$ u of SO_2. Ethanol for example has a substantially lower molecular weight ($M = 46.1$ u) but also a lower diffusion coefficient ($D = 0.12\,cm^2\,s^{-1}$) at room temperature.

Figure 4 clearly demonstrates that the removal efficiency rises when the sample flow rate is reduced. This statement is valid for all sets of measurements. For the example of H_2O at room temperature a decrease of the sample flow rate from 2 sl min^{-1} to 0.5 sl min^{-1} increases the removal efficiency from 42% to 95%. Depending on the application, not the removal efficiency but the penetration can be the measure of interest. For this example an increase of the sample flow rate by a factor of 4 leads to an increase of the relative penetration by a factor of 11.6.

Another general trend that can be observed is the increased efficiency at elevated temperature. This behavior is reasonable because the increased diffusion coefficient at high temperatures ($\propto T^{\approx 1.5}$) overcompensates the decreased residence time due to a higher volumetric flow rate ($\propto T^{-1}$) at a constant mass flow rate. However, toluene ($M = 92.1$ u) and α-pinene ($M = 136.2$ u) do not follow this trend. For these two substances the observed removal efficiency at room temperature exceed the values measured at elevated temperature. Figure 5 shows the measured removal efficiencies at room temperature (left) and elevated temperature (right) as a function of the dimensionless parameter $\mu = \frac{Dl}{Q_{s,vol}}$. This representation facilitates the comparison of experimental data gathered under different conditions and the predictions of the theoretical model. The temperature dependence of the volumetric flow rate and the diffusion coefficients are accounted for in the calculation. For the sake of clearness the uncertainty in μ caused by the uncertainty of the sample flow measurement is not represented in the form of error bars. The relative uncertainties in μ amount to 10%, 5% and 2.5% for the data points measured for sample flows of 0.5 sl min^{-1}, 1.0 sl min^{-1} and 2.0 sl min^{-1} respectively.

It is obvious at first glance at the two plots in Fig. 5 that the chosen experiment parameters are very suitable for the characterization of the aerosol gas exchange system, because the evaluated removal efficiencies are spread over a large range (6–99%). The removal efficiency shows a large dependence on μ in the experimentally covered range of μ. This allows for a comprehensive comparison with the efficiencies that are predicted by the theory. Hagino evaluated the removal efficiency under experimental conditions that lead to relatively high values of μ. This is the reason why removal efficiencies $\geq$89% for all investigated substances are reported[13]. Consequently, the fact that the theoretical model applied is not suitable was not conspicuous because the applied model also predicts removal efficiencies close to 100% for the respective values of μ. In the plot for the data collected at room temperature, all experimental data points are reasonably close to the line that represents the theoretical prediction (<10% deviation). However, the majority of the measured efficiencies are located below the theoretical efficiencies. The plot that shows the efficiencies at elevated temperature shows similar behavior but a higher deviation from the theoretical efficiency. A reason for this higher deviation can be that the sample line was not perfectly isothermal due to heat losses. The point representing GSA shows a significantly higher removal efficiency than other substances at comparable values of μ. The dashed black line in the plot shows the theoretical removal efficiency for substances that adhere to the wall of denuder[17]. This is the curve used by Hagino[13] to predict the performance of

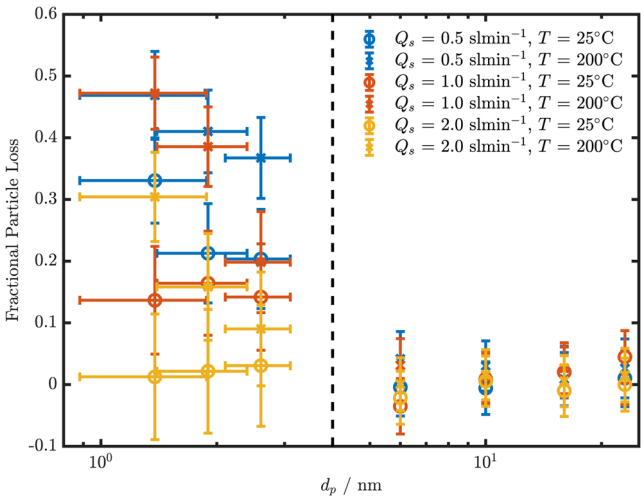

Figure 6. Fractional particle losses as a function of the particle size for different sample flows. The data point to the left of the dashed line (<4 nm) are determined by using the a polydisperse aerosol and the PSM. The data points to the right of the dashed line (>4 nm) are determined using monodisperse aerosol and the DMA-CPC approach.

the counter flow denuder for all substances. The experimental data shows that the assumption of gas molecules adhering to the wall is only valid for sulfuric acid amongst the test substances. For the case of wetted surfaces there are strongly varying values of the GSA mass accommodation or "sticking" coefficient reported in the literature[24,26,27]. However, due to the very large surface area of the porous glass tube we can assume here that this "sticking coefficient" is very close to unity for GSA in our device. This means that it can be assumed that a GSA molecule adheres to the surfaces similarly to condensation, when it gets in contact with the membrane. For the majority of compounds the boundary condition described in Eq. 2 has to be applied and consequently the calculation of the removal efficiency has to be performed using the formula in Eq. 6.

The plot in Fig. 5 showing the data of the experiment at 200 °C shows that the agreement of the measured data with the theoretical behavior is not of equal quality for all substances investigated. The CO_2 removal efficiencies measured at different flow rates agree well with the behavior predicted by the model. For H_2O the removal efficiency at a sample flow rate of $Q_s = 0.5$ sl min^{-1} ($\mu = 1.0$) agree well with theory but the deviation increases for higher flow rates. The observation made in Fig. 4 that the removal efficiency of toluene and α-pinene at elevated temperatures are lower than expected is evident also in Fig. 5. Also the measured removal efficiencies of isopropanol and ethanol show a relatively high deviation to the values predicted by the model. In general it can be said the the model derived overestimates the removal efficiencies of hydrocarbons at high temperatures.

Particle penetration. The particle size dependent fractional particle losses induced by the AGES are shown in Fig. 6. The fractional particle losses are measured and calculated similarly as for the exchange rate of gaseous compounds. The focus is on the sub-23 nm regime, where diffusion is the dominant loss mechanism. The losses of a comparable device in this particle size regime are not covered in the literature to the best of our knowledge. For particle losses at 6 nm, 10 nm, 16 nm and 23 nm were determined for monodisperse aerosol using a DMA and a CPC, as described in the methods section. The particle losses at 1.4 nm, 1.9 nm and 2.6 nm were measured with a PSM for a polydisperse particle-size distribution with a mode at approximately 2 nm.

The particle losses determined with the DMA-CPC approach are below 5% under all tested conditions and particle sizes. No trend for the particle losses at increasing temperatures or flow rates can be identified.

The data measured with the PSM shows particle losses between 1% and 47%. As expected, there is a clear trend for increased particle losses at lower flows and higher temperatures. The particle losses determined at room temperature and a sample flow rate of $Q_s = 2$ sl min^{-1} are below 5% at all size bins. However, the measurement uncertainties of both particle size and particle losses are too high to draw stressable conclusions except the observations of general trends.

Discussion

We found that the AGES is a potential tool to be used in several applications where removal of gases is required with simultaneous low losses of nanoparticles. The model describing gas exchange was first verified with oxygen and later studied with several inert gases having molecular masses between 18 u and 135 u. The experimental findings agree very well with the model based on the boundary condition that the mass flux through the SPG membrane is proportional to the difference between the concentrations at the inner and outer walls. However, the model seems to overestimate the removal efficiency of hydrocarbons at elevated temperatures. This unexpected behavior is subject to further investigations. With non-sticky gases, the removal of the lightest compounds can exceed 90% efficiency at the flow rates used. Larger molecules do not have enough time to diffuse away from the sample to reach removal efficiency larger than 50%. Thus, the AGES in the current configuration would work as an efficient drying element (no necessary need for dilution) or it could be used in front of a mass spectrometer to

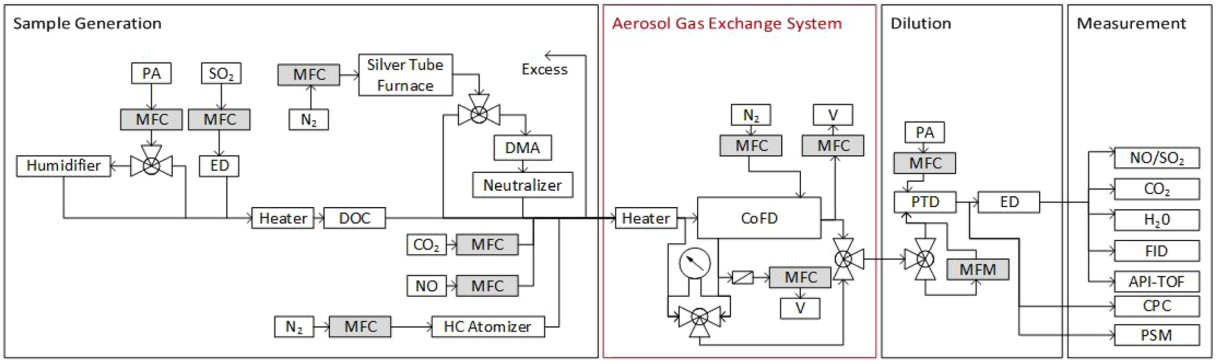

Figure 7. Schematic drawing of the experimental setup.

exchange main gases. In several applications, like automotive nonvolatile PN measurement, it is beneficial also to remove larger molecules like e.g. large poly aromatic hydrocarbons (PAH) that tend to be found in the particle phase. AGES could be used to remove gaseous (at 200 °C) large molecules but in the current form the diffusion time is not long enough to reach significant efficiency. For applications requiring high removal efficiency of large molecular masses, a redesign of the AGES would be needed. According to the model derived, better performance could be reached with (1) lower sample flow rate, (2) longer porous glass tube or (3) having several parallel porous glass tubes parts in parallel. The maximal operation temperature of 200 °C is limited by the PTFE sealing between the SPG membrane and the stainless steel housing. The application of more heat resistant materials instead will increase the maximal operation temperature and further extend the range of possible applications of the AGES.

The removal of sticky gases was studied with GSA. The measurements results agreed with the model with boundary condition of zero concentration at the wall. As GSA sticks to walls efficiently, the porous glass part has no additional functionality, rather it is probable and possibly problematic that GSA will be stored on the walls of the porous medium. In applications having high concentrations of GSA, this could lead to periodic regeneration or replacement needs of the porous part.

We identified very small particle losses in the AGES at 6 nm particle size (<5%), and further increased diffusion losses in the PSM size range down to 1.2 nm. Thus, the measured losses are smaller than one would expect based on the results of Hagino[13], where already 6% losses were detected at 20 nm particle size. In general, one would expect only small losses since the porous glass part is practically a 20 cm long isothermal tube. The AGES particle losses presented here are much smaller than previously presented for thermodenuders[10] or catalytic strippers[28]. In general, in all of these gas removal systems diffusion is the physical mechanism to collect or remove gaseous compounds but also at the same time collect the smallest nanoparticles. AGES and TD share the trait of the whole surface being active whereas CS systems can have also catalytically inactive sites. The advantage of AGES and TD applications compared to CS is that they are not chemically active, thus the risk of unwanted chemical reactions is lower than in the CS. On the other hand, the advantage of AGES and CS applications compared to the TD is that the removal regime can be sustained isothermal at the elevated temperature whereas in TD cooling is required for the activated charcoal. After the AGES, sample gas can be kept hot or then cooled with a desired method having optimal performance. In our tests, the gas was cooled in an uninsulated metal tube, but also the reference aerosol was sampled the same way. Thus similar thermophoresis was expected and also confirmed by the findings from sampling upstream and downstream locations. In general, if one optimized the gas exchange in the AGES with either having lower sample flow, longer porous glass tube or several parallel sections, one would also see increased losses of nanoparticles. However, an application targeted design of the AGES, can significantly improve measurement results of aerosol experiments by lowering the partial pressure of undesired gaseous compounds without the necessity to dilute the sample.

Methods

Laboratory experiments were performed to characterize the performance of the AGES. The experiments focused on (1) gas exchange of inert inorganic and organic gases, (2) gas exchange of sticky gaseous sulfuric acid (GSA) and (3) nonvolatile particle loss characterization down to 1.2 nm in particle size.

The measurement setup is presented in Fig. 7. The setup is divided into four parts: sample generation, the Aerosol Gas Exchange System (AGES), dilution and measurement.

Sample generation. The generation part consisted of a main line, to which silver particles and different gaseous species were injected. By adjusting the main line mass flow controller (MFC) setting, the concentration of species in test was adjusted to a desired value. The main line flow was operated at the range of 3–20 sl min^{-1}. The sample humidity/dryness was set by leading the flow either through a humidifier unit or bypassing it.

The gaseous species used for the experiments, their molecular masses and diffusion coefficients in air, typical main line concentrations and the measurement instruments are listed in Table 1. The substances chosen for the experiments were water (H_2O), nitrogen monoxide (NO), carbon dioxide (CO_2), sulfur dioxide (SO_2), ethanol (C_2H_5OH), isopropanol ($CH_3CHOHCH_3$), toluene (C_7H_8), sulfuric acid (H_2SO_4) and α-pinene ($C_{10}H_{16}$).

The hydrocarbon vapors were generated by setting a flow through an atomizer with a mass flow controller operating at 0.2–0.5 sl min^{-1}. The other gaseous species except sulfuric acid were also injected to the main line

with mass flow controllers, straight from gas bottles. The gas feeds were changed according to the desired concentration, which depended on the respective measurement instrument limitations.

For sulfuric acid generation a platinum coated diesel oxidation catalyst (DOC)[29] was used. Upstream the DOC sulfur dioxide was injected to the sample line through an ejector diluter (ED). In the DOC, the sulfur dioxide is oxidized, forming sulfur trioxide, which reacts with water forming sulfuric acid.

$$2SO_2 + O_2 \xrightarrow{Pt} 2SO_3$$

$$SO_3 + H_2O \rightarrow H_2SO_4$$

Since the aim was to determine the removal efficiency of gaseous sulfuric acid, the sulfuric acid concentration was kept low enough to keep it from nucleating. The particle number concentration was monitored with a condensation particle counter to make sure that only gas phase was present.

For the particle loss measurements, silver particles were generated[30]. A ceramic vessel containing a small amount of silver was placed inside a quartz glass tube, which again was placed inside a tube furnace (Carbolite Gero CWF Model 23 Litre). A nitrogen flow of 2 l min^{-1} was then set through the tube to the main line. Adjusting the furnace temperature allowed for manipulation of the silver particle size distribution, higher temperatures resulting in higher mean sizes. The furnace was operated between 1000 °C and 1200 °C. The particles were fed to the line either straight from the furnace or through a TSI Model 3085 Differential Mobility Analyzer (DMA) coupled with a neutralizer. The neutralizer was used to generate the equilibrium charge distribution of the particles and to consequently reduce electrophoretic particle losses.

Sampling and dilution. The sample flow through the AGES was created with a combination of a porous tube diluter (PTD) and an ejector diluter. The ejector diluter was operated with a dilution air pressure of 1–2 bar. Changing the pressure allowed for manipulation of the secondary dilution ratio and the ejector inlet flow. The PTD dilution air flow was then chosen accordingly to reach the desired sample flow through the AGES. The sample flow was measured with a TSI model 4140 mass flow meter. The flows chosen in the measurements were 0.5, 1.0 and 2.0 sl min^{-1}. The valve system of the measurement setup was built so that it was possible to draw sample before the AGES, after it and from the purge gas flow.

Measurement instruments. The instruments used for gaseous species concentration measurements were LI-COR LI-840A for CO_2 and H_2O, SIDOR gas analyzer for SO_2 and NO and an Atmospheric Pressure Interface Time Of Flight (API-TOF) mass spectrometer[31] for gaseous sulfuric acid. The API-TOF was operated with an Eisele-type nitrate inlet for chemical ionization[32]. Baseline Series 9000 NHMC flame ionization detector (FID) was used for the measurement of hydrocarbons. The FID has a different response for each different substance, but as the quantity to be determined was the removal efficiency (and not absolute concentration) for each substance, the response difference does not interfere with the data analysis.

For total particle number concentration measurement an Airmodus A10 Particle Size Magnifier (PSM) coupled with an A20 CPC and a TSI CPC model 3775 were used. The PSM allows for manipulation of the saturator flow and thus the cutoff size of the PSM-CPC pair. Periodically changing the saturator flow allows for calculation of particle concentrations in the size bins determined by the chosen saturator flows. In this measurement, saturator flows of 1.22, 0.298, 0.191 and 0.102 sl min^{-1} were used, which correspond to cutoff sizes of 1.17, 1.63, 2.21 and 3.07 nm, respectively.

Test matrix. The substances presented in Table 1 were chosen to get a representation of both inorganic and organic molecules and to have variation in molecular mass and vapor pressure to see if it has an effect on the species' storage on the porous glass surfaces.

Measurement procedure. Concentrations of the gas species were measured upstream and downstream of the AGES for the removal efficiency determination. The measurement procedure also included a dilution air background measurement, which meant sampling only dilution air. This was done to monitor drifts in measurement instrument zero levels and to correct the concentrations accordingly in the data processing phase. All measurements were conducted with a hot system (AGES heaters at 200 °C) and a cold system (AGES heaters off), with the exception of GSA, with which only the hot system was used. For the most part, the measurements were made for one substance at a time, but H_2O, CO_2 and SO_2 were also coupled with other substances.

The GSA concentration had to be kept low in order to prevent it from nucleating. The appropriate concentration was found by adjusting the SO_2 feed, main line flow and flow through the humidifier until no particles were detected with the CPC. It was observed that in order to prevent the nucleation a very low concentration of GSA was required. Because of this the background signal was approximately half of the measured signal. The background signals for the sampling points were measured by sampling only air from the main line and it was observed that the background signal was different for each sampling point (upstream and downstream). The reason for this can be that even with the DOC heaters and SO_2 feed turned off there was some trace amount of GSA released from the main- and sampling lines or the DOC. For this reason, background signal levels of all sampling points were measured to calculate the removal efficiency accurately.

Due to relatively long integration times (>5 min) and accurately mass flow controlled sources of substances the measurement uncertainty for gas measurements is found to be dominated by the sample flow measurement. The uncertainty of this measurement amounts to 0.05 sl min^{-1}.

Particle loss measurements. We used two different experimental approaches for the determination of particle size dependent losses. The first approach was to inject monodisperse particles and calculate the losses from concentrations measured by a TSI CPC 3776. Particles of 6, 10, 16 and 23 nm in diameter were classified using a TSI model 3085A Nano DMA and injected into the main line. Observations of the particle source showed that the particle number concentration varies by approximately 2% between two consecutive measurements that were used to determine the particle losses. The uncertainties for the fractional particle losses were calculated from the uncertainty caused by the particle source variation, the Poisson counting statistics uncertainties and the application of Gaussian propagation of uncertainties.

The second approach was to inject polydisperse particles from a tube furnace and calculate the losses from size distributions measured by the PSM upstream and downstream the AGES. This transient measurement method enables the measurement of smaller particles but exhibits higher measurement uncertainties than the approach with monodisperse aerosol.

The uncertainty of the PSM particle size bins positions is subject to a number of effects including particle composition dependent detection probability, CPC calibration with differently charged particles and limited DMA resolution due to Brownian motion[33]. The combination of these effects is estimated to yield an uncertainty of ± 0.5 nm.

We observed that the generated particle number concentrations vary by approximately 5% between two successive measurement points. This uncertainty, which is caused by the particle source is added to the Poisson uncertainty for the determination of the uncertainty of the fractional particle losses.

Data availability

The data sets and codes used and analysed in this study are available from the corresponding author on reasonable request.

Received: 20 June 2019; Accepted: 29 October 2019;
Published online: 20 November 2019

References

1. Amanatidis, S. *et al*. Comparative performance of a thermal denuder and a catalytic stripper in sampling laboratory and marine exhaust aerosols. *Aerosol Sci. Technol*., https://doi.org/10.1080/02786826.2017.1422236 (2018).
2. Rönkkö, T. *et al*. Nucleation mode particles with a nonvolatile core in the exhaust of a heavy duty diesel vehicle. *Environ. Sci. Technol.* **41**, 6384–6389, https://doi.org/10.1021/es0705339 (2007).
3. Swanson, J. J., Franklin, L. M., Bika, A. S. & Kittelson, D. B. Size and volatility of particle emissions from an ethanol-fueled HCCI engine. *Aerosol Sci. Technol.* **51**, 614–625, https://doi.org/10.1080/02786826.2017.1286289 (2017).
4. Alanen, J. *et al*. Comparison of primary and secondary particle formation from natural gas engine exhaust and of their volatility characteristics. *Atmospheric Chem. Phys.* **17**, 8739–8755, https://doi.org/10.5194/acp-17-8739-2017 (2017).
5. Cao, L.-M., Huang, X.-F., Li, Y.-Y., Hu, M. & He, L.-Y. Volatility measurement of atmospheric submicron aerosols in an urban atmosphere in southern China. *Atmospheric Chem. Phys.* **18**, 1729–1743, https://doi.org/10.5194/acp-18-1729-2018 (2018).
6. Grieshop, A., Logue, J., Donahue, N. & Robinson, A. Laboratory investigation of photochemical oxidation of organic aerosol from wood fires 1: . . . . *Atmospheric Chem. And Phys.* 1263–1277 (2009).
7. Huffman, J. A. *et al*. Chemically-resolved aerosol volatility measurements from two megacity field studies. *Atmospheric Chem. Phys.* **9**, 7161–7182, https://doi.org/10.5194/acp-9-7161-2009 (2009).
8. Giechaskiel, B. *et al*. Measurement of automotive nonvolatile particle number emissions within the european legislative framework: a review. *Aerosol Sci. Technol.* **46**, 719–749 (2012).
9. Saha, P. K., Khlystov, A. & Grieshop, A. P. Determining Aerosol Volatility Parameters Using a "dual Thermodenuder" System: Application to Laboratory-Generated Organic Aerosols. *Aerosol Sci. Technol.* **49**, 620–632, https://doi.org/10.1080/02786826.2015.1056769 (2015).
10. Rönkkö, T. *et al*. Diesel exhaust nanoparticle volatility studies by a new thermodenuder with low solid nanoparticle losses. *15th ETH Conf. on Combust. Gener. Nanoparticles* (2011).
11. Abdul-Khalek, I. & Kittelson, D. Real Time Measurement of Volatile and Solid Exhaust Particles Using a Catalytic Stripper. *SAE Tech. Pap*. 950236 (1995).
12. Swanson, J., Kittelson, D., Giechaskiel, B., Bergmann, A. & Twigg, M. A Miniature Catalytic Stripper for Particles Less Than 23 Nanometers. *SAE Int. J. Fuels Lubr*. **6**, 2013–01–1570, https://doi.org/10.4271/2013-01-1570 (2013).
13. Hagino, H. Laboratory evaluation of nanoparticle penetration efficiency in a cylindrical counter flow denuder for nonspecific removal of trace gases. *Aerosol Sci. Technol.* **51**, 443–450 (2017).
14. Tarik, M., Foppiano, D., Hess, A. & Ludwig, C. A practical guide on coupling a scanning mobility sizer and inductively coupled plasma mass spectrometer (smps-icpms). *JoVE Journal Vis. Exp*. e55487 (2017).
15. Hess, A., Tarik, M. & Ludwig, C. A hyphenated smps–icpms coupling setup: Size-resolved element specific analysis of airborne nanoparticles. *J. Aerosol Sci.* **88**, 109–118 (2015).
16. Yamazaki, N., Yuyama, H., Nagai, M., Ma, G.-H. & Omi, S. A comparison of membrane emulsification obtained using spg (shirasu porous glass) and ptfe [poly (tetrafluoroethylene)]. *membranes. J. dispersion science technology* **23**, 279–292 (2002).
17. Gormley, P. & Kennedy, M. Diffusion from a stream flowing through a cylindrical tube. In *Proceedings of the Royal Irish Academy. Section A: Mathematical and Physical Sciences*, vol. 52, 163–169 (JSTOR, 1948).
18. Murphy, D. M. & Fahey, D. W. Mathematical treatment of the wall loss of a trace species in denuder and catalytic converter tubes. *Anal. Chem*. **59**, 2753–2759 (1987).
19. Walker, R. Chemical reaction and diffusion in a catalytic tubular reactor. *The Phys. Fluids* **4**, 1211–1216 (1961).
20. Brown, R. Tubular flow reactors with first-order kinetics. *J. Res. Natl. Bur. Stand* **83**, 1–8 (1978).
21. Renkin, E. M. Filtration, diffusion, and molecular sieving through porous cellulose membranes. *The J. general physiology* **38**, 225–243 (1954).
22. Satterfield, C. N., Colton, C. K. & Pitcher, W. H. Jr. Restricted diffusion in liquids within fine pores. *AIChE J.* **19**, 628–635 (1973).
23. Crank, J. *et al*. *The mathematics of diffusion*. (Oxford university press, 1979).
24. Pöschl, U. *et al*. Mass accommodation coefficient of h_2so_4 vapor on aqueous sulfuric acid surfaces and gaseous diffusion coefficient of h_2so_4 in n2/h2o. *The J. Phys. Chem. A* **102**, 10082–10089 (1998).
25. Kolb, C. *et al*. Laboratory studies of atmospheric heterogeneous chemistry. In *Progress and problems in atmospheric chemistry*, 771–875 (World Scientific, 1995).

26. Van Dingenen, R. & Raes, F. Determination of the condensation accommodation coefficient of sulfuric acid on watersulfuric acid aerosol. *Aerosol Sci. Technol.* **15**, 93–106 (1991).
27. Clement, C. F., Kulmala, M. & Vesala, T. Theoretical consideration on sticking probabilities. *J. Aerosol Sci.* **27**, 869–882 (1996).
28. Amanatidis, S. *et al*. Evaluation of an oxidation catalyst ("catalytic stripper") in eliminating volatile material from combustion aerosol. *J. Aerosol Sci.* **57**, 144–155, https://doi.org/10.1016/j.jaerosci.2012.12.001 (2013).
29. Karjalainen, P. *et al*. Sulfur driven nucleation mode formation in diesel exhaust under transient driving conditions. *Environ. science & technology* **48**, 2336–2343 (2014).
30. Harra, J. *et al*. Size-controlled aerosol synthesis of silver nanoparticles for plasmonic materials. *J. Nanoparticle Res*. (2012).
31. Junninen, H. *et al*. A high-resolution mass spectrometer to measure atmospheric ion composition. *Atmospheric Meas. Tech.* **3**, 1039–1053, https://doi.org/10.5194/amt-3-1039-2010 (2010).
32. Eisele, F. L. & Tanner, D. J. Measurement of the gas phase concentration of h_2so_4 and methane sulfonic acid and estimates of h_2so_4 production and loss in the atmosphere. *J. Geophys. Res. Atmospheres* **98**, 9001–9010, https://doi.org/10.1029/93JD00031 (1993).
33. Kangasluoma, J. & Kontkanen, J. On the sources of uncertainty in the sub-3 nm particle concentration measurement. *J. Aerosol Sci.* **112**, 34–51 (2017).
34. Brus, D. *et al*. Temperature-dependent diffusion coefficient of h_2so_4 in air: Laboratory measurements using laminar flow technique. *Atmos. Chem. Phys. Discuss*., https://doi.org/10.5194/acp-2016-398 (2016).
35. Silva, C. M., Cláudio Filho, A., Quadri, M. B. & Macedo, E. A. Binary diffusion coefficients of a-pinene and b-pinene in supercritical carbon dioxide. *The J. supercritical fluids* **32**, 167–175 (2004).
36. Chapman, S., Cowling, T. G. & Burnett, D. *The mathematical theory of non-uniform gases: an account of the kinetic theory of viscosity, thermal conduction and diffusion in gases*. (Cambridge university press, 1990).
37. Cussler, E. L. *Diffusion: mass transfer in fluid systems*. (Cambridge university press, 2009).

Acknowledgements

This work is conducted in the framework of the H2020 project DownToTen. This project has received funding from the European Union's Horizon 2020 research and innovation programme under grant agreement Nr. 724085. P.K. additionally acknowledges funding from two Academy of Finland projects: UPCE decision Nr. 318940 and EFFi decision Nr. 322120.

Author contributions

M.B. and S.M. contributed equally to this work, M.B. conceived the theoretical description, M.B. performed the CFD simulations, M.B., S.M. and P.K. conceived and conducted the experiments, M.B. and S.M. analysed the results, M.B. prepared the graphics and diagrams, M.B., S.M. and P.K. wrote the manuscript, J.K. and A.B. gave technical support and conceptual advice, All authors reviewed the manuscript.

Competing interests

The authors declare no competing interests.

Additional information

Correspondence and requests for materials should be addressed to M.B.

Reprints and permissions information is available at www.nature.com/reprints.

Publisher's note Springer Nature remains neutral with regard to jurisdictional claims in published maps and institutional affiliations.

Paper 3

Particle Number Measurements within Periodic Technical Inspections: A First Quantitative Assessment of the Influence of Size Distributions and the Fleet Emission Reduction

Particle Number Measurements within Periodic Technical Inspections: A First Quantitative Assessment of the Influence of Size Distributions and the Fleet Emission Reduction

Markus Bainschab[a], Mario A. Schriefl[a,b], Alexander Bergmann[a]

[a] *Institute of Electrical Measurement and Sensor Systems, Graz University of Technology, 8010 Graz, Austria*
[b] *AVL DiTEST GmbH, 8020 Graz, Austria*

Abstract

The enforcement of more and more stringent type approval emission standards de facto mandate manufacturers to equip vehicles with particle filters, which reduces the particle number concentration in automotive emissions to levels below typical ambient concentrations. Soon, the overall automotive particle emissions will be dominated by highly emitting vehicles with malfunctioned after-treatment systems, making tests of in-service compliance with emission standards inevitable. These tests are especially for diesel-powered because broken diesel particle filters can increase the particle emissions by several orders of magnitude. For spark-ignition vehicles, the possible effect is significantly lower, and the implementation of corresponding tests is technically challenging. For the first time, we provide a quantitative assessment of the possible emission reduction impact of identifying malfunctioned after-treatment systems utilizing particle number measurements in the course of periodic technical inspections. We found that the enforcement of particle number measurements within periodic technical inspections can reduce the overall particle emissions of the actual fleet by more than 80 %. This substantial improvement requires reliable identification of high emitters. Based on data from a dedicated measurement campaign and simulations, we demonstrate that this can be achieved, even in extreme cases where instruments barely meet any under discussion specifications. Mandating the tests to be performed in low idle operation would further facilitate a reliable discrimination between low and high emitters, compared to high idle

tests. The corresponding increased accuracy would allow for the application of more-cost efficient measurement equipment and support the introduction of a comprehensive in-service compliance testing of vehicles to significantly lower automotive emissions of particulate matter.

Keywords: Automotive Particle Number Emissions, Periodic Technical Inspections, Particle Size Distributions, Instrument Specificatons, Impact Assessment

1. Introduction

Particulate matter emitted by motor vehicles continues to contribute to air pollution, causing adverse health effects (Oberdörster et al., 2005; Brook et al., 2010; Peters et al., 2004). Policymakers around the globe regulate particulate mass (PM) and particulate number (PN) emissions from internal combustion engine-driven vehicles to improve the air quality, and as a result, people's health and quality of living. Many of the current regulations are based on type approval testing (TAT). In these tests, the compliance of new vehicle models with emission regulations is checked, by testing a limited number of vehicles of the respective model. A well-controlled environment, high-end measurement equipment, and testing facilities guarantee a high degree of accuracy and reproducibility. However, these tests only ensure compliance with the emission standards at the beginning of vehicles' life cycles and well-defined driving conditions. In real-world situations, varying environmental conditions, aggressive driving, or malfunctioned exhaust after-treatment systems can lead to emissions that deviate significantly from the values determined during type approval testing (Pant and Harrison, 2013).

Boveroux et al. (2019) assessed the particle emissions of more than 300 EURO5 and EURO6 diesel vehicles. They found that 15 % of vehicles could be identified as high emitters employing particle number concentration measurement during low idle operation, while only less than 1 % failed the opacity test currently prescribed during the periodic technical inspection (PTI) in several countries. The emissions of the 15 % of high emitters are estimated to be responsible for 97 % of the total particle emissions of the studied fleet. Multiple studies show that the emitted particle concentration in idle speed is in good correlation with the total number of emitted particles over type approval compliant driving cycles (NEDC or WLTC) (Kadijk et al., 2017; Giechaskiel et al., 2018).Hence, tailpipe PN concentration measurements can

be a useful and reliable tool for identifying particulate filter malfunctions (Kadijk et al., 2017).

In the last decades, the emission limits around the globe have become more and more rigorous, and accordingly, the exhaust after-treatment systems have become increasingly complex to meet these emission limits. If this trend is prolonged, soon, not only diesel cars but also the majority of gasoline vehicles will be equipped with particle filters to meet the legal emission requirements (Andersson, 2019). This development could further increase the need for in-service functionality checks of after-treatment systems and, therefore, increase the impact of particle number concentration measurements in the course of PTIs.

Based on an initiative of the Verification of Emission Reduction Technologies (VERT) association, the New Periodic Technical Inspection (NPTI) working group was established to define a procedure and a reasonable limit value, as well as instrument specifications for the particle number measurement during the PTI (VERT, 2019).

Countries like Germany, Belgium, and the Netherlands are about to introduce PTI particle number regulations. Regulatory instrument specifications will have a substantial influence on the costs and benefits of these regulations. The defined instrument specifications should ensure reliable detection of high emitters (i.e., DPF failures) while allowing for instruments that have a limited degree of complexity.

In this paper, we present the results of a PTI PN measurement campaign testing 21 vehicles during low idle and high idle operation. Laboratory grade particle size distribution measurement instruments were used for a comprehensive analysis of the emitted aerosol.

Simulations based on the measurement results demonstrate how regulatory specifications for PTI particle measurement instruments may affect the accuracy of measurement results and, hence, the categorization of low and high emitters.

Several studies claim that PN PTI measurements can significantly contribute to particle emission reduction and improvement of air quality (Boveroux et al., 2019; Burtscher et al., 2019; VERT, 2019; Kadijk et al., 2016, 2017). While there is a comprehensive qualitative agreement, up to now, no estimations of the effects' magnitude are published. For the first time, we provide a quantitative assessment of the effect of PN PTI measurements on particle emissions of an actual fleet considering different scenarios of PTI schedules, particle filter aging behavior, and fleet vehicle age distributions.

2. Material and Methods

2.1. Vehicles Tested

In this study, the particle emissions of 21 light-duty vehicles in low and high idle operations were assessed in terms of particle number concentration and particle size distribution. Table 1 lists the 21 vehicles tested during this study. The vehicles were chosen from a broad range of manufacturers, mileages, and emission standards. Four vehicles are experimental vehicles deviating from production vehicles in some technical aspects. The other cars are privately owned and used on an everyday basis. Six out of the 21 vehicles are gasoline cars and 15 run on diesel. Five out of the six gasoline vehicles employ direct injection (DI). One of them utilized port fuel injection (PFI) technology. The years of construction range from 1997 to 2019. More than half (13) of the vehicles were equipped with particulate filters. Vehicles 9 and 19 are identical cars except that the diesel particulate filter was removed for the measurements on vehicle 19.

Table 1: List of tested vehicles. Every vehicle is assigned a vehicle number indicating the order the measurements were done. The manufacturer of the vehicles 2,3,4 and 10 is not published because the according vehicles are experimental vehicles deviating from production vehicles in several technical aspects.

Vehicle number	Manufacturer	Model	Year of construction	Displacement [ccm]	Power [hp]	Euro standard	Fuel	Mileage [km]	Particle Filter
0	Ford	Galaxy	2016	1997	150	6	Diesel	105426	Yes
1	Hyundai	Terracan	2002	2900	150	3	Diesel	135814	No
2	experimental vehicle		2016	2967	270	6	Diesel	43827	Yes
3	experimental vehicle		2017	1995	190	6[1]	Diesel	37529	Yes
4	experimental vehicle		2017	3993	550	6	Gasoline DI	34000	Yes
5	Mini	Cooper S	2007	1598	175	4	Gasoline DI	98644	No
6	VW	Lupo 3L	2003	1200	60	3	Diesel	158627	No
7	Mercedes-Benz	C200	2002	2148	116	3	Diesel	152347	Yes
8	Mazda	3 Skyactiv-X	2019	2000	179	6	Gasoline DI	421	Yes
9	VW	Polo	2015	1422	90	6[2]	Diesel	4357	Yes
10	experimental vehicle		2018	1995	231	6[3]	Gasoline DI	16897	Yes
11	Honda	CR-V	2012	2176	150	5	Diesel	220000	Yes
12	VW	Golf	2014	1197	86	5	Gasoline DI	45910	No
13	Mercedes-Benz	Viano	2013	2987	224	5	Diesel	193551	Yes
14	VW	Passat	2015	1968	150	6[2]	Diesel	114000	Yes
15	Renault	Megane	2006	1870	110	4	Diesel	168646	Yes
16	Mahindra	XUV500	2012	2179	140	5	Diesel	101900	Yes
17	experimental vehicle		1997	1797	169	2	Gasoline PFI	130000	No
18	Mini Cooper	D Countryman	2018	1995	150	6[3]	Diesel	23300	Yes
19	VW	Polo	2015	1430	90	6[2]	Diesel	4357	No
20	Opel	Astra	1998	1600	82	2	Diesel	68400	No

[1] 6/c
[2] 6/b
[3] 6/dTmp

2.2. Instrumentation

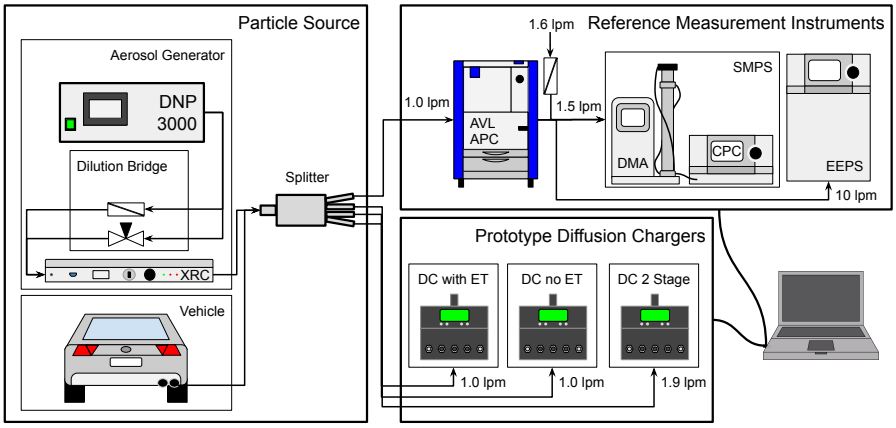

Figure 1: Drawing of the experimental setup. The Palas DNP 3000, in conjunction with the Palas XRC 049 were used as a particle source for the instrument comparison measurements. The AVL APC was used as a PMP compliant solid particle number reference. Additionally, the diluted exhaust exiting the APC was fed into the SMPS, and the EEPS for size distribution measurements. Three prototype diffusion charger devices were used in the measurements. One DC was equipped with an evaporation tube (ET) to remove volatile particles. One DC was equipped with an evaporation tube (ET) to remove volatile particles. Another DC comprises a second charging stage, which enables the measurement of the mean particle size and the PN concentration.

Figure 1 shows the experimental setup used to measure the particle number concentrations and particle size distributions in low and high idle operation. The Palas DNP 3000 (Helsper et al., 1993), in conjunction with the Palas XRC 049, were used as a stable, reproducible particle source for the initial instrument comparison measurements. As indicated in Figure 1, the applied measurement instruments are divided into reference measurement equipment and prototype devices. The AVL APC acts as a reference instrument for particle number concentration measurement. The inlet flow rate of the APC was $1\,\mathrm{l\,min^{-1}}$. The exhaust flow of the AVL APC (particle concentration reduction factor of 100), is fed into a TSI SMPS (scanning mobility particle sizer) and a TSI 3090 EEPS (engine exhaust particle sizer). These two instruments acted as reference instruments for particle size distribution measurements. The SMPS consists of a TSI 3080 classifier with a 3081 differential mobility analyzer and a 3088 soft x-ray neutralizer for size classification and a condensation particle counter 3775 for particle counting. It

was operated in high flow mode (1.5 l min^{-1} inlet flow rate, 15 l min^{-1} sheath flow rate). The SMPS provides high particle size resolution (64 channels per decade) and counting accuracy but lacks high temporal resolution (120 s per scan). To enable capturing rapid changes in size distributions during transient events, an EEPS measured the size distribution in parallel to the SMPS with a high temporal resolution (1 Hz). The inlet flow rate of the EEPS was 10 l min^{-1}. The flow drawn by the SMPS and the EEPS was 1.6 l min^{-1} higher than the APC exhaust flow. The additional 1.6 l min^{-1} were supplied from the ambient air using a T-piece and a HEPA filter. The dilution introduced (dilution factor $DF = 1.17$) by the additional particle-free air was accounted for in the data processing. Three prototype low-cost diffusion charger devices were installed to measure the particle number concentration of the emitted aerosol. One of the prototype instruments was equipped with an evaporation tube (ET) to remove volatile particles. Another prototype device was applied as a two-stage version, enabling the determination of a mean particle size (Schriefl et al., 2019). The inlet flow rate of the 2-stage device was 1.9 l min^{-1}. The inlet flow rates of the single-stage diffusion charger devices were 1 l min^{-1}. Both single stage devices utilize dilution with dry, particulate-free air at a dilution ratio of 4 to avoid condensation in the instruments' gas path.

2.3. Calibration Procedure

The prototype diffusion charger devices were compared with the reference instrumentation in a set of calibration measurements. For these measurements, the Palas DNP 3000 was used as a particle source. The particles generated with this device may be highly charged due to the spark generation process. These highly charged particles may influence the measurement results of charge based instruments like the EEPS or diffusion chargers. A Palas XRC 049 soft x-ray neutralizer downstream of the aerosol generator was used to prevent undesired effects from highly charged particles. The high concentration of ions generated by the x-rays establishes a particle charge distribution close to equilibrium. A dilution bridge (needle valve in parallel to HEPA filters) between the aerosol generator and the neutralizer was used to adjust the particle number concentration to be $(1.0 \pm 0.2) \times 10^6$ cm^{-3} (reading of AVL APC). For the calibration measurements, the nitrogen flow rate was set to 5 l min^{-1}, and the dilution air flow rate was set to 15 l min^{-1}. The excess aerosol flow was fed into an extraction system. The generation voltage was set to 2500 V and the generation frequency was varied between 100 Hz

and 500 Hz in 100 Hz intervals. The outlet of the neutralizer was connected to a TSI 3708 flow splitter with conductive tubing. The four outlet ports of the flow splitter were connected to the APC and the three diffusion charger prototype instruments using conductive tubing. The particle concentrations and size distributions at the different generation frequencies were measured for approximately 200 s each to provide enough time for the SMPS to complete at least one full scan.

The results of the measurements performed are shown in Figure 2. The left plot shows the geometric mean diameter (GMD) as given by the scanning mobility particle sizer (SMPS) and the engine exhaust particle sizer (EEPS) for different generation frequency settings of the particle generator. Additionally, there are dashed lines showing the GMD evaluated by fitting the size distribution measured by the SMPS and the EEPS with log-normal distributions. As shown in Figure 2, the change in generation frequency resulted in changing the geometric mean diameter of the generated size distribution. The change in frequency did not significantly affect the width of the distribution (GSD $=1.72 \pm 0.03$). For the SMPS data, the agreement of the GMD value from the fit with the directly evaluated value is very good (< 1 nm deviation).

The GMDs from the fitted EEPS data is 2 nm to 6 nm lower than the GMD given by SMPS. This deviation is caused by the relatively high noise level of the EEPS leading to high artifact particle concentrations below 10 nm. This measurement artifact causes a shift of the fitted log-normal distributions towards lower particle diameters. The effect of these artifacts on the GMDs directly calculated from the EEPS data is more pronounced and leads to a deviation from the SMPS data of 4 nm to 14 nm. As the EEPS is only used to detect transient events on timescales below the SMPS' temporal resolution, these deviations between the EEPS and SMPS results are acceptable.

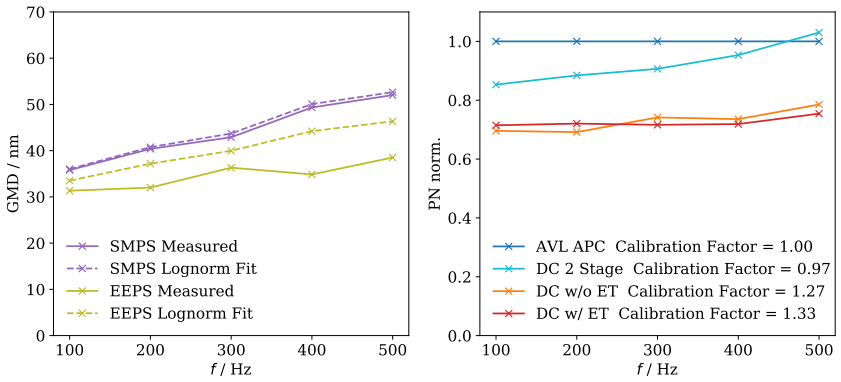

Figure 2: Instrument responses to spark generated graphite aerosol for different generation frequencies. The left plot shows geometric mean diameter (GMD) as given by the SMPS and EEPS. The dashed lines show the GMD resulting from fitting the SMPS and EEPS size distribution data with log-normal distributions. The right plot shows the particle number response of the three prototype diffusion charger devices and the AVL APC normalized with the AVL APC data.

The right plot in Figure 2 shows the response of the diffusion charger prototypes normalized by the AVL APC PN measurement results for different particle generation frequencies. It can be seen that all three DCs show increased responses for higher frequencies. This increase is associated with the increasing mean diameters of the particle size distributions generated at higher frequencies and the particle size-dependent response of the diffusion chargers (Schriefl et al., 2019). The two single-stage DC instruments were calibrated beforehand to have a 100 % counting efficiency at 80 nm, while the counting efficiency is decreasing towards smaller particle sizes (Schriefl et al., 2020). This explains the underestimation by about 30 % for the size distributions measured. The results of the comparison measurements have been used to calibrate the prototype diffusion chargers for the vehicle measurements. For the calibration, the measurement point at a generation frequency of 500 Hz has been used. At this measurement point, the GMD of the size distribution is 53 nm (SMPS). This geometric mean diameter is suitable because it is well in the range of the mean particle sizes that are expected in diesel (40 nm to 120 nm) and gasoline (40 nm to 80 nm) exhaust (Harris and Maricq, 2001). The applied calibration factors for the prototype diffusion charger instruments are shown in the legend of the right

plot in Figure 2. The authors are well aware that the primary particles of spark generated graphite agglomerates are considerably smaller (3 nm to 10 nm) than those of combustion generated soot particles(Olfert and Rogak, 2019). Furthermore, the effective density of the spark-generated particles is smaller. These differences have been shown to cause significant deviations in the response of measurement instruments. These deviations can be particularly pronounced for incandescence-based detection methods(Gysel et al., 2012). Due to the increased surface area related to the smaller effective density, charge-based methods can also exhibit deviations of the measurement response. The charging efficiency of particles is dependent on the surface area. However, Mamakos showed that the ratio between the number of single and multiple charged particles in an electrically neutralized aerosol is very comparable for soot and graphite aggregates(Mamakos, 2016). Comparative measurements showed that the response of the diffusion charger prototypes used in this study could be up to 20 % higher for spark-generated particle than for soot in the relevant size range below 150 nm. These results are part of another study that will be published soon.

2.4. Vehicle Measurement Procedure

The exhaust particles emitted by the vehicles tested during this study were sampled directly from the tailpipe using a metal probe, which was clipped onto the tailpipe. The tailpipe probe was connected to a TSI 3708 flow splitter with conductive tubing. The four outlet ports of the flow splitter were connected to the APC and the three diffusion charger prototype instruments using conductive tubing. The vehicles were operated in low-speed driving and idling for at least 10 min before the measurements to avoid effects from cold starts. After the warm-up, the low idle measurements were conducted. For these measurements, the vehicles were operated at idle speed without pushing the gas pedal. High idle measurements succeeded the low idle measurements. For these measurements, the gas pedal was used to keep the rotational frequency of the engine (1500 ± 100) rpm above the rotational frequency at low idle speed. Both the low idle and high idle measurements were performed for at least 4 min to provide enough time to perform two full SMPS scans (120 s scan time). At specific points during the measurement campaign, two of the diffusion chargers stopped working correctly after being exposed to high concentrations of water vapor emitted by gasoline vehicles. For the two-stage DC, which was operated without diluting the exhaust gas with dried, particulate-free air, this happened after the measurement of vehi-

cle 6 (Mini Cooper S). The DC with the evaporation tube equipped went into error mode during the measurement of vehicle 17 (Honda Civic). The high moisture levels in gasoline exhaust are generally very challenging for particle measurement equipment. Also, the commercially available PMP compliant system AVL APC could not be run entirely without errors. Multiple times, water accumulating in the sampling line or the primary diluter had to be removed by running a dedicated drying procedure to reconstitute the full functionality of the instrument.

3. Theory and Calculation

3.1. Assessment of Instrument Specifications

In this section, the procedure applied to assess the effectiveness of different PTI instrument specifications is described. For automotive measurements, particle number counters (PNC) need to comply with specific counting efficiency (CE) requirements. The CE defines the ratio of the number of particles counted by the instrument and the actual number of particles at specific particle diameters and thus, specifies the particle size dependency of the sensor response.

The CE requirements are defined differently by various regulations. The particle measurement programme (PMP), for example, specifies a lower particle size limit, defined by the d_{50} cut-off (i.e. 50 % counting efficiency), at 23 nm, whereas for particles larger than 41 nm, the counting efficiency must be greater than 90 % (United Nations Economic Commission for Europe, 2006). The CE criteria for PMP(United Nations Economic Commission for Europe, 2006) , real driving emission (RDE)(EC, 2017) , the Swiss PTI regulation for off-road machinery (VAMV)(EJPD, 2006) and the CE criteria as suggested by the NPTI (Ministry for Infrastructure and Public Works, 2019) working group are listed in Table 2 and indicated by the circular markers in Figure 3.

Table 2: Counting efficiency limits for different automotive particle number measurement regulations

d_p / nm	Counting Efficiency Criteria [%]			
	PMP	RDE	VAMV	NPTI
23	38 – 62	20 – 60	<50	20 – 60
30	–	30 – 120	–	–
41	>90	–	>40	–
50	–	60 – 130	–	60 – 130
70	–	70 – 130	–	–
80	–	–	70 – 130	70 – 130
100	–	70 – 130	–	–
200	–	50 – 200	<300	–

In this study, we assess if the different CE criteria are sufficient for the unambiguous assignment of vehicles into one of the two regimes of high and low emitters. To do so, we calculate the particle number an instrument barely meeting the criteria (upper and lower) would report. We calculate the deviation from the actual solid particle number, δN, according to Equation 1.

$$\delta N = \frac{1}{N_{\mathrm{tot}}} \int f^i_{\mathrm{lim}}(d_{\mathrm{p}}) p(d_{\mathrm{p}}) d(d_{\mathrm{p}}) - N_{\mathrm{tot}} \tag{1}$$

with

$$N_{\mathrm{tot}} = \int p(d_{\mathrm{p}}) d(d_{\mathrm{p}}) \tag{2}$$

the total particle number N_{tot}, measured by the instrument is calculated by integrating over the particle size distribution $p(d_{\mathrm{p}})$. As the removal of (semi-)volatile particles (Kittelson, 1998) is required for particle measurement systems (Giechaskiel et al., 2012), only the accumulation mode, which predominantly consists of solid particles, is considered for this assessment. The size distribution is weighted by the limit functions f^i_{lim} shown in Figure 3 as the border of the filled compliance areas, before the integration over the particle diameter (Equation 1).

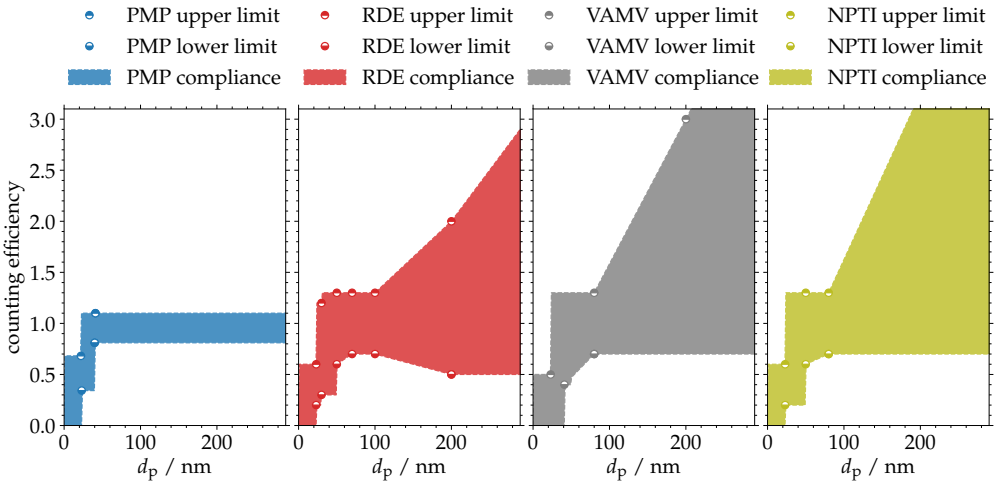

Figure 3: Visualization of regulative counting efficiency limit functions used for the calculation of the total particle number deviation according to Equation 1. These functions are obtained by step-wise interpolation below 50 nm and linear interpolation above 50 nm between the specified CE criteria that are indicated by circular markers. A linear increase is assumed above the largest specified particle sizes.

The limit functions are obtained by interpolating between the specified CE criteria that are indicated by circular markers. Depending on the particle size, two different modes of interpolation were applied to account for the characteristics of state-of-the-art particle number measurement devices. Below 50 nm, the specified points are interpolated with step functions to account for counting efficiency characteristics of condensation particle counters, that can exhibit steep slopes in the size regime below 50 nm. In the size regime above 50 nm, the defined points are linearly interpolated because the response of conventional diffusion charging based instruments scales approximately linearly with particle size (Nishida et al., 2019; Schriefl et al., 2020). A linear function that intersects the criterion at the largest specified particle diameter and the point (0,0) is the extrapolation of the upper counting efficiency limits beyond the largest specified particle diameter. The lower limit functions for all standards are assumed to be constant beyond the largest specified particle size.

The PMP regulation does not explicitly state an upper counting efficiency limit apart from the one at 23 nm (62 %). It was necessary to define an

upper limit of the counting efficiency for larger particle sizes to perform the described calculations. This additional definition was done on the basis that all commercially available PMP compliant measurement systems rely on CPC technology. This fact theoretically limits the counting efficiency to 100 %. Based on the experience of the authors, an estimated margin of 10 % (possibly arising from uncertainties of internal flow measurements and calibration) was added to the points specified in Table 2 to be in line with the other specifications' limit functions, which seek to map worst-case scenarios. Furthermore, an additional point at 41 nm and a counting efficiency of 110 % was added to the PMP specifications for the calculations described.

3.2. PTI Emission Reduction Impact

The reduction potential of the overall particle emissions of a fleet consisting of vehicles equipped with DPFs (Euro 5 and Euro 6) is assessed. It is assumed that a malfunctioned DPF can be detected with a reliability of $p_{\text{detect}} = 100\,\%$ in the course of a PTI by the application of particle number concentration measurements. Based on the findings of published studies (Boveroux et al., 2019), it is assumed that vehicles with improperly working DPFs are responsible for $F_{\text{broken DPF}} = 97\,\%$ of the particle emissions of the examined fleet. The available data on the aging behavior and breakage occurrence of DPFs is very limited. Therefore, five different scenarios of the probability density function for the occurrence of a particle filter malfunction are evaluated. The upper section of Figure 4 shows these scenarios. In the first scenario (constant), it is presupposed that the probability of the occurrence of a DPF malfunction is time-independent. The second (linear) and third (quadratic) scenarios assume a linearly and a quadratically rising probability, respectively. The fourth (onset linear) and fifth (onset constant) scenarios map that the DPF does not break in the first five years of operation. After five years, linearly increasing and constant probabilities are assumed, respectively. It is presupposed that the DPF of the vehicle will not break again if it was already repaired/replaced once. Upon the occurrence of a malfunction, it is presumed that the number of particles emitted by the vehicles is linearly proportional to the driven distances. The driven distances are assumed to be directly proportional to the times in circulation. A maximum vehicle age of 15 years is presumed to map the current and near-future fleet of EURO5 and EURO6 vehicles. For the vehicle age distribution, three different scenarios are assessed. The three scenarios are illustrated in the middle part of Figure 4. In the first scenario, the vehicle age distribution is

assumed to be flat (there is the same number of vehicles at each age between 0 and 15 years). This scenario simulates declining numbers of sold vehicle units. In the second scenario, the population of vehicles declines linearly with age, so that there is half the number of vehicles that are 15 years old compared to the number of new vehicles. This scenario maps the current fleet of vehicles in Germany in good approximation (KBA, 2019a). In the third scenario, which is more drastic, also a linear decline with age is assumed, but with the difference that the population of vehicles with the age of 15 years or older is assumed to be zero. This scenario would apply for a market where the number of vehicles sold is rising. The assessment is performed for the currently prescribed temporal PTI strategies of Germany, the Netherlands, and Belgium, which are the first European countries that are about to introduce particle number measurements in the course of PTI soon. In Germany, PTIs are foreseen every other year after four years. In Belgium, PTIs are scheduled every year after year four, and in the Netherlands, there is one inspection after two years and PTIs every year after four years. The lower section in Figure 4 shows the prescribed PTI schedules in the countries mentioned above. Three different PTI schedules, three different vehicle age distributions, and five different DPF aging scenarios yield a total number of 45 scenarios evaluated.

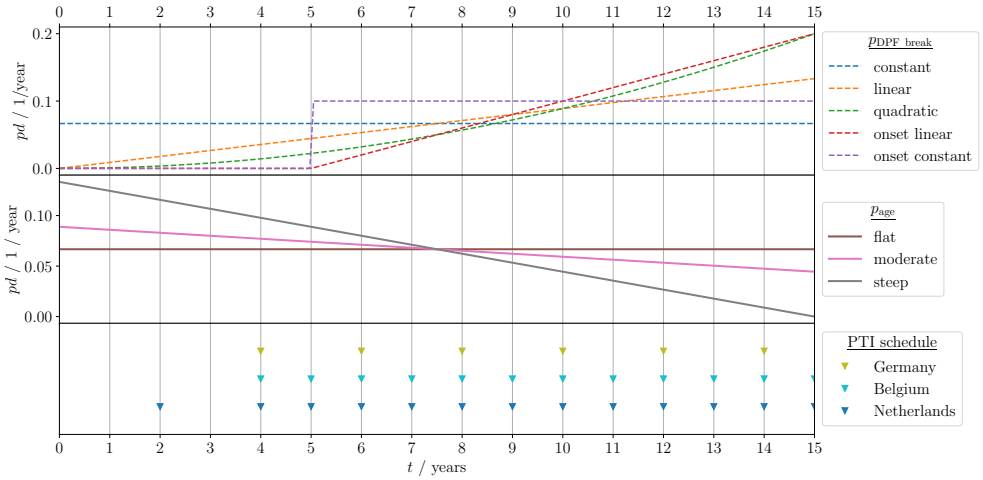

Figure 4: Illustration of different scenarios for DPF aging (top), vehicle population age distribution (middle) in the form of probability density (*pd*) functions and PTI schedules (bottom).

For these scenarios, the relative particle emission reduction R is calculated as described in Equation 3. The inner integral over t' calculates the contribution of one PTI to the reduction of time a vehicle with a broken particle filter is in circulation. This calculation consists of multiple steps. First, the probability that a particle filter breaks between a specific PTI and the previous one is evaluated, by integrating over the probability density function from the time of the previous PTI $t' = t_{PTI,i}$ to the time of the current PTI $t' = t_{PTI,i+1}$. Second, the obtained value is multiplied with the time difference between the age of the vehicle t and the time of the PTI $t_{PTI,i+1}$. Third, the contributions of all PTIs performed in the lifetime of the vehicle are summed up. The outer integral integrates the reduction of time in circulation weighted according to the distribution of vehicle ages from zero to maximal vehicle age ($T_{\max}$), which is 15 years for this assessment. Finally, the total reduction of time in circulation is normalized with the normalization factor Z, which is the total time, vehicles with broken particle filters were in circulation if the malfunctions were not repaired (Equation 4). The calculation of the potential reduction for each scenario was done numerically

using Python and the `scipy.integrate.quad` integration method.

$$R = \frac{F_{\text{DPF broken}}}{Z} \int_0^{T_{\max}} p_{\text{age}}(t) \sum_{t_{\text{PTI},i<t}} \int_{t'=t_{\text{PTI},i}}^{t'=t_{\text{PTI},i+1}} p_{\text{DPF break}}(t')(t - t_{\text{PTI},i+1}) dt' dt \tag{3}$$

$$Z = \int_0^{T_{\max}} p_{\text{age}}(t) \int_{t'=0}^{t'=t} p_{\text{DPF break}}(t')(t - t') dt' dt \tag{4}$$

Extenuating effects like possible tampering of the after-treatment system and temporary functionality restoration for the PTI are not considered.

4. Results and Discussion

4.1. Particle Number Concentration Measurements

The emitted particle number concentrations of a total number of 21 vehicles in low idle and high idle operation have been measured using three diffusion charger prototype instruments and a commercially available particle number reference instrument (AVL APC). The measurement procedure and the vehicles tested (Table 1) are described in section 2. Figure 5 shows the time-averaged results of the particle number concentration measurements. A black dashed line at a concentration of $2.5 \times 10^5\,\text{cm}^{-3}$ divides the measurement results into two regimes. The origin and motivation of this value are discussed in section 3. Concentrations below this line indicate a functional particle filter. Concentrations exceeding $2.5 \times 10^5\,\text{cm}^{-3}$ indicate that no particulate filter is installed, or the filter is not fully functional. A grey dashed line at $1 \times 10^3\,\text{cm}^{-3}$ shows the approximate noise level of the prototype diffusion chargers. Black, red and blue descriptions indicate diesel, GDI, and PFI vehicles, respectively.

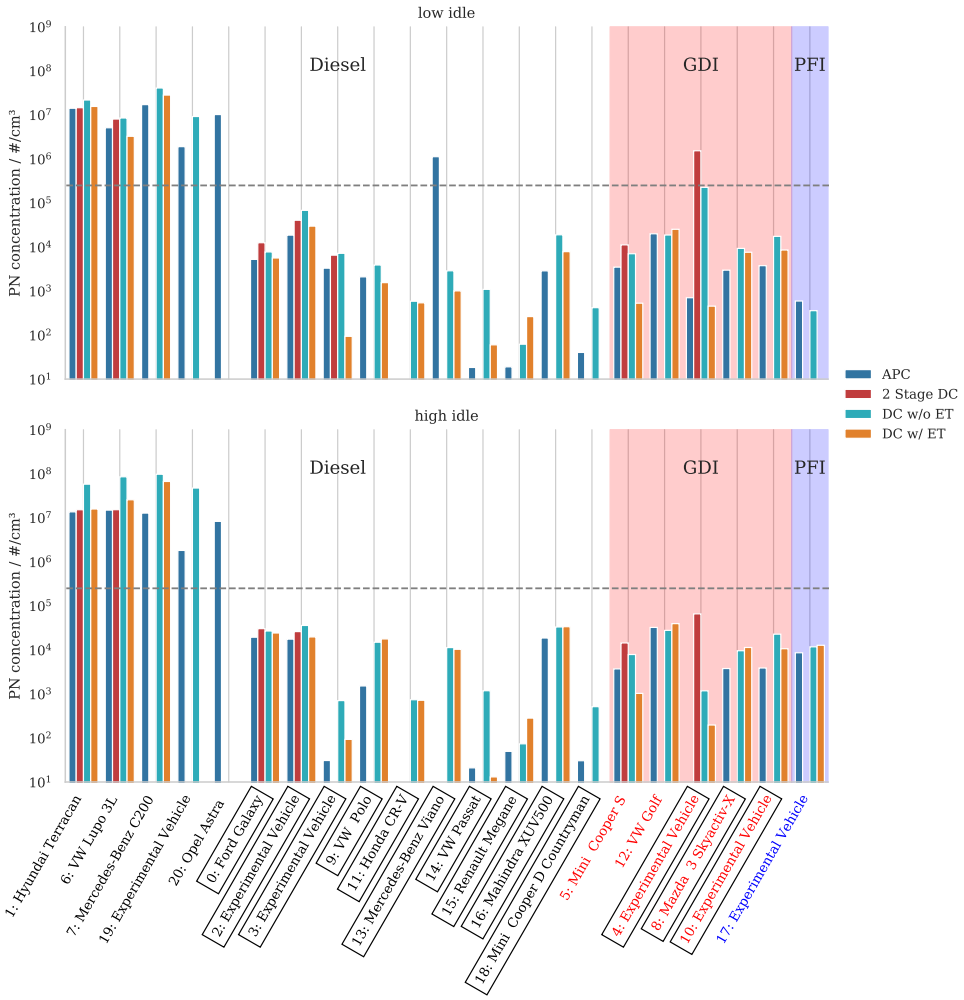

Figure 5: Number concentrations on a logarithmic scale as measured by the AVL APC and the three diffusion charger prototype instruments. A gray dashed line is drawn at a concentration of $2.5 \times 10^5\,\mathrm{cm}^{-3}$. Concentrations below this line indicate a functional particle filter. The upper and lower plot shows the results from the measurements in low and high idle, respectively. Red and blue vehicle descriptions indicate GDI and PFI vehicles, respectively. Black ones are powered by diesel. Vehicles with boxes around the descriptions are equipped with a particle filter.

4.1.1. Diesel Vehicles

Figure 5 shows that there are five high emitters (vehicles 1,6,7,19 and 20) among the 21 tested vehicles. The particle concentrations at the tailpipe of these five vehicles considerably exceed the threshold level of $2.5 \times 10^5\,\mathrm{cm}^{-3}$ in low and high idle operation. These exceedances were reliably detected by all measurement devices applied. All the high emitters are diesel cars without particulate filters. Vehicle 19 is a EURO 6 compliant diesel vehicle, where the DPF was removed. The other high emitters are EURO 3 or lower. Apart from the identified high emitters, there are two more singular measurement results exceeding the threshold value of $2.5 \times 10^5\,\mathrm{cm}^{-3}$. These are the low idle measurements of the two-stage DC of vehicle number four and the AVL APC measurement of the vehicle 13 in low idle operation. Both these events can be assigned to instrument malfunctions due to high water vapor concentrations in the gasoline engine exhaust. In the case of the measurement of vehicle number four, which is a high-performance SUV (550 hp), both the two-stage DC and the single-stage DC without evaporation tube reported elevated particle concentration levels compared to the APC and the DC with evaporation tube. These elevated particle concentrations demonstrate that measurement instruments without volatile particle remover are very prone to erroneous measurements due to high moisture levels. Apart from the immediate impact on measurement results, the high water content in gasoline exhaust can also have adverse effects on successive measurements. This indirect effect is clearly demonstrated by the measurement of vehicle 13, which is a EURO 6 compliant diesel with particle filter. Despite a fully functional exhaust after-treatment system, the AVL APC reported particle concentration values indicating a malfunctioned particle filter in the low idle test and stopped working during the high idle measurement. This behavior can be assigned to water that accumulated in the sampling line during the measurement of the gasoline vehicle before and entered the APC in the liquid phase during the measurement of vehicle 13. The liquid water that entered the primary diluter of the APC was evaporated and formed volatile particles downstream at the second dilution stage. Events like these, caused by the ingress of water, have been reported previously (Giechaskiel et al., 2019). Figure 6 shows two nucleation mode formation events (mode at 11 nm) lasting approximately 10 s each. The shown data was captured with the EEPS during the low idle measurement. The relatively small mean particle size and the absence of a second mode indicate that particles detected during these

events are volatile and formed by nucleation.

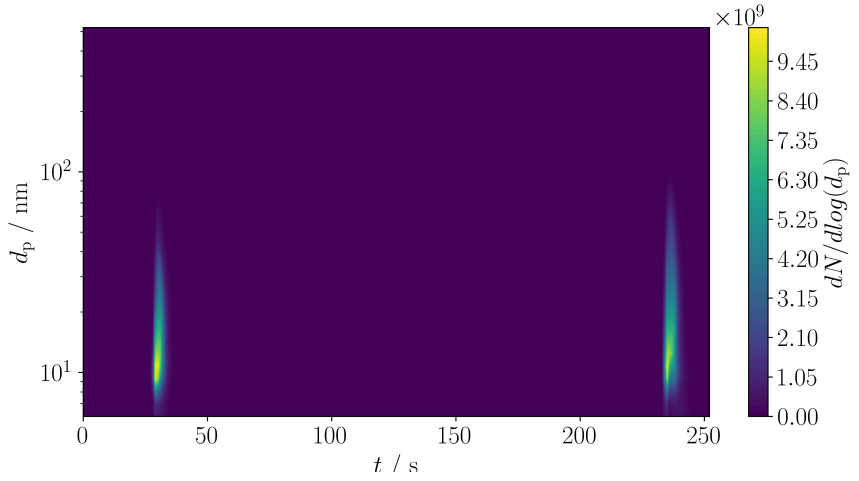

Figure 6: EEPS measurement of vehicle 13 (Mercedes-Benz Viano). There are two clearly visible nucleation mode formation events after 30 s and 235 s, both lasting approximately 10 s. An ingress of liquid water most probably causes the two events. Water condensed during the measurement of a gasoline vehicle shortly before. These two events dominate the overall particle number count in this measurement.

4.1.2. Gasoline Vehicles

During the low and high idle measurements of the gasoline vehicles, only once a concentration value above the threshold of $2.5 \times 10^5\,\mathrm{cm}^{-3}$ was reported by a measurement device. The 2 stage DC reported a concentration of more than $1 \times 10^6\,\mathrm{cm}^{-3}$ during the low idle measurement of vehicle 4. As discussed above, this can be assigned to a measurement instrument error caused by very high moisture levels. The only PFI vehicle investigated exhibited particle number concentrations well below the threshold value of $2.5 \times 10^5\,\mathrm{cm}^{-3}$ in high and low idle operation. The particle emissions of PFI vehicles are generally significantly less intense than the particle emissions of GDI vehicles.When the fuel is injected into the port, there is more time for fuel droplets to evaporate and mix with the oxidation. Directly injecting the fuel into the cylinder improves the fuel economy for the cost of increased particle emissions due to a less homogeneous mixture of fuel and air(Karavalakis et al., 2014; Bielaczyc et al., 2014; Graves et al., 2017). Three out of the five

GDI vehicles were equipped with particle filter. The measurement results shown in Figure 5 illustrate clearly that the difference between particle concentrations from GDI vehicles with and without particle filter is much lower than the difference between diesel vehicles with and without particle filters. The APC reported that the particle concentration levels of vehicle number 5, which are not equipped with a GPF are very similar to those from vehicles 8 and 10, which are equipped with GPFs. Although the sample size in this study is limited, the results from the gasoline vehicle measurements demonstrate that the definition of a threshold particle concentration level for the discrimination between functional and malfunctioned/removed gasoline particle filter is much more complicated than for diesel vehicles. Furthermore, the high moisture levels make the assessment of particle number concentration much more technically challenging. The DC prototype instruments are designed for the moisture levels that are expected in diesel exhaust. The adaption for the reliable measurement of particle number concentration in gasoline exhaust would require additional dilution, higher operation temperatures, or the implementation of a dedicated drying system. The adaption would, in any case, significantly increase the costs and complexity of the measurement instrument.

4.2. Size Distribution Measurements

Particle size distributions of the 21 vehicles in high and low idling operation were measured with an SMPS and an EEPS. The SMPS data was analyzed and interpreted during post-processing. The EEPS data was used for online monitoring during the measurements and the identification of possible transient events that would not be captured by the SMPS. The results from the SMPS and EEPS were generally in good agreement. Except for the water ingress event during the measurement of vehicle 13, no transient events were detected with the EEPS. In measurements where the particle number concentration exceeded $1 \times 10^4\,\mathrm{cm}^{-3}$, the SMPS signal was high enough to allow for the identification of distinct modes. The averages of the SMPS size distributions measured for each measurement point were fitted with a bimodal log-normal function.

The results from the particle size distribution measurements and the corresponding bimodal fits are listed in Table 3. Except for vehicle 8 in high idling operation, all size distributions were bimodal. The bimodal size distributions consisted of a nucleation mode and an accumulation mode. For the conditioning of the exhaust, the dilution system (rotating disc diluter,

Table 3: Table listing the measurements where the particle number concentration was sufficiently high ($> 1 \times 10^4\,\mathrm{cm}^{-3}$) to measure size distributions with reasonable signal-to-noise ratios. The geometric mean diameters (GMD) and geometric standard deviations (GSD) are listed for the nucleation mode and the accumulation mode.

Vehicle information			Nucleation Mode		Accumulation Mode		
Number	Type	Operation	GMD / nm	GSD / 1	GMD nm	GSD / 1	Total PN / cm^{-3}
1	Hyundai Terracan	low idle	5	1.60	60	2.06	1.5e+07
1	Hyundai Terracan	high idle	5	1.50	35	1.91	2.1e+07
2	Experimental Vehicle	low idle	11	1.31	62	1.99	5.5e+04
6	VW Lupo 3L	low idle	6	1.41	65	2.03	7.6e+06
6	VW Lupo 3L	high idle	8	1.43	42	1.68	4.8e+07
7	Mercedes-Benz C200	low idle	14	1.66	77	2.03	1.9e+07
7	Mercedes-Benz C200	high idle	-	-	48	1.79	6.3e+07
16	Mahindra XUV500	high idle	9	1.45	39	1.92	3.2e+04
19	VW Polo (DPF removed)	low idle	9	1.34	63	1.82	1.6e+07
19	VW Polo (DPF removed)	high idle	11	1.35	48	1.60	4.6e+07
20	Opel Astra	low idle	15	1.33	70	1.82	5.2e+07
20	Opel Astra	high idle	11	1.30	40	1.62	8.5e+07

evaporation tube, porous tube diluter) of the AVL APC was used. Considering that raw exhaust measurements were performed, a relatively low dilution ratio ($DR = 100$) was chosen. This dilution ratio was chosen to get sufficient signal for particle size distribution measurements. As a result, conditioning the exhaust lowered the number concentration and size of nucleation mode particles but did not inhibit their formation entirely (Giechaskiel et al., 2019; Giechaskiel, 2020; Zheng et al., 2011). The nucleation mode geometric mean diameters (GMD) observed in this study are between 5 nm and 15 nm. The accumulation mode GMDs range from 35 nm to 77 nm. These values are well in line with previously published studies on diesel exhaust particle size distributions (Harris and Maricq, 2001; Kittelson et al., 1998; Abdul-Khalek et al., 1998). The accumulation mode GMD is notably larger, while the geometric standard deviation (GSD) is lower in the low idle measurement compared to the high idle measurement.. This phenomenon is probably related to different residence times in the cylinder, where the coagulation rate is high due to a high particle concentration. In high idle, the residence time is lower, and as a result, the emitted particles are smaller. (Hinds, 2001).

4.3. Assessment of Instrument Specifications

Previous studies and the particle number measurement results of this study show that vehicles that are equipped with functional particle filters exhibit exhaust PN concentrations below $5 \times 10^4\,\mathrm{cm}^{-3}$. The exhaust of diesel vehicles without or with malfunctioned DPF emit more than $1 \times 10^6\,\mathrm{cm}^{-3}$

(Burtscher et al., 2019). Accordingly, vehicles can be categorized into low emitters($< 5 \times 10^4\,\mathrm{cm}^{-3}$) or high emitters ($> 1 \times 10^6\,\mathrm{cm}^{-3}$). As a threshold level for this categorization, a value of $2.5 \times 10^5\,\mathrm{cm}^{-3}$ has been defined by the NPTI working group (VERT, 2019; Ministry for Infrastructure and Public Works, 2019) and for the PTI test of off-road machinery in Switzerland according to the Swiss regulation SR 941.242 for exhaust measurement instruments (VAMV) (EJPD, 2006). We assessed if the instrument specifications, shown in Figure 3, are sufficient to reliable categorize vehicles into high or low emitters assuming a threshold value of $2.5 \times 10^5\,\mathrm{cm}^{-3}$. To demonstrate the method of calculating the maximal possible deviations specification compliant instruments can exhibit, described in subsection 4.3, we assume a typical diesel solid particle number size distribution with a GMD of 70 nm and a GSD of 1.7 (Harris and Maricq, 2001).

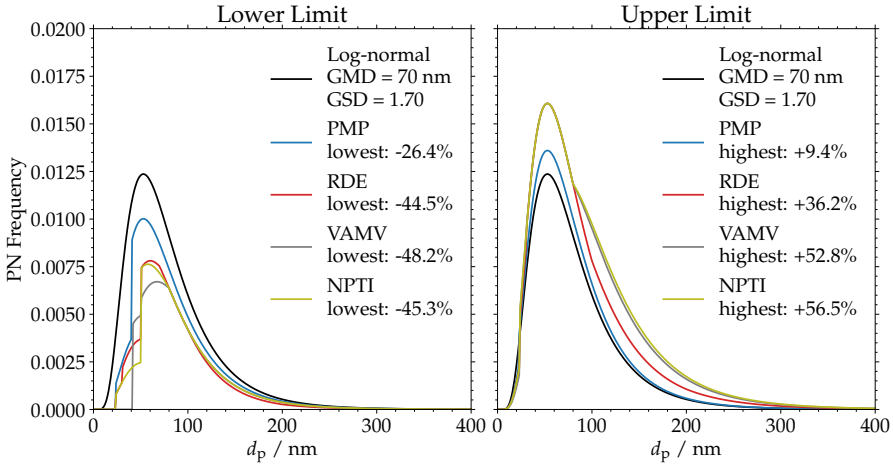

Figure 7: Visualization of size dependent maximum theoretical particle number concentration underestimation (left) and overestimation (right) for a typical diesel size distribution that is weighted by regulative counting efficiency limit curves. The figure legends show the calculated values for the maximum theoretical underestimation and overestimation.

The left plot in Figure 7 shows this size distribution curve, and the same curve weighted by the lower limit functions. It can be seen that weighing this size distribution with the lower CE limit functions leads to underestimating the total particle number. The maximal underestimations of the total parti-

cle number concentration for this size distribution range between 18.3 % for a PMP compliant instrument and 48.2 % for a VAMV compliant instrument. The right plot in Figure 7 shows the maximal overestimation of the typical diesel exhaust size distribution for the different counting efficiency criteria. The values range between 4.4 % (PMP) and 56.5 % (NPTI). Under the assumption of a limit value of $2.5 \times 10^5\,\mathrm{cm}^{-3}$ and a maximum overestimation of 56.5 % for the NPTI upper limit, a vehicle that emits $1.6 \times 10^5\,\mathrm{cm}^{-3}$ would pass the PTI test. As mentioned before, a vehicle with a working DPF will emit less than $5 \times 10^4\,\mathrm{cm}^{-3}$. Hence, any of the evaluated upper counting efficiency limits are sufficiently low to exclude false fail scenarios of vehicles emitting particles with a typical diesel exhaust size distribution (GMD =70 nm, GMD = 1.70).

In the same manner, the results from the lower counting efficiency limits can be used to assess the possibility of false pass cases. Assuming a limit value of $2.5 \times 10^5\,\mathrm{cm}^{-3}$ and a maximum underestimation of 48.2 %, a vehicle that emits $4.8 \times 10^5\,\mathrm{cm}^{-3}$ would just pass the PTI test. However, literature results (Gloor, 2018; Burtscher et al., 2019; Buekenhoudt et al., 2019; Yamada, 2019), and our measurements have shown that a broken or removed DPF will cause emissions clearly above $1 \times 10^6\,\mathrm{cm}^{-3}$. Therefore, false pass scenarios can be excluded for instruments complying with any of the evaluated counting efficiency limits if the emitted particle size distribution is that of typical diesel exhaust

Of course, it cannot be assumed that the size and widths of vehicle emission particle size distributions are always in the range of typical values. The method demonstrated above for a typical diesel exhaust particle size distribution is applied for the size distributions measured within this study and consecutively generalized for unimodal log-normal size distributions to deduce a more general statement on the validity of the counting efficiency specifications under discussion. The results from the calculation evaluating the maximal underestimations/overestimations of PN concentrations of a measurement device that is compliant with the specifications shown in Figure 3 and the size distributions measured in this study are listed Table 4.

Table 4: Maximal over and underestimations of particle number concentration for different instrument specifications and the size distributions measured in the course of the measurement campaign of this study sorted by the GMD.

GMD / nm	GSD / 1	Operation	PMP		RDE		VAMV		NPTI	
			lower	upper	lower	upper	lower	upper	lower	upper
35	1.9	high idle	-55%	+0%	-69%	+12%	-78%	+14%	-72%	+18%
39	1.9	high idle	-50%	+2%	-65%	+17%	-73%	+21%	-67%	+24%
40	1.6	high idle	-47%	+6%	-64%	+20%	-75%	+22%	-68%	+24%
42	1.7	high idle	-45%	+6%	-62%	+21%	-72%	+24%	-65%	+26%
48	1.8	high idle	-40%	+6%	-57%	+24%	-65%	+31%	-60%	+34%
48	1.6	high idle	-37%	+8%	-56%	+26%	-65%	+30%	-60%	+31%
60	2.1	low idle	-35%	+7%	-53%	+35%	-57%	+53%	-53%	+59%
62	2.0	low idle	-34%	+7%	-51%	+35%	-56%	+53%	-52%	+58%
63	1.8	low idle	-31%	+8%	-49%	+34%	-54%	+49%	-50%	+52%
65	2.0	low idle	-33%	+7%	-51%	+38%	-54%	+59%	-51%	+65%
70	1.8	low idle	-28%	+9%	-46%	+38%	-50%	+58%	-47%	+62%
77	2.0	low idle	-29%	+8%	-47%	+48%	-49%	+76%	-46%	+84%

As expected, the most severe possible underestimations of particle number concentration are found for the particle size with the smallest geometric mean diameters (GMD = 35 nm to 48 nm). All these size distributions were measured in high idle operation. The maximal possible underestimations exceed 60 % for the RDE, VAMV, and NPTI specifications. The highest possible underestimation is found to be 78 % for the VAMV limits and the distribution with a GMD of 35 nm and a GSD of 1.9. Following the thoughts above, underestimations exceeding 75 % would theoretically threaten the unambiguous categorization into low and high emitters. A vehicle that exhibits particle number concentrations of $1 \times 10^6\,\mathrm{cm}^{-3}$, which could indicate a malfunctioned after-treatment system, would pass the test with a threshold value of $2.5 \times 10^5\,\mathrm{cm}^{-3}$. The maximal possible negative measurement deviations for the evaluated instrument specifications and unimodal log-normal size distributions are shown in three-dimensional plots in Figure 8 in the form of planes as functions of the size distributions' GMD and GSD. The data in Table 4 is illustrated as green crosses (low idle) and circles (high idle). A black horizontal plane indicates the threshold of an underestimation of the particle number concentration of 75 %, which threatens the exclusion of false pass cases. It can be seen that the points from the high idle measurements approach this threshold for the RDE and NPTI specifications. As discussed above, one measured size distribution leads to a maximal possible underestimation of 78 % for the VAMV specifications, exceeding the indicated threshold value.

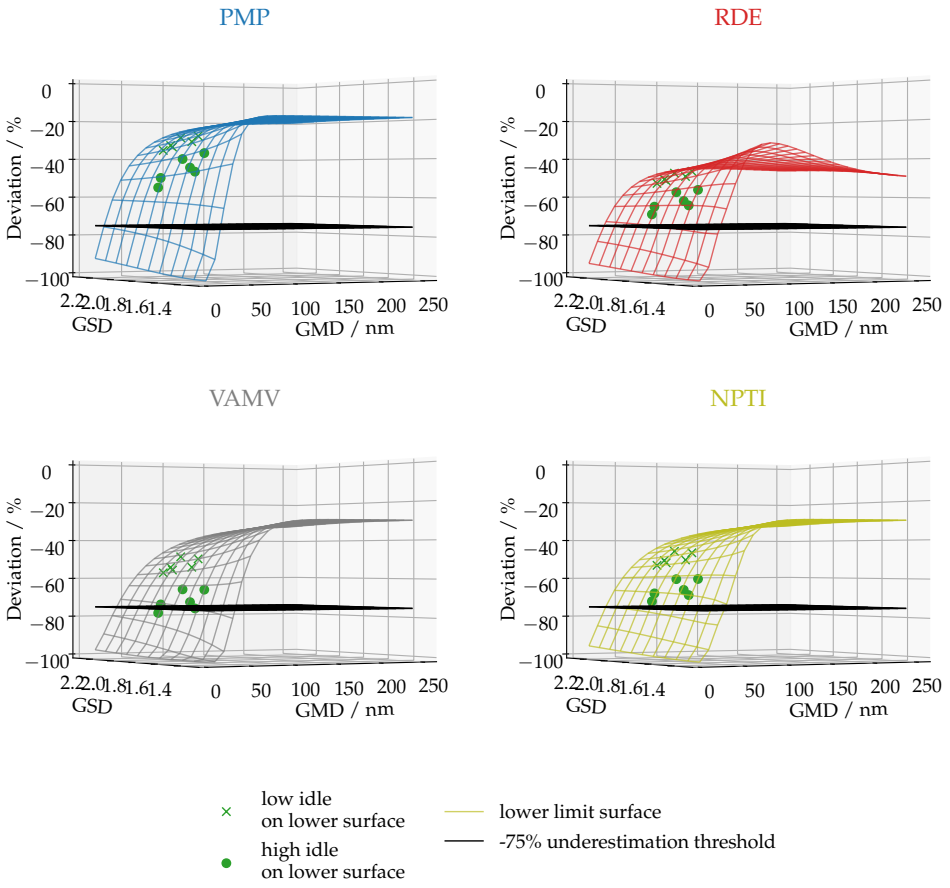

Figure 8: The wireframe surfaces indicate the lower maximal measurement deviations by instruments complying with the respective regulation as a function of the GSD and the GMD of unimodal log-normal distributions. The green crosses (low idle) and circles (high idle) indicate the positions of the evaluated measured size distributions on these surfaces (data as listed in Table 4).

Overestimations exceeding 30 % are obtained for various cases with the RDE, the VAMV, and the NPTI upper limits (see Table 4). The most considerable overestimation (84 %) is obtained applying the NPTI upper limit function for the size distribution with the largest GMD measured. This overestimation would mean, that a vehicle with an actual emission of $1.36 \times 10^5\,\mathrm{cm}^{-3}$ would fail the PTI test. Following the thoughts above, this case does not threaten the unambiguous categorization of vehicles in high or low emitters. As vehicles with working DPFs emit less than $5 \times 10^4\,\mathrm{cm}^{-3}$, with a threshold value of $2.5 \times 10^5\,\mathrm{cm}^{-3}$ an overestimation of 400 % could be accepted.

Analogously to Figure 8, the maximal possible positive measurement deviations for the evaluated instrument specifications and unimodal log-normal size distributions are shown in three-dimensional plots in Figure 9 respectively, in the form of planes as functions of the size distributions' GMD and GSD. The data in Table 4 is illustrated as red (upper limit) crosses (low idle) and circles (high idle). For the evaluated instrument specifications, deviations exceeding 400 % can only theoretically occur for size distributions with GMDs beyond 200 nm assuming reasonable GSDs below 2.3. To the best of our knowledge, no automotive exhaust particle size distributions with comparable high geometric mean diameters have been reported in the literature. Thus, we conclude that any of the evaluated CE criteria are sufficiently strict about excluding false fail scenarios reliably.

It has to be stressed that the performed evaluations seek to provide upper and lower boundaries for the measurement deviations. Worst-case scenarios have been constructed, that would be technically extremely challenging to replicate in realistic measurement scenarios. Under the assumption of these unrealistic worst-case scenarios, one of the size distribution measured would theoretically barely allow for an underestimation of particle number concentration by a VAMV compliant measurement instrument so that a false pass scenario cannot be entirely excluded. While DC-based instruments fulfilling one of the regulations mentioned, tend to overestimate the signal, underestimation can be a problem for CPC based devices, especially if they are calibrated with materials other than soot (Wang et al., 2010). Although the constructed worst-case scenario is not very probable in reality, we conclude that performing tests in low idle speed would be advantageous compared to high idle speed. Due to higher GMDs and GSDs of the emitted size distributions, the maximal possible underestimation is reduced. The reduced possible underestimation can also be seen in the plots in Figure 8, where the size distributions measured during low idle speed and high idle speed form

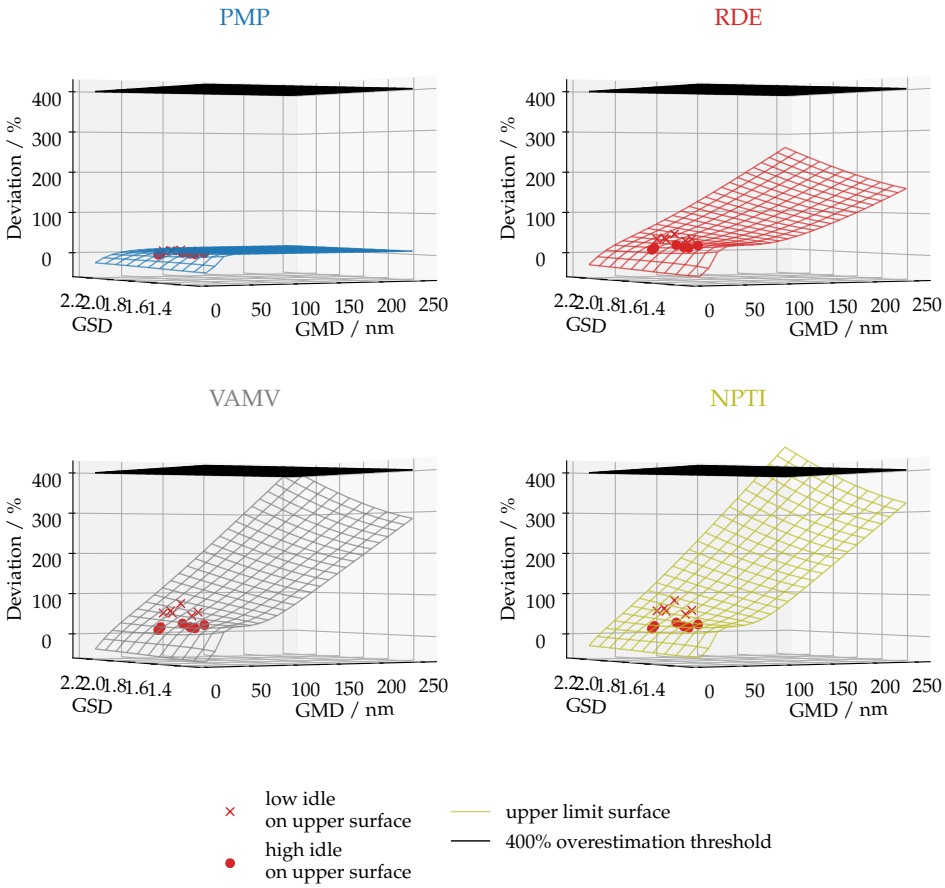

Figure 9: The wireframe surfaces indicate the upper maximal measurement deviations by instruments complying with the respective regulation as a function of the GSD and the GMD of unimodal log-normal distributions. The red crosses (low idle) and circles (high idle) indicate the positions of the evaluated measured size distributions on these surfaces (data as listed in Table 4).

two distinct clusters with the low idle cluster being located in a regime where much lower magnitudes of underestimations are possible. Furthermore, performing tests in low idle speed does not raise the risk of false fail scenarios. As illustrated in Figure 9, the maximal overestimations associated with the size distributions measured in low idle operation are by no means close to critical levels. Performing tests in low idle is an effective means to improve the measurement accuracy without mandating stricter instrumentation specifications.

4.4. PTI Emission Reduction Impact

The possible impact of PTI particle number measurements on the fleet emissions was evaluated as described in subsection 3.2. Figure 10 shows the results of the PTI impact assessment. The most pessimistic scenarios predict a particle emission reduction of 60 % (German PTI schedule, constant or onset linear DPF aging, steep vehicle age distribution). The most optimist scenarios predict a reduction by 83 %.

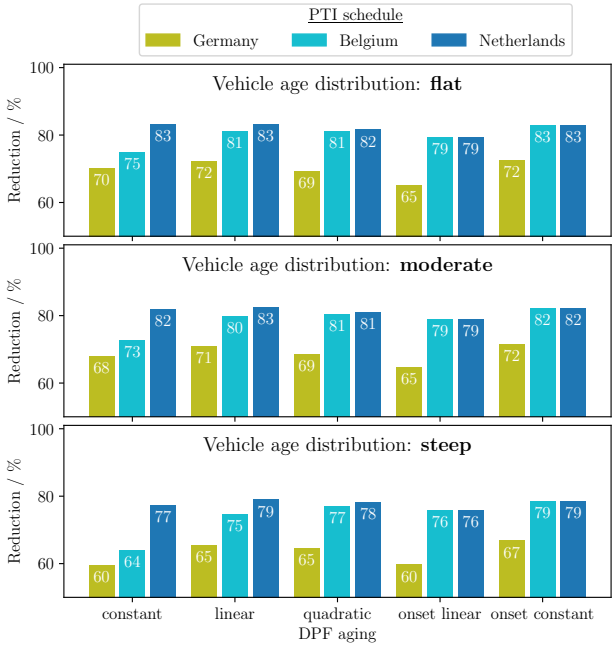

Figure 10: Illustration of maximal particle emission reduction potential calculated for different DPF aging scenarios, fleet age distributions and prescribed PTI schedules in selected European countries.

Due to a lack of available data, the highest degree of uncertainty is attributed to the DPF aging scenario in this assessment. The highest deviation (15 %) due to the variation of the DPF aging scenario occurs for the Belgian PTI schedule and a steep vehicle age distribution. For the German PTI schedule, the maximal deviation due to the variation of the DPF aging scenario amounts to 7 %. The Dutch PTI schedule is the most robust one in this aspect, with a maximal deviation of 4 %. For all DPF aging scenarios, the German PTI schedule combined with a steep vehicle age distribution, predicts the lowest improvement and the Dutch PTI schedule with a flat vehicle age distribution predicts the highest impact. For all evaluated scenarios, the relative reduction of particle emissions due to PN PTI measurements is higher, the flatter the vehicle age distribution is. Hence, the relative reduction of particle emissions in a market with declining numbers of sold vehicles exceeds the reduction in markets with increasing numbers of sold vehicles. The comparison between the German PTI schedule and the Dutch

PTI schedule shows the impact of doubling the frequency of PTIs. Depending on the scenarios for DPF aging and vehicle age distribution, the higher PTI frequency in the Netherlands yields a further reduction of fleet particle emissions between 17 % (constant DPF aging, steep vehicle population) and 11 %. Although this assessment is based on some assumptions and idealizations, it is evident that PN measurements in the course of PTI have the potential to reduce the overall particle emissions of diesel vehicles that are equipped with DPFs by more than 50 %. Consequently, PTI PN measurements can contribute significantly to air quality improvement by identifying malfunctioned exhaust after-treatment systems.

5. Conclusion

The measurement results from this study demonstrate that diesel vehicles with properly working after-treatment systems can be reliably distinguished from vehicles with removed or malfunctioned particle filters employing particle number concentration measurements during low idle or high idle operation, which is in agreement with previously published data (Burtscher et al., 2019; Boveroux et al., 2019; Kadijk et al., 2017). Measurements of this kind can be performed in regular workshops within periodic technical inspections. The particle concentrations measured at the tailpipes of vehicles without DPFs exceed the concentrations measured at the tailpipes of vehicles with functional DPFs by more than one order magnitude. This large discrepancy allows for the application of relatively inexpensive measurement equipment to reliably distinguish between low emitters and high emitters. The measurement results from the examined gasoline vehicles demonstrate that the assessment of the functionality/existence of a GPF through particle concentration measurements is much more complex and challenging than for diesel vehicles. The detected particle concentration levels of vehicles with and without particle filter can be on the same order of magnitude. The high moisture levels of gasoline exhaust are a technical challenge for particle number measurement devices in general. We furthermore observed that condensed water that accumulated during the measurement of a gasoline vehicle caused erroneous results in subsequent measurement of a diesel vehicle.

The results from particle size distribution measurements show a clear trend towards broader size distributions and larger geometric mean diameters during low idle operation compared to high idle speed. In the assessment of instrument specifications under discussion, the larger particle sizes

observed in low idle operation were found to facilitate the exclusion of false pass scenarios in PTI PN tests. Simulating worst-case scenarios, the small particle sizes emitted in high idle operation could theoretically lead to false pass scenarios. Therefore, performing tests in low idle operation is preferable over tests in high idle speed.

We assessed the possible impact of introducing particle number concentration measurements over periodic technical inspections on the overall particle emissions from vehicles equipped with diesel particle filters. Different scenarios of fleet age distributions, DPF aging behaviors, and PTI schedules were evaluated. The expected reductions for the different scenarios range between 60 % and 83 %. These numbers demonstrate that PTI PN measurements can contribute significantly to the improvement of air quality by identifying malfunctioned exhaust after-treatment systems. The effect can be especially pronounced in European countries where the amount of diesel-powered passenger cars is substantial (e.g., 32.1 % in Germany in 2019 (KBA, 2019b)) and the majority of vehicles is compliant with the EURO 5 or newer standards (KBA, 2019a). In the future ,particle emissions caused by vehicles with improperly working after-treatment system may be further reduced by the implementation of remote sensing for particulates. Remote sensing is an established technique for gaseous pollutants like nitric oxide, carbon monoxide, and hydrocarbons (Smit et al., 2010; Smit and Bluett, 2011). The extension towards remote sensing of particulate emissions is currently under development in the course of the EU Horizon2020 project CARES (CARES, 2019). Remote particle emission sensing could be realized by mobile laboratories (Pirjola et al., 2004) that chase cars to evaluate their emissions or stationary roadside measurements. Identifying possible high emitters directly on the road and mandating PTI-like checks in a nearby workshop would enable repairing or replacing particle filters shortly after a malfunction occurs. Furthermore, with the mechanism of remote sensing, tampering with particle filters for improved fuel consumption could be tackled effectively. These illegal actions could be prevalent for commercial light-duty and heavy-duty vehicles, contributing significantly to air pollution. They cannot be effectively counteracted with PN PTI measurements because vehicle owners can reestablish the functionality of after-treatment systems temporarily to pass the technical inspections.

In summary, it can be said that the introduction of particle number measurements in the course of periodic technical inspections can lead to significant short term improvements of the air quality in Europe and there is

potential for an even more significant impact in the future by the combination with remote sensing of particulate emissions.

Acknowledgement

The authors thank Jason Olfert for providing constructive comments and suggestions that significantly improved the paper's quality.

The authors acknowledge Christos Dardiotis, Thanasis Mamakos and Martin Kupper from AVL GmbH for providing and calibrating the laboratory-grade measurement equipment. We further thank Tristan Reinisch, Manuel Neuhold, and Philipp Geistlinger from AVL DiTEST for supporting the measurements and Martin Kammerhofer for his help regarding OBD data. Furthermore, we thank Michael Zallinger, Florian Ansperger, and their teams for providing the facilities for the experiments. Special thanks go to Simon Teppernegg for his high helpfulness, which went far beyond his professional duties.

References

Abdul-Khalek, I.S., Kittelson, D.B., Graskow, B.R., Wei, Q., Brear, F., 1998. Diesel Exhaust Particle Size: Measurement Issues and Trends. SAE Transactions 107, 683–696. URL: http://www.jstor.org/stable/44736561.

Andersson, J., 2019. Sub-23 nm particle measurement methodology roadmap. 50th PMP Meeting URL: https://wiki.unece.org/download/attachments/75532498/20190403_PMP_sub23_roadmap.pdf.

Bielaczyc, P., Woodburn, J., Szczotka, A., 2014. Particulate Emissions from European Vehicles Featuring Direct Injection Spark Ignition Engines Tested Under Laboratory Conditions. SAE International Journal of Fuels and Lubricants 7, 580–590. doi:10.4271/2014-01-1608.

Boveroux, F., Cassiers, S., Buekenhoudt, P., Chavatte, L., De Meyer, P., Jeanmart, H., Verhelst, S., Contino, F., 2019. Feasibility study of a new test procedure to identify high emitters of particulate matter during periodic technical inspection. SAE Technical Papers 2019-April, 2–9. doi:10.4271/2019-01-1190.

Brook, R.D., Rajagopalan, S., Pope, C.A., Brook, J.R., Bhatnagar, A., Diez-Roux, A.V., Holguin, F., Hong, Y., Luepker, R.V., Mittleman, M.A., Peters, A., Siscovick, D., Smith, S.C., Whitsel, L., Kaufman, J.D., 2010. Particulate matter air pollution and cardiovascular disease: An update to the scientific statement from the american heart association. doi:10.1161/CIR.0b013e3181dbece1.

Buekenhoudt, P., De Meyer, P., Chavatte, 2019. PN study - New fine particle emission measurement for the assessment of the quality of the particulate filter during the periodic inspection of diesel vehicles, in: Presentation for 10 years VERT Forum on 14th of March 2019, Dübendorf.

Burtscher, H., Lutz, T., Mayer, A., 2019. A New Periodic Technical Inspection for Particle Emissions of Vehicles. Emission Control Science and Technology doi:10.1007/s40825-019-00128-z.

CARES, 2019. CARES — City Air Remote Emission Sensing. URL: https://cares-project.eu/.

EC, 2017. Commission Regulation (EU) 2017/1154. Official Journal of the European Union URL: https://eur-lex.europa.eu/eli/reg/2017/1154/oj.

EJPD, 2006. SR 941.242 Verordnung des EJPD vom 19. März 2006 über Abgasmessmittel für Verbrennungsmotoren (VAMV). URL: https://www.admin.ch/opc/de/classified-compilation/20051389/index.html.

Giechaskiel, B., 2020. VOLATILE REMOVAL EFFICIENCY & PARTICLE LOSSES IN PMP SYSTEMS. URL: https://www.researchgate.net/publication/338644148_Volatile_removal_efficiency_particle_losses_in_PMP_systems.

Giechaskiel, B., Lahde, T., Suarze-Bertoa, R., Clairotte, M., Grigoratos, T., Zardini, A., Perujo, A., Martini, G., 2018. Particle number measurements in the European legislation and future JRC activities. Combustion Engines 174, 3–16. doi:10.19206/CE-2018-301.

Giechaskiel, B., Mamakos, A., Andersson, J., Dilara, P., Martini, G., Schindler, W., Bergmann, A., 2012. Measurement of automotive non-volatile particle number emissions within the European legislative frame-

work: A review. Aerosol Science and Technology 46, 719–749. doi:10.1080/02786826.2012.661103.

Giechaskiel, B., Mamakos, A., Woodburn, J., Szczotka, A., Bielaczyc, P., 2019. Evaluation of a 10 nm Particle Number Portable Emissions Measurement System (PEMS). Sensors 19, 5531. URL: https://www.mdpi.com/1424-8220/19/24/5531, doi:10.3390/s19245531.

Gloor, B., 2018. Survey about functional efficiency of DPF during PTI in Zürich. ETH-Conference URL: http://www.nanoparticles.ch/archive/2018_Gloor_FO.pdf.

Graves, B.M., Koch, C.R., Olfert, J.S., 2017. Morphology and volatility of particulate matter emitted from a gasoline direct injection engine fuelled on gasoline and ethanol blends. Journal of Aerosol Science 105, 166–178. doi:10.1016/j.jaerosci.2016.10.013.

Gysel, M., Laborde, M., Mensah, A.A., Corbin, J.C., Keller, A., Kim, J., Petzold, A., Sierau, B., 2012. Technical Note: The single particle soot photometer fails to reliably detect PALAS soot nanoparticles. Atmospheric Measurement Techniques 5, 3099–3107. URL: https://www.atmos-meas-tech.net/5/3099/2012/, doi:10.5194/amt-5-3099-2012.

Harris, S.J., Maricq, M., 2001. Signature size distributions for diesel and gasoline engine exhaust particulate matter. Journal of Aerosol Science 32, 749–764. doi:10.1016/S0021-8502(00)00111-7.

Helsper, C., Mölter, W., Löffler, F., Wadenpohl, C., Kaufmann, S., Wenninger, G., 1993. Investigations of a new aerosol generator for the production of carbon aggregate particles. Atmospheric Environment Part A, General Topics 27, 1271–1275. doi:10.1016/0960-1686(93)90254-V.

Hinds, W., 2001. Aerosol Technology. Methods of Biochemical Analysis 2, 0–471. doi:10.1037/023990.

Kadijk, G., Elstgeest, M., Ligterink, N.E., van der Mark, P.J., 2016. Investigation into a Periodic Technical Inspection (PTI) test method to check for presence and proper functioning of Diesel Particulate Filters in light-duty diesel vehicles. URL: www.tno.nlhttps://publications.tno.nl/publication/34620651/rrjJYZ/TNO-2016-R10735.pdf.

Kadijk, G., Elstgeest, M., Ligterink, N.E., van der Mark, P.J., 2017. Investigation into a Periodic Technical Inspection (PTI) test method to check for presence and proper functioning of Diesel Particulate Filters in light-duty diesel vehicles - part 2. Technical Report. Earth, Life & Social Sciences. Den Haag. URL: www.tno.nl.

Karavalakis, G., Short, D., Vu, D., Villela, M., Asa-Awuku, A., Durbin, T.D., 2014. Evaluating the regulated emissions, air toxics, ultrafine particles, and black carbon from SI-PFI and SI-DI vehicles operating on different ethanol and iso-butanol blends. Fuel 128, 410–421. doi:10.1016/j.fuel.2014.03.016.

KBA, 2019a. Kraftfahrt-Bundesamt - Bestand. URL: https://www.kba.de/DE/Statistik/Fahrzeuge/Bestand/bestand_node.html.

KBA, 2019b. Kraftfahrt-Bundesamt - Umwelt - Bestand an Pkw am 1. Januar 2019 nach ausgewählten Kraftstoffarten. URL: https://www.kba.de/DE/Statistik/Fahrzeuge/Bestand/Umwelt/2019_b_umwelt_dusl.html?nn=663524.

Kittelson, D.B., 1998. Engines and nanoparticles: A review. Journal of Aerosol Science 29, 575–588. doi:10.1016/S0021-8502(97)10037-4.

Kittelson, D.B., Watts, W.F., Arnold, M.J., Department of Mechanical Engineering, C.o.D.R., 1998. Review of diesel particulate matter sampling methods. Supplemental report #2. Aerosol dynamics, laboratory and on-road studies. Report on EPA grant 2, 60.

Mamakos, A., 2016. Methodology to quantify the ratio of multiple-to single-charged fractions acquired in aerosol neutralizers. Aerosol Science and Technology 50, 363–372. doi:10.1080/02786826.2016.1153034.

Ministry for Infrastructure and Public Works, 2019. Regulation of the Minister for Environment and Housing of November 21, 2019, No. IENW / BSK-2019/202498, amending the Vehicle Regulations to enable the control of diesel particulate filters with a particle counter and a number of other technical changes. Technical Report. Ministry for Infrastructure and Public Works.

Nishida, R.T., Yamasaki, N., Schriefl, M.A., Boies, A.M., Hochgreb, S., 2019. Modelling the effect of aerosol polydispersity on unipolar charging and

measurement. Journal of Aerosol Science 130, 10–21. URL: https://doi.org/10.1016/j.jaerosci.2019.01.003, doi:10.1016/j.jaerosci.2019.01.003.

Oberdörster, G., Oberdörster, E., Oberdörster, J., 2005. Nanotoxicology: An emerging discipline evolving from studies of ultrafine particles. Environmental Health Perspectives 113, 823–839. doi:10.1289/ehp.7339.

Olfert, J., Rogak, S., 2019. Universal relations between soot effective density and primary particle size for common combustion sources. URL: https://www.tandfonline.com/doi/full/10.1080/02786826.2019.1577949, doi:10.1080/02786826.2019.1577949.

Pant, P., Harrison, R.M., 2013. Estimation of the contribution of road traffic emissions to particulate matter concentrations from field measurements: A review. Atmospheric Environment 77, 78–97. URL: http://dx.doi.org/10.1016/j.atmosenv.2013.04.028, doi:10.1016/j.atmosenv.2013.04.028.

Peters, A., Von Klot, S., Heier, M., Trentinaglia, I., Hörmann, A., Wichmann, H.E., Löwel, H., 2004. Exposure to traffic and the onset of myocardial infarction. New England Journal of Medicine 351, 1721–1730. URL: http://www.nejm.org/doi/abs/10.1056/NEJMoa040203, doi:10.1056/NEJMoa040203.

Pirjola, L., Parviainen, H., Hussein, T., Valli, A., Hämeri, K., Aaalto, P., Virtanen, A., Keskinen, J., Pakkanen, T.A., Mäkelä, T., Hillamo, R.E., 2004. "Sniffer" - A novel tool for chasing vehicles and measuring traffic pollutants. Atmospheric Environment 38, 3625–3635. doi:10.1016/j.atmosenv.2004.03.047.

Schriefl, M.A., Bergmann, A., Fierz, M., 2019. Design principles for sensing particle number concentration and mean particle size with unipolar diffusion charging. IEEE Sensors Journal 19, 1392–1399. doi:10.1109/JSEN.2018.2880278.

Schriefl, M.A., Nishida, R.T., Knoll, M., Boies, A.M., Bergmann, A., 2020. Characterization of particle number counters based on pulsed-mode diffusion charging. Aerosol Science and Technology , 1–18doi:10.1080/02786826.2020.1724257.

Smit, R., Bluett, J., 2011. A new method to compare vehicle emissions measured by remote sensing and laboratory testing: High-emitters and potential implications for emission inventories. Science of the Total Environment 409, 2626–2634. doi:10.1016/j.scitotenv.2011.03.026.

Smit, R., Ntziachristos, L., Boulter, P., 2010. Validation of road vehicle and traffic emission models - A review and meta-analysis. doi:10.1016/j.atmosenv.2010.05.022.

United Nations Economic Commission for Europe, 2006. Regulation No 83 of the Economic Commission for Europe of the United Nations (UN/ECE) – Uniform provisions concerning the approval of vehicles with regard to the emission of pollutants according to engine fuel requirements. Publications Office of the European Union URL: https://op.europa.eu/en/publication-detail/-/publication/2f8f0ce5-66fb-4a38-ae68-558ae1b04a5f/language-en.

VERT, 2019. VERT initiative for "New periodic technical inspection" (NPTI). URL: https://www.vert-dpf.eu/j3/index.php/projects/technology-projects/9-cat-projects/50-inspection-diesel-and-gasoline-motors.

Wang, X., Caldow, R., Sem, G.J., Hama, N., Sakurai, H., 2010. Evaluation of a condensation particle counter for vehicle emission measurement: Experimental procedure and effects of calibration aerosol material. Journal of Aerosol Science 41, 306–318. doi:10.1016/j.jaerosci.2010.01.001.

Yamada, H., 2019. Improving Methodology of Particulate Measurement in Periodic Technical Inspection with High-Sensitivity Techniques: Laser Light Scattering Photometry and Particle Number Method. Emission Control Science and Technology 5, 37–44. doi:10.1007/s40825-019-0108-z.

Zheng, Z., Johnson, K.C., Liu, Z., Durbin, T.D., Hu, S., Huai, T., Kittelson, D.B., Jung, H.S., 2011. Investigation of solid particle number measurement: Existence and nature of sub-23nm particles under PMP methodology. Journal of Aerosol Science 42, 883–897. doi:10.1016/j.jaerosci.2011.08.003.

Appendix

Appendix A.

Publications and Conference Contributions

The publications and conference contributions generated and contributed to within this thesis are listed below.

Journal Publications

1. Markus Bainschab, Lukas Landl, Jon Andersson, Athanasios Mamakos, Stefan Hausberger, and Alexander Bergmann. "Measuring Sub-23 Nanometer Real Driving Particle Number Emissions Using the Portable DownToTen Sampling System." In: *Journal of Visualized Experiments* (2020). DOI: doi:10.3791/61287. URL: https://www.jove.com/video/61287

2. Markus Bainschab, Sampsa Martikainen, Jorma Keskinen, Alexander Bergmann, and Panu Karjalainen. "Aerosol gas exchange system (AGES) for nanoparticle sampling at elevated temperatures: Modeling and experimental characterization." In: *Scientific Reports* (2019). DOI: 10.1038/s41598-019-53113-5. URL: https://www.nature.com/articles/s41598-019-53113-5

3. Markus Bainschab, Mario Anton Schriefl, and Alexander Bergmann. "Particle Number Measurements within Periodic Technical Inspections: A First Quantitative Assessment of the Influence of Size Distributions

and the Fleet Emission Reduction." Graz, 2020

4. Paul Maierhofer, Georg Röhrer, Markus Bainschab, and Alexander Bergmann. "On the Inherent Variability of Particulate Matter Concentrations on Small Scales and the Consequences for Miniaturized Particle Sensors." In: *Aerosol and Air Quality Research* 20.2 (2020), pp. 271–280. ISSN: 16808584. DOI: 10.4209/aaqr.2019.01.0048

Conference Proceedings

1. Markus Bainschab and Alexander Bergmann. "An Intrinsically Pressure Insensitive Low Cost Particle Number Diluter Featuring Flow Monitoring." In: *Proceedings* 2.13 (Dec. 2018), p. 981. ISSN: 2504-3900. DOI: 10.3390/proceedings2130981. URL: http://www.mdpi.com/2504-3900/2/13/981

Oral Presentations

1. M Bainschab, A Bergmann, S Martikainen, P Karjalainen, and J Keskinen. "A Counter Flow Denuder for Engine Exhaust Conditioning: First Laboratory Experiments." In: *Aerosol Technology*. Bilbao, 2018. URL: https://pure.tugraz.at/ws/portalfiles/portal/26898316/20180620_AT_talk_JK_MB.pdf

2. M Bainschab, A Bergmann, S Martikainen, P Karjalainen, J Keskinen, J Andersson, A Mamakos, T Lähde, C Haisch, O Piacenza, A Tomboulides, Z Toumasatos, L Ntziachristos, and Z Samaras. "A Versatile Portable Exhaust Particle Sampling System to Extend Particle Number Measurements Below 23 Nanometers." In: *International Aerosol Conference*. St. Louis, MO: AAAR, 2018. URL: https://pure.tugraz.at/ws/portalfiles/portal/26898309/20180823_IAC_DTT.pdf

3. M Bainschab, A Bergmann, S Martikainen, P Karjalainen, and J Keskinen. "Aerosol Gas Exchange System (AGES) for Engine Exhaust

Conditioning." In: *UK Combustion Aerosol Conference*. Cambridge, 2019. URL: https://pure.tugraz.at/ws/portalfiles/portal/26898320/20190625_UKCA_talk.pdf

4. M Bainschab, A Bergmann, S Martikainen, P Karjalainen, and J Keskinen. "Aerosol Gas Exchange System (AGES) for Engine Exhaust Conditioning." In: *AAAR Conference*. Portland, OR: AAAR, 2019. URL: https://pure.tugraz.at/ws/portalfiles/portal/26898320/20190625_UKCA_talk.pdf%20https://pure.tugraz.at/ws/portalfiles/portal/26898320/20190625_UKCA_talk.pdf

Poster Presentations

1. M Bainschab, A Bergmann, P Karjalainen, J Keskinen, J Andersson, A Mamakos, B Giechaskiel, C Haisch, O Piacenza, L Ntziachristos, and Z Samaras. "Extending Particle Number Limits to below 23 nm: First Results of the H2020 DownToTen Project." In: *European Aerosol Conference*. Zürich, 2017. URL: https://pdfs.semanticscholar.org/9e9b/80ef6604aeed3d8485e28abf78ad4d89c3b8.pdf

2. M Bainschab, A Bergmann, J Andersson, A Mamakos, P Karjalainen, J Keskinen, B Giechaskiel, T Lähde, C Haisch, K Thaler, O Piacenza, L Ntziachristos, A Tomboulides, Z Toumasatos, and Z Samaras. "First Results of Vehicle Technology Effects on Sub-23 nm Exhaust Particle Number Emissions Using the DownToTen Sampling and Measurement System." In: *Cambridge Particle Meeting*. Cambridge, 2018. URL: https://pure.tugraz.at/ws/portalfiles/portal/19373485/20180612_DTT_Poster.pdf

3. Markus Bainschab and Alexander Bergmann. "An Intrinsically Pressure Insensitive Low Cost Particle Number Diluter Featuring Flow Monitoring Introduction Flow Measurement." In: *Eurosensors*. Graz, 2018. URL: https://pure.tugraz.at/admin/files/27781583/20180824_ES_poster.pdf

4. M Bainschab, S Martikainen, P Karjalainen, J Keskinen, and A Bergmann. "A Counter Flow Denuder for Engine Exhaust Conditioning: First Laboratory Experiments." In: *Transport Airt Pollution*. Thessaloniki, 2019. URL: https://pure.tugraz.at/ws/portalfiles/portal/26898357/20190301_TAP_poster.pdf

Co-authorships of Conference Contributions

1. P Karjalainen, A Bergmann, M Bainschab, J Keskinen, A Mamakos, J Andersson, B Giechaskiel, L Ntziachristos, and Z Samaras. "Implications for the Sampling System in Extending Automotive Particle Regulations Below 23 nm. First Results of the DownToTen Project." In: *AAAR COnference*. Rayleigh, 2017. URL: https://graz.pure.elsevier.com/en/activities/implications-for-the-sampling-system-in-extending-automotive-part

2. Sampsa Martikainen, Panu Karjalainen, Antti Rostedt, Markus Bainschab, Alexander Bergmann, Jonathan Andersson, and Leonidas Ntziachristos. "Dependence of Dilution Performance of a Prototype Setup for Sampling Non- volatile Engine Exhaust Particles down to ten Nanometer in Diameter on Pressure Variations in Sample Line." In: *22nd ETH Conference on Combustion Generated Particles*. Zürich, Switzerland, 2018, p. 1. URL: http://www.nanoparticles.ch/2018_ETH-NPC-22/2018_ETH-NPC-22_book_of_abstracts_posters.pdf

3. Jon Andersson, Athanasios Mamakos, Andreas Klug, Markus Bergmann Alexander Bainschab, Panu Karjalainen, Jorma Keskinen, Barouch Giechaskiel, Tero Lahde, Christoph Haisch, Klemens Thaler, Oriana Piacenza, Leonidas Ntziachristos, and Zissis Samaras. "First results of vehicle technology effects on sub-23nm exhaust particle number emissions using the DownTo10 sampling and measurement system." In: *22nd ETH-Conference on Combustion Generated Nanoparticles*, Zurich, Switzerland, 2018. URL: https://www.nanoparticles.ch/archive/2018_Andersson_PR.pdf

4. Jonathan Symonds, David Walker, Tyler Johnson, Robert Nishida, Kingsley Reavell, Markus Bainschab, and Alexander Bergmann. "Uniformity of Particle Concentration after Mixing Aerosol Flows." In: *International Aerosol Conference 2018*. St. Louis, MO: AAAR, Sept. 2018. URL: https://www.researchgate.net/publication/327624013_Uniformity_of_Particle_Concentration_after_Mixing_Aerosol_Flows

Appendix B.

DownToTen Sampling System: Supplementary Information

The supplementary information about the DownToTen sampling system provided in this chapter covers aspects that are not described as detailed in **Paper 1**. The information provided here has partially been reported in Deliverable 4.1 of DownToTen in a similar form.

B.1. Overview Schematic and Wiring Diagram

Figure B.1 shows a schematic drawing of the DownToTen sampling system, including its key components. This schematic is mainly used to demonstrate the working principle of the system to a non-expert audience. The schematic shows the first two dilution elements that are supplied by porous tube diluters, including mixing elements (PDn+Mixer), the catalytic stripper (CS), and the optional tertiary dilution stage (D3) that is realized by the bifurcated flow diluter described in Appendix D. Two CPCs with 10 nm and 23 nm cut points are indicated as particle number concentration sensing elements. The pressurized air (PA) can be supplied by a gas bottle for mobile measurements or a stationary supply for static measurements. Mass flow controllers (MFC) and mass flow meters (MFM) are used for flow management in the system. The directions of the flows are indicated with arrows. A cooling coil and filters protect the MFMs from heat and pollution. A pump downstream of the MFMs establishes the required underpressure.

Red sections indicate that the respective section is heated (typically 350 °C). The grey sections are close to room temperature during operation.

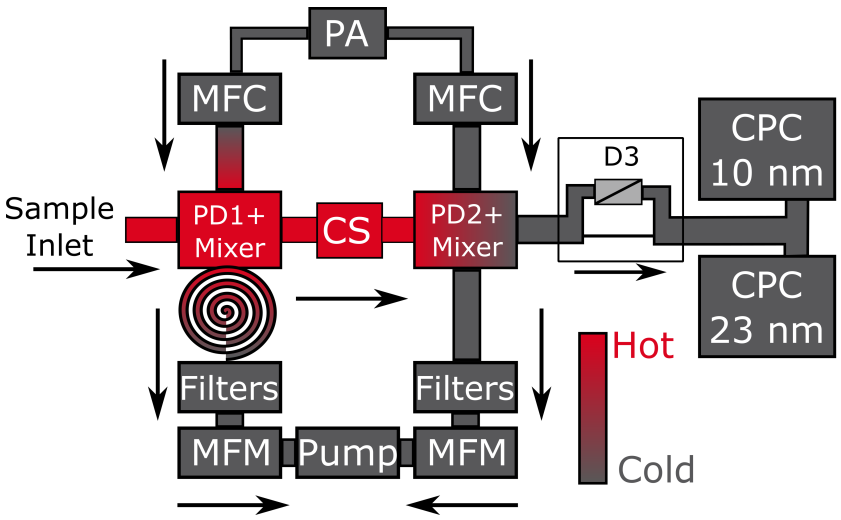

Figure B.1.: Schematic drawing of the mobile DownToTen system.

Figure B.2 shows a wiring diagram of the DownToTen sampling system. The relevant components included are directly labeled in the diagram. Bold black connections indicate tubing for aerosol or dilution air. Thinner black and yellow lines represent cables for the transmission of digital and analog electrical signals, respectively. Green connections represent non-amplified analog signals from thermocouples, and red connections indicate cables for AC or DC power supply.

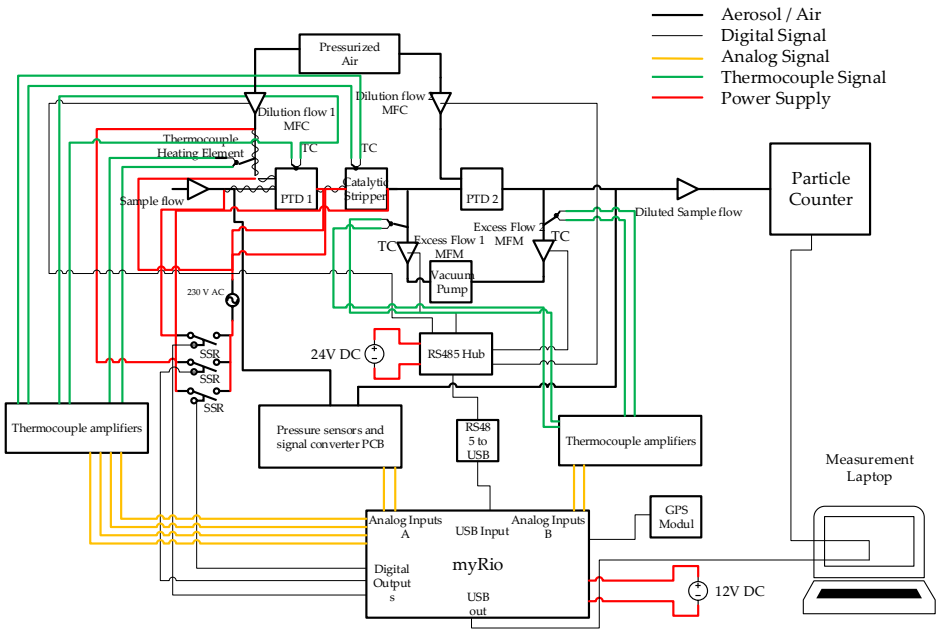

Figure B.2.: Wiring diagram of the DownToTen sampling system

B.2. Dilution Ratio Uncertainty

The dilution ratio introduced by the first two dilution stages, and the error propagation of the MFC accuracies to the dilution ratio were assessed using the GUM workbench [111]. Figure B.3 shows a schematic of the first two dilution stages, including the corresponding dilution and excess flows.

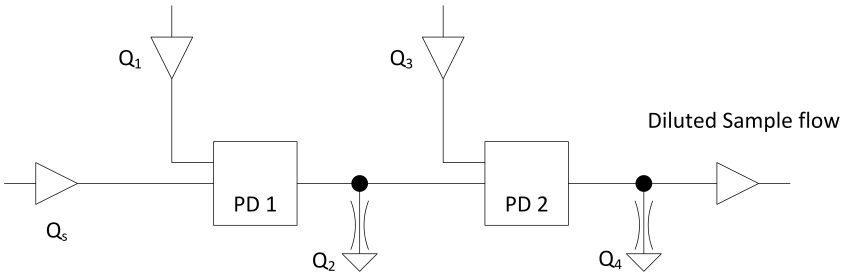

Figure B.3.: Schematic of the flows in the first two dilution stages of the DownToTen sampling system.

The dilution ratio DR introduced at the first two dilution stages supplied by porous tube diluters is the product of the dilution ratios introduced in each stage. The dilution ratio of one dilution stage is defined as the sum of the sample flow (Q_s) and the dilution air flow (Q_{dil}) divided by the sample flow:

$$DR = \frac{Q_{dil} + Q_s}{Q_s} = \frac{Q_{dil}}{Q_s} + 1 \tag{B.1}$$

Q_s is controlled by the total flows of the measurement instruments situated downstream of the last dilution stage and the differences between the dilution air flows, and the excess flows in the first two dilution stages. The sampling system is usually operated in a way that Q_s amounts to approximately 1 lpm.

For two dilution stages in series, the total dilution ratio DR is the product of dilution ratios of the two dilution stages DR_1 and DR_2. Concerning the labeling of the flows in Figure B.3, the total dilution ratio is calculated as follows:

$$DR = DR_1 \times DR_2 = \left(\frac{Q_1}{Q_s} + 1\right) \times \left(\frac{Q_3}{Q_s + Q_1 - Q_2}\right) \tag{B.2}$$

For the calculation of the DR-uncertainty, typical values were used for the sample flow and the flows that are measured by the MFCs and MFMs. The measurement uncertainties of the MFCs (Q_1,Q_3) and MFMs (Q_2,Q_4) are $\pm 0.3\,\%$ of the full-scale value plus $\pm 0.5\,\%$ of the measured value, according to the datasheet. The relative uncertainty of Q_s has been estimated to be

$\pm 5\,\%$ of the measured value, based on according measurements.

$Q_s = (1.00 \pm 0.05)\,\mathrm{lpm}$
$Q_{1-4} = (10.0 \pm 0.1)\,\mathrm{lpm}$

The model described above, the absolute values of the flow rates and the respective measurement uncertainties, were implemented in the GUM workbench[111]. With this tool, the uncertainty of the dilution ratio was evaluated analytically and numerically. The analytical evaluation yielded a dilution ratio of $DR = 121 \pm 11$, which is in good agreement with the results from a numerical Monte Carlo simulation shown in Figure B.4

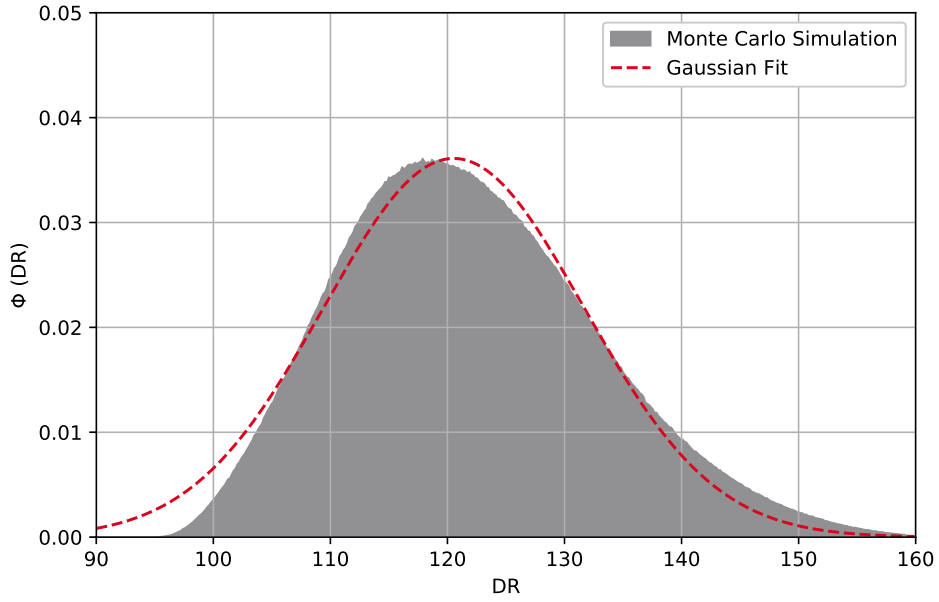

Figure B.4.: Illustration of the result of a Monte Carlo simulation with 2 000 000 sweeps to calculate the dilution ratio DR and the respective uncertainty.

It can be said that the uncertainty of the dilution ratio that is introduced by the measurement uncertainties of the MFCs and MFMs amounts to

approximately 9 % for typical operating parameters.

B.3. DownToTen System: Manual

A user manual for the DownToTen system has been written to provide step-by-step instructions for the system's operation. This manual has proven to be especially useful for the operation of the unit used by Ricardo Ltd. (Shoreham-by-Sea, United Kingdom), where the distance aggravates direct instructions, support, and troubleshooting. However, the manual is also valid for the operation of the unit owned by the Institute of Internal Combustion Engines and Thermodynamics (Graz University of Technology). The reprint of the manual is attached below.

DownToTen Sampling System Manual

Markus Bainschab

January 2019

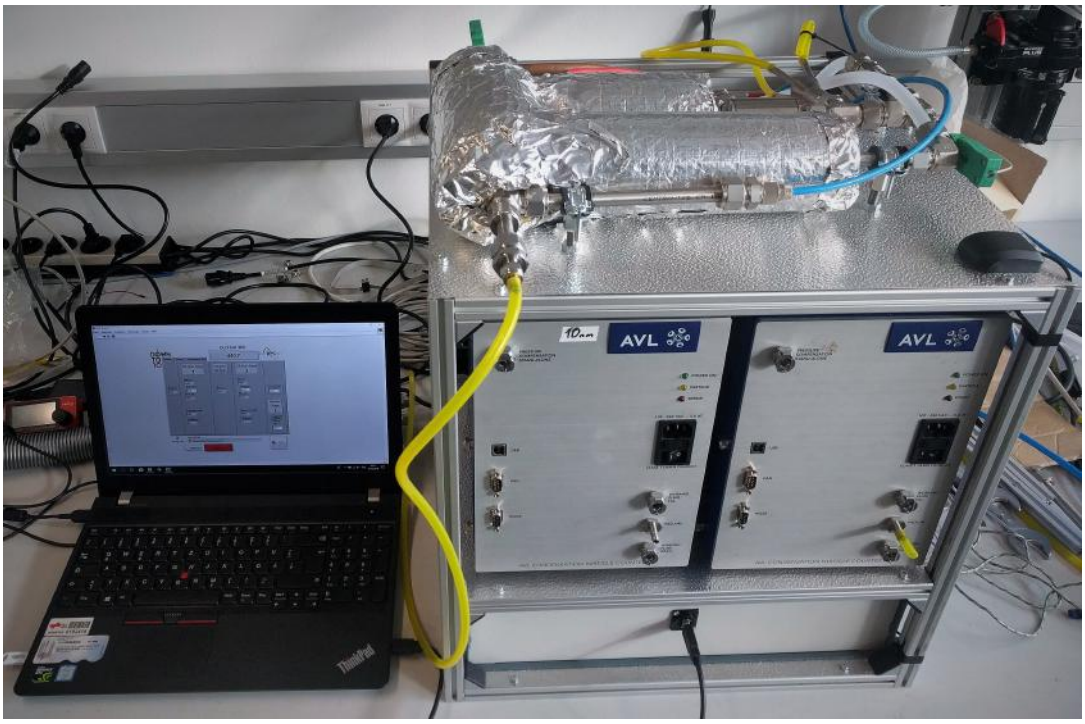

Contents

1 Software Installation

To operate the **DownToTen** sampling system, first install the LabVIEW software on a computer running Windows version 7 or later. If you do not have the installation files, contact Markus Bainschab (TUG).

- In the "Volume" folder of the installer, double click the "setup" icon indicated below.

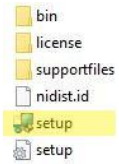

- Choose a destination directory:

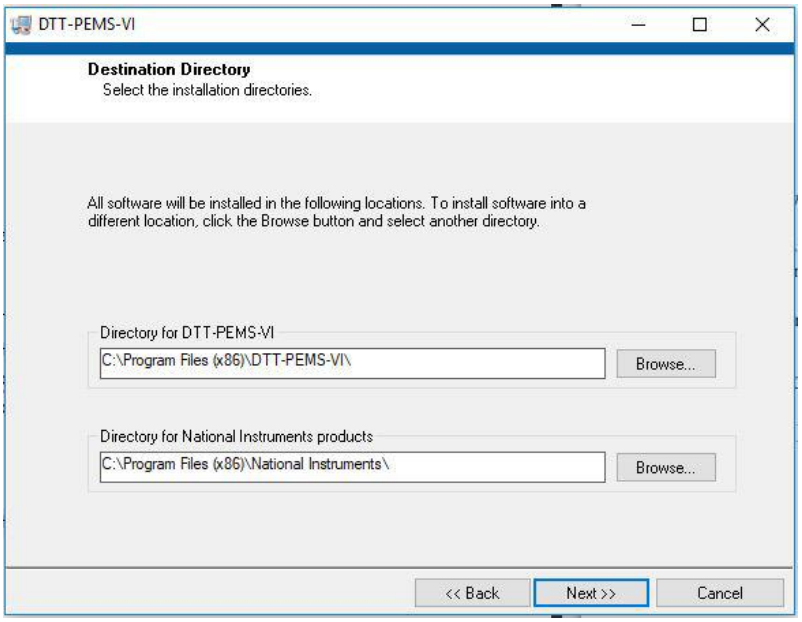

- Press "Next >>" twice to start the installation. After the installation has finished, you can find the application you need to operate the sampling system in the folder you defined before.

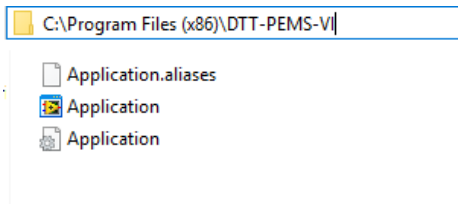

2 Hardware Installation

If you want to operate the DTT sampling system in a laboratory or at a dynamometer, follow the steps below for an appropriate installation.

- Place the sampling system as close as possible to your particle source or measurement port
- Place the measurement devices you want to use at the middle deck of the system (like in the picture below) or nearby. Connect the measurement devices to power and vacuum if needed. Connect them to the computer you want to control the **DTT** system with (to ensure the time in the measurement files of the system and the measurement devices match). Make sure this computer has the required software to communicate with the measurement devices.

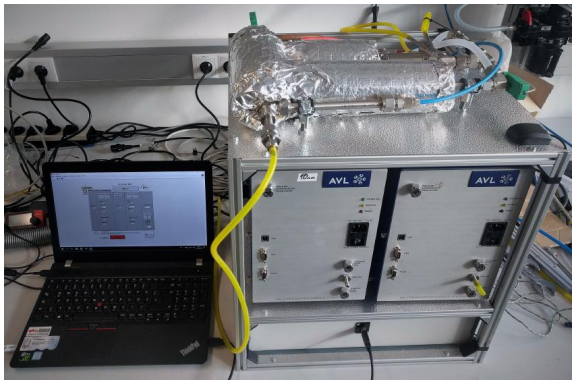

- If the dilution ratio ($DR \approx 100$) introduced by the first two dilution stages of the sampling system is sufficient, connect the measurement devices' inlets to the outlet ports of the system and plug the ports that are not used. Use anti static or conducting tubing and make the tubes the same length for all measurement devices and as short as possible.

- If the third dilution stage is needed to attenuate the particle number dilution by an additional factor of ≈ 15, plug all but one outlet port of the system and connect the bifurcated flow diluter to the one remaining outlet. Connect the measurement devices' inlets to the outlet ports of the bifurcated flow diluter and plug the ports that are not used. Use anti static or conducting tubing and make the tubes the same length for all measurement devices and as short as possible.

- Connect the two Mass Flow Controllers (MFC) to clean compressed air (5 bar)

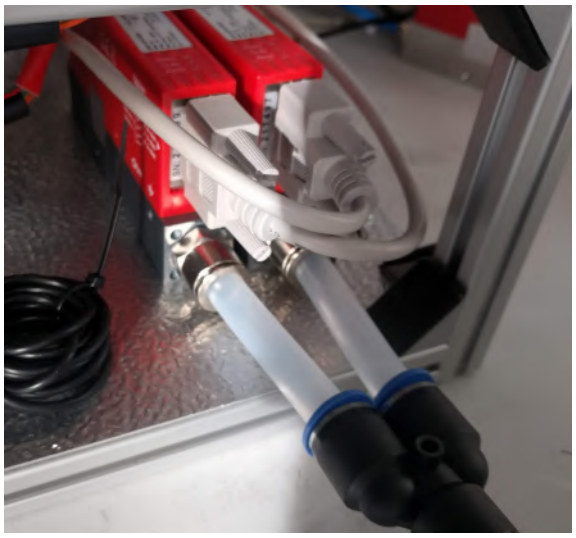

- Connect the Mass Flow Meters (MFM) to needle valves and a vacuum source

- Connect the system to a 230 V AC power source

- Connect the sampling system to a computer with the **DTT** application installed. The installation process is described in section 1.

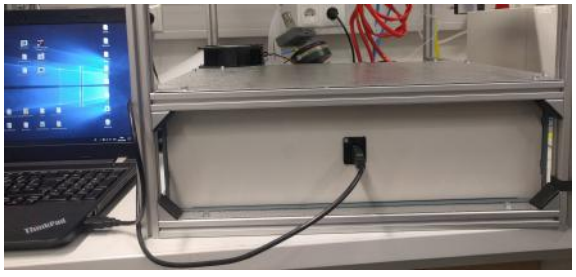

- Connect the inlet of the **DTT** system to the particle source using a heated (150 °C) sampling tube

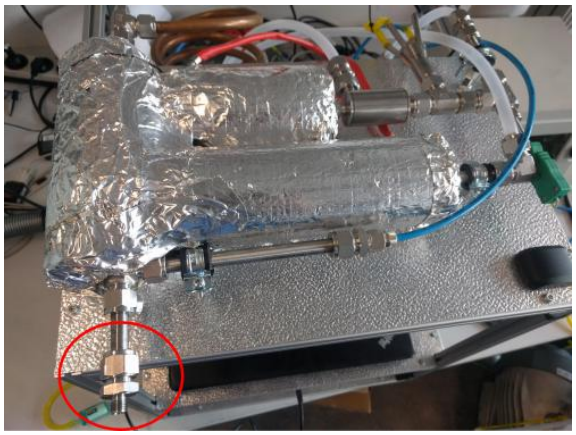

3 Heat up and Preparation

Execute the following steps at least 30 minutes before performing measurements of solid particle number concentrations using the DTT sampling system to ensure that the system is heated up before the measurements start.

- Switch on the measurement devices and their external vacuum supply, if needed
- Open the applications communicating with the measurement devices on your measurement computer and make sure the connection is working
- Close the needle valves downstream the MFMs completely

- Switch on the vacuum source for the DTT sampling system
- Switch on the sampling system by pushing the red shining switch down

- Open the LabVIEW DTT application on your computer

- The GUI of the application now displays the flows in and out at dilution stages 1 and 2, which should show 0.00 lpm now. If the values differ from 0, double check if the needle valves are closed properly.

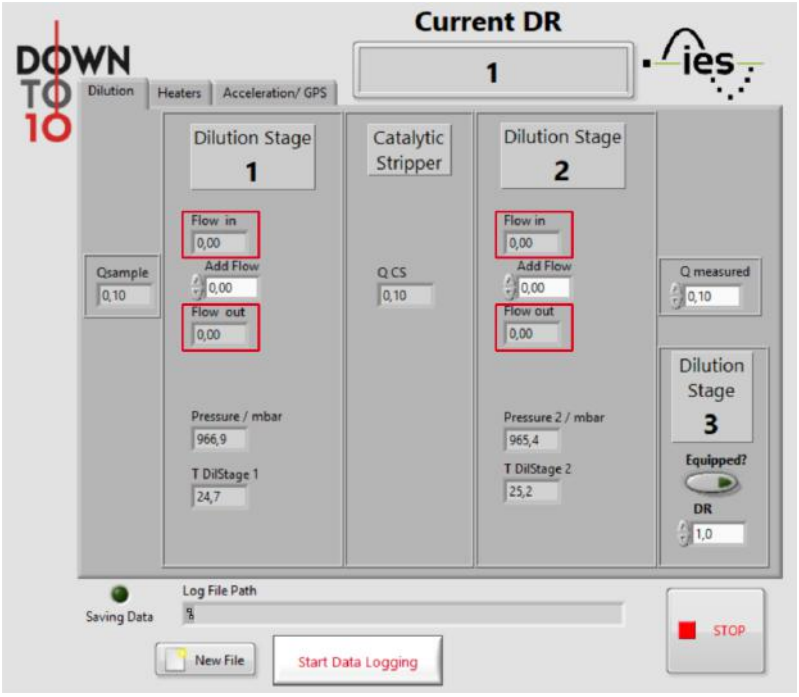

- Enter the mass flow (in slpm) drawn by the connected measurement instruments. If you don't know the flow drawn by the instruments, measure it using a mass flow meter.

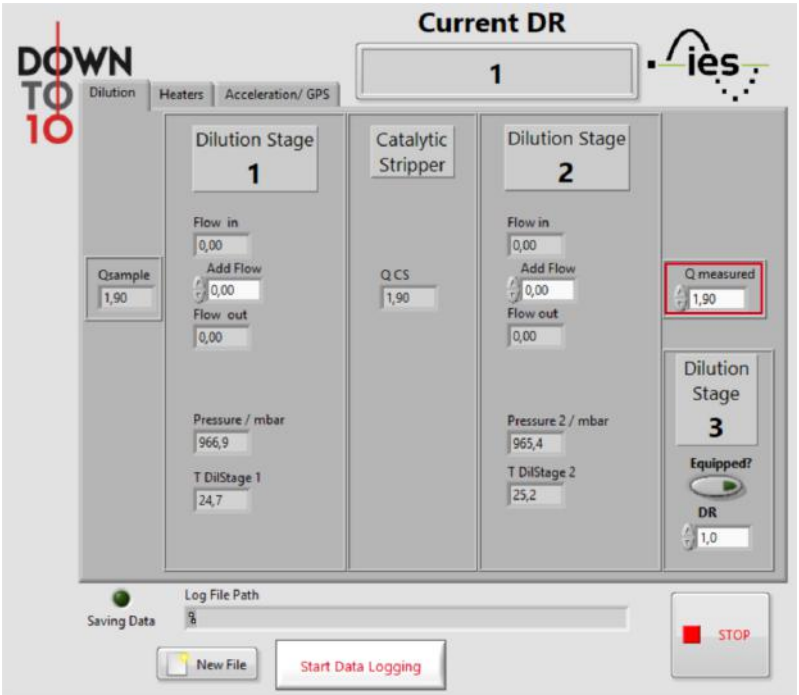

- Slowly open the needle valves until both "Flows out" reach 10.0 ± 0.5 slpm. Both "Flows in" will also increase to the same values as the corresponding "Flows out".

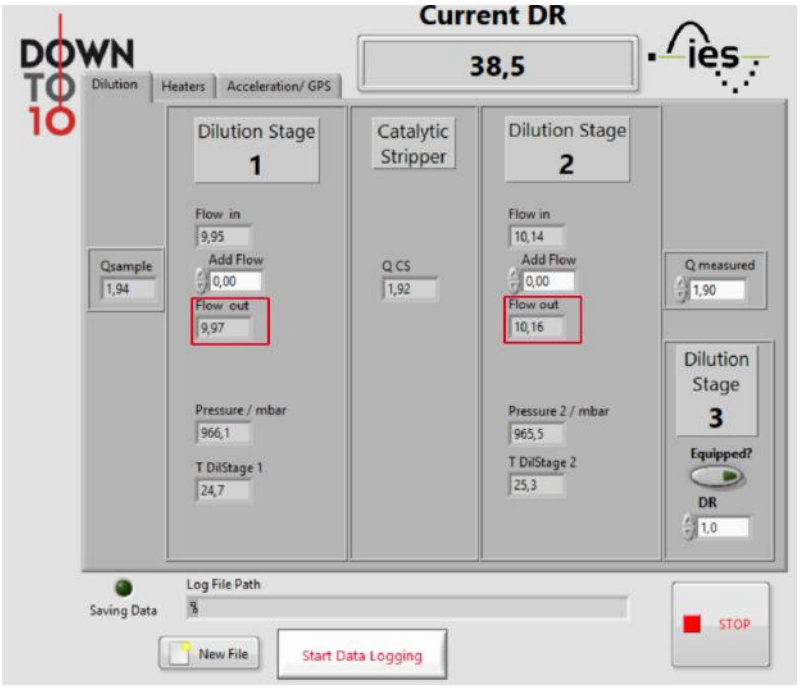

- Adjust the "Add Flow" (difference between dilution air flow and excess flow) of both dilution stages to get the desired flow through the catalytic stripper (Q CS) and sample flow (Qsample).

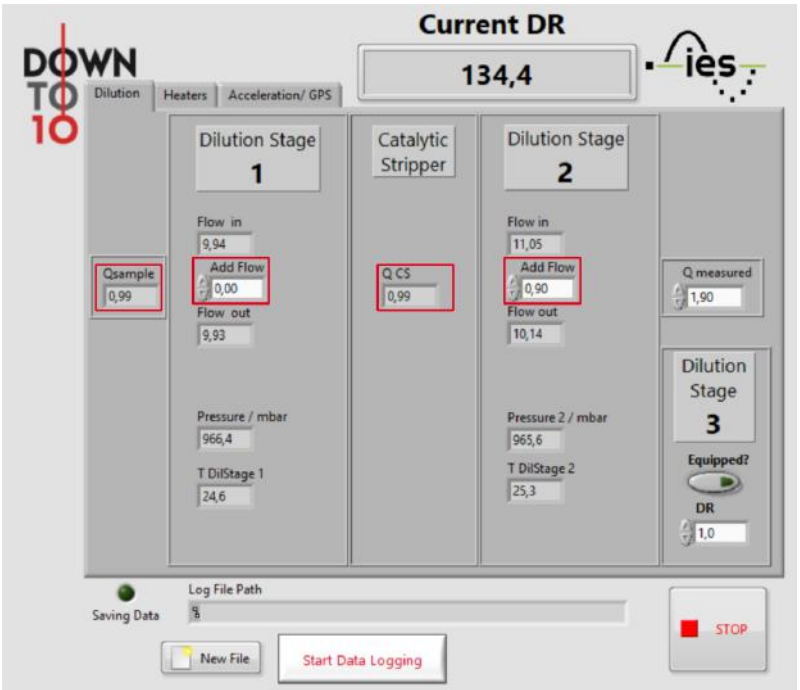

- If the bifurcated flow diluter is connected to the sampling system, press the button below the "Equipped?" text in the "Dilution Stage 3" box and enter the DR "dilution ratio" introduced by the additional diluter. The value entered there is automatically multiplied to the DR value calculated using the flows in the system.

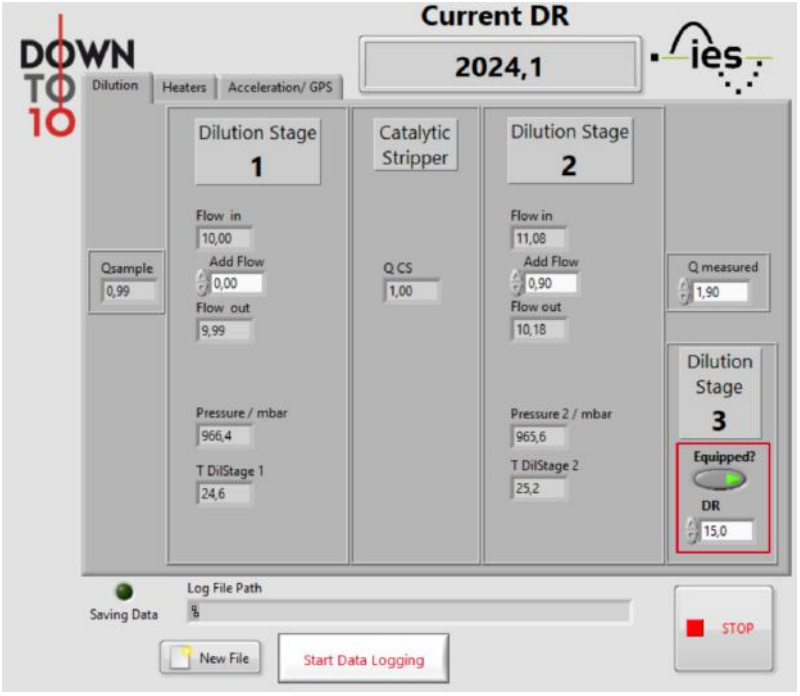

- Click on the "Heater" tab to get to the interface where you can set the heater temperatures

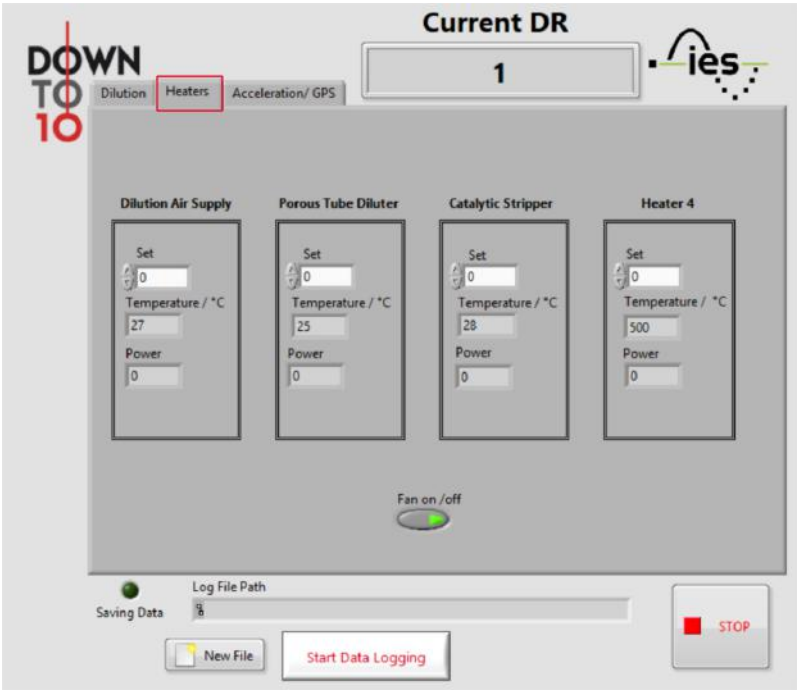

- Set the heater temperatures of the dilution air supply, the first porous tube diluter and the catalytic stripper to the desired temperatures (usually 350 °C). The system will now start to heat up. Below the "Set" interfaces the current temperature and heating power (in %) is displayed. "Heater 4" outputs and inputs are not connected to any heating element. This interface can be ignored.
  Note that all heaters are automatically switched off if the dilution air flow of dilution stage 1 drops below 2 slpm, to prevent overheating and melting of the connected plastic tubes.

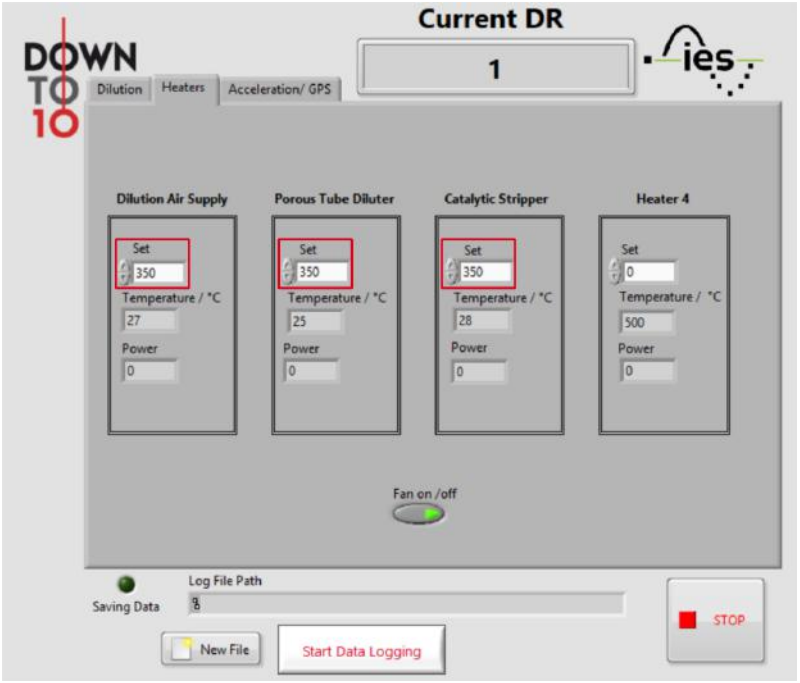

- Wait until the temperature at dilution stage 1 reaches 290 °C (if set temperatures are 350 °C) before starting measurements

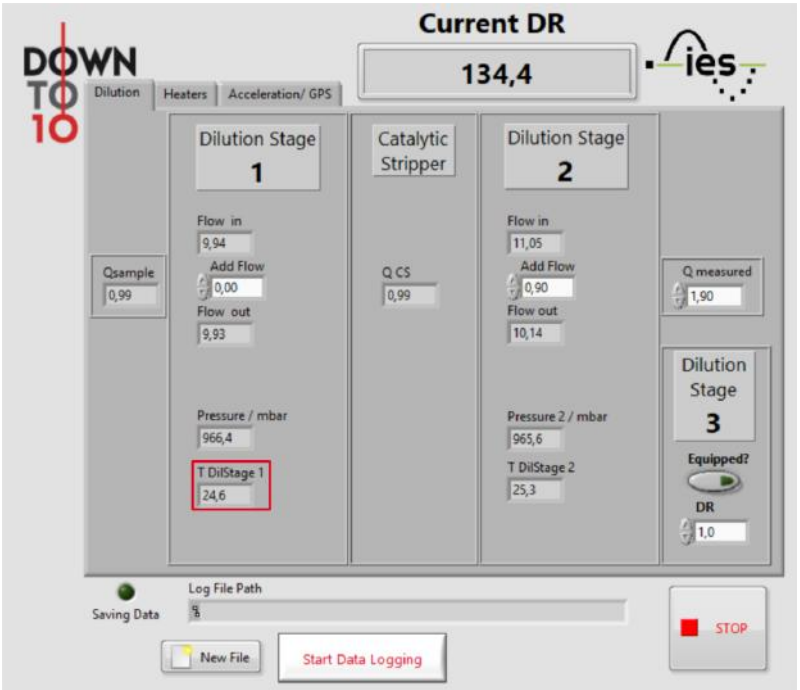

4 Operation and Data Logging

When the system reaches a thermally stable operation point it is ready to be used for measurements.

- Start to log the data on the measurement devices connected to the **DTT** sampling system.
- Start to log the data of the sampling system by pressing the "Start Data Logging" button and choose a path and a file name in the pop up window.

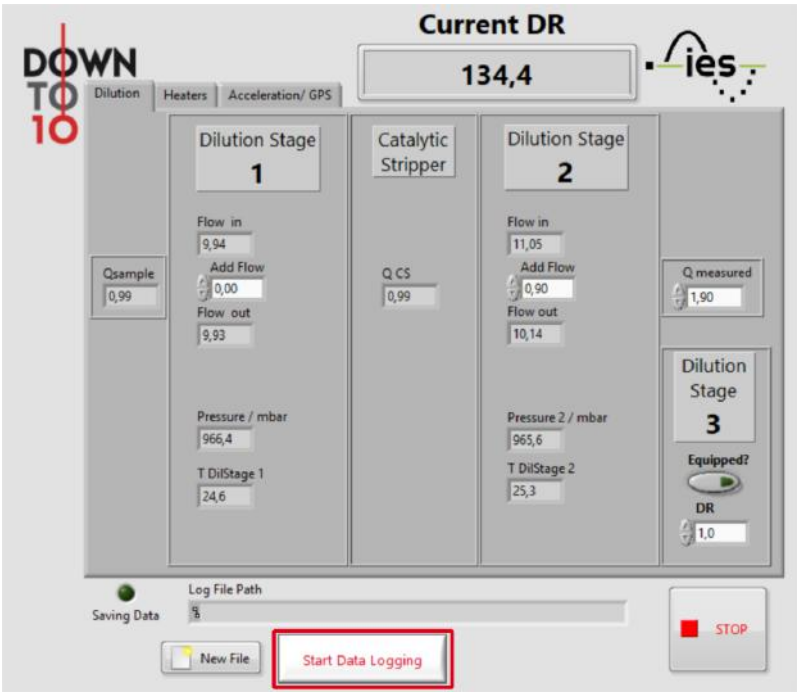

- Now the log file path is displayed and the green light indicates that data is saved. The systems' data is logged at a frequency of 2 Hz

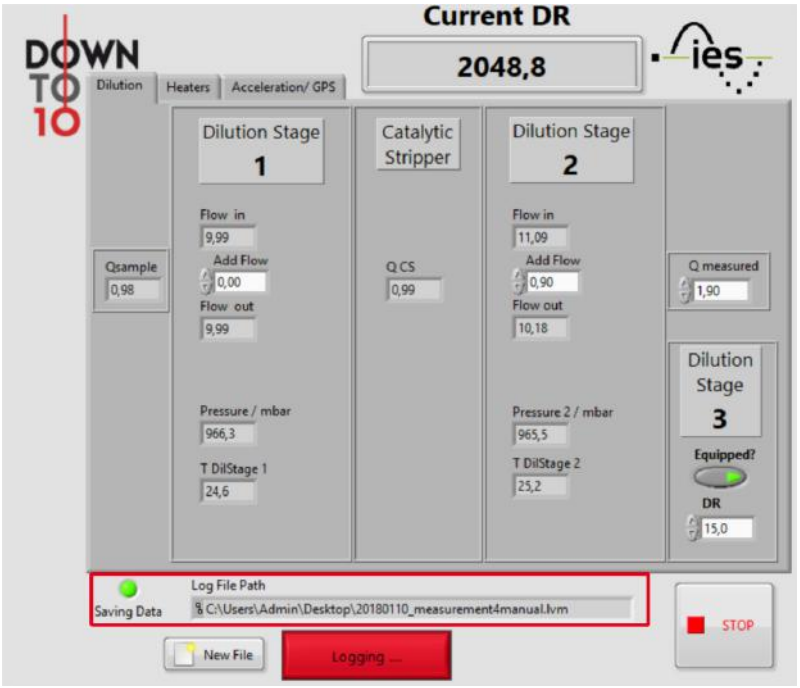

- Press "Logging ..." to stop recording data
- If you want to append data to the file defined before, simply press "Start Data Logging" again
- If you want to create a new log file press "New File" and then press "Start Data Logging". Now the pop up window where you can define a path and a file name appears again.
- The created measurement file is a tab separated text file. The filename extension ".LVM" stands for LabVIEW Measurement File. It can be imported to excel or other applications for data analysis.
- The following values are logged:

Variable name in file	Unit	Description
X_value	s	Time relative to the time the data logging started. The start time can be found in the header of the file
MFC 1 out / lpm	slpm	Flow out in dilution stage 1 in slpm
MFC 1 in / lpm	slpm	Dilution air flow in dilution stage 1 in slpm
MFC 2 out / lpm	slpm	Flow out in dilution stage 2 in slpm
MFC 2 in / lpm	slpm	Dilution air flow in dilution stage 2 in slpm
Temperature 1 / °C	°C	Aerosol temperature after dilution stage 1
Temperature 2 / °C	°C	Aerosol temperature after dilution stage 2
Pressure 1 / mbar	mbar	Pressure at the inlet of the sampling system
Pressure 2 / mbar	mbar	Pressure at the outlet of the sampling system
Temperature Heater 1/ °C	°C	Temperature of the dilution air supply heater
Temperature Heater 2/ °C	°C	Temperature of the porous tube heater
Temperature Heater 3/ °C	°C	Temperature of the catalytic stripper heater
Temperature Heater 4/ °C	°C	Temperature of heater 4. If there is no heating element connected it shows 500 °C
Sample Flow / lpm	slpm	Flow at the inlet of the sampling system. Calculated from the MFC values and the entered "Flow drawn by Instruments / lpm".
Flow drawn by Instruments / lpm	slpm	Flow at the outlet of the sampling system. This flow has to be entered manually in the user interface under "Q measured".
Dilution Ratio	1	Total dilution ratio. Calculated using the MFC values and the entered DR3 value. Particle losses are not taken into account.
Latitude / deg	°	Latitudinal position of the system. If there is no GPS signal, it shows 0 .
Longitude / deg	°	Longitudinal position of the system. If there is no GPS signal, it shows 0 .
DR3 equipped	-	1 if DR3 is equipped. 0 if DR3 is not equipped.
DR 3	1	Shows the dilution ratio introduced by the bifurcated flow diluter. This value is entered manually in the user interface.

Appendix C.

DownToTen Sampling System with SUREAL-23 Catalytic Stripper

DownToTen and SUREAL-23 are two EU-funded projects tackling automotive exhaust particle number measurement below the current regulatory threshold of 23 nm in particle diameter. Despite the same overall topic of the projects, the projects are mostly complementary. Examples for the complementarity are SUREAL-23 covering novel particle measurement instrumentation, while DownToTen also investigates non-solid particle emissions.

At the Transport Research Arena event in Vienna in April 2018, representatives of both projects met and discussed research questions, and the project progresses. The extensive efforts of SUREAL-23 in developing a catalytic stripper (CS), which is designed for particle number measurements below 23 nm, were identified as also possibly very advantageous for DownToTen. A catalytic stripper with low diffusional particle losses could further improve the performance of the low particle loss sampling system developed within DownToTen. The SUREAL-23 consortium expressed their willingness to provide a catalytic stripper to DownToTen for the evaluation of the CS as a part of the DownToTen sampling system. The face-to-face discussions in Vienna were followed by telephone conferences and further face-to-face discussions between members of the two project consortia at the joint event in Thessaloniki in October 2018. After agreeing on the technical specifications of the device, SUREAL-23 manufactured a CS and could provide it to DownToTen for the period between March and September 2019. The SUREAL-23 CS has been implemented in the DownToTen sampling system.

The change in size-dependent particle penetration efficiency has been experimentally evaluated and compared with the system's performance in the original configuration. Figure C.1 shows the catalytic stripper developed by SUREAL-23. A detailed analysis of this catalytic stripper has been published by Melas et al.[94]

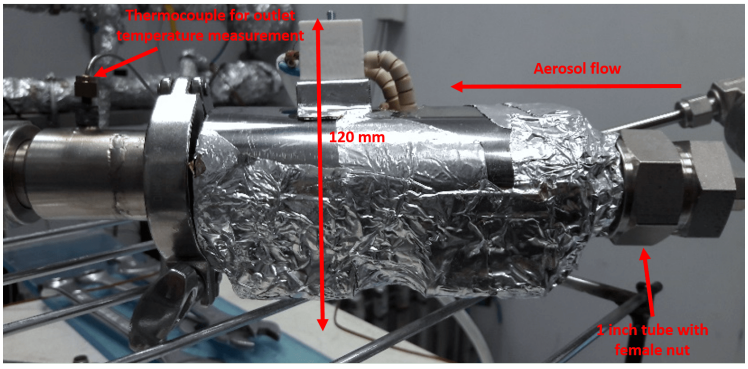

Figure C.1.: Picture of the SUREAL-23 catalytic stripper

Experimental Evaluation

One of the main differences between the catalytic stripper used in the DownToTen system and the catalytic stripper developed by SUREAL-23 is the designated aerosol flow rate. The CS used in the DTT is designed for a flow rate of ≈ 1 lpm, whereas the SUREAL-23 CS is designed for a flow rate of ≈ 12 lpm. At these flow rates, the volatile removal efficiencies are high enough to substantially lower the risk of nucleation and growth of sub-cut size particles. In contrast, diffusional particle losses are limited to acceptable levels. Replacing the CS used in the DTT system with the SUREAL-23 CS would lead to an operation of the SUREAL-23 CS far off the targeted flow rates and, therefore, high diffusional particle losses. However, the DTT system's versatility allows for the incorporation of the SUREAL-23 CS in a location where the target conditions can be met. In the DTT system the flow rate downstream the first dilution stage is approximately 11 lpm (1 lpm inlet flow, 10 lpm dilution airflow). To meet the target flow rate of the DTT CS, 10 lpm are extracted from the sample line upstream entering the

CS. Changing the location where the 10 lpm are extracted from upstream the CS to downstream the CS leads to a flow rate of 11 lpm at the CS. This value is reasonably close to the target value of 12 lpm. The described modifications have been performed to incorporate the SUREAL-23 CS in the DTT system. The modification of the system is schematically illustrated in Figure C.2. Figure C.3 shows pictures of the DTT system before and after the modification.

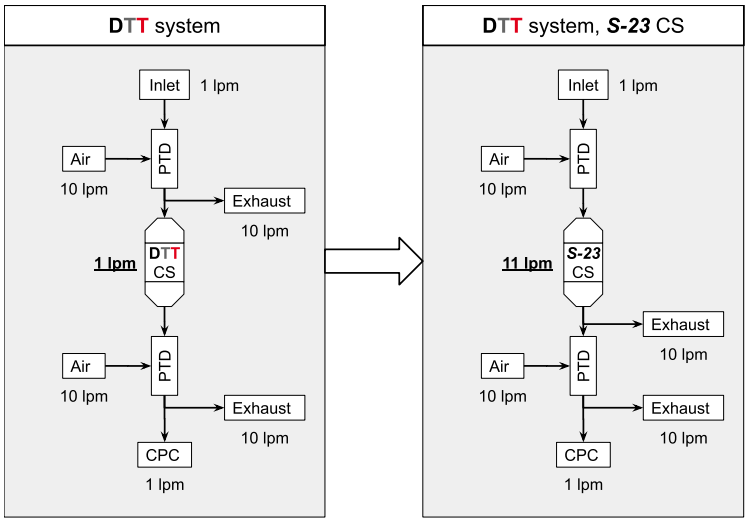

Figure C.2.: Schematic drawing and approximate flow rates at selected locations of the original DTT system and the modified system incorporating the SUREAL-23 CS.

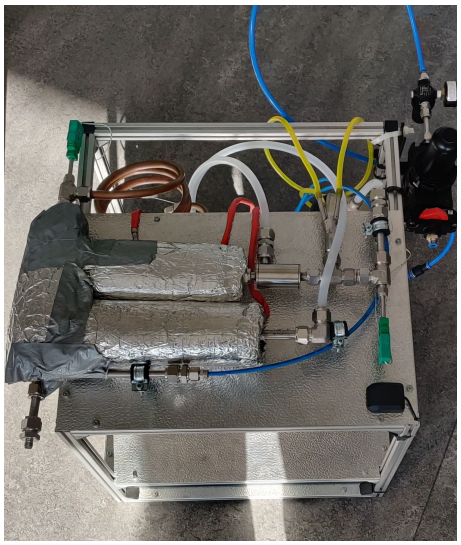

(a) DownToTen system

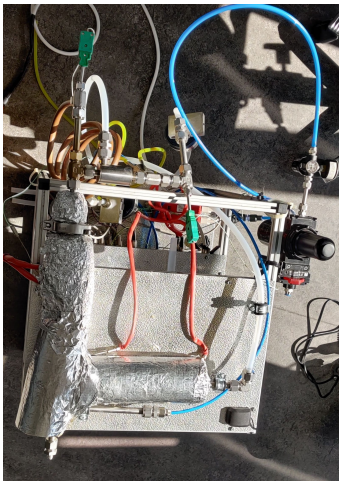

(b) Modified DownToTen system with SUREAL-23 catalytic stripper.

Figure C.3.: Top view of the DownToTen sampling system (a) before and (b) after the modification to incorporate the SUREAL-23 catalytic stripper.

CPC Comparison

Particle number concentrations upstream and downstream of the sampling system were measured simultaneously using two condensation particle counters TSI 3775 ($d_{50} = 4\,\mathrm{nm}$) to assess the penetration efficiency of the DownToTen system with the SUREAL-23 CS. The counting efficiencies of the CPCs at different particle diameters are compared before the particle penetration measurements. Possible differences in counting efficiencies would have to be corrected for evaluating the data of the particle penetration measurements. Figure C.4 shows a schematic drawing of the experimental setup used for the counting efficiency comparison tests. A Jing miniCAST burning propane was used as a particle source. The generated soot was passed through a catalytic stripper to remove possibly abundant volatile particles. A dilution bridge is used to adjust the particle number concentration. A TSI 3082 electrostatic classifier, together with a TSI 3085 differential mobility analyzer (nano DMA), is used for the size selection of particles. Downstream

the DMA, the two CPCs measured the particle number concentration in parallel.

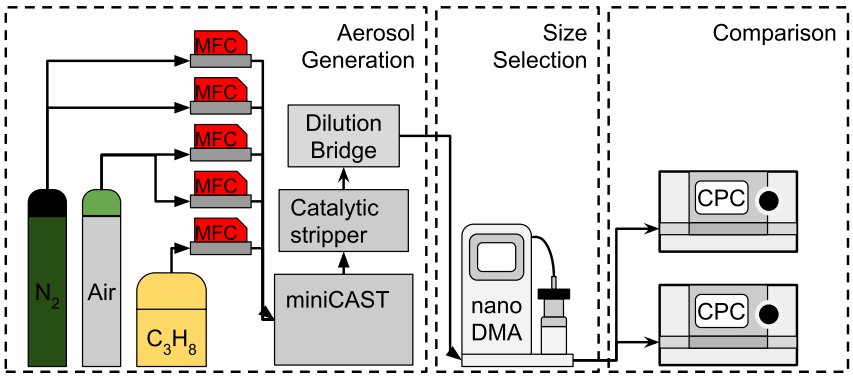

Figure C.4.: Drawing of the experimental setup used for comparative counting efficiency measurements of the two CPCs.

Figure C.5 shows the relative counting efficiencies of the two CPCs at different particle mobility diameters. At particle diameters where multiple measurements have been performed, the mean value of the determined efficiencies is taken for further data evaluation.

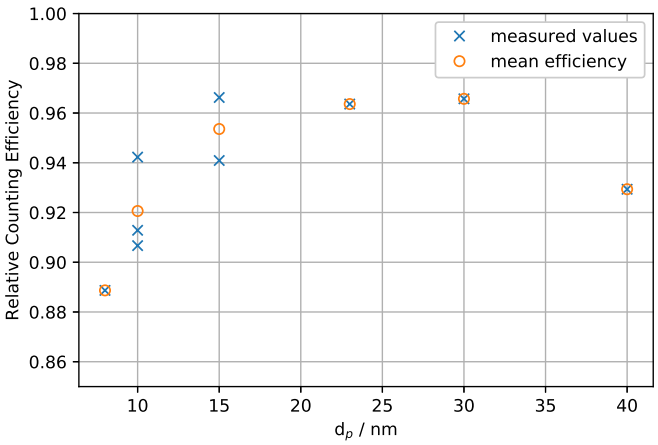

Figure C.5.: Relative counting efficiency of CPC2 compared to CPC1.

Particle Penetration

The particle penetration efficiency measurements were performed using the experimental setup shown in Figure C.6. The particle generation and size selection are the same as used for the CPC comparison. Downstream the size selection, one CPC measures the particle number concentration upstream of the sampling system. The other CPC measures the concentration downstream of the sampling system.

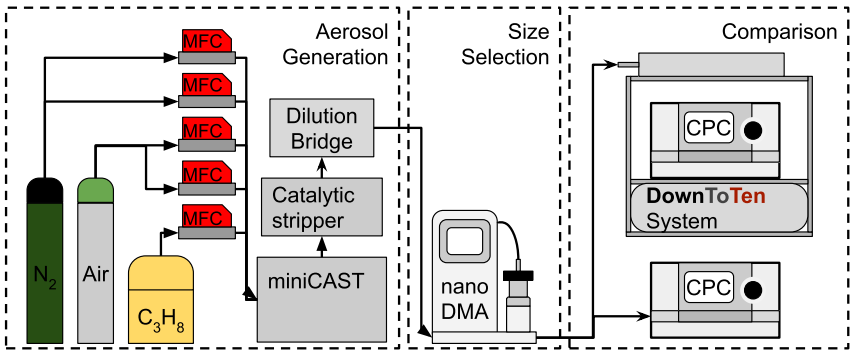

Figure C.6.: Drawing of the experimental setup used for the particle penetration measurements.

The concentration data from the downstream CPC is multiplied with the dilution ratio of the sampling system and corrected for counting efficiency deviation to determine the particle penetration efficiencies. Figure C.7 shows the particle penetration measurement results using the DownToTen system with the SUREAL-23 CS. Additionally, the results of particle penetration measurements with the DTT system in the original modification are shown. The penetration efficiency at 10 nm is $\approx 50\,\%$ for both modifications. Also the performance at 15 nm is very similar ($\approx 60\,\%$). There is a deviation of $\approx 10\,\%$ for particle sizes of 30 nm and larger with the original DTT system showing higher penetration efficiencies. The data shows that particle size independent thermophoretic losses are $\approx 10\,\%$ lower for the original DTT system compared to the modified one, including the SUREAL-23 CS. The particle size-dependent diffusional losses are reduced with the modified system. The reduced diffusional losses equalize the higher baseline thermophoretic losses at a particle size of 10 nm.

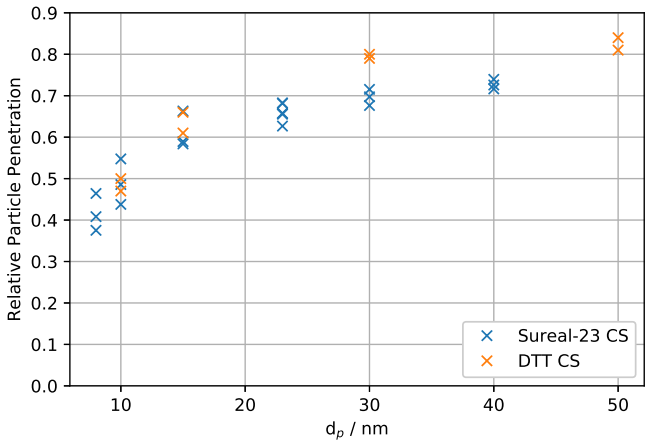

Figure C.7.: Relative particle penetration as a function of the particle mobility diameter for both the DTT system with the original CS and the system with the SUREAL-23 CS.

Discussion

It can be stated that a possible synergy between the complementary projects DownToTen and SUREAL-23 has been identified and successfully exploited in a fruitful collaboration. The DTT system's versatility allowed for the incorporation of CS developed and optimized for low diffusional particle losses by SUREAL-23. We could show that applying the SUREAL-23 CS in the DownToTen sampling system reduces diffusional particle losses. Thermophoretic losses could most probably be reduced with geometric modifications of the catalytic stripper and the sampling system. Overall, the application of the SUREAL-23 catalytic stripper leads to a performance improvement for particle number measurements below 23 nm because of the lower particle size dependence of the penetration efficiency. This reduced dependence leads to a less pronounced under-estimation of particle number concentrations in the size-range between 23 nm and 10 nm and more accurate measurement results.

Appendix D.

Bifurcated Flow Diluter

The conference proceedings paper attached below describes the bifurcated flow diluter (section 3.3) that was used as an optional tertiary dilution stage in DownToTen system to attenuate further the particle number concentration downstream the firs two dilution stages. In the measurements performed with the DownToTen system, this diluter was used as an entirely passive element. The monitoring of the flow was not applied in field-measurements with the DownToTen system, for the sake of simplicity.

proceedings

MDPI

Proceedings

An Intrinsically Pressure Insensitive Low Cost Particle Number Diluter Featuring Flow Monitoring †

Markus Bainschab * and Alexander Bergmann

Institute of Electronic Sensor Systems, Graz University of Technology, 8010 Graz, Austria; alexander.bergmann@tugraz.at

* Correspondence: m.bainschab@tugraz.at; Tel.: +43-316-873-3349

† Presented at the Eurosensors 2018 Conference, Graz, Austria, 9–12 September 2018.

Published: 10 December 2018

Abstract: We present a low cost Particle Number (PN) diluter including mass flow monitoring. The device consists of a commercial hypodermic needle, a High Efficiency Particulate Air (HEPA) filter. and a custom-made flow sensor. The flow sensor is used to monitor the diluter's performance and enable in-time replacement of the low cost elements used. Neither the sampling flow rate nor the pressure drop drastically change the dilution factor introduced by the presented device. This makes the presented device especially useful for particle number measurements at positions close to the tailpipe of internal combustion engine powered vehicles, where aggravating, fast pressure pulsations complicate correct sampling.

Keywords: engine exhaust; particle number; dilution; flow monitoring

1. Introduction

The particle number emitted by vehicles has been regulated by European emission standards since 2011 (Euro 5b). The high PN concentrations in raw automotive exhaust exceed the upper measurement limits of state-of-the-art PN sensors, which makes dilution inevitable.

It is common practice to apply two dilution stages [1]. In some applications (e.g., raw exhaust sampling in real driving emission measurements) these two dilution stages may not sufficiently attenuate the particle number concentration, which makes a third dilution stage necessary. The introduced dilution stage must not distort the particle size distribution and should be robust against pressure fluctuations or drifts. Commonly used dilution solutions like the ejector diluter show a strong dependence of the dilution factor on the pressure level [2]. The device presented is designed to be insensitive to pressure fluctuations and drifts. It is made of low cost components and comprises flow monitoring to enable the replacement of these components before clogging compromises the device's performance.

2. Results

The presented diluter consists of a hypodermic needle, a HEPA filter and custom made circuit for flow monitoring. The majority (≈95%) of the aerosol that runs through the diluter passes through the HEPA filter, where more than 99.97% of particles are removed. The rest of the sample passes through the hypodermic needle and is then mixed again with the filtered part of the sample [3]. Figure 1 shows the geometry and the flow velocities in the diluter as predicted by CFD simulations.

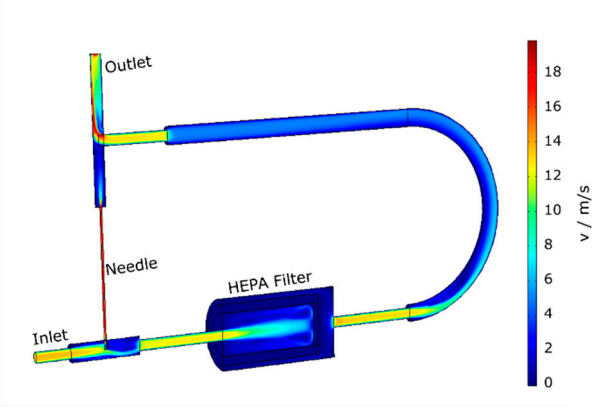

Figure 1. Velocities at the centered cut plane of the diluter at a total flow rate of $Q_{tot} = 2.1 \frac{l}{min}$. CFD simulation performed using COMSOL.

2.1. Theoretical Description

The diluter attenuates the particle number concentration by a factor that is called dilution ratio *DR*. For the presented diluter, *DR* is only dependent on the ratio between the flow rate through the filter Q_f and the flow rate through the needle Q_n:

$$DR = \frac{Q_{tot}}{Q_n} = \frac{Q_f + Qn}{Q_n} = \frac{Q_f}{Q_n} + 1 \quad (1)$$

where Q_{tot} is the total flow rate through the diluter. The flow rate through the needle as a function of the pressure drop Δp can be theoretically described with the Darcy-Weisbach equation. For the case of a hypodermic needle (0.6 mm inner diameter) and the relatively small pressure drop of approximately 10 mbar where the Reynolds number is below 10, the form for laminar flow can be used [4].

$$Q_n = \frac{\pi}{128} \frac{D^4}{\mu L_n} \Delta p \quad (2)$$

with μ being the dynamic viscosity of the fluid, D the hydraulic diameter of the needle and L_n the length of the needle. The fluid flow rate through a porous medium as a function of the pressure drop is described by Darcy's law. The low Reynolds number justifies the theoretical description of the flow through the HEPA filter by this law [5]:

$$Q_n = \frac{\kappa}{\mu} \frac{A}{L_f} \Delta p \quad (3)$$

A is the cross-sectional area, L_f is the length of the filter and k is the permeability of the medium. Inserting Equations (2) and (3) into Equation (1) yields:

$$DR = \frac{128 L_n}{\pi D^4} \frac{\kappa A}{L_f} + 1 \quad (4)$$

Equation (4) shows that the *DR* does not depend on the pressure drop over the diluter. This pressure drop insensitivity is very advantageous for the application in engine exhaust sampling where short and long time related pressure fluctuations occur. The device faces moderate temperatures and particle concentration levels if it is employed as a tertiary dilution stage. Therefore, the performance of the device is not significantly compromised by the deposition of particles, even at relatively long operation times.

2.2. Dilution Ratio in Simulation and Experiment

The flow through the filter and the needle at different pressure drops were measured using a Gilian Gilibrator 2 bubble flow meter. The measurements were done for the three different orientations of the needle orifice relative to the aerosol shown in Figure 2. Figure 3 shows the results

of these measurements. The obtained measurement points where fitted with a power law: $Q = a * \Delta p^b$ At ideal conditions the exponents b of all four fitted curves should amount to 1 according to Equations (2) and (3). The deviation of the observed values can be assigned to entrance and exit effects for the needle and to several turns and tapers in the filter path. For the needle turned by 180°, both fit parameters are larger than for the other orientations. In this case the aerosol is not only pushed through the needle by the static pressure drop but also by the dynamic pressure caused by the fluid flow. An illustration of the flow velocities for a total flow of $2.1 \frac{l}{min}$ predicted by CFD simulations is shown in Figure 1.

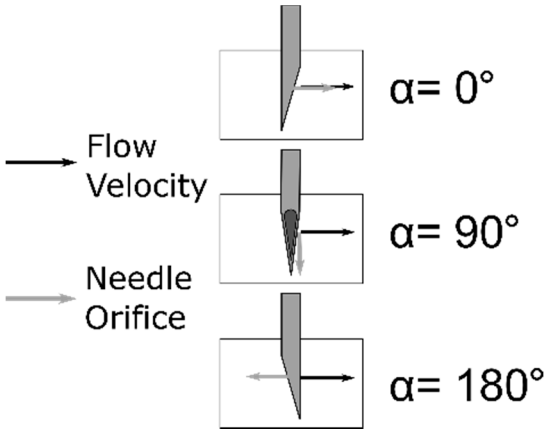

Figure 2. Schematic illustration of different needle orifice orientations relative to the flow. The angle between the needle orifice and the flow velocity is described by α.

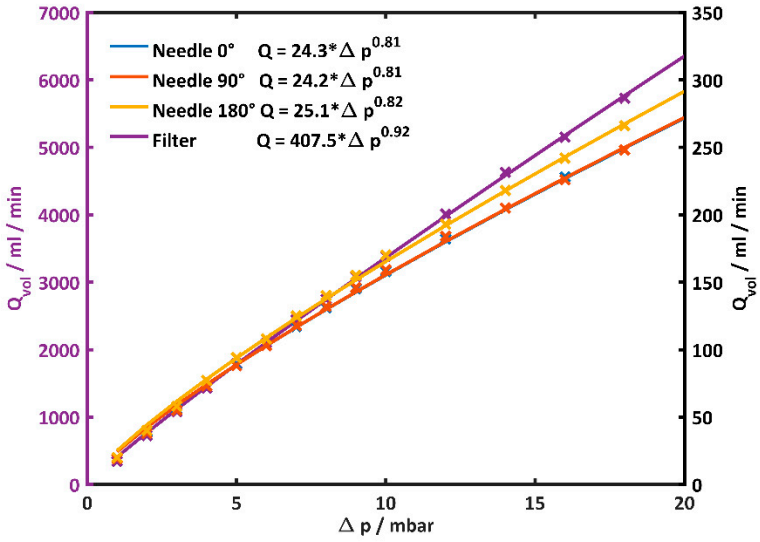

Figure 3. Flow rate as a function of total pressure drop for different needle orientations (right y-axis) and the HEPA filter (left y-axis).

Figure 4 shows the *DR* for different total flow rates calculated from the data shown in Figure 3 and the dilution ratio as predicted by 3-D CFD simulations performed using COMSOL. The experimental and the simulation data agree reasonably well. At low flow rates, the influence of the orientation decreases, because the dynamic pressure effects scale quadratically with the flow rate. The diluter with the $\alpha = 180°$ needle orientation shows a smaller pressure drop sensitivity than the one with $\alpha = 0°$. The *DR* shows a very small dependency on the total flow rate compared to the ejector diluter and it can be further reduced by geometry optimizations.

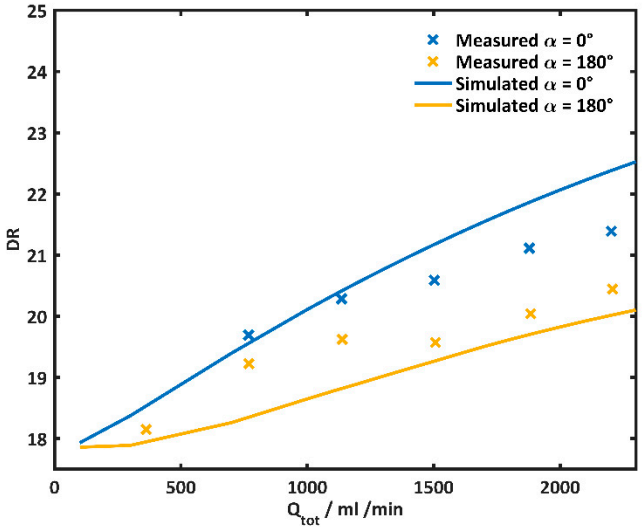

Figure 4. Comparison of the dilution ratio determined by flow measurements and simulations using COMSOL, for two different needle orientation angles α.

2.3. Flow Monitoring

An agglomeration of deposited particles inside the needle or the filter can lead to a change in the pressure drop to flow characteristics, which consequently changes the *DR* of the device. To enable in-time replacement of the needle or the filter, the flow through the needle is monitored. If the total flow rate is known (this is usually the case), monitoring the flow rate through the needle enables the direct calculation of the dilution ratio (Equation (1)).

Figure 5 shows a schematic of the flow sensor. The shown system is heated by the resistor to keep the NTC resistance at 22 kΩ (42.5 °C). The higher the flow through the needle, the more heat is transported away, thus the more voltage has to be applied to the resistor to keep the NTC at 42.5 °C. Figure 6 shows the dependence of the applied voltage, on the flow rate through the needle. The measured data is fitted with a second degree polynomial. The flow through the needle can be monitored by measuring the voltage applied to the heating resistor. The measurements have been successfully reproduced after changing the bypassing needle.

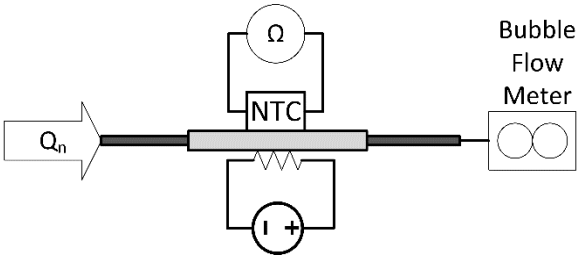

Figure 5. Schematic of the flow sensor and the calibration setup. The flow sensor consists of a 38 Ω heating resistor and a NTC soldered onto hypodermic needle. An electronic circuit controls the heating power to keep the NTC resistance at same values as a referenceresistor.

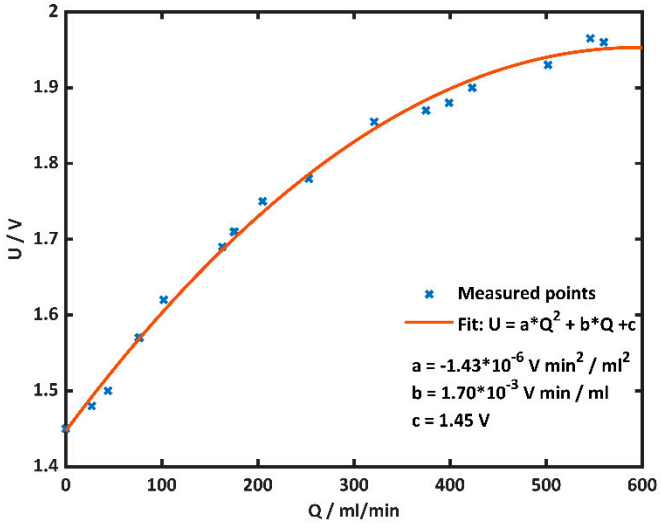

Figure 6. Voltage applied to the heating resistor to keep the NTC resistance at 22 kΩ for different flow rates. The sample temperature and the ambient temperature were 26.0°C. The parameters of the quadratic polynomial fit are given below the legend.

3. Conclusions and Outlook

We designed a device which attenuates the particle number concentration. The costs of the components used do not exceed 40 €. Laws that describe the pressure drop dependence of the flow rate in tubes and porous media, predict that the magnitude of this attenuation is independent of the total flow rate. Flow measurements and CFD simulations showed that the dependence on the total flow does not cancel out perfectly, but the sensitivity of the *DR* is very low compared to other devices. It has been shown that the orientation of the needle orifice relative to the aerosol flow has a significant influence on the dilution ratio and its dependence on the flow rate. Geometry modifications will be performed to further improve the robustness of the dilution ratio. A flow sensor enables monitoring of the introduce dilution ratio. The measured signal shows a quadratic dependence on flow rate. The needle that bypasses the HEPA filter can be exchanged without changing the characteristics of the flow sensor. The influence of the sample temperature and the ambient temperature on the measured signal will be investigated in detail and implemented into the model function. Furthermore, particle losses within the device will be studied in detail and accounted for by defining a Particle Dilution Ratio PDR. The presented device is used for engine exhaust particle number measurements in the framework of the H2020 project DownToTen.

Author Contributions: M.B.: Methodology, Software, Validation, Formal Analysis, Investigation, Writing—Original Draft Preparation, Visualization. A.B.: Conceptualization, Writing—Review & Editing, Supervision, Project Administration, Funding Acquisition

Funding: This work is conducted in the framework of the H2020 project DownToTen. This project has received funding from the European Union's Horizon 2020 research and innovation programme under grant agreement Nr. 724085.

References

1. Giechaskiel, B.; Dilara, P.; Sandbach, E.; Andersson, J. Particle measurement programme (PMP) light-duty inter-laboratory exercise: comparison of different particle number measurement systems. *Meas. Sci. Technol.* **2008**, *19*, 095401.
2. Bergmann, M.; Vogt, R.; Szente, J.; Maricq, M.; Benter, T. Using ejector diluters to sample vehicle exhaust at elevated pressures and temperatures. *SAE Int. J. Engines* **2008**, *1*, 1167–1178.
3. Fuchs, N.; Sutugin, A. Coagulation rate of highly dispersed aerosols. *J. Colloid Sci.* **1965**, *20*, 492–500.

4. Brown, G.O. The history of the Darcy-Weisbach equation for pipe flow resistance. In *Environmental and Water Resources History*; **2003**; pp. 34–43. American Society of Civil Engineering. Washington D.C., United States
5. Al-Hussainy, R.; Ramey, H., Jr.; Crawford, P. The flow of real gases through porous media. *J. Pet. Technol.* **1966**, *18*, 624–636.

Appendix E.

Rotating Disk Diluter: Particle Loss Assessment

Two rotating disk diluters from AVL List GmbH were characterized concerning particle number losses dependent on the particle size, the rotation speed of the dilution disk, and the dilution airflow. Figure E.1 shows a drawing of the diluter used. There was 80 cm of particle loss relevant Viton tube (30 cm "Probe" inlet, 50 cm "Aerosol" outlet) connected to the dilution disk. In the rotating disk, there are two pitch circles. The outer one with $n_o = 8$ (number of holes), $d_o = 2\,\text{mm}$ (hole diameter) holes is used to achieve high dilution ratios. The inner one with $n_i = 15$, $d_i = 4\,\text{mm}$ is used for low dilution ratios. The disk has a thickness of $h = 4\,\text{mm}$. So the transferred volumes per revolution for the outer circle (V_o) and the inner circle (V_i) are:

$$V_o = \frac{d_o^2}{2}\pi h n_o = 9.4 \times 10^{-4}\,\text{L/rev} \tag{E.1}$$

$$V_i = \frac{d_i^2}{2}\pi h n_i = 1.3 \times 10^{-4}\,\text{L/rev} \tag{E.2}$$

The disk can be rotated with speeds between $f_{min} = 5\,\text{rev/min}$ and $f_{max} = 300\,\text{rev/min}$. With a dilution air flow of $Q_{dil} = 1\,\text{L}\,\text{min}^{-1}$. This yields dilution ratio ranges DR_o (outer circle) and DR_i (inner circle) of:

$$DR_o = \frac{Q_{dil}}{V_o f_{max}} - \frac{Q_{dil}}{V_o f_{min}} = 3.5 - 212 \tag{E.3}$$

$$DR_i = \frac{Q_{dil}}{V_i f_{max}} - \frac{Q_{dil}}{V_i f_{min}} = 26.5 - 1592 \tag{E.4}$$

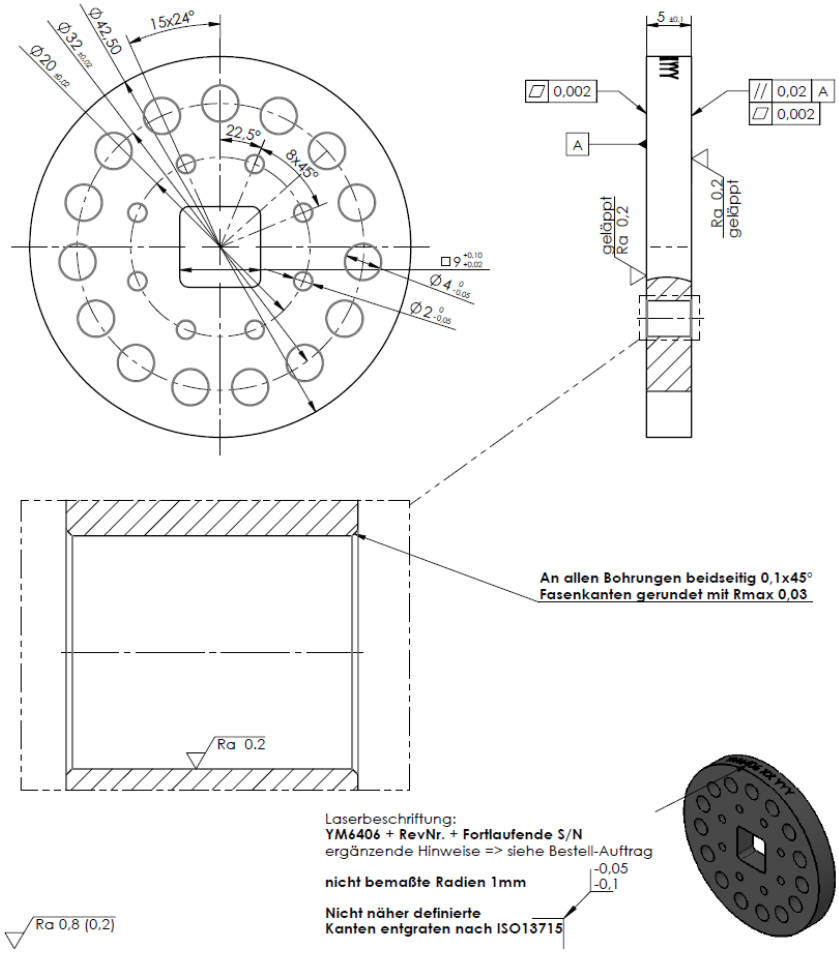

Figure E.1.: Drawing of the AVL rotating disk diluter.

The Topas ATM 220 was used as an aerosol generator. A 0.005 % NaCl solution was atomized. The geometric mean diameter of the particle number distribution was $GMD \approx 30\,\text{nm}$ and the geometric standard deviation $GSD \approx 1.65$. The particle size distributions were measured using a scanning mobility particle sizer (SMPS) comprising a TSI 3082 (long) or 3085 (nano) differential mobility analyzer (DMA) and a TSI 3775 condensation particle counter (CPC) with a cut size of 4 nm. The total number concentration was set to $\approx 6.5 \times 10^5\,\#/\text{cm}^3$ by operating the ATM 220 at 3 bar and using a dilution bridge as depicted in Figure E.3. The tubes were kept as short as possible to minimize diffusional losses to increase the signal to noise ratio, especially at small particle sizes. A typical generated NaCl particle size distribution is shown in Figure E.2.

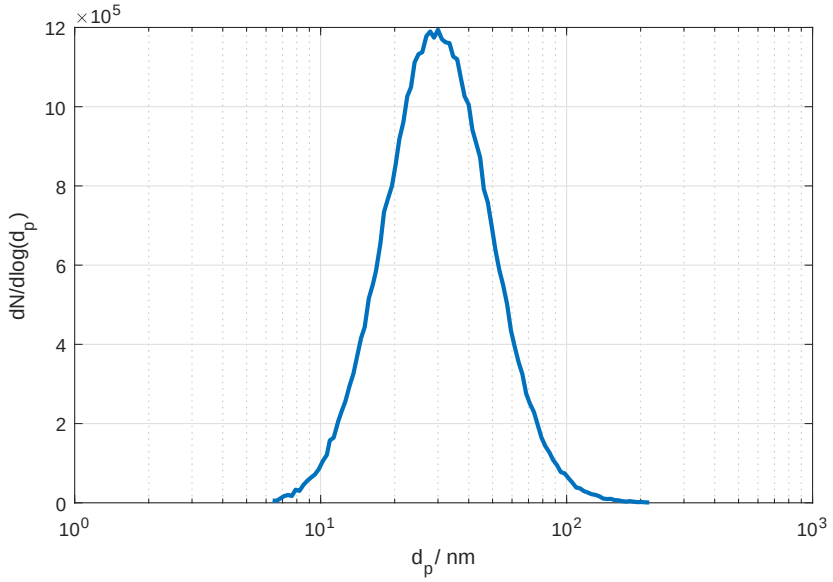

Figure E.2.: A typical generated NaCl particle size distribution

Measurement Schedule, Data Processing, and Diluters Comparison

As a first step, the particle losses of the two diluters were compared. The comparison was made by performing measurements using the long DMA 3082 and a similar setup to the one depicted in Figure E.3. The only difference is that there was no needle valve at the exhaust of the rotating disk diluter. The absence of this needle valve resulted in different pressures in the sampling line when measuring with or without diluter. This absence might affect the generated aerosol in terms of number concentration and particle size. Because of this possible effect, these measurements were only used to compare the two diluters. The measurement of the total particle losses was performed using the more stable setup depicted in Figure E.3. To decrease the effects of possible drifts of the generated number concentration, mean particle size, or other properties, the measurement strategy described in the following lines is applied:

A certain number $N+1$ of size distribution of the undiluted sample is recorded. Between two raw sample measurements, one diluted size distribution is measured with the same settings by switching the two 3-way valves resulting in a total number of $2N+1$ size distributions per measurement set. In data processing, the average of two adjacent undiluted measurements is compared with the dilution ratio multiplied with the diluted sample measured between the undiluted one. This results in N size-dependent loss curves per measurement set. As a final step, the average of these five curves is calculated. The data processing and measuring strategy is described mathematically in the following:

$$1 \leq n \geq N, n \in \mathbb{Z}$$

Undiluted distributions	$c(d_p)_{2n-1}, c(d_p)_{2N+1}$
Diluted distributions	$c(d_p)_{2n}$
Reference distributions	$c(d_p)_{ref,n} = \frac{c(d_p)_{2n-1}+c(d_p)_{2n+1}}{2}$
Loss curves	$L(d_p)_n = \frac{c(d_p)_{ref,n}-c(d_p)_{2n}*DR}{c(d_p)_{ref,n}}$
Mean Losses	$L(d_p)_{mean} = \frac{1}{N}\sum_1^N L(d_p)_n$

Table E.1.: Settings used to compare the two rotating disk diluters' particle loss characteristics.

Pitch Circle	f / rev/min	Q_{dil}/L min^{-1}	DR	N
outer	5	1.35	286.5	5
outer	44	1.35	32.5	5
outer	204	1.35	7.0	5
inner	44	1.35	244.2	5
inner	204	1.35	52.7	5

The described measurements and data processing were performed for both diluters and the dilution settings listed in Table E.1. The results of the measurements are not shown here explicitly because the absolute loss values may be incorrect due to the backpressure issue described above. The particle loss characteristics of the two diluters do not show a significant difference. The following measurements are only performed for one of them, and it is assumed that the other one shows the same behavior.

Size Dependent Particle Losses at a Constant Dilution Flow Rate

The measurement setup for particle number losses with a constant flow rate is schematically depicted in Figure E.3. The pressure difference between the sample line and ambient measured by the pressure gauge in the "Over pressure valve 1" is kept constant at 30 mbar for both sampling raw and diluted aerosol using the two needle-valves at the "Over pressure valve 1" and the "Exhaust" tube of the diluter. This keeps the aerosol generation very stable. In the SMPS system, the TSI 3085 nano DMA was used in order to decrease diffusional particle losses in the SMPS and increase the signal to noise ratio in the loss curves, especially for small particle sizes.

The size range bounds were set to 5.05 nm and 30.5 nm. The scan time was set to 100 s. The measurement and data processing strategies described in section E were applied. The dilution airflow, which equals the sample flow into the SMPS, was set to $\approx 1.5\,\mathrm{L\,min^{-1}}$ and was read out automatically. The

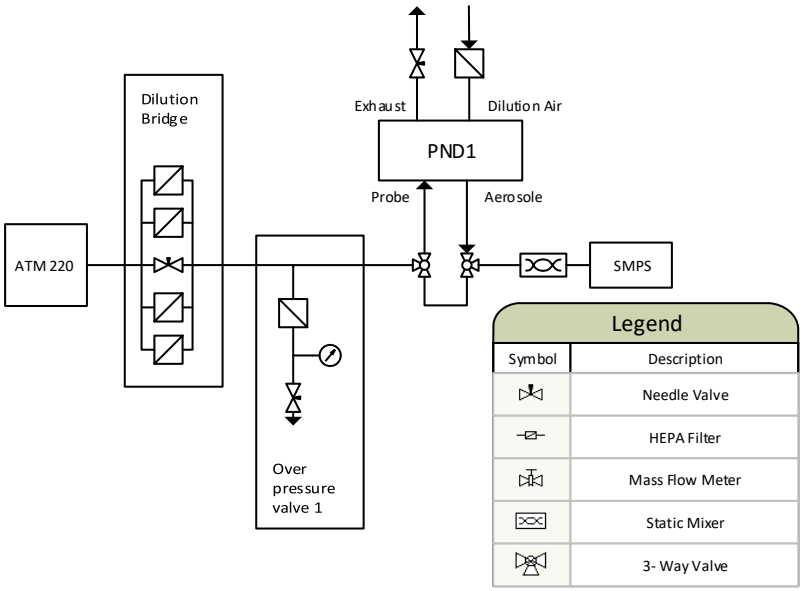

Figure E.3.: Schematic of the setup used for the particle loss measurement with a constant dilution flow rate.

Table E.2.: Dilution settings to assess the particle loss characteristics.

Pitch Circle	f / rev/min	Q_{dil}/L min^{-1}	DR	N
outer	5	1.50	318.3	3
outer	44	1.50	36.2	2
outer	204	1.50	7.8	2
inner	44	1.50	271.3	5
inner	204	1.50	58.5	3

dilution settings and the number of measured samples per measurement set N are listed in Table E.2.

Figure E.4 shows the size dependent particle losses for the settings listed in Table E.2. The left plot in Figure E.4 shows the particle size-dependent losses of the outer pitch circle for three different rotation frequencies. The losses for particles with $d_p > 25\,\text{nm}$ show the lowest losses for $f = 44\,\text{rev/min}$ and the highest for $f = 5\,\text{rev/min}$. Although this is the size range with the highest signal-to-noise ratio, the difference of the three loss-levels is still within the measurement uncertainty, and a clear statement in which rotation frequency leads to the lowest losses cannot be made. The right plot showing the losses using the inner pitch circle, and therefore a higher dilution ratio reveals that both circles have insignificantly different loss characteristics. There is no significant influence of the dilution settings on the particle loss characteristics. More reliable data could be acquired with a different setup using a DMA as a static classifier and measuring the particle number concentration with two CPCs in parallel upstream and downstream the RDD. However, the realization of a corresponding experimental setup was not possible for the described measurement campaign, because the required additional CPC was available during the availability time frame of the rotating disk diluter.

Dilution Flow Rate Variation

The influence of the dilution air flow rate on the particle losses was assessed using the setup depicted in Figure E.5. The dilution air flow was

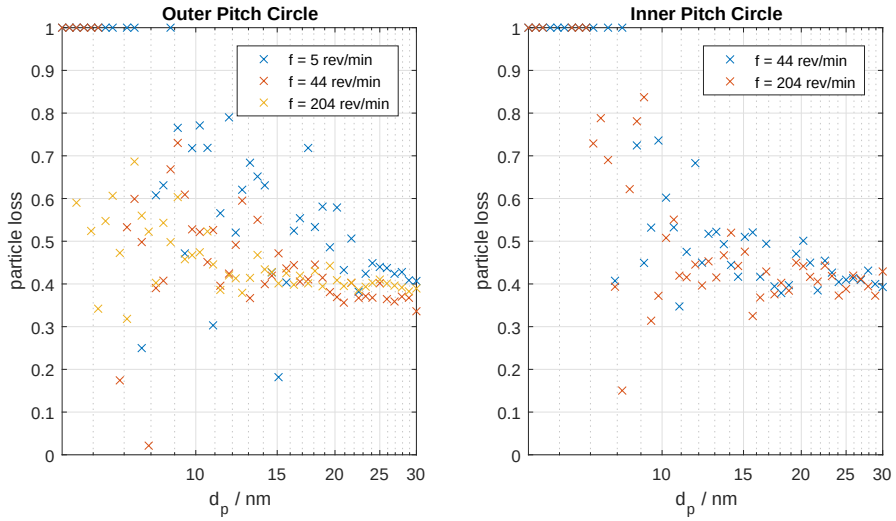

Figure E.4.: Number particle losses for five different dilution settings of the rotating disk diluter.

Table E.3.: Dilution settings to assess the particle loss characteristics.

Pitch Circle	f / rev/min	Q_{dil}/L min^{-1}	DR	N
outer	44	1.38	33.2	5
outer	44	2.50	60.3	5
outer	44	4.00	96.5	5

controlled using the mass flow meter at the "Dilution Air" inlet of the diluter. The "Over pressure valve 2" was used to keep the flow into the SMPS at 1.38 L min^{-1}. The measurement and data processing strategies described in section E were applied. 60 s scans between 5.05 nm and 50.5 nm were performed. The following settings were used:

Figure E.6 shows the particle losses of the diluter operated with the outer pitch circle at 44 rev/min and different dilution flow rates. Figure E.6 shows that the dilution air flow rate does not have a significant influence on the particle losses.

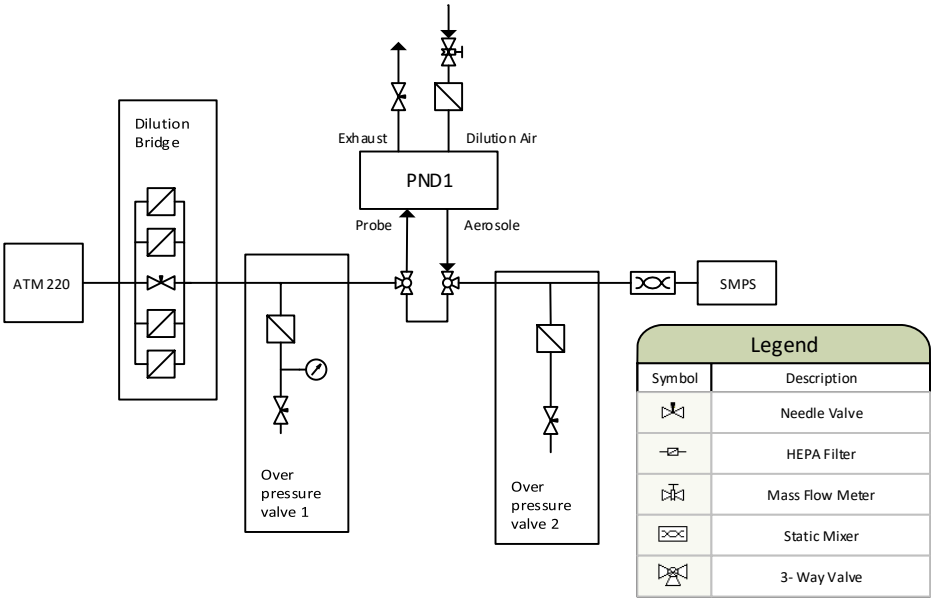

Figure E.5.: Schematic of the setup for measuring particle losses at different dilution flow rates.

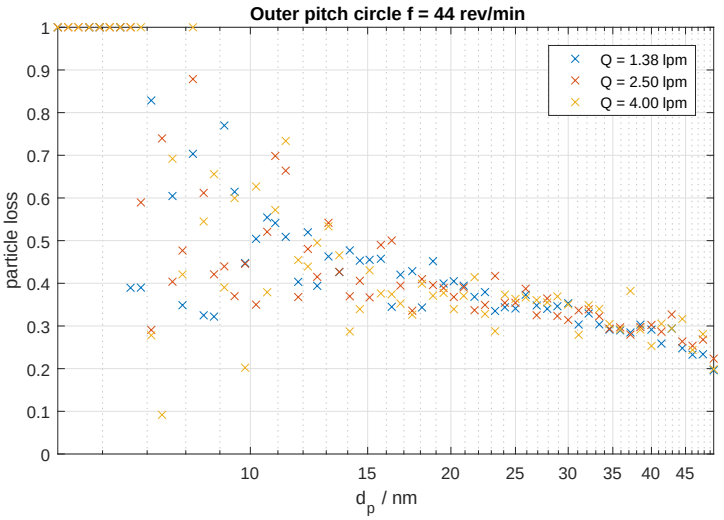

Figure E.6.: Particle size dependent losses of the rotating disk diluter operated with 44 rev/min and the outer pitch circle.

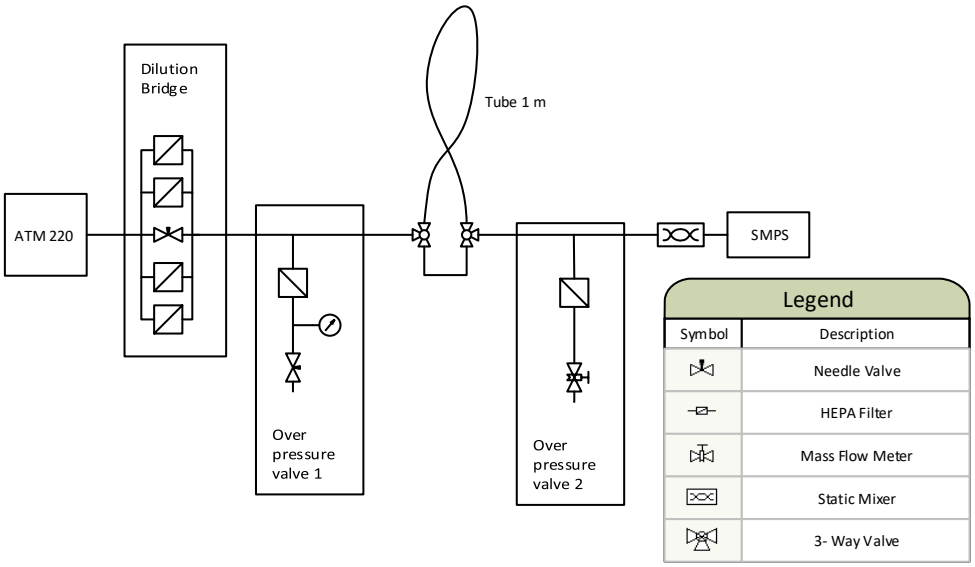

Figure E.7.: Measurement setup for the assessment of particle losses in a Viton and a silicone tube.

Particle Losses in Viton and Silicone Tube

The AVL RDD can be connected to other components and aerosol sources using tubes either made of Viton or Silicone. The particle losses in a 1 m Viton tube and a 1 m Silicone tube was experimentally assessed to examine if the different materials influence the particle losses. The measurement setup depicted in Figure E.7 was used for the corresponding measurements. Both tubes' particle losses were measured at flow rates of $Q = 1.35\,\mathrm{L\,min^{-1}}$ and $Q = 2.66\,\mathrm{L\,min^{-1}}$. The flow rates were controlled by operating the ATM 220 at 1.1 bar and 4.0 bar respectively. The flow measured with the mass flow meter in the "Over pressure valve 2" was added to the flow into the SMPS. The measurement and data processing strategies described in section E were applied. Figure E.8 shows the size-dependent particle losses of the tube at two different flow rates and the theoretical values described in subsection 2.4.2.

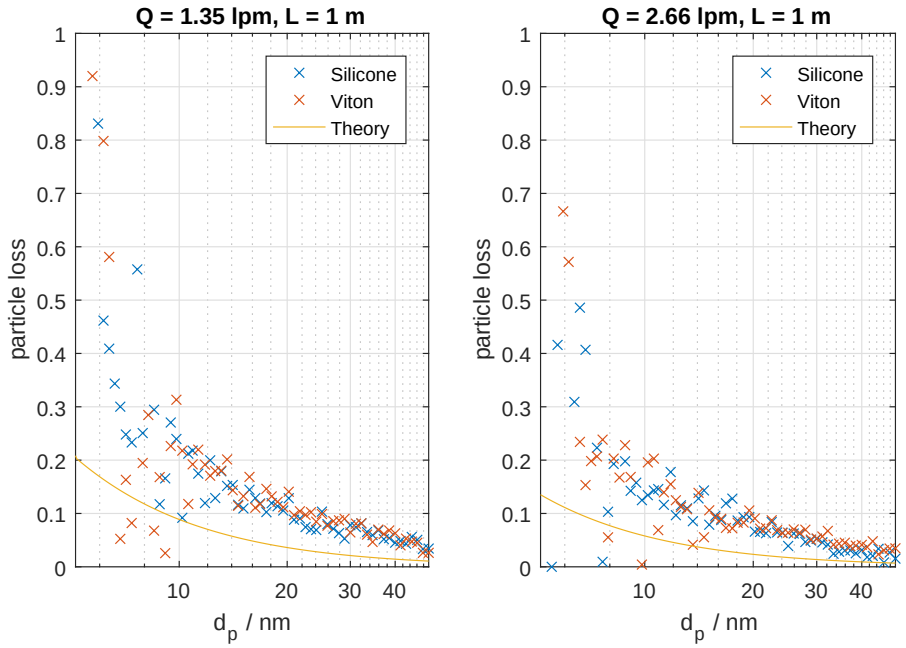

Figure E.8.: Particle losses in a viton and a silicone tube at different flow rates.

The results shown in Figure E.8 indicate that the different materials do not influence the particle losses in the investigated particle size range. Both tubes show the same loss characteristics. The deviations to the theoretical values are of a reasonable magnitude considering that the theoretical description assumes ideal conditions and only takes into account diffusional losses.

Appendix F.

Patent: Particle Magnifier and Particle Counter for Particles in a Flow

The patent application attached below was composed by the patent attorney Bernhard Voith, based on an invention disclosure by Alexander Bergmann (30 %) and the author of this thesis (70 %). The invention describes an instrument for the magnification and counting particles in a flow. The significant difference to state-of-the-art CPCs is that the operating temperature of the described instrument can significantly exceed room temperature. This higher temperature is enabled by the application of a counter flow denuder as described in **Paper 2** for the injection of the working fluid.

Particle Magnifier and Particle Counter for Particles in a Flow

The present invention relates to a particle magnifier for magnifying particles carried by a carrier gas in a flow, comprising a conditioner for conditioning the flow with a working gas, a cooler for cooling the conditioned flow such that working gas condenses on the particles, and a first conduit for guiding the flow in a flow direction successively through the conditioner and the cooler. The invention further relates to a particle counter comprising the particle magnifier.

Particle magnifiers are typically used in particle counters, however, they are not limited to such a use. For detecting and counting particles in an aerosol, i.e., in a dispersion of solid and/or liquid particles carried by a carrier gas, different types of particle counters are known. Usually, particle counters for aerosols have an optical detector, e.g., a source for a laser light directed at the aerosol flow and a photosensor detecting particles in the flow on the basis of the laser light scattered by each particle. However, the sizes of particles to be measured, e.g., in air pollution monitoring or in particle concentration measurement of combustion engine exhausts, decrease due to an evolution in combustion processes and/or in statutory requirements. Light scattered by particles of very small size is yet hard or even impossible to be detected with conventional means. To solve this problem, particle magnifiers have been developed that exploit the properties of the particles to act as condensation nuclei and grow (“mag-

nify") the particles in the flow by condensation of a working gas, e.g., water or butanol vapour, on the particles until they are sufficiently large to be detected in the particle detector. To this end, a wick is soaked with, e.g., liquid water, butanol etc., and exposed to the flow such that the liquid is vaporised by the flow, thereby saturating the flow with the vapour, i.e., the working gas; when subsequently cooling the flow, the working gas condenses on the particles.

This process used, e.g., in known particle counters - also referred to as "condensation nuclei counters" or "condensation particle counters" - very much depends on the temperature and on the equilibrium vapour pressure which is working gas specific. Moreover, the maximum operation temperature of such condensation nuclei counters is generally limited to room temperature or slightly above, e.g. to 35°C or 40°C, mainly due to the wick and its vaporisation of the liquid. In many cases, though, only non-volatile particles are to be counted, i.e., particles that are not vaporised at a temperature of typically 350°C; volatile particles, that vaporise only between the operation temperature of the particle counter and said, e.g., 350°C, substantially impair the counting result in these cases.

For countering this drawback, it has been proposed by *N. Collings et al.*, "A Condensation Particle Counter Insensitive to Volatile Particles", Journal of Aerosol Science 73 (2014), 27 - 38, to use a silicon carbide diesel particle filter as a wick in a through-flow device to saturate an auxiliary gas first, e.g., clean air or Nitrogen, at a temperature of 150°C

to 200°C with a special working gas suitable for such elevated temperatures, e.g., with per-fluorinated polyether or poly-phenyl-ether. The auxiliary gas saturated with the working gas is then conveyed into the cooler into which the aerosol flow is injected at the same elevated temperature. Thereby, the operation temperature of the particle counter can be raised with respect to previous particle counters. However, the proposed particle counter has a complex structure and still substantially depends on temperature and equilibrium vapour pressure. Furthermore, the applicability is limited by the availability of a suitable working gas for the required operation temperature as well as the particles to be counted: For condensing on the particles, the working gas has to wet their surfaces. While the maximum operation temperature reachable with such a particle counter is expected to be 300°C at best, this is still lower than generally required, e.g., for monitoring combustion processes.

A different solution has been proposed by *M. Bainschab et al.*, "Aerosol Gas Exchange System (AGES) for Nanoparticle Sampling at Elevated Temperatures: Modeling and Experimental Characterization", Sci Rep 9, 17149 (2019) doi: 10.1038/s41598-019-53113-5. According thereto, the aerosol flow is heated (in the proposed example to a temperature of 200°C, with higher temperatures to be achieved) and the carrier gas and the volatile particles that are vaporised at this temperature are exchanged to a clean purge gas by means of a so-called counter flow denuder, described, e.g., in *H. Hiroyuki*, "Laboratory Evaluation

of Nanoparticles Penetration Efficiency in a Cylindrical Counter Flow Denuder for non-specific Removal of Trace Gases", Aerosol Science and Technology, 51:4, 443 - 450, doi: 10.1080/02786826.2016,1271939. The remaining non-volatile particles now carried by the purge gas in the flow can later be counted at any convenient temperature by means of a conventional condensation nuclei counter connected to the counter flow denuder.

It is an object of the present invention to provide a particle magnifier and a particle counter which are reliable, flexibly usable, less dependent on temperature and pressure, also applicable at higher temperature, and the structures of which are straightforward.

According to a first aspect, this object is achieved with a particle magnifier of the type mentioned at the outset, which is distinguished in that the conditioner has a second conduit for the working gas, wherein the first and second conduit are in fluid communication via a membrane that is permeable to both the carrier gas and the working gas and impermeable to the particles, such that at least part of the carrier gas in the flow can be substituted by the working gas.

This particle magnifier does not require a complex structure and particularly has a continuous, straightforward flow through the first conduit. As the working gas in this case is gaseous before being brought into the flow, the particle magnifier is suitable for any temperature above the boiling point or the dew point of the working gas. Therefore, the present particle magnifier can be flexibly used with a huge variety of known

and easily available substances including water and butanol. This is not impaired by the fact that both the boiling point and the dew point depend on the pressure as known to the skilled person, because the pressure is easy to handle with the present straightforward design. Moreover, by substituting carrier gas by working gas the particle magnifier is less dependent on the temperature and independent, or at least largely independent, of the equilibrium vapour pressure and thus more reliable than particle magnifiers of prior art particle counters.

In an advantageous embodiment, the particle magnifier further comprises a heating or cooling device which is heat-conductively connected to the first conduit upstream the conditioner and configured to bring the flow to a predetermined temperature. The heating or cooling device facilitates a matching of the flow's temperature with the predetermined temperature of the process in the particle magnifier. Thereby, the particle magnifier becomes independent of the temperature of the flow fed into the first conduit; an optimum process temperature can be achieved.

It is favourable when the conditioner comprises a pressuriser which is conductively connected to the second conduit and configured to keep a pressure difference between the second conduit and the first conduit below a predetermined threshold. A reliable substitution of the carrier gas by the working gas can thereby be achieved in the conditioner. Moreover, this supports a substitution of the carrier gas by the working gas by diffusion rather than by convective mass transport through the

membrane, thus achieving a high substitution rate, without affecting the flow in the first conduit.

In a preferred embodiment, the conditioner is configured to create a counterflow in the second conduit along the membrane with respect to the flow direction in the first conduit. The efficiency of substituting the carrier gas by the working gas is particularly high in such a condition. Experiments have shown that up to or even above 99% of the carrier gas can be substituted by working gas when using a counterflow.

It is favourable when the conditioner comprises a reservoir for a working substance upstream the second conduit and a heater for vaporising the working substance in the reservoir to the working gas. By storing and vaporising the working substance and providing the working gas by the conditioner, the particle magnifier is self-contained while keeping a small overall size.

In a beneficial embodiment, the conditioner comprises a cooled container downstream the second conduit for condensing unused working gas. The unused working gas can thereby be collected for an optional later reuse.

A variety of different designs of the first and second conduit and the membrane may be used in the particle magnifier, e.g., a parallel plate membrane etc. It is, however, particularly advantageous when the membrane is substantially tubular, wherein the first conduit is inside and the second conduit is outside the tubular membrane. This provides a specifically

large surface of the membrane for efficient substitution of carrier gas by working gas.

The membrane may be of any suitable type and material. It is favourable, though, when the membrane is made of a porous glass. Porous glass is heat resistant, reliable and very durable as a membrane.

The cooler may, e.g., use a heat exchanger for cooling the first conduit and/or its wall. In a beneficial embodiment, the cooler is configured to inject a cooling gas into the first conduit for cooling the flow. A cooler of this type achieves a simple and reliable way of cooling the flow and effectively prohibits condensation of working gas on the first conduit's wall and/or on a heat exchanger's surface.

In a second aspect, the present invention creates a particle counter for counting particles carried by a carrier gas in a flow, which particle counter comprises a particle magnifier of the aforementioned type and a detector, wherein a first conduit is configured to guide the flow in a flow direction successively through a conditioner and a cooler of the particle magnifier and through the detector, and wherein the detector is configured to detect, in the flow, and to count the particles with working gas condensate thereon.

With respect to further embodiments of the particle counter and advantages thereof, it is referred to the above statements on the particle magnifier.

The invention shall now be explained in further detail below on the basis of an exemplary embodiment thereof with reference to the accompanying drawings, in which:

Fig. 1 shows a particle counter comprising a particle magnifier according to the present invention in a schematic side view;

Fig. 2 shows a first conduit of the particle magnifier and the particle counter of Fig. 1 in a fragmentary sectional view; and

Fig. 3 shows a temperature and saturation profile in the first conduit of Fig. 2 in a schematic diagram over the length of the first conduit.

Figs. 1 and 2 schematically show a particle magnifier 1 which magnifies particles 2 that are carried by a carrier gas 3 in a flow 4, and a particle counter 1' comprising the particle magnifier 1 for counting the particles 2 in the flow 4. The particles 2 are solid or liquid, have sizes in a range from 1 nm to several 100 nm, i.e., they are nanoparticles, and may be of natural origin or man-made, e.g., resulting from combustion. The carrier gas 3 may be a mixture of different gases and is symbolised in the enlarged depiction of Fig. 2 by hatched dots representing carrier gas molecules 3' which are substantially smaller than the particles 2 in the flow 4. It shall be noted in this context, that Fig. 2 is not drawn to scale.

With reference to Figs. 1 to 3, details and embodiments of the particle magnifier 1 and the particle counter 1' shall now be explicated in detail. For easier reference, Figs. 1 to 3 are

consistently sectioned according to functions, in a direction 6 of the flow 4, into: an optional heating or cooling section 7, a subsequent conditioner section 8, a cooler section 9 following the conditioner section 8, and, finally, an optional detector section 10. In accordance therewith, a first conduit 11 guides the flow 4 in the flow direction 6 between an inlet 12 and an outlet 13 of the first conduit 11 successively at least through a conditioner 14 and a cooler 15 of the particle magnifier 1 and, in case of the particle counter 1', also through a detector 16 of the particle counter 1'. The conditioner 14, the cooler 15 and the detector 16 are located in the conditioner section 8, the cooler section 9, and the detector section 10, respectively.

The conditioner 14 conditions the flow 4 with a working gas 17. To this end, the conditioner 14 has a second conduit 18 for the working gas 17, and the first and second conduit 11, 18 are in mutual fluid communication via a membrane 19. The membrane 19 is permeable to both the carrier gas 3 and the working gas 17 but is impermeable to the particles 2. As symbolised by small arrows in Fig. 2, molecules 3' of the carrier gas 3 diffuse from the first to the second conduit 11, 18 and molecules 17' of the working gas 17, represented by open dots in Fig. 2, diffuse from the second to the first conduit 18, 11 through the membrane 19. Thereby, at least part of the carrier gas 3 in the flow 4 is substituted by the working gas 17 in the conditioner 14, as will be explicated in greater detail further below.

From the conditioner 14, the first conduit 11 guides the flow 4 conditioned with working gas 17 to the cooler 15. The cooler 15 cools the conditioned flow 4 such that working gas 17 condenses. The working gas 17 is suited for condensing on the particles 2 when sufficiently cooled; this includes that the working gas wets the particles' surfaces. Thereby, the particles 2 in the flow 4 are grown ("magnified") in the particle magnifier 1 before leaving the cooler section 9 and, thus, the particle magnifier 1.

In case of the particle magnifier 1 being comprised in the particle counter 1', the first conduit 11 further guides the cooled flow 4 from the cooler 15 to the detector 16 of the particle counter 1'. The detector 16 is of any type known in the art that is capable of detecting, in the cooled flow 4, each particle 2 that has working gas condensate 17" thereon, e.g., an optical detector 16 having a laser light source 20 emitting a laser light 21 into the flow 4 and onto a photo-sensor 22. In this case, the photo-sensor 22 detects a particle 2 by the laser light 21 scattered by the particle 2 and/or the working gas condensate 17" thereon as known in the art. The detector 16 is further configured to count the detected particles 2.

Optionally the particle magnifier 1 further comprises a heating or cooling device 23. The heating or cooling device 23 heats or cools the flow 4 when it is not at a predetermined temperature T_p at the inlet 12 of the first conduit 11. To this end, the heating or cooling device 23 is heat-conductively connected to the first conduit 11 in the heating or cooling sec-

tion 7 upstream the conditioner 14 and has, e.g., a heat exchanger 24 abutting on a wall 25 of the first conduit 11. The temperature T_p is predetermined based on the respective requirements; in a case where only non-volatile particles 2 in the flow 4, i.e., particles 2 that do not vaporise below a certain temperature, e.g., 350 °C, shall be counted, this temperature will be used as the predetermined temperature T_p. In other cases, a different temperature T_p may be predetermined.

In the present example, the heating or cooling device 23 heats the flow 4 to raise the temperature T thereof to the predetermined temperature T_p in the heating or cooling section 7, as depicted by the dashed line over the length L of the particle counter 1 in Fig. 3. When, on the other hand, the flow 4 at the inlet 12 of the first conduit 11 would have a temperature T above the predetermined temperature T_p, the heating or cooling device 23 would cool the flow 4 to the predetermined temperature T_p. Moreover, the carrier gas 3 sometimes comprises some gas of the same type as the working gas 17, e.g., when the working gas 17 is water vapour and the carrier gas 3 is an exhaust gas of a combustion engine, which also comprises water vapour. In such a case, a (low) saturation S of the flow 4 with, e.g., water vapour further decreases when heating the flow 4 in the heating or cooling section 7 as depicted by the solid line in the example of Fig. 3.

Generally, the first and second conduits 11, 18 are at the same or a similar pressure level. However, the conditioner 14 may optionally comprise a pressuriser 26 which is conductively

connected to the second circuit 18, e.g., upstream or downstream the membrane 19. The pressuriser 26 is configured to keep a pressure difference between the second circuit 18 and the first circuit 11, i.e., the absolute value of the pressure difference, below a predetermined threshold of, e.g., 10 mbar, 1 mbar, 0.5 mbar or even less. To this end, the pressuriser 26 may comprise a pump and/or a control valve 27 and may measure and compare a respective pressure both in the first and in the second conduit 11, 18 as known in the art.

Moreover, the conditioner 14 optionally creates a counterflow in the second conduit 18 along the membrane 19 with respect to the flow direction 6 in the first conduit 11, i.e., a flow in a direction 28 opposed to the flow direction 6 of the first conduit 11, e.g., by means of the pressuriser 26.

As depicted in Fig. 3, the saturation S of the flow 4 with working gas 17 reaches a level L_S in the conditioner 14 at the downstream end of the conditioner section 8, whereas the temperature T in the first conduit 11 is substantially stable throughout the conditioner section 8. The saturation level L_S is close or equal to 100% saturation S. However, at least part of the carrier gas 3 may remain in the flow 4 downstream the conditioner 14 as symbolised by the few molecules 3' of carrier gas 3 in the cooler section of Fig. 2.

In an optional embodiment, the conditioner 14 further comprises a reservoir 29 for a working substance 30, i.e., the working gas 17 in its liquid or solid state. In this embodiment, the conditioner 14 further comprises a heater 31, which

is heat-conductively connected to the reservoir 29 and vaporises the working substance 30 in the reservoir 29 to the working gas 17 which is provided to the second conduit 18.

In the optional case where the working substance 30 in the reservoir 29 is solid, the heater 31 melts and vaporises the working substance 30 or, depending on the working substance 30, sublimates the working substance 30 to the working gas 17, which shall all be comprised by the term “vaporising” the working substance 30 in the present context. Similarly, a deposition of working gas 17 as a solid working substance 30 on a particle 2 or a freezing of working gas condensate 17" thereon in the cooler section 9 shall also be comprised by the term “condensing” on the particle 2 in the present context.

The optional pump and/or control valve 27 of the pressuriser 26 may control the pressure of working gas 17 provided from the reservoir 29 to the second conduit 18 in the example of Fig. 1. In this example, the pump and/or control valve 27 of the pressuriser 26 is located at an optional outlet 32 of the second conduit 18 downstream the membrane 19. Moreover, the second conduit 18 may optionally have an inlet 33 for admixing a further gas 34 to the working gas 17 upstream the membrane 19; said admixing may be controlled, e.g., by a further pressuriser 35 at the inlet 33 of the second conduit 18 and/or by the abovementioned pressuriser 26.

It shall be understood that the working gas 17 in the second conduit 18 is, generally, at the same or a similar temperature as the temperature T_p predetermined for the flow 4 in the

first conduit 11. To this end the working gas 17 is either provided to the conditioner 14 at this temperature, or, e.g., the heater 31 heats the working gas 17 to this temperature.

In the shown example, the conditioner 14 further comprises an optional cooled container 36 downstream the second conduit 18 and connected thereto. In the cooled container 36, working gas 17 that has not been used in the second conduit 18 for substituting carrier gas 3 is condensed and contained in liquid or solid form as working substance 30, e.g., for later reuse.

The membrane 19 may be of any shape, type and material known in the art. Similarly, the first and second conduits 11, 18 may be of any suitable cross-sectional shape. For example, the membrane 19 may be a porous plate between the first and second conduit 11, 18 which have, e.g., rectangular or semi-circular cross-sectional shape in this case. Optionally, the membrane 19 may be formed by two parallel porous plates, between which the first conduit 11 runs, and outside each of which a respective part of the second conduit 18 runs. In the example of Figs. 1 and 2, however, the membrane 19 is substantially tubular and the first conduit 11 is inside the tubular membrane 19, whereas the second conduit 18 is outside the tubular membrane 19 such that it has, e.g., an annular cross-section and is enclosed by a wall 37. It shall be understood, that the membrane 19 may be composed of a plurality of membranous members, e.g., a plurality of tubular membranes of the abovementioned type, together forming the membrane 19. Furthermore, the membrane 19 is optionally made of a porous glass,

e.g., of a glass known as Shirasu Porous Glass, produced by SPG Techno Co., Ltd. of Japan.

In the cooler section 9, the temperature T of the flow 4 is decreased by means of the cooler 15. To this end, the cooler 15, similar to the heater or cooler device 23, may be equipped with a heat exchanger that is heat-conductively connected to the first conduit 11. In the example of Fig. 1, however, the cooler 15 injects a cooling gas 38 into the first conduit 11 for cooling the flow 4. The cooling gas 38 does not contain any further particles that might affect the counting of the particles 2 in the flow 4 as shall be understood.

As a consequence of cooling, the flow 4 becomes supersaturated with working gas 17 in the cooler section 9, i.e., it reaches a level of super saturation L_{SS} (Fig. 3). Hence, the working gas 17 condenses on the particles 2, i.e., the surfaces thereof, as the particles 2 act as condensation nuclei for the condensing working gas 17. This is depicted in Fig. 2 by an increasing number of working gas molecules 17' condensing as condensate 17" on the particles 2. As known on the art, the condensation of the working gas 17 occurs when the saturation vapour pressure falls below the partial pressure of the working gas 17. Due to the substantially constant pressure in the first conduit 11 of the present particle magnifier 1, the temperature T is the main parameter of influence, however.

In the optionally subsequent detector section 10, the particles 2 of the flow 4 are detected by the detector 16 of the particle counter 1'. Due to the increased size of the particles

2 which have working gas condensate 17" thereon, the photosensor 22 can detect the scattered laser light 21, such that they can be counted.

The invention is not restricted to the specific embodiments described in detail herein, but encompasses all variants, combinations and modifications thereof that fall within the frame of the appended claims.

Claims:

1. A particle magnifier for magnifying particles (2) carried by a carrier gas (3) in a flow (4), comprising a conditioner (14) for conditioning the flow (4) with a working gas (17), a cooler (15) for cooling the conditioned flow (4) such that working gas (17) condenses on the particles (2), and a first conduit (11) for guiding the flow (4) in a flow direction (6) successively through the conditioner (14) and the cooler (15),

characterised in that

the conditioner (14) has a second conduit (18) for the working gas (17), wherein the first and second conduit (11, 18) are in fluid communication via a membrane (19) that is permeable to both the carrier gas (3) and the working gas (17) and impermeable to the particles (2), such that at least part of the carrier gas (3) in the flow (4) can be substituted by the working gas (17).

2. The particle magnifier according to claim 1, characterised by a heating or cooling device (23) which is heat-conductively connected to the first conduit (11) upstream the conditioner (14) and configured to bring the flow (4) to a predetermined temperature (T_p).

3. The particle magnifier according to claim 1 or 2, characterised in that the conditioner (14) comprises a pressuriser (26) which is conductively connected to the second conduit (18) and configured to keep a pressure difference between the

second conduit (18) and the first conduit (11) below a predetermined threshold.

4. The particle magnifier according to any one of claims 1 to 3, characterised in that the conditioner (14) is configured to create a counterflow in the second conduit (18) along the membrane (19) with respect to the flow direction (6) in the first conduit (11).

5. The particle magnifier according to any one of claims 1 to 4, characterised in that the conditioner (14) comprises a reservoir (29) for a working substance (30) upstream the second conduit (18) and a heater (31) for vaporising the working substance (30) in the reservoir (29) to the working gas (17).

6. The particle magnifier according to any one of claims 1 to 5, characterised in that the conditioner (14) comprises a cooled container (36) downstream the second conduit (18) for condensing unused working gas (17).

7. The particle magnifier according to any one of claims 1 to 6, characterised in that the membrane (19) is substantially tubular, wherein the first conduit (11) is inside and the second conduit (18) is outside the tubular membrane (19).

8. The particle magnifier according to any one of claims 1 to 7, characterised in that the membrane (19) is made of a porous glass.

9. The particle magnifier according to any one of claims 1 to 8, characterised in that the cooler (15) is configured to inject a cooling gas (38) into the first conduit (11) for cooling the flow (4).

10. A particle counter for counting particles (2) carried by a carrier gas (3) in a flow (4), characterised by a particle magnifier (1) according to any one of claims 1 to 9 and a detector (16), wherein a first conduit (11) is configured to guide the flow (4) in a flow direction (6) successively through a conditioner (14) and a cooler (15) of the particle magnifier (1) and through the detector (16), and wherein the detector (16) is configured to detect, in the flow (4), and to count the particles (2) with working gas condensate (17") thereon.

Abstract:

Particle Magnifier and Particle Counter for Particles in a Flow

The present invention relates to a particle magnifier (1) for magnifying particles (2) carried by a carrier gas (3) in a flow (4), comprising a conditioner (14) for conditioning the flow (4) with a working gas (17), a cooler (15) for cooling the conditioned flow (4), and a first conduit (11) for guiding the flow (4) in a flow direction (6) successively through the conditioner (14) and the cooler (15), wherein the conditioner (14) has a second conduit (18) for the working gas (17), wherein the first and second conduit (11, 18) are in fluid communication via a membrane (19) that is permeable to both the carrier gas (3) and the working gas (17) and impermeable to the particles (2). The invention further relates to a particle counter (1') comprising the particle magnifier (1).

(Fig. 1)

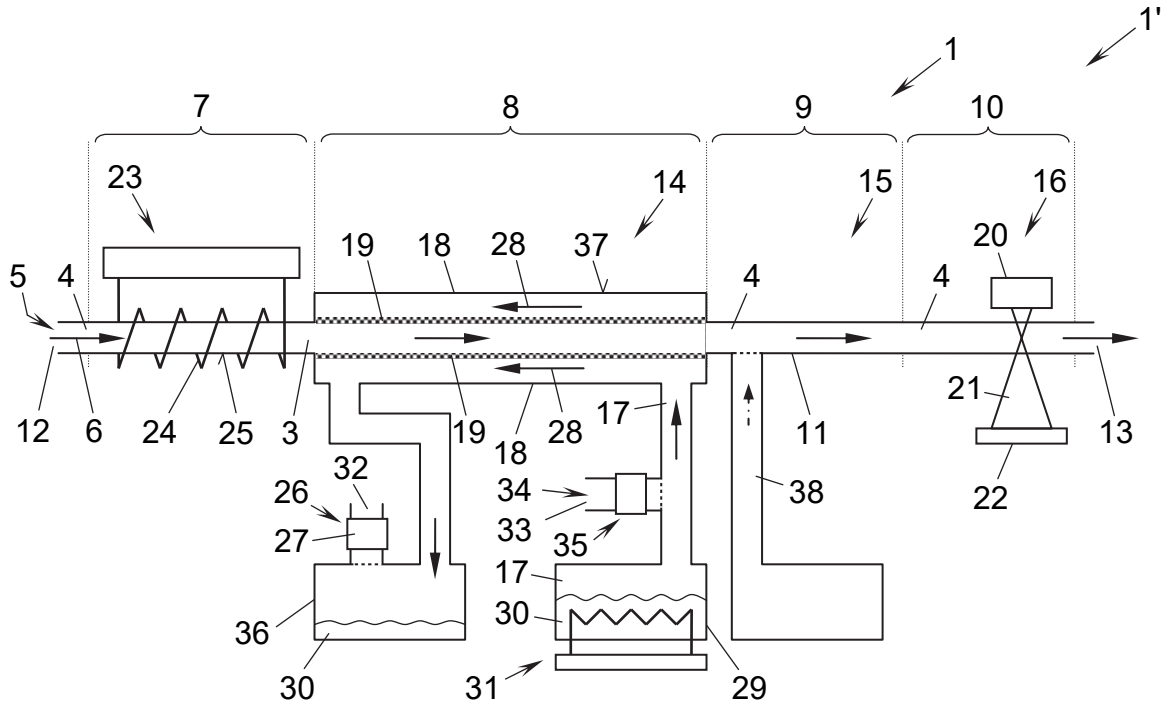

Fig. 1

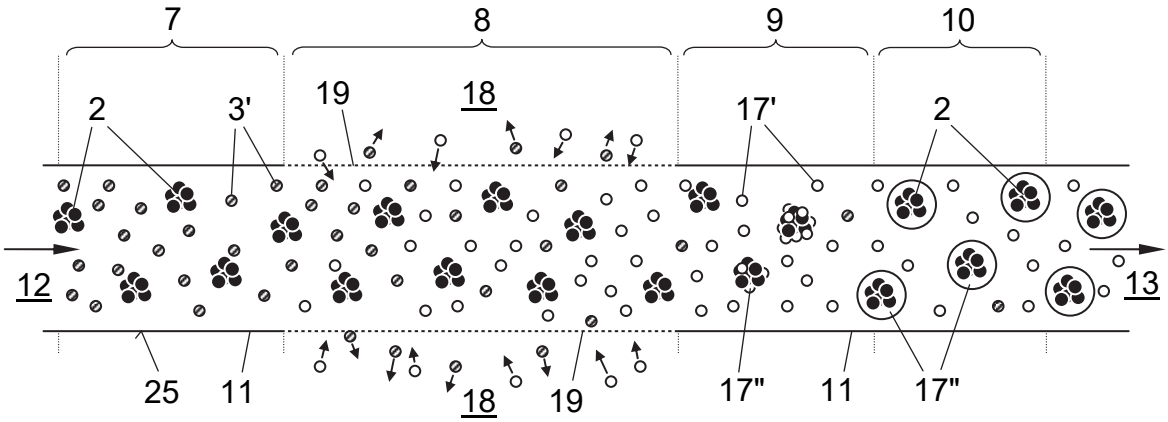

Fig. 2

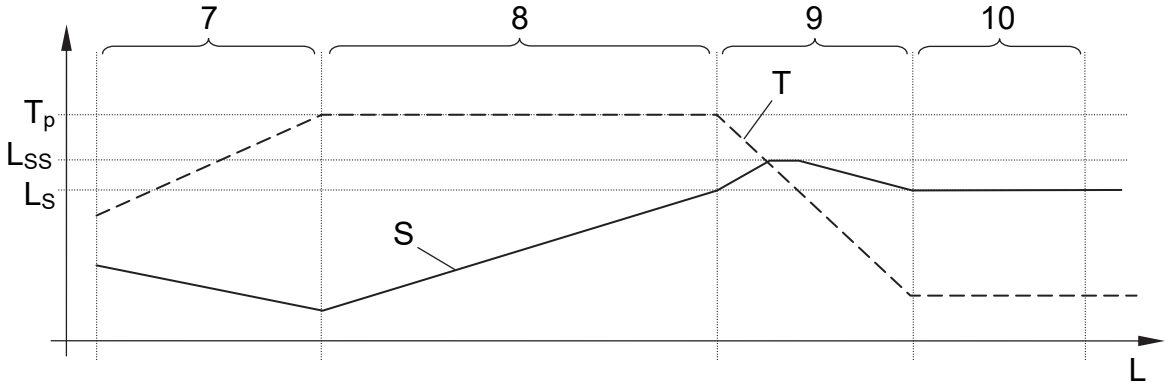

Fig. 3